The Roles of Factor XIII-A and Transglutaminase 2 in the Vasculature

Kingsley Simpson

Submitted in accordance with the requirements for the degree of

Doctor of Philosophy

The University of Leeds
Faculty of Medicine and Health
School of Medicine
Leeds Institute of Cardiovascular and Metabolic Medicine (LICAMM)
Division of Cardiovascular and Diabetes Research (DCDR)

March 2017

Intellectual Property and Publication Statements

The candidate confirms that the work submitted is his own, except where work which has formed part of jointly authored publications has been included. The contribution of the candidate and the other authors to this work has been explicitly indicated below. The candidate confirms that appropriate credit has been given within the thesis where reference has been made to the work of others.

Work that forms part of a jointly authored publication is found on pg16, figure 1-5 (chapter 1) and is from “Normal Bone Deposition Occurs in Mice Deficient in Factor XIII-A and Transglutaminase 2.” Cordell PA, Newell LM, Standeven KF, Adamson PJ, Simpson KR, Smith KA, Jackson CL, Grant PJ, Pease RJ. Matrix Biology (Apr 2015). I carried out maintenance of mouse lines and produced real time PCR data. PAC, LMN, KFS, PA and KAS conducted experimental work. PAC, LMN, KFS and RJP conducted ongoing data analysis. RJP, PAC and PJG prepared the manuscript.

Acknowledgements

I would like to recognise and thank wholeheartedly my PhD supervisors, Dr Richard Pease and Professor Peter Grant, without them this opportunity would never have arisen. Their support and guidance over these past three years has been appreciatively received.

I would also like to take the opportunity to thank the following:

The British Heart Foundation for their financial support in the form of a non-clinical PhD studentship (FS/13/36/30243), without this the work would not have been possible.

Dr Kathryn Griffin for her invaluable advice, support and for her massive expenditure of effort in establishing the aneurysm model, for all of which I am hugely grateful.

Dr Cora Beckers for her support with the cardiac fibrosis study and Mrs Jane Brown for her assistance with the FXIII-A activity assays.

The members of the Grant group for welcoming me into the “family” and for the memorable experiences.

Dr Karen Porter and Dr Kerrie Smith for their pastoral support and guidance throughout the whole PhD process.

I would also like to thank the CBS staff, particularly Mr Andrew Horner, for their help and guidance with all aspects of animal husbandry and experimental procedures.

Finally, a heartfelt thank you to my parents, family, Helen, Marc and Chris for being there for me through the highs and lows of the PhD process and for generally making life a joy, without you all I would never have made it this far.

Abstract

Transglutaminases catalyse the formation of isopeptide bonds which covalently link proteins together and these enzymes have been previously implicated in cardiovascular repair processes. This thesis explores the transglutaminases, Factor (F)XIII-A and Transglutaminase (TG)2, and their roles within the vasculature. To do this, we bred and characterised single and double knockout mice deficient for FXIII-A and/or TG2.

Previously, a protective role has been postulated for FXIII-A, as humans and mice lacking FXIII-A fail to maintain pregnancy potentially due to a failure of remodelling within the placental artery. This finding was also repeated in this study and further to this a significant decrease in the number of FXIII-$A^{-/-}$ pups born to FXIII-$A^{+/-}$ mothers was seen. FXIII-$A^{-/-}$ mice develop cardiac fibrosis and suffer significant mortality following injury and this phenotype is exacerbated with additional loss of TG2, highlighting the importance of FXIII-A and TG2 as protective enzymes.

Interestingly, despite being present in the blood at µg/mL concentrations, the cellular source that maintains the plasma pool of FXIII-A has not been identified. FXIII-A is known to be produced by megakaryocytes, chondrocytes, osteoclasts, monocytes and macrophages and the prevailing view is that platelets are the most likely cellular source.

To delineate the cellular source of plasma FXIII-A, we commissioned a *de novo* FXIII-A floxed mouse which was bred with tissue specific cre recombinase mice. These novel models were used to determine plasma and platelet FXIII-A activity, together with FXIII-A gene expression in the aorta and

heart. The results presented here discount the platelet as the cellular source of plasma FXIII-A. Mouse bone marrow transplants and gene expression in whole and fractionated organs instead implicate a resident tissue cell, possibly a macrophage, in the wall of the aorta (and perhaps the heart) as the cellular source of FXIII-A.

Beyond its repair role, TG2 has been suggested to potentiate apoptosis in response to stress signalling. However, previous studies have utilised monodansylcadaverine and hence have not inhibited TG2 directly. Here, transglutaminase activity assays and characterisation of MAPK signalling in wildtype and $TG2^{-/-}$-derived vascular smooth muscle cells are used to demonstrate that TG2 is the main transglutaminase involved in calphostin C-induced apoptosis.

The findings shown here explore the common and distinct functions of these enzymes and details potential avenues for translation into therapy.

Table of Contents

List of Figures

List of Tables

List of Abbreviations

BLAST	Basic Local Alignment Search Tool
AAA	Abdominal Aortic Aneurysm
AGM	Aorta-Gonad-Mesonephros
ATF	Activating Transcription Factor
ATP	Adenosine Triphosphate
BCA	Bicinchoninic Acid Assay
bp	Base Pair
BSA	Bovine Serum Albumin
Ca^{2+}	Calcium Dication
$CaCl_2$	Calcium Chloride
CCR2	C-C Chemokine Receptor Type 2
CD11b	Integrin Alpha M
CD11c	Integrin Alpha X
CD163	Cluster of Differentiation 163
CD31	Platelet Endothelial Cell Adhesion Molecule-1
CD68	Cluster of Differentiation 68
Cdc42	Cell Division Control Protein 42 Homolog
cDNA	Complementary Deoxyribonucleic Acid
Clodrosomes	Clodronate Encapsulated Liposomes
(c-)Mpl	Thrombopoietin Receptor
CMV	Cytomegalovirus
CO_2	Carbon Dioxide
cre	Cre Recombinase
Ct	Crossing Point

CTAD	Citrate, Theophylline, Adenosine and Dipyridamole
DAPI	4',6-Diamidino-2-Phenylindole
DEXA	Dual Energy X-Ray Absorptiometry
DiI	1,1'-Dioctadecyl-3,3,3',3'-Tetramethylindocarbocyanine Perchlorate
DLK	Dual Leucine-Zipper Bearing Kinase
DMSO	Dimethyl Sulphoxide
DNA	Deoxyribonucleic Acid
DTT	Dithiothreitol
E. Coli	*Escherichia coli*
E8.5	Embryonic Day 8.5
ECL	Enhanced Chemiluminescence
ECM	Extracellular Matrix
EDTA	Ethylenediaminetetraacetic Acid
EGF	Epidermal Growth Factor
ER	Endoplasmic Reticulum
F4/80	EGF-Like Module-Containing Mucin-Like Hormone Receptor-Like 1
FACS	Fluorescence Assisted Cell Sorting
FCS	Fetal Calf Serum
$FeCl_3$	Iron (III) Chloride
FITC	Fluorescein Isothiocyanate
Flt3	FMS-Like Tyrosine Kinase 3
FXIII	Factor XIII
FXIII-A	Factor XIII Subunit A

FXIII-B	Factor XIII Subunit B
GAPDH	Glyceraldehyde 3-Phosphate Dehydrogenase
gDNA	Genomic Deoxyribose Nucleic Acid
GDP	Guanosine Diphosphate
GTP	Guanosine Triphosphate
h	Hour
HO-1	Heme Oxygenase-1
HSC	Haematopoietic Stem Cell
IL-1β	Interlukin-1β
IL-6	Interlukin-6
IGF-1	Insulin-like Growth Factor 1
IPTG	Isopropyl B-D-1-Thiogalactopyranoside
IRS-1	Insulin Receptor Substrate 1
JNK	C-Jun N-Terminal Kinase
JP(E)G	Joint Photographic Experts Group File Format
KCl	Potassium Chloride
kDa	Kilodalton
LC-MS	Liquid Chromatography–Mass Spectrometry
LED	Light Emitting Dioide
LOX	Lysyl Oxidase
LoxP (Flox)	Locus of X-Over P1
LT-HSC	Long-Term Haematopoietic Stem Cells
LysM	Lysozyme 2
MAPK	Mitogen Activated Protein Kinase
M-CSF	Macrophage Colony Stimulating Factor

Min	Minute
MMP	Matrix Metalloproteinase
mRNA	Messenger Ribonucleic Acid
NaCl	Sodium Chloride
NaOH	Sodium Hydroxide
NAPQI	*N*-acetyl-*p*-benzoquinone imine
NGF	Neuronal Growth Factor
nm	Nanometer
^{o}C	Degrees Celsius
PBS	Phosphate Buffered Saline
PCR	Polymerase Chain Reaction
PF4	Platelet Factor 4
PFA	Paraformalydehyde
Pfu	*Pyrococcus furiosus* DNA Polymerase
PKC	Protein Kinase C
PVDF	Polyvinylidene Difluoride
qPCR	Quantitative Real Time Polymerase Chain Reaction
Rac1	Ras-Related C3 Botulinum Toxin Substrate 1
RFP	Red Fluorescent Protein
RIPA	Radio-Immunoprecipitation Assay Buffer
RNA	Ribose Nucleic Acid
ROTEM	Rotational Thromboelastometry
RPL32	Ribosomal Protein L32
RPMI	Roswell Park Memorial Institute Medium

SAPK	Stress Activated Protein Kinase
SDS	Sodium Dodecyl Sulphate
SDS-PAGE	Sodium Dodecyl Sulphate-Polyacrylamide Gel Electrophoresis
s	Second
SEK	SAPK/Erk Kinase
SEM	Scanning Electron Microscopy
ST-HSC	Short-Term Haematopoietic Stem Cells
TAE	Tris, Acetic Acid, EDTA
Taq	*Thermus aquaticus* DNA Polymerase
TBS	Tris-Buffered Saline
TBS-T	Tris Buffered Saline-Tween 20
TCA	Trichloroacetic Acid
TE	Tris-EDTA
TG	Transglutaminase
TGF	Transforming Growth Factor
Thy1(.2)	Thy-1 Cell Surface Antigen, CD90(.2)
TIFF	Tagged Image File Format
TM	Melting Temperature
TNF	Tumour Necrosis Factor
Tris-HCl	Tris(hydroxymethyl)aminomethane) Hydrochloride
VSMC	Vascular Smooth Muscle Cell
vWF	Von Willebrand Factor
WT	Wildtype
xg	Times Gravity

α-elastin	Alpha Elastin
αSMA	Alpha Smooth Muscle Actin
β-actin	Beta Actin

Chapter 1 – General Introduction

1.1 Transglutaminases

Mammals express 8 catalytically active transglutaminases, most of which have restricted functions and tissue expression patterns. These are transglutaminase (TG) 1 through 7 and FXIII-A, all of which contain the 5 consensus transglutaminase active site residues Gly-Gln-Cys-Trp-Val (Korsgren et al., 1990). Mammals also express a 9th protein known as erythrocyte band 4.2 which appears to function as a structural membrane protein in red blood cells, and although it possesses the consensus transglutaminase active site sequence, it has an alanine mutation of the active site cysteine and is therefore catalytically inactive (Korsgren et al., 1990).

Transglutaminase activity involves calcium-dependent covalent crosslinking of two proteins through a glutamine-lysine isopeptide bond (Folk and Finlayson, 1977). First, a glutamine residue on a protein is targeted by the transglutaminase, the active site cysteine displaces the -NH_2 group of the side chain thereby deamidating the glutamine to a glutamic acid and eliminating an ammonia group. This intermediate complex with the transglutaminase covalently attached is then displaced by a primary acyl acceptor, a lysine residue on an adjacent protein, thereby releasing the transglutaminase from the complex and forming the isopeptide, ε-(γ-glutamyl) lysine, bond (depicted in Figure 1-1). Other reactions are described later.

The transglutaminase family members are reported to have roles in blood coagulation (FXIII-A), keratinocyte differentiation and skin-barrier formation (TG1 and 3), extracellular-matrix assembly (FXIII-A and TG2), semen

coagulation in rodents (TG4) and brain plaque stabilisation (TG2). Deficiency of the transglutaminases is rare but causes spontaneous haemorrhage (FXIII-A), lamellar ichthyosis (TG1) and hereditary spherocytosis (Band 4.2) (Lorand and Graham, 2003; Greenberg et al., 1991).

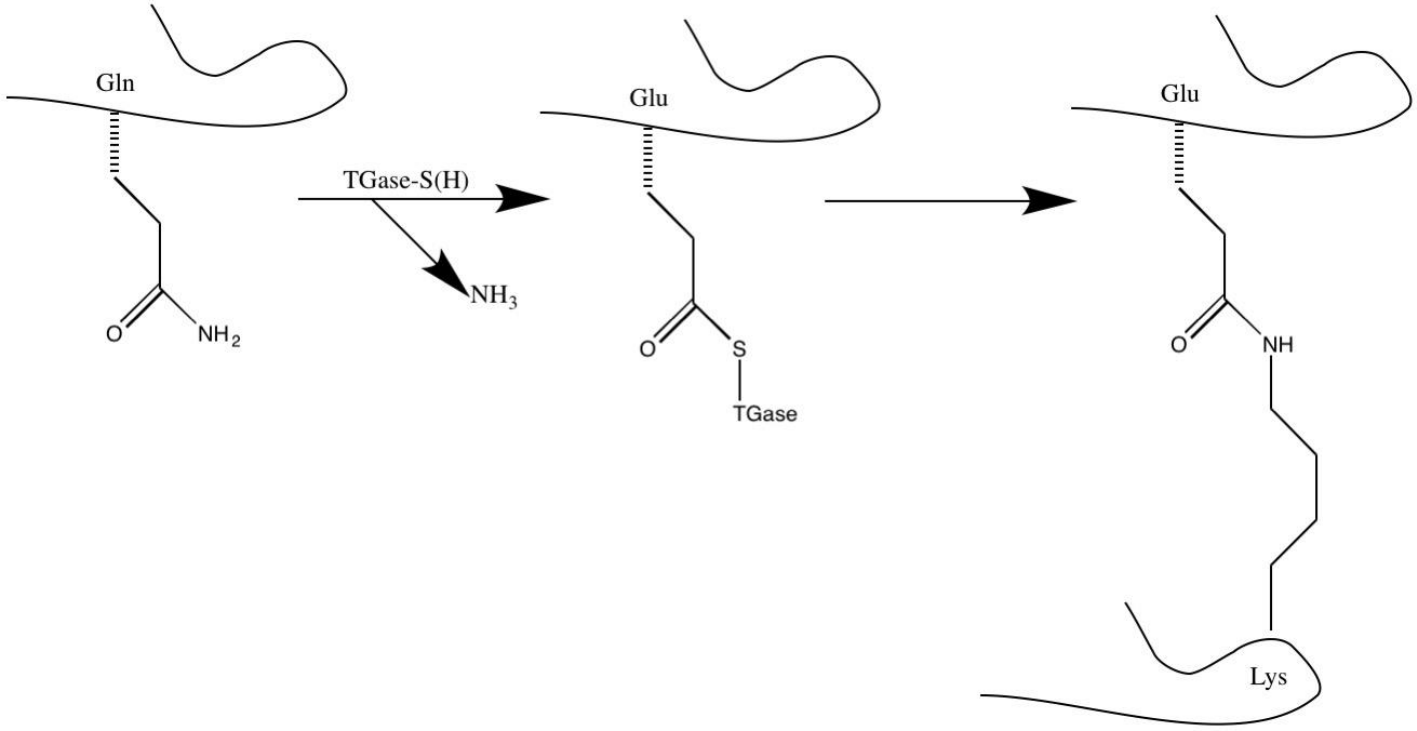

Figure 1-1 – Depiction of a typical transglutaminase catalysed reaction

The formation of a glutamyl-lysyl bond involves the free cysteine in the catalytic site of a transglutaminase forming an intermediate with a glutamine side chain, which is located within a transglutaminase recognition motif. The formed intermediate is available for attack by the primary amine group of an adjacent lysine residue which displaces the active site cysteine from the intermediate and results in the formation of the stable amide isopeptide bond.

1.1.1 Factor XIII-A

Plasma FXIII (also known as Laki-Lorand factor or fibrin stabilising factor) is a 320 kDa heterotetrameric (A_2B_2) complex consisting of 2 catalytic A subunits and 2 carrier B subunits. The A subunit is 83 kDa in size and contains 2 β-barrel domains, a catalytic core domain including the triad of Cysteine-314, Histidine-373 and Aspartate-396 (human co-ordinates), a β-sandwich and an NH_2-terminal activation peptide (Schwartz et al., 1973; Ichinose et al., 1990). The B subunit is a 76.5 kDa glycoprotein consisting of 10 sushi domains, each stabilised by a pair of disulphide bridges (Schwartz et al., 1973; Komáromi et al., 2011).

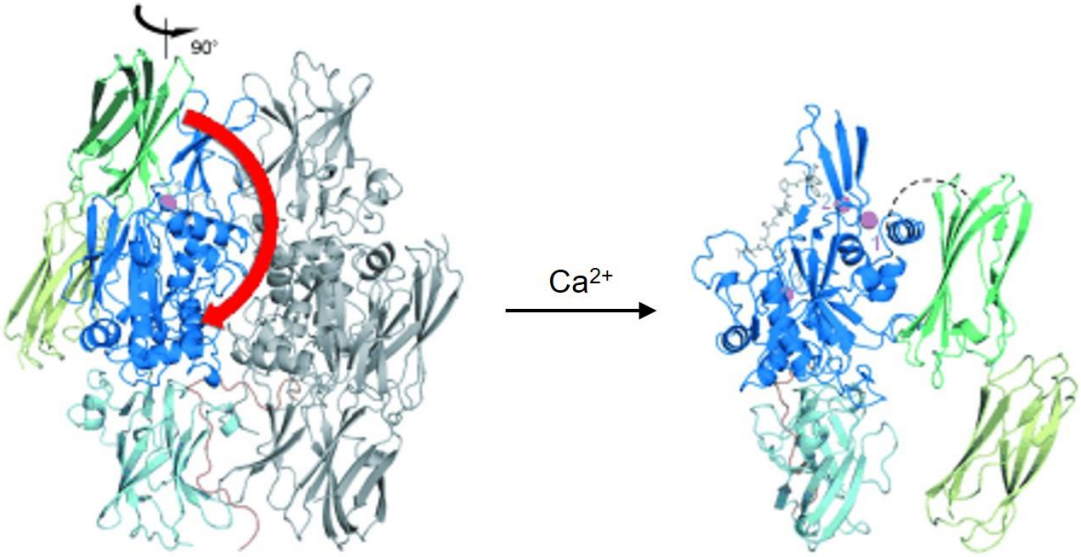

Figure 1-2 – Crystal structure of FXIII-A

FXIII-A exists as a homodimer of two A subunits (one coloured) which when inactive show a 'closed' conformer. Activation of FXIII-A requires binding of calcium dications which causes the two β-barrel domains (green and yellow) to undergo a large steric movement (denoted by the red arrow) revealing the activation peptide (orange) and the active site. Adapted from (Stieler et al., 2013).

FXIII-A is expressed as a pro-transglutaminase, which when activated by the enzymatic cleavage of thrombin and in the presence of calcium ions, plays an important role in the final part of the clotting cascade by crosslinking exposed glutamine and lysine residues (generating ε(γ-glutamyl)lysyl bonds) (Aeschlimann and Paulsson, 1994; Lorand and Conrad, 1984; Folk and Finlayson, 1977) between opposing fibrin α- and γ- chains (Muszbek et al., 1999). FXIII-A is known to also catalyse the covalent linkage of the serpin α_2-antiplasmin to the insoluble fibrin mesh. This crosslinking of the fibrin chains enables the clot to resist mechanical lysis (i.e. shear-stress) and incorporation of serpins imparts resistance against enzymatic fibrinolysis (e.g. by plasmin) (Muszbek et al., 2011). Lorand has proposed that inhibition of FXIII-A may be considered as a safe therapeutic candidate for the treatment of atherosclerosis, coronary heart disease and thrombosis (Lorand, 2000).

FXIII-A is present in moderate abundance in the plasma (7-14 μg/mL in humans) (Yorifuji et al., 1988) and has a short half-life of 5 to 10 days (Ponce et al., 2005; Inbal et al., 2004; Hsieh and Nugent, 2008). While the secretory source is unknown, the abundance and short half-life suggest that plasma FXIII-A is unlikely be maintained by a rare cell type.

Expression of the FXIII-A homodimer occurs in the bone marrow and specifically in megakaryocytes, monocyte/macrophages (Henriksson et al., 1985; Töröcsik et al., 2005; Muszbek et al., 1985) and dendritic cells (Caux et al., 1996; Nestle et al., 1993) and is secreted, through an uncharacterised, non-classical pathway, into the blood circulation (Kaetsu et al., 1996). Expression of the FXIII-B homodimer takes place in hepatocytes and is subsequently secreted into the plasma in excess of FXIII-A. This excess

promotes rapid formation of the A_2B_2 quaternary structure of circulating FXIII. FXIII-A_2B_2 formation is important for haemostasis with the key responsibility of FXIII-B_2 being to protect FXIII-A_2 from oxidation of its cysteine residues in the circulation (Robinson et al., 2000).

There is an emerging view in the literature that FXIII-A is not just involved in maintenance of haemostasis. Recently, (Nikolajsen et al., 2014) identified 147 substrates of plasma FXIII-A, of which 48 were cross linked into the insoluble fibrin clot. The other non-clot incorporated substrates which include members of the complement cascade, monocyte differentiation antigen and immunoglobulin chains led the authors to suggest that FXIII-A has roles in complement activation, inflammation and immune response. However, immune defects would be expected but are not seen in FXIII-A deficient patients and mice and hence this substrate crosslinking activity is either non-essential or is compensated for by another enzyme.

A whole range of potential functions have been postulated for FXIII-A in both the intracellular and extracellular spaces.

Intracellularly, FXIII-A_2 is present in the cytoplasm and the nucleus of certain cell types where it been suggested that it has functions in cytoskeletal organisation (e.g. crosslinking actin, myosin, filamin and vinculin in platelets and Fcγ-mediated phagocytosis in monocyte-macrophages (Sárváry et al., 2004; Richardson et al., 2013)) and remodelling (Muszbek et al., 2011). FXIII-A has also been identified in the nucleus of monocyte-macrophages, by electron microscopy, co-localised with the electron-dense nuclear material and shown to be catalytically active in this location by fluorescent monodansylcadaverine incorporation assay (Adány et al., 2001).

In the extracellular space FXIII-A is suggested to be involved in crosslinking proteins to the extracellular matrix (ECM) such as von Willebrand factor (Hada et al., 1986) which regulates cell-matrix and cell-cell interactions, and also catalysing collagen/fibronectin interactions (Adány and Bárdos, 2003).

1.1.2 Deficiency of FXIII-A

Homozygous loss of FXIII-A has a frequency of 1 in 5,000,000 people (Board et al., 1993) and affects people of all races. Sixty-nine mutations have so far been mapped in FXIII-A and 7 in FXIII-B. Deficiency of the A subunit produces a phenotype consisting of severe bleeding, spontaneous intracranial haemorrhage, poor wound healing and miscarriage (Hsieh and Nugent, 2008). However, treatment with recombinant FXIII-A has shown remarkable success in deficient patients and is used routinely in clinical practice.

Rotational thromboelastometry (ROTEM) is used clinically for detecting coagulopathies in people. The system detects clot “stiffness” and as FXIII-A activity is responsible for 60-70% of the overall clot strength, it is sensitive to FXIII-A deficient states (Nielsen et al., 2004). Patients with FXIII-A deficiency show, by ROTEM, delayed clot formation time and reduced overall clot stiffness (Nielsen et al., 2007).

Mouse models deficient for FXIII-A have shown: spontaneous uterine bleeding and miscarriage (Koseki-Kuno et al., 2003), development of fatal cardiac fibrosis in male, but not female, mice within 12 months as determined by the presence of histochemical haemosiderin and collagen positive staining in the myocardium (Souri et al., 2008) and left ventricular cardiac rupture following coronary artery ligation which could be mitigated with FXIII-A_2B_2 replacement therapy (Nahrendorf et al., 2006).

1.1.3 Transglutaminase 2

TG2 is a 78 kDa monomeric protein which, unlike the other transglutaminases, is ubiquitously expressed. As with FXIII-A, TG2 is secreted by a non-classical pathway into the extracellular space (van den Akker et al., 2012). Activation of TG2 requires the binding of Ca^{2+} and guanosine diphosphate (GDP) which induces the “open” active conformation. Conversely, in states where Ca^{2+} is low and in the presence of bound guanosine triphosphate (GTP), TG2 adopts the “closed” inactive conformer.

While the presence of TG2 in the extracellular space is undisputed, its extracellular activity under normal conditions is less well defined. Beyond the Ca^{2+}/GTP reciprocal control described earlier, a further level of post-translational control is evident extracellularly. In this mechanism, a disulphide bridge between two vicinal cysteine residues in the open conformation is reduced to enable transamidation to occur (Pinkas et al., 2007; Stamnaes et al., 2010). Reduction of this bond has been proposed to occur in states of tissue damage in which the enzyme thioredoxin is released from cells (Jin et al., 2011) (Figure 1-3). Within the ECM, two roles are proposed to exist for TG2; the first is a repair function whereby TG2 becomes activated following cellular damage and functions to assist in rebuilding the ECM. A second function for TG2 is in the establishment of the basal structure of the ECM whereby TG2 is suggested to constitutively crosslink a number of matrix proteins (e.g. fibronectin, osteonectin and osteopontin) (Kim et al., 2002) as well as proteinase inhibitors (e.g. elafin) which protect the ECM from proteolytic degradation (Nara et al., 1994). However, this constitutive function appears to be at odds with the strict activation mechanisms of extracellular TG2 (i.e. the requirement for Ca^{2+}, GDP and the reduction of cysteine

residues) and it is unclear how this activation would occur in the developing ECM.

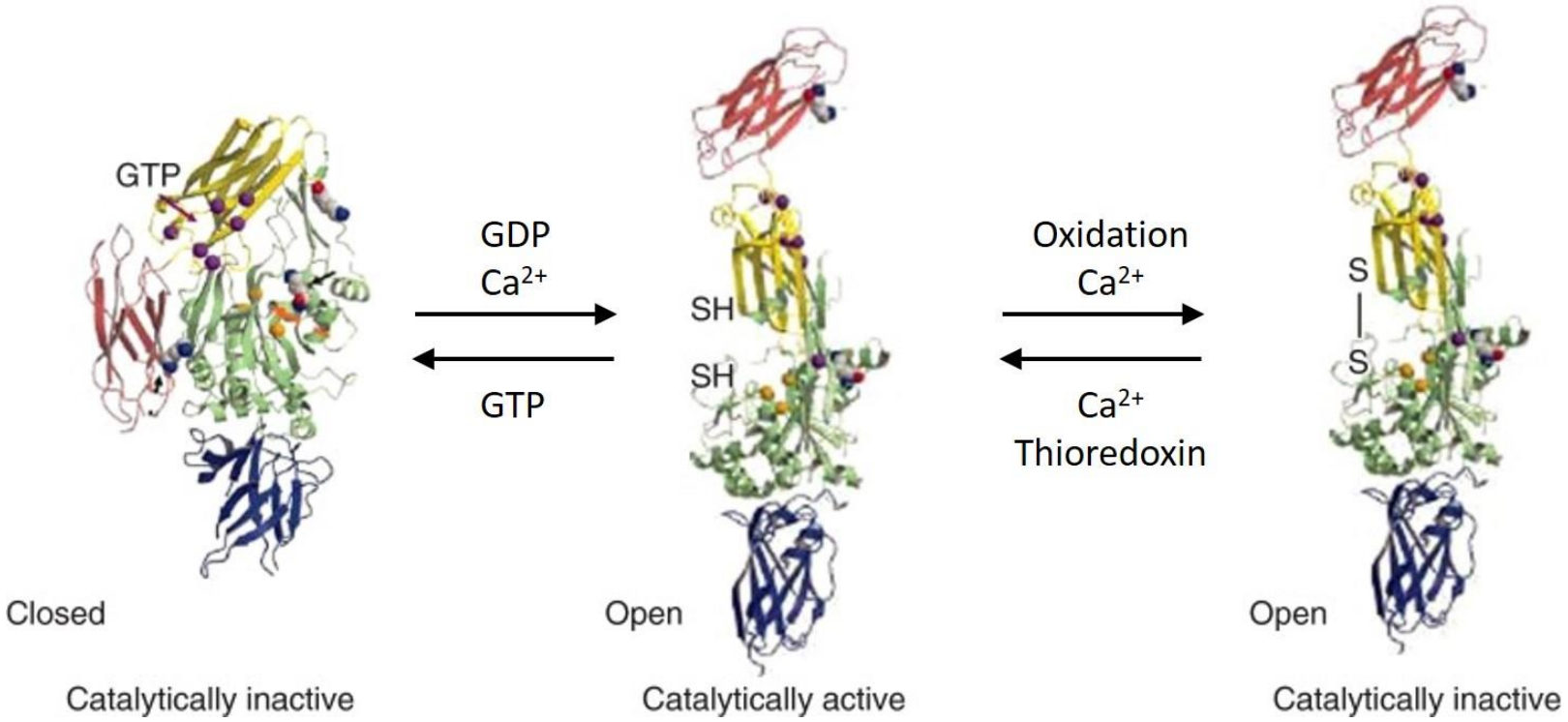

Figure 1-3 – Structure and post-translational control of TG2

TG2 is known to adopt two steric conformations; ‘closed’ and ‘open’. Binding of GTP locks TG2 in the closed conformer, while Ca^{2+} and GDP allows the large conformational change to the catalytically open conformer. Extracellularly, a disulphide bridge is formed between two vicinal cysteines due to the oxidative environment. This bridge inactivates TG2 until a reducing agent, thought to be thioredoxin, is released from cells following tissue damage. Adapted from (Eckert et al., 2014).

Intracellularly, TG2 has been implicated in modulating cell signalling and can supposedly function as a G-protein and also as a protein kinase (Mishra and Murphy, 2006; Stephens et al., 2004). However, these functions are the subject of debate within the field.

A common pro-apoptotic stimulus is the rapid influx of calcium into the cell which should result in the activation of intracellular TG2. This activation may under certain circumstances cause large-scale crosslinking of intracellular proteins, which potentially keeps the contents of the dying cell intact and prevents the leakage of intracellular proteins into the ECM (Park et al., 2010; Fesus et al., 1996). Besides protecting against the consequences of apoptosis, TG2 may also itself induce apoptosis. The earliest pro-apoptotic report of TG2 was described by (Fesus et al., 1987), when TG2 activity and antigen were shown to be significantly increased in hepatocytes undergoing apoptosis following lead nitrate induced hyperplasia.

TG2 has also been implicated in neurodegenerative conditions (e.g. Alzheimer's and Parkinson's disease) whereby accumulation and hyper-phosphorylation of tau and amyloid β proteins in neurons and glial cells results in cell death followed by a steady decline in cognitive function. TG2 is known to crosslink and stabilise these protein aggregates and symptoms of Huntington's disease were ameliorated in $TG2^{-/-}$ mice (Mastroberardino et al., 2002). TG2 also plays an important role in the development of coeliac disease whereby glutamine residues (Figure 1-4) in wheat proteins are selectively deamidated to glutamic acid due to a lack of proximal amines in the protein structure to displace TG2 and form the isopeptide bond. In this instance, water is able to act as the acyl acceptor allowing the release of TG2. In certain

individuals, these peptides can be recognised as neo-antigens thus triggering an immune reaction (Klöck et al., 2012).

There are two TG2 knockout mouse lines available, one produced by Professor Gerry Melino (De Laurenzi and Melino, 2001) which has been reported to show a number of pathological phenotypes such as defective clearance of apoptotic cells by macrophages and impaired glucose-stimulated insulin secretion (Szondy et al., 2003; Bernassola et al., 2002) and a second created by Professor Robert Graham (Nanda et al., 2001) which does not show either of these phenotypes (Nanda et al., 2001). Whilst both lines are deficient in TG2, it remains to be determined whether the Melino mouse carries further underlying mutations which produce the deleterious phenotypes seen. However, what does seem clear is that the lack of a phenotype seen in the Graham mouse is not due to a compensatory rescue mutation, since the TG2 knockout mouse has been backcrossed from the founder onto distinct mouse lines without producing any pathology.

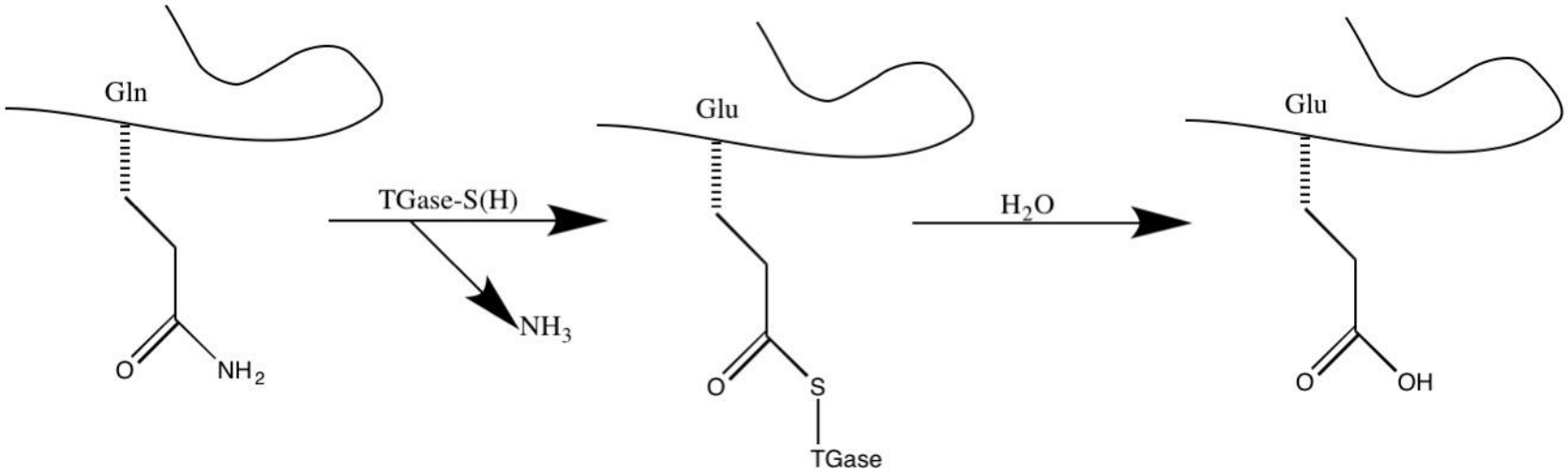

Figure 1-4 – Reaction mechanism of TG2-catalysed deamidation

While TG2 is known for its transamidation activity, it can also catalyse a second reaction when the pH is acidified and a lack of appropriately positioned primary amines are available to act as acyl acceptors. In this instance, a water molecule is able to act as the acceptor and results in the glutamine residue being deamidated to a glutamic acid. In certain individuals this reaction causes wheat proteins, namely gliadin, to be seen as neoantigens resulting in the body mounting an immune reaction leading to coeliac disease.

1.1.4 Redundancy between FXIII-A and TG2

There is a commonly held belief that there is significant crossover in activity between FXIII-A and TG2 due to the findings that they both perform the same catalytic transamidation activity and are present both intra- and extracellularly.

An example of this suggested overlap of function is in skeletal tissue formation whereby the enzymes are externalised into the extracellular space prior to mineralisation and they also function in chondrocyte differentiation (Aeschlimann et al., 1993; Nurminskaya et al., 1998; Nurminskaya and Kaartinen, 2006). It was suggested by (Tarantino et al., 2009) that in states of TG2 deficiency no skeletal defects are observed in mice due to FXIII-A and TGF-β being upregulated in response. However, this seems improbable due to the different activation mechanisms of the two enzymes which have been previously discussed. Further to this, work carried out in a collaboration between our group and Dr Christopher Jackson (Bristol) showed no skeletal defects (Figure 1-5) in FXIII-$A^{-/-}$.$TG2^{-/-}$ double knockout mice by DEXA scanning (Cordell et al., 2015).

However, while both FXIII-A and TG2 crosslink proteins at glutamine residues, it has been shown that each has differing substrate specificities using phage display peptide libraries. It was shown that FXIII-A prefers glutamines residing in motifs containing QxxΦxWP (Φ = hydrophobic) residues whereas TG2 favours QxPΦ, QxPΦD(P) and QxxΦDP motifs (Sugimura et al., 2006).

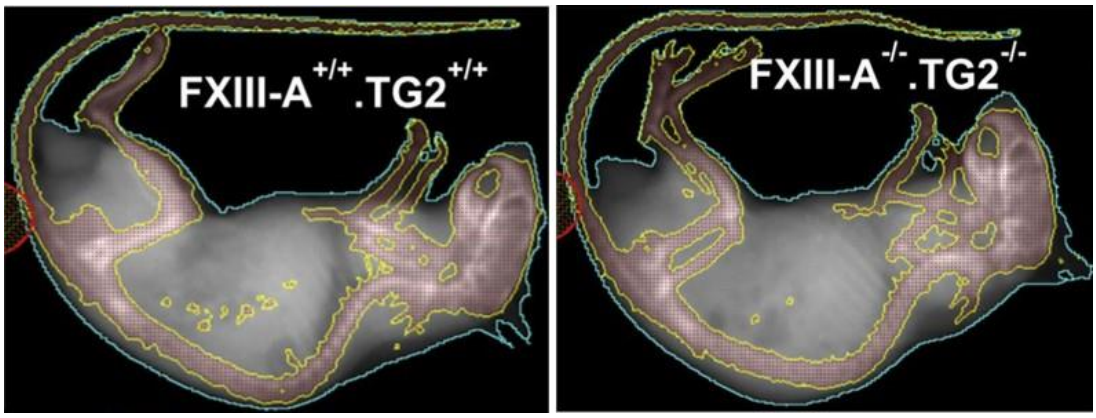

Figure 1-5 – DEXA scans of FXIII-A$^{+/+}$.TG2$^{+/+}$ and FXIII-A$^{-/-}$.TG2$^{-/-}$ mice

Representative images from dual-energy X-ray absorptiometry which showed no difference in skeletal morphology or mineral density between wildtype and double knockout mice. Adapted from (Cordell et al., 2015).

On the other hand, (Bakker et al., 2006) provided substantial evidence for compensation between the two enzymes in a model of inward arterial vessel remodelling. They showed that in TG2$^{-/-}$ mice, remodelling was delayed but still occurred, with transglutaminase mediated crosslinks present in the vessel wall and an increase in local FXIII-A content. This compensation was suggested to be the result of increased numbers of FXIII-A positive macrophages in the vessel wall. When these cells were depleted with the cytotoxic drug clodronate, FXIII-A levels decreased and inward remodelling was further reduced.

A further complication which clouds the understanding of redundancy between the two enzymes is the mechanism of secretion into the extracellular space. As neither FXIII-A nor TG2 have a secretory signal sequence they cannot be released from the cell by the classical Golgi-ER pathway. However, the non-classical mechanism by which TG2 is secreted from the cell is understood. TG2 has been shown in smooth muscle cells to be secreted as a result of TG2 crosslinking itself to secretory microparticles (van den Akker et

al., 2012). In contrast, FXIII-A externalisation has yet to be convincingly demonstrated; suggesting that it must occur by a distinct pathway.

1.2 The Platelet Hypothesis of Plasma FXIII-A

There is a long standing view in the literature that the cellular source of FXIII-A is the platelet due, primarily, to the fact that platelets contain approximately 50% of the total FXIII-A in the blood (Adány and Bárdos, 2003). It has been argued that simple turnover of these platelets, whereby the intracellular FXIII-A is released into the blood, is sufficient to explain the high plasma FXIII-A concentration. However, no explanation to date has been suggested as to the mechanism of release from platelets, and simple “bursting” seems improbable as other platelet proteins are not seen in the plasma at comparable concentrations.

The first report of platelets as the cellular source of FXIII-A was by (Wölpl et al., 1987), in a case series of three patients who had undergone bone marrow transplantation with donor cells carrying a different electrophoretic variant of FXIII-A. They found that as early as 6 days post-transplant the recipient plasma and platelet FXIII-A phenotype had changed to match the donor and this persisted to at least 361 days with no reports of the phenotype reverting back to the original recipient variant.

(Poon et al., 1989) also described patients who had received allogenic stem cell transplantation (following myeloablation) again with donor bone marrow which carried a different electrophoretic variant of FXIII-A. They showed that even though the recipient’s bone marrow had been completely replaced by the donor’s, there was a delay of between 115–458 days until the plasma FXIII-A phenotype changed to match that of the donor. This is far longer than

the plasma half-life of FXIII-A of 5-10 days (Ponce et al., 2005; Inbal et al., 2004; Hsieh and Nugent, 2008)). The authors concluded that there was insufficient evidence to discount *either* circulating platelets or monocytes derived from the bone marrow as the plasma source, and they hypothesised that there may be an extrahaematological source of FXIII-A such as the liver.

(Pihusch et al., 2002) provided the first evidence to suggest a cellular source of FXIII-A originating from outside of the bone marrow. They described that plasma FXIII-A levels declined *slightly* following autologous bone marrow transplantation (which may suggest a haematological origin), however, the levels remained within the normal range. The authors concluded that this was as a result of secretion from “long-living” macrophages residing in the liver, spleen and lungs. Evidence to discount the liver and spleen as the tissue source of plasma FXIII-A is provided later in this thesis.

However, upon reappraisal of the original literature, it does appear that some groups have jumped to the conclusion that platelets are the cellular source even though their results point to a distinct origin.

Despite the work of Pihusch et al, more recent literature, (Inbal et al., 2004) has again suggested that platelets are the source of plasma FXIII-A. Inbal et al followed 20 patients with various forms of lymphoma and myeloma, who received autologous blood stem cell transplantation. They concluded that the observed drop in platelet, but not blood monocyte, numbers following high-dose chemotherapy to ablate the bone marrow resulted in a commensurate drop in FXIII-A concentration which they attributed to impaired megakaryocyte activity during the myeloablative treatment. However, the conclusions they provided do not match the results they reported. They

showed that a >90% drop in platelet count resulted in only a modest 15% maximal drop in FXIII-A plasma activity, which does not appear to be consistent with a platelet derived source of FXIII-A.

The above findings also suggest that the circulating monocyte cannot maintain the plasma pool as like the platelet, the monocyte has a short half-life of just 1 to 3 days (Yona et al., 2013; Yang et al., 2014).

Work from our group has provided the first substantial evidence that platelets do not maintain the plasma levels of FXIII-A (Cordell et al., 2010). In this study we observed unchanged plasma FXIII-A levels in two different lines of thrombocytopenic mice (Bcl-$x^{plt20/plt20}$ and $Mpl^{-/-}$). The Bcl-$x^{plt20/plt20}$ mice, possess a homozygous missense mutation in the anti-apoptotic gene Bcl-xL which causes the mice to produce platelets which are rapidly cleared with a life span of 1 day (Mason et al., 2007). These Bcl-x mice also argue against the slow, continual, release of FXIII-A from the platelet over its lifetime rather than release from megakaryocytes or at death, as the platelets are born and die at the same rate yet the plasma FXIII-A levels remain unchanged. The $Mpl^{-/-}$ mice have a targeted deletion of the thrombopoietin receptor which vastly reduces megakaryocyte precursor cell numbers and therefore platelet production (Alexander et al., 1996; Ng et al., 2014). Due to the low levels of platelet biogenesis and clearance in these mice, early or late release of FXIII-A from the platelet is also excluded as it would be expected that the altered equilibrium of platelet synthesis would affect the amount of FXIII-A in the plasma. These findings implicated nucleated cells as the secretory source of plasma FXIII-A. Our lab also showed - using ^{35}S-methionine labelling experiments in THP-1 human monocyte cells - that under conditions where

the paradigm non-classically secreted protein, IL-1β, is released from the cell, no FXIII-A is secreted.

These findings support the notion that a cell maintained outside of the megakaryocyte lineage is responsible for maintaining the plasma pool of FXIII-A and the identity of this cell is addressed in this thesis.

1.3 Haematopoiesis

Based on previous literature in the area and the range of cells known to express FXIII-A, plasma FXIII-A is expected to be secreted from a haematopoietic cell type.

Haematopoiesis is the process by which all blood cells are generated. These cells arise from a common stem cell, the haematopoietic stem cell (HSC). Cytokines control the proliferation and differentiation patterns of these stem cells by regulating distinct sets of transcription factors. External factors, such as blood oxygen saturation, can also stimulate production of mature cells; for example, red blood cell (RBC) production is upregulated in states of hypoxia.

There are three stages of haematopoiesis, divided into early embryogenesis (primitive), postnatal and adult (definitive). Of these, the primitive and definitive stages are clearly defined and differ markedly from each other whilst the post-natal stage is intermediate between the other two and could be described as a “handover” stage in haematopoiesis.

1.3.1 Foetal Haematopoiesis

During embryogenesis, macrophages are present in the yolk sac and within the developing embryo. These cells are found prior to the start of definitive haematopoiesis and before monocytes are seen in the foetal circulation (Perdiguero and Geissmann, 2016; Samokhvalov, 2014; Garcia and Larina,

2014). Early works detected these cells (Naito et al., 1990; Takahashi et al., 1983; Takahashi et al., 1989) in the blood islands of the yolk sac and also later in development, in the foetal liver. These macrophages lacked phagocytic activity and showed weak expression of the widely used macrophage marker F4/80 (Naito et al., 1990; Takahashi et al., 1989) and it was shown by peroxidase staining of foetal rat liver that the resident macrophages were capable of self-replication (Deimann and Fahimi, 1978).

Primitive haematopoiesis involves rapid differentiation of stem cells into mature cells and appears to skip a number of intermediary differentiation stages (Ginhoux and Jung, 2014; Takahashi et al., 1989).

As the embryo develops (E8.5-10.5), the first early HSCs emerge in the aorta-gonad-mesonephros (AGM) and begin production of all lineages of blood cells.

After this (E10.5 to the perinatal period), the foetal liver functions as the major site of haematopoiesis following the migration of the HSCs in the AGM migrating to the liver. However, it is only perinatally that the transition to traditional (adult) haematopoiesis in the bone marrow occurs (Orkin and Zon, 2008).

1.3.2 Adult Haematopoiesis

Occurring in the bone marrow, adult haematopoiesis produces all of the blood cells required from birth onwards. The pivotal cell involved in this process is the HSC which is able to undergo mitosis to maintain its number and is able to differentiate into the multi-potential progenitor (MPP) cell.

There are known to be two differentiated states of HSCs; the long term (LT-) and short term (ST-) HSC. LT-HSCs are responsible for maintaining the cell

number of the HSC pool. These cells are able to differentiate into the ST-HSC through a Flt3-dependent mechanism. These ST-HSCs have a limited self-renewal capacity and further differentiate into the MPP. The MPP cells have a reduced potential for self-renewal but have the ability to differentiate into all the lineages of blood cells (Kondo et al., 2003).

Both HSCs and MPPs require the transcription factor c-myb for the processes of self-renewal and differentiation, and targeted disruption of the c-myb gene produces mice with a depleted HSC pool and reduced numbers of all mature blood cells (Lieu and Reddy, 2009).

The MPPs are able to differentiate into two precursor cells, the common myeloid precursor (CMP) and common lymphoid precursor (CLP). These cells are lineage committed; with the CMP producing the megakaryocyte/erythroid/granulocyte/macrophage cells and the CLP producing the T- and B-lymphocyte cells. Adult haematopoiesis is summarised in Figure 1-6.

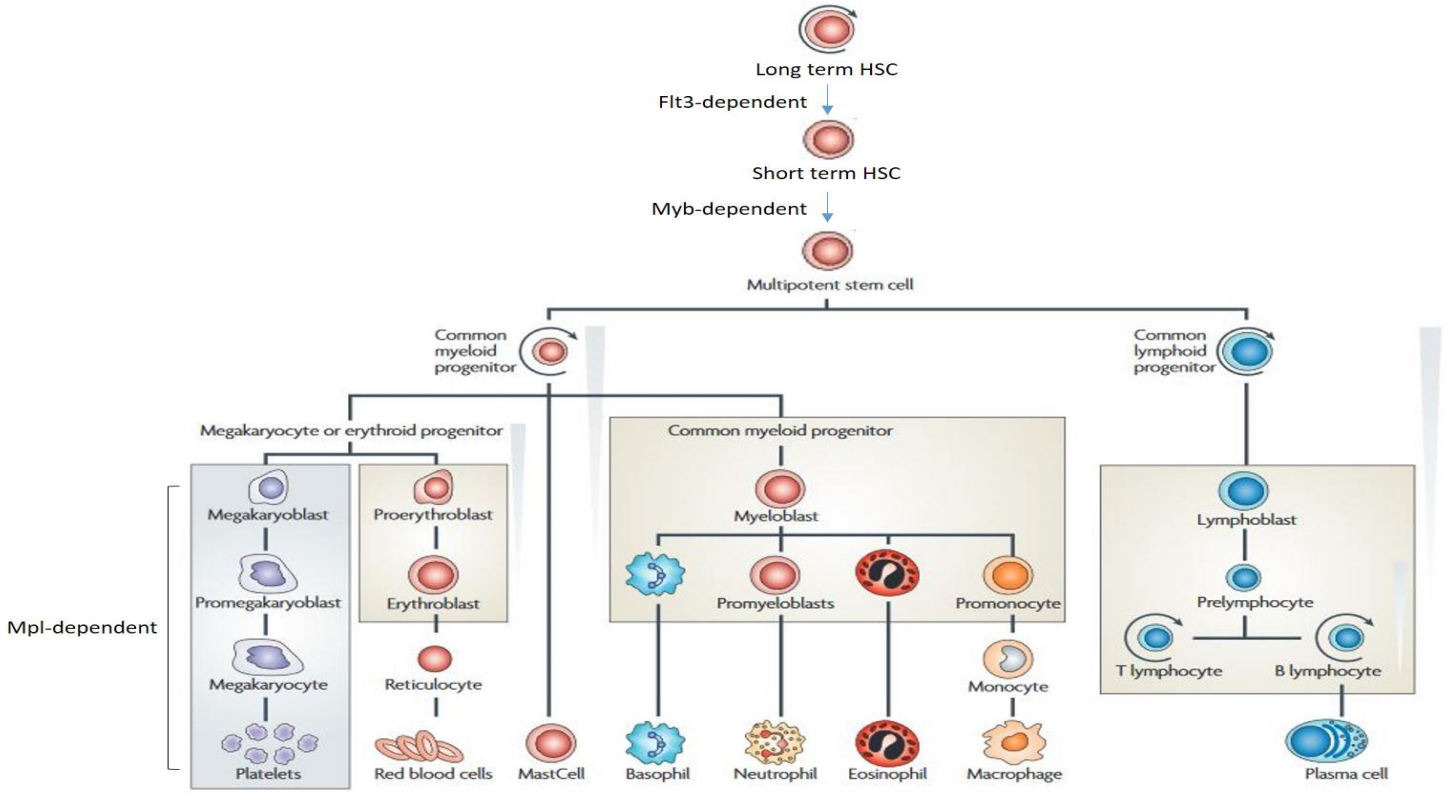

Figure 1-6 – Overview of adult haematopoiesis

Adult haematopoiesis occurs in the bone marrow and follows a tightly regulated scheme. All haematopoietic cells originate from the long term-haemopoietic stem cell (LT-HSC), which maintains the HSC pool. The LT-HSC is able to differentiate into the short term-haemopoietic stem cell (ST-HSC) through a Flt3-dependent pathway and again through a myb-dependent pathway to the multipotent progenitor (MPP). The MPP is able to give rise to the common myeloid progenitor (CMP) and the common lymphoid progenitor (CLP) which are able to produce all the adult blood cells. As the cells becomes more differentiated they lose the ability to self-replicate (adapted from (Ramsay and Gonda, 2008)).

1.3.2.1 Platelet Production

Megakaryocytes in the adult bone marrow shed platelets into the blood stream through fenestrations in the capillaries that run adjacent to the bone marrow.

Work by (Ng et al., 2014) and colleagues recently clarified the expression patterns of PF4-cre and endogenous Mpl within the megakaryocyte lineage. PF4 is a protein released from platelet alpha-granules on platelet activation, which binds heparin with high affinity to modulate coagulation. Mpl is also known as the thrombopoietin receptor, a known regulator of megakaryocyte differentiation. These authors concluded that PF4-cre is only expressed in the precursor cell directly before the megakaryocyte (and in the megakaryocyte and platelet) but not in the granulocyte/monocyte precursor (Figure 1-7). The group also revised the mechanism by which the body senses platelet number. They showed that the Mpl receptor is expressed on all megakaryocyte precursors (and not the granulocyte/monocyte precursor). However, the purpose of this receptor on the megakaryocyte and platelet is to “mop up” and degrade free thrombopoietin. Therefore, increased numbers of these cells result in less circulating thrombopoietin to stimulate the precursors. This enables megakaryocytes (and therefore platelets) to self-regulate their number whilst still being able to rapidly respond to thrombocytopenic events when more free thrombopoietin is available to stimulate stem cell expansion.

While the previous study by Ng et al showed quite specific and limited expression of PF4 (and therefore PF4-cre), earlier lineage tracing experiments had not (Calaminus et al., 2012). Calaminus et al described the use of a PF4-cre crossed stop-floxed RFP mouse which showed RFP expression, and therefore recombination, in platelets as expected, but wider cell analysis

showed RFP expression in a number of other cells types. Their results suggested that PF4-cre had shown recombination in approximately 50% of stem and primitive progenitor cells meaning that various haematopoietic cell types could show the effects of recombination. This theme will be returned to in the experimental work presented in this thesis.

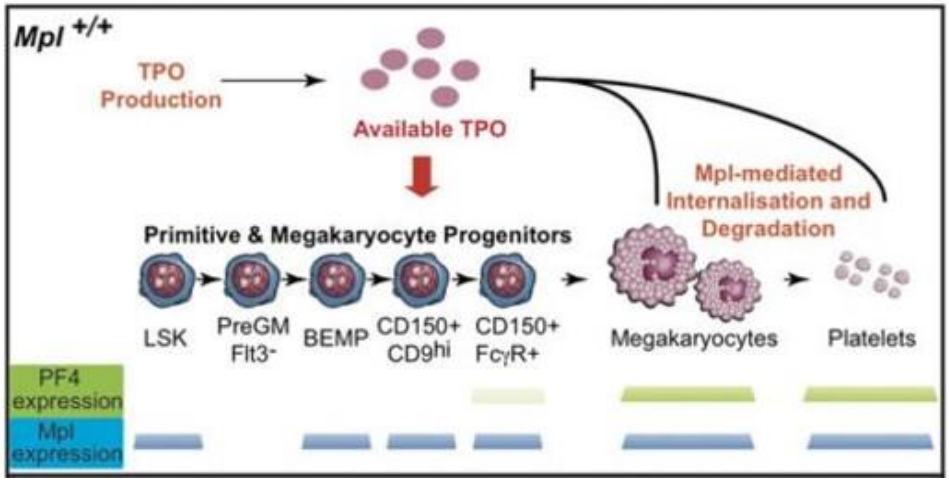

Figure 1-7 – PF4 and Mpl expression in bone marrow cells

The thrombopoietin receptor (Mpl) is expressed on all cells of the megakaryocyte lineage (including stem cells) and the receptor is activated by the cytokine, thrombopoietin (TPO) which stimulates proliferation of the megakaryocyte precursors. The function of the Mpl receptors on megakaryocytes and platelets is to mop up and degrade free TPO which therefore limits proliferation of the precursors and reduces the rate of platelet production. In thrombocytopenic states, the TPO is not degraded as quickly and therefore more is available to activate the Mpl receptors on the stem cell precursors which results in their expansion and therefore increases platelet production to counter the thrombocytopaenia (Ng et al., 2014).

1.4 Cre-Lox Recombination

In light of the significant uncertainty regarding the cellular source of FXIII-A, this thesis aims to employ the use of cre-lox technology to generate mice with reduced FXIII-A gene expression.

Mutations in any mouse gene can now be induced by either conventional gene knockout (i.e. homologous recombination to irreversibly inactivate the gene) or, through conditional gene targeting with cre-lox technology which allows for temporal and/or spatial control of gene recombination depending on the type of cre recombinase construct used.

The cre-lox system (Sauer and Henderson, 1988) works by flanking the gene of interest with small palindromic sequences known as LoxP sites which act as recognition motifs for the Cre DNA recombinase enzyme.

Cre recombinase cleaves and reattaches the flanked DNA sequences and depending upon the orientation of the LoxP sites, can result in deletions (same orientation), inversions (opposing orientation), insertions and translocations to the sequence. These processes are summarised in Figure 1-8.

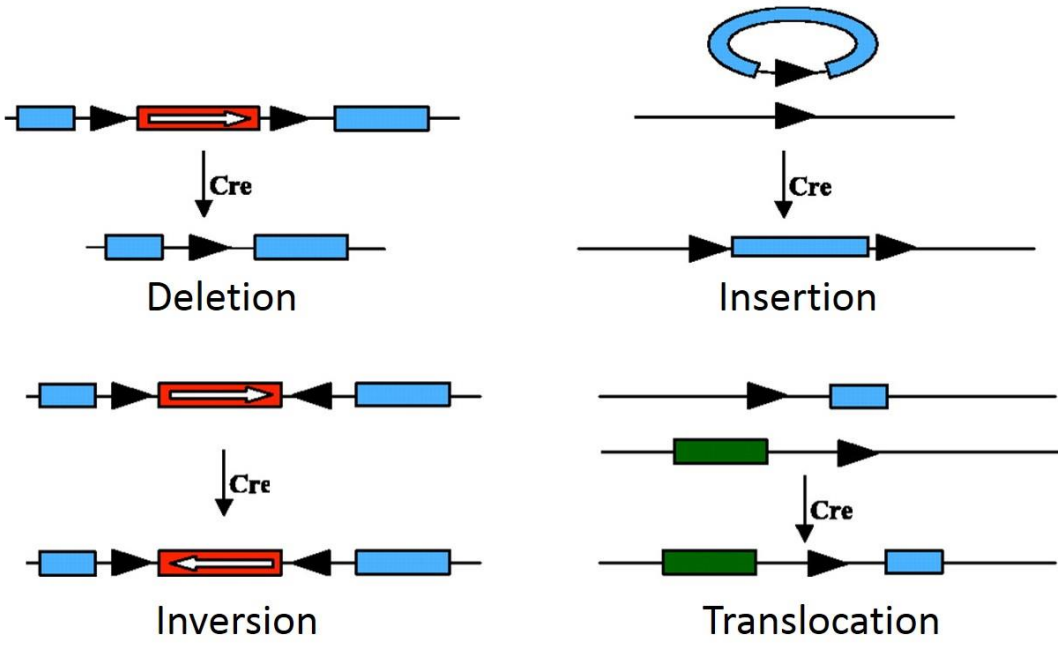

Figure 1-8 – An overview of cre-lox recombination events

Cre-lox mediated recombination requires the action of; **(1)** a DNA recombinase (cre), and **(2)** recombination signalling DNA markers (LoxP sites). Depending on the orientation and position of these markers, cre recombinase can perform 4 separate actions on DNA; deletion of bases between the LoxP sites, insertion of DNA between the sites, inversion of the DNA between the sites or translocation of a region of DNA. Adapted from (Bockamp et al., 2002).

The expression pattern of the cre recombinase can be determined by replacing the promoter sequence of the cre gene with either a promoter to enable whole body expression (e.g. the immediate early promoter of human cytomegalovirus, CMV) or a promoter that has a defined cell expression pattern (e.g. PF4-cre which was presumed to be expressed in cells of the megakaryocyte lineage (Tiedt et al., 2007; Ng et al., 2014)). A further level of (temporal) control, can be added to this system by creating a fusion protein whereby the cre recombinase is attached to a ligand binding domain of a mutant form of the oestrogen receptor. This then requires injection of tamoxifen into the mouse which causes the release of the tethered cre enzyme from the cytoplasm and therefore initiation of recombination. This

control avoids issues with embryonic lethality and developmental problems which can occur with classical gene knockout models.

With cre-lox recombination, especially for conditional cre constructs, it is important to know that the cre gene is only expressed in the tissues of interest. One method for testing the expression pattern is through the use of a stop-floxed mouse. A stop-flox mouse contains a transgene in which expression of a marker gene (e.g. LacZ (Soriano, 1999) or fluorescent protein marker (Muzumdar et al., 2007) are interrupted by a floxed region of DNA (usually an in-frame stop codon). This floxed region disrupts expression of the reporter gene until excision by cre recombinase.

When a floxed mouse is crossed with a mouse expressing a cre construct, the resulting pups contain both the floxed and cre genes. These pups, depending on the expression pattern of the cre gene, will either undergo recombination immediately and in most cells (i.e. CMV-cre, which has a 90% recombination efficiency) and generate a stable germline mutation (after the F_2 generation), or later and in limited cells (i.e. PF4-cre) and be a non-germline *de novo* mutation in every litter. Figure 1-9 shows an overview of potential cre-lox recombination strategies for gene knockout.

It has been noted in the literature that insertion of short DNA sequences (i.e. LoxP sites) can alter expression patterns of the target and also off target genes at distances of >100 Kb away (Meier et al., 2010). Therefore, it is important to first determine any effects which are due to the insertion of the ectopic sequence before any interpretations are made about the effects of ablation of the target gene.

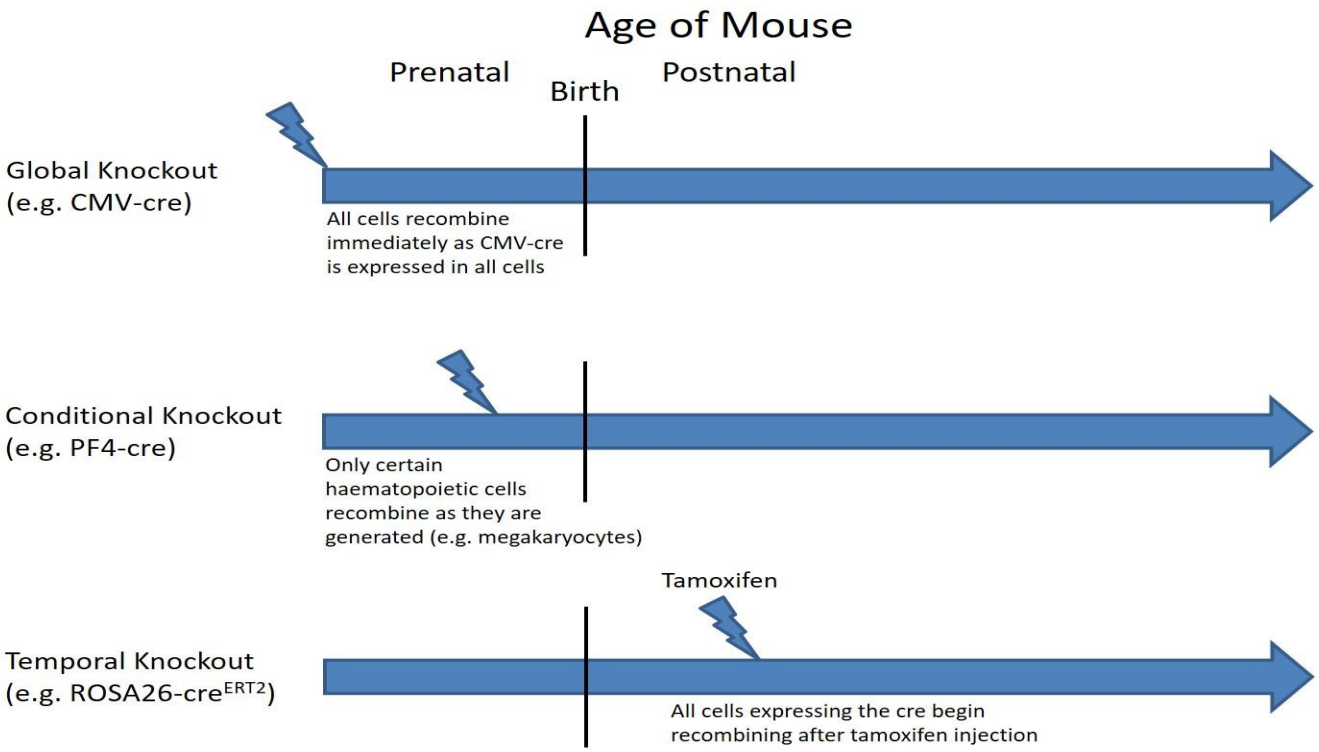

Figure 1-9 – An overview of cre-lox recombination strategies

Cre-lox is amenable for use in a number of different ways. Global knockout mice can be easily produced by generating gene fusions with the viral cytomegalovirus promoter (CMV) which is transcriptionally active in cells of all lineages and therefore produces germline recombination. Gene fusions can also be made with tissue specific promoters (such as the supposedly megakaryocyte-specific gene, PF4) which restricts recombination to these cells. A further layer of control is possible in both of the above situations by fusing the cre-promoter gene to a modified version of the oestrogen receptor. This allows temporal control of recombination by administration of a synthetic activator of the receptor (e.g. tamoxifen).

1.5 The Blood Vessel

The work in this thesis also focusses on cells within the arterial wall and their functions. The arterial wall consists of three main layers; tunica intima, tunica media and the tunica adventitia which are bound together by two internal elastin-rich layers. These layers are the internal elastic lamina (between the intima and media) and external elastic lamina (between the media and the adventitia).

The intimal layer consists of a single layer of squamous endothelial cells which control vascular barrier function and allow the passage of blood solutes ranging from small molecules (e.g. metabolites) up to whole cells (e.g. immune cells following inflammation) from the circulation into the surrounding tissue space and vice versa. The endothelial cells also play a key role in detecting changes in shear-stress through cell-surface mechanoreceptors and signalling to the smooth muscle layer to contract to resist this change. They also mediate blood vessel dilation in response to neuronal signals by releasing nitric oxide (Bauer and Sotníková, 2010; Alberts B, Johnson A, 2002).

The medial layer is made up of elastin fibres (arranged as fenestrated elastic lamellae) along with a high density of vascular smooth muscle cells. This layer is responsible for maintaining the contractile tone of the vessel and the width of the layer is variable depending on the size of the vessel.

The adventitial layer is comprised of collagenous fibres, elastic fibres, fibroblasts, macrophages and the perivascular nerves. This layer is thought to contain resident progenitor cell niches which are primed to respond to vascular injury and is also a major site of immune surveillance and

inflammatory cell trafficking in response to foreign antigens. The adventitia is also in physical contact with the tissue surrounding the vessel and is thought to mediate the exchange of signals between the tissue and the vessel (Majesky et al., 2011).

1.5.1 The Vascular Smooth Muscle Cell

Vascular smooth muscle cells (VSMCs) are the most abundant cell type found within the vascular wall. Located within the medial layer of the artery, these stromal cells are responsible for maintaining local blood pressure (in resistance vessels) as well as providing the vessel with the means to withstand the high pressure blood flow through it.

During development, these cells are responsible for synthesising the ECM of the medial layer and throughout adult life are capable of remodelling and repairing the ECM in response to injury (Lacolley et al., 2012).

VSMCs are known to be a heterogeneous cell type. Two phenotypes known as contractile and synthetic sit at two ends of a spectrum with cells showing phenotypes between the two. The contractile cells, which comprise the majority of VSMCs, perform the classical functions of the smooth muscle cell, i.e. maintaining vascular tone, whereas the synthetic cells are thought to be a dedifferentiated form of the VSMC which perform the remodelling of the ECM (Owens et al., 2004). In states of chronic inflammation, stress (both oxidative and mechanical) and chemokine activation tip the balance in favour of the synthetic cells and results in overactive remodelling of the ECM and, if prolonged, the destruction of the ECM and weakening of the vessel (e.g. in aortic aneurysm disease) (Rensen et al., 2007).

VSMCs are also known to be key mediators of atherosclerosis and restenosis after angioplasty. Both conditions show the characteristic migration of VSMCs from the media into the intimal layer of the vessel where they accumulate, proliferate and promote formation of atheromatous plaques (Hao et al., 2003). These cells are then known to undergo apoptosis and it has been hypothesised that this cell death causes the destabilisation of the shoulder regions of the plaque leading to rupture (Davies et al., 1993; Geng and Libby, 1995; Bauriedel et al., 1999; Bennett and Boyle, 1998).

It has been shown previously, albeit in rats, that aortic vascular smooth muscle cells express both transglutaminase 1 and 4 (Johnson et al., 2012) as well as the ubiquitously expressed transglutaminase 2.

1.6 Vascular Disease Models in Mice

This thesis explores the roles of the two transglutaminases FXIII-A and TG2 in the vasculature and their roles in repair. Parallel work within the group employs two disease models to study them in this context; aortic aneurysm and cardiac fibrosis. Other models have subsequently been investigated and are presented later in this thesis.

1.6.1 Abdominal Aortic Aneurysm

Abdominal aortic aneurysms (AAA) are localised dilatations of the abdominal aorta occurring primarily between the renal arteries which, in human patients, may rupture with fatal consequences. The pathophysiology of AAA includes four specific events; infiltration of the aortic wall by inflammatory macrophages, destruction of the elastic media and adventitia by matrix metalloproteinases leading to a reduced elastin:collagen ratio, rapid proliferation and invasion of VSMCs into the lumen from the tunica media

followed by apoptosis causing thinning of this layer of the vessel, and neovascularisation (Ailawadi et al., 2003).

Several AAA mouse models are described in the literature, these are adventitial application of calcium chloride (Gertz et al., 1988), infusion of angiotensin II into hypercholesterolaemic mice (Daugherty et al., 2000) and peri-aortic application of elastase (Pyo et al., 2000). Of these, our group chose to use the calcium chloride model due to the presence of the following features which mimic the human condition: calcification, inflammatory cell invasion, MMP activation, elastin loss and fibre fragmentation and VSMC apoptosis. The model requires neither genetically altered mice (i.e. ApoE deficient male mice are required for the angiotensin model) nor weakening of the vessel to start the process (i.e. the elastase model).

1.6.2 Cardiac Fibrosis

Progressive organ fibrosis is a hallmark of aging which affects the heart, kidney, liver and lung and is characterised by deposition of collagen and loss of organ function (Biernacka and Frangogiannis, 2011). In the heart, this is seen as a loss of ventricular compliance and impaired diastolic function (Lakatta, 2003).

In mice, increased microvascular permeability can result in the development of spontaneous cardiac fibrosis. This permeability causes microvascular haemorrhage and stimulates the invasion of inflammatory cells into the cardiac tissue which in turn carry out remodelling of the ECM and lead to the increased deposition of ECM components (Wynn, 2008). Previous reports in the literature have postulated roles for numerous clotting factors in the protection of the myocardium from fibrosis, with deficiency of Factor VII (Xu et

al., 2009), plasminogen activator inhibitor-1 (Xu et al., 2010), tissue factor (Pawlinski et al., 2002) and FXIII-A and FXIII-B in male mice (Souri et al., 2008) all causing spontaneous cardiac fibrosis. In our hands, cardiac fibrosis developed spontaneously in FXIII-$A^{-/-}$.$TG2^{-/-}$ mice irrespective of high fat feeding and this is explained in detail later in 3.5.1.

1.7 SAPK/JNK Signalling Pathway

It has been hypothesised by (Robitaille et al., 2004; Robitaille et al., 2008) that a transglutaminase is able to crosslink and activate the upstream protein kinase in the MAPK signalling pathway and thus promote pro-apoptotic signalling within the cell.

The MAPK signalling pathway provides the cell with the machinery to relay, magnify and incorporate signals from a vast range of exterior stimuli. In mammals, these responses involve; proliferation, differentiation, inflammation and initiation of programmed cell death (Weston and Davis, 2007).

Activation of the MAPK pathway by “stress” factors (e.g. IL-1β, IL-6, TNF-α and nitric oxide) allows the cell to respond to extracellular stimuli and chronic activation of this pathway typically results in apoptosis of the cell (Cafueri et al., 2012; Verma and Datta, 2010).

The components of signal transduction in the MAPK pathway involve a 3 tier array of kinases with each tier being able to modulate the function of the next through phosphorylation of key residues on specific substrates. The three tiers are referred to as; MAP kinase kinase kinase (MAP3K or MAPKKK), MAP kinase kinase (MAP2K or MAPKK) and MAP kinase (MAPK).

Activation of the pro-apoptotic MAPK pathway results in recruitment of dual lineage kinase (also referred to as DLK or MAP3K12) to the cell surface where

it is activated by phosphorylation and oligomerisation followed by covalent crosslinking, which is catalysed by a transglutaminase (Robitaille et al., 2004; Robitaille et al., 2008). Once activated, DLK is able to phosphorylate both SEK1 (MKK4) and SEK2 (MKK7) which in turn are able to phosphorylate JNK1 (MAPK8) and JNK2 (MAPK9) (Cui et al., 2007). Activated JNK (phosphorylated at threonine-183 and tyrosine-185 residues (Fleming et al., 2000)) has been shown to be able to phosphorylate a range of substrates such as the nuclear transcription factors c-Jun, ATF and c-Fos (Gupta et al., 1995) allowing the cell to switch on and off expression of many stress response genes.

JNK comprises a family of three genes; JNK 1 and 2 are widely expressed whereas JNK 3 is exclusively expressed in neurones. All three genes have been individually “knocked out” by homologous recombination in mice and these JNK-deficient mice are viable but show defects in apoptotic and immune signalling (Coffey, 2014). Whilst JNK is predominantly known as a pro-apoptotic mediator, growth factors (e.g. IGF-1, EGF and NGF) are also able to activate JNK through a separate pathway resulting in a proliferative cellular phenotype (O’Blenes et al., 2000). Compound knockout mice ($JNK1^{-/-}$.$JNK2^{-/-}$) show early embryonic lethality (Kuan et al., 1999); embryonic fibroblasts isolated from these mutants show a resistance to stress-induced apoptosis but also have decreased rates of proliferation (Tournier et al., 2000) suggesting that JNK activation is necessary for these functions in addition to mediating cell death.

The apoptotic and proliferative arms of MAPK signalling are summarised in Figure 1-10.

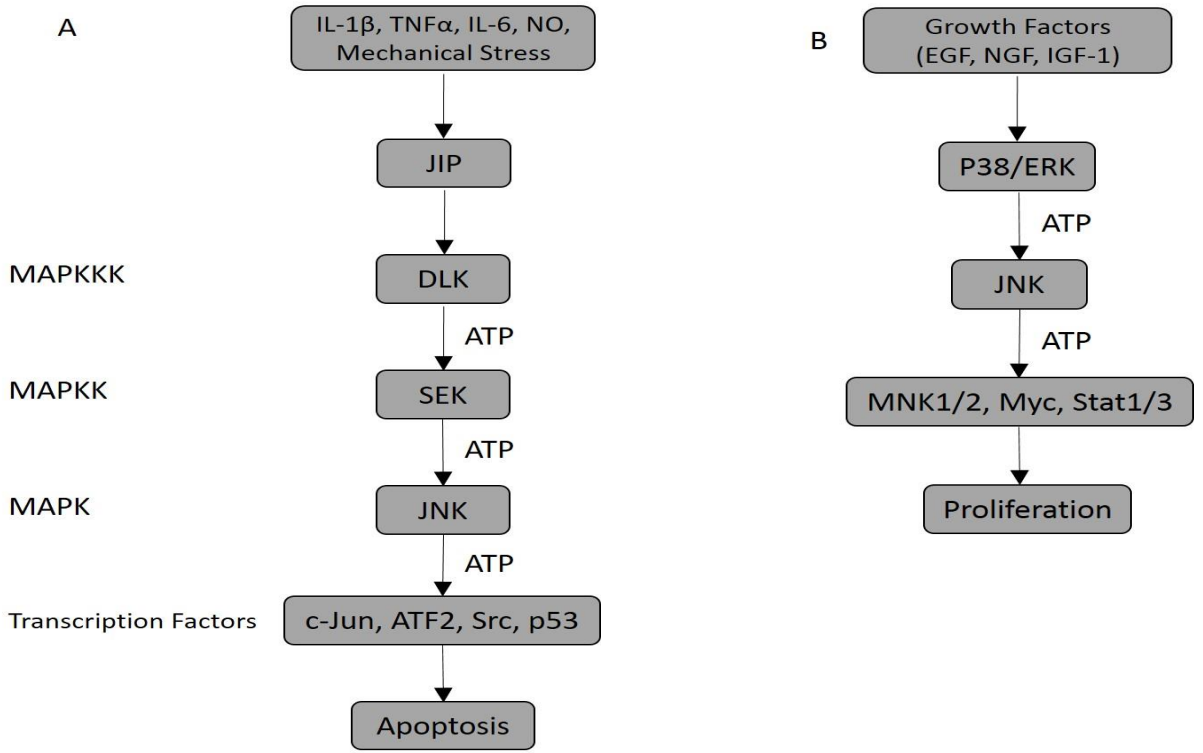

Figure 1-10 – MAPK apoptotic and proliferation signalling pathway

The mitogen activated protein kinase pathway comprises two pathways, apoptotic and proliferative, which both require JNK to effect changes within the cell. The two pathways are activated by different stimuli and switch on different transcription factors. Global inhibition of JNK to stop cell death, therefore, appears unwise as it would result in the loss of the proliferative capability.

1.7.1 Global JNK inhibition in previous studies

c-Jun N-terminal kinase (JNK) has been implicated as the major factor in AAA pathogenesis. (Yoshimura et al., 2006) reported that JNK activation was markedly increased in the walls of human AAA resulting in the induction of the ECM degrading enzyme matrix metalloproteinase-9 (MMP-9) and suppression of ECM synthesis through the down-regulation of lysyl oxidase (LOX).

Inhibition of JNK by the small molecule SP600125 (an ATP competitor) followed by AAA induction with 0.5 M $CaCl_2$ in mice did not lead to a significant increase in aortic diameter or damage to the vessel when compared to controls. However, whilst Yoshimura et al describe SP600125 as a specific inhibitor of JNK (Yoshimura et al., 2006), it appears to also inhibit closely related kinases such as protein kinase B and C, as shown in Table 1-1 (Bennett et al., 2001). It may be that it is the inadvertent inhibition of one of these other kinases that prevents the vessel dilatation and aneurysm formation, either in concert with JNK inhibition, or independently. Additionally, due to the requirement of JNK activation for non-apoptotic signalling (namely proliferation), wholesale JNK inhibition may not prove to be a viable long-term therapeutic strategy. This notion is also reflected in the findings of the compound JNK1 and 2 deficient mice (Tournier et al., 2000).

SP600125 has also been shown to protect mice from small intestinal injury caused by diclofenac (Ramirez-Alcantara et al., 2009), hepatic fibrosis resulting from either bile duct ligation or carbon tetrachloride injury (Kluwe et al., 2010). JNK has been implicated in both acute liver injury resulting from

paracetamol overdose (Win et al., 2011) and appears necessary for macrophage differentiation into foam cells (Rahaman et al., 2006).

Beyond this, significant interest is being focussed on MAPK inhibitors for use in the treatment of traumatic brain injury and stroke as well as in neurodegenerative conditions such as Alzheimer's disease and Huntington's disease (Kim and Choi, 2010; Coffey, 2014).

Enzyme	IC50 (μM)
JNK1	0.04
JNK2	0.04
JNK3	0.09
MKK4	0.4
MKK6	1.0
PKB (AKT)	1.0
MKK3	1.5
PKCa	1.5
p56Lck	4.3
MKK7	5.1
ERK2	>10
p38-2	>10
Chk1	>10
EGF-TK	>10
IKK-1	>10
IKK-2	>10
MEKK1	>10
PKA	>10

Table 1-1 – Inhibitory profile of SP600125

The most promising and widely cited JNK inhibitor is known as SP600125. While it is known to inhibit the kinase activity of all 3 JNK genes it also is known to inhibit numerous other kinases with a similar affinity (Bennett et al., 2001).

1.7.2 Transglutaminases in Cell Apoptosis and Survival

Many authors have reported that intracellular TG2 activity is pro-apoptotic in the *in vitro* situation (Robitaille et al., 2004; Robitaille et al., 2008; Hébert et al., 2000). For example, Robitaille et al (2004) undertook work in a monkey kidney fibroblast like-cell line transformed with a T7-tagged DLK vector and used an inhibitor (monodansylcadaverine, MDC) to block the action of TG2.

They induced apoptosis in culture using the fungi metabolite calphostin C which is able to specifically inhibit protein kinase C (PKC) by a light-dependent mechanism. Inhibition of PKC causes rapid mobilisation of intracellular calcium ion stores, resulting in induction of apoptosis and this increase in [Ca^{2+}] should activate intracellular TG2 as described previously (Zhang et al., 1998). Robitaille et al found that initiation of apoptosis resulted in the formation of higher-order oligomers of DLK which corresponded with a direct increase in phosphorylated JNK, caspase cleavage and cellular apoptosis. These effects could be significantly reduced by pre-treating the cells with an inhibitor of transglutaminase activity, MDC.

However, the use of an immortalised cell line in this work is problematic, as defects in apoptotic signaling may result from the immortalisation process thus rendering these cells unsuitable to study the apoptotic role of TG2. Furthermore, the use of MDC as an inhibitor means that all transglutaminase activity is inhibited (not simply TG2 activity) as MDC acts as a primary amine acceptor i.e. as a competitive substrate in the transamidation reaction. MDC is also known to block TNF-α receptor internalisation which is a MAPK activating signal (Schütze et al., 1999) and can also act as a lysosomotropic agent which causes the breakdown of intracellular ion gradients and therefore causes an increase in cellular acidity (Niemann et al., 2000) both of which could disrupt the normal apoptotic signaling pathway.

Paradoxically, TG2 has also been seen to play a role in cell survival. This dual function appears to be dependent on whether or not the stressor results in an increase in transamidation activity (Tucholski and Johnson, 2002; Milakovic et al., 2004), with activation promoting apoptosis (as described above) and no

activation repressing apoptosis. This anti-apoptotic response could be, in part, due to TG2's ability to bind calreticulin in a GTP-dependent manner at a site distinct from the transamidation catalytic site (Feng et al., 1999) as overexpression of calreticulin is known to sensitise the cell to apoptotic signals (Nakamura et al., 2000).

1.8 General Aims

a) To determine if FXIII-A and TG2 individually or co-operatively influence the outcome of cardiac fibrosis and abdominal aortic aneurysm in mice.
b) To find the cell responsible for secreting and maintaining the levels of plasma FXIII-A using a novel FXIII-A floxed mouse and several tissue specific cre mice.
c) To describe the role TG2 plays in apoptosis using a cell based model and TG2-knockout mice.

Chapter 2 – General Methods

2.1 Mouse Husbandry

All animal husbandry, housing and procedures were carried out in line with the regulations and guidelines of the University of Leeds Central Biologicial Services facility and under the authority of a United Kingdom Home Office approved Project licence (Dr Stephen Wheatcroft – 70/8115) and my own Personal licence (Mr Kingsley Simpson – 70/25614). All mice were maintained on a 12 h light/dark cycle and had access to water and standard laboratory chow diet at all times.

2.2 Origins of the Mice

2.2.1 Thrombocytopenic (Mpl Knockout)

The Mpl (thrombopoietin receptor) knockout mice were obtained from Professor Warren Alexander (Walter and Eliza Hall Institute, Australia) on a defined C57BL/6 background. Despite a severe bleeding phenotype following injury, female homozygote knockouts breed normally. The $Mpl^{-/-}$ males were crossed with $Mpl^{-/-}$ females, in trios, to produce $Mpl^{-/-}$ pups.

2.2.2 TG2 Knockout

$TG2^{+/-}$ knockout mice, on a C57BL/6 background, were a kind gift from Professor Robert Graham (Victor Chang Institute, Australia). These mice have a targeted deletion of exons 6-8 of the TG2 gene which was carried out using cre-lox recombination of a TG2 floxed mouse (Nanda et al., 2001). $TG2^{+/-}$ x $TG2^{+/-}$ breeding was established to produce $TG2^{-/-}$ offspring at an expected ratio of 1 in 4. Following this, $TG2^{-/-}$ pups from distinct litters were crossed in trios to produce pure litters of $TG2^{-/-}$ pups which were used for study.

2.2.3 FXIII-A Floxed Mouse

Figure 2-1 shows the process by which C57BL/6:129/Sv chimeric offspring habouring the FXIII-A targeted locus were backcrossed onto a C57BL/6 mouse expressing Flp recombinase to remove the neomycin resistance cassette from the homologous recombination targeting vector. The offspring produced contain one wildtype allele and one floxed allele (FXIII-$A^{+/flox}$). This mouse was then backcrossed onto either a wildtype C57BL/6 mouse (to generate backcrossed heterozygous floxed mice, FXIII-$A^{+/flox}$) or a C57BL/6 mouse expressing CMV-cre (to produce FXIII-A heterozygous knockouts, FXIII-$A^{+/-}$). At this stage the mice were 75% C57BL/6 and were further backcrossed to >93.75% C57BL/6 to remove stain differences.

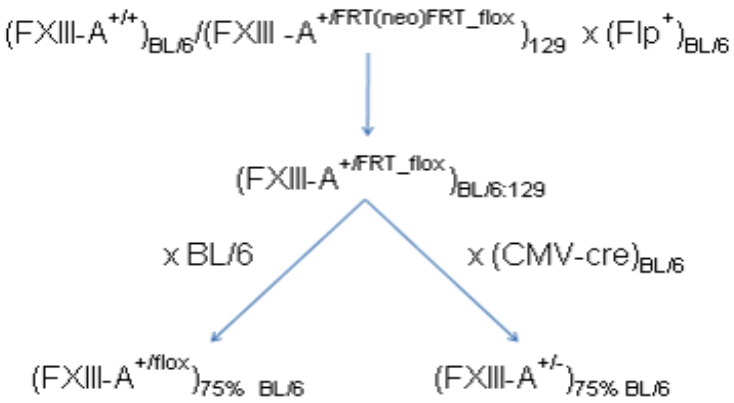

Figure 2-1 – Schematic of the FXIII-A breeding strategy used by GenOway

Chimeric floxed C57BL/6:129Sv mice were backcrossed onto a C57BL/6 background and the neomycin resistance cassette excised by Flp recombinase. FXIII-A floxed and global knockout mice were produced by crossing either with wildtype C57BL/6 or CMV-cre expressing C57BL/6 mice respectively. The background was then further enriched by backcrossing with C57BL/6 mice.

2.3 Flox Sequencing

Genomic DNA was isolated from livers as per 2.10 below. The entire FXIII-A floxed locus was amplified by PCR with primers that hybridised both upstream and downstream of the two LoxP sites, using a proofreading Pfu/Taq polymerase mix (Bio-Rad). The primer sequences used are detailed in Table 8-1.

Taq polymerase adds a single adenosine nucleotide overhang to the 3' end of each amplicon and the PCR product was ligated into a pCR4-TOPO vector (ThermoFisher Scientific) which possesses 5' thymidine overhangs. The system utilises topoisomerase to recircularise the vector once the Taq amplified product has hybridised. *E. coli* DH5-α cells were transformed by heat shocking the cells at 42^{o}C in the presence of the plasmid, spread onto an agar plate containing ampicillin (100 µg/mL) and allowed to replicate overnight at 37 ^{o}C. Single colonies were selected and grown overnight at 37 ^{o}C with shaking (225 rpm) in lysogeny broth containing ampicillin (100 µg/mL). The plasmid was recovered using Qiagen miniprep kits as per the manufacturer's recommended instructions and diluted to 20 ng/µL in ultrapure water. The DNA sequencing was performed by DNA Sequencing & Services (MRCPPU, College of Life Sciences, University of Dundee, Scotland, www.dnaseq.co.uk) using Applied Biosystems Big-Dye Ver 3.1 chemistry on an Applied Biosystems model 3730 automated capillary DNA sequencer.

2.4 Generation of *de novo* FXIII-A Knockout Mice

2.4.1 FXIII-A Knockout

All FXIII-A global and conditional knockout mice in this study were generated using cre-lox technology. A floxed FXIII-A mouse was commissioned by GenOway which had LoxP sites inserted, flanking exon 8 (coding exon 7) within intron 7 and intron 8 of the FXIII-A gene (Figure 2-2). Recombination of these sites in cells expressing cre recombinase produces a truncated mRNA, which lacks the catalytic domain.

Homozygous global FXIII-A knockout mice were produced by crossing non-sibling pups from separate FXIII-$A^{+/-}$ litters.

Due to FXIII-A deficient females being unable to survive pregnancy, the breeding strategy consisted of trios of a FXIII-$A^{-/-}$ male and two FXIII-$A^{+/-}$ females. This was expected to give a frequency of 1 in 2 for $FXIII^{-/-}$ pups however, as described later in 3.4.2, the frequency of homozygous knockout pups obtained was markedly below expectation.

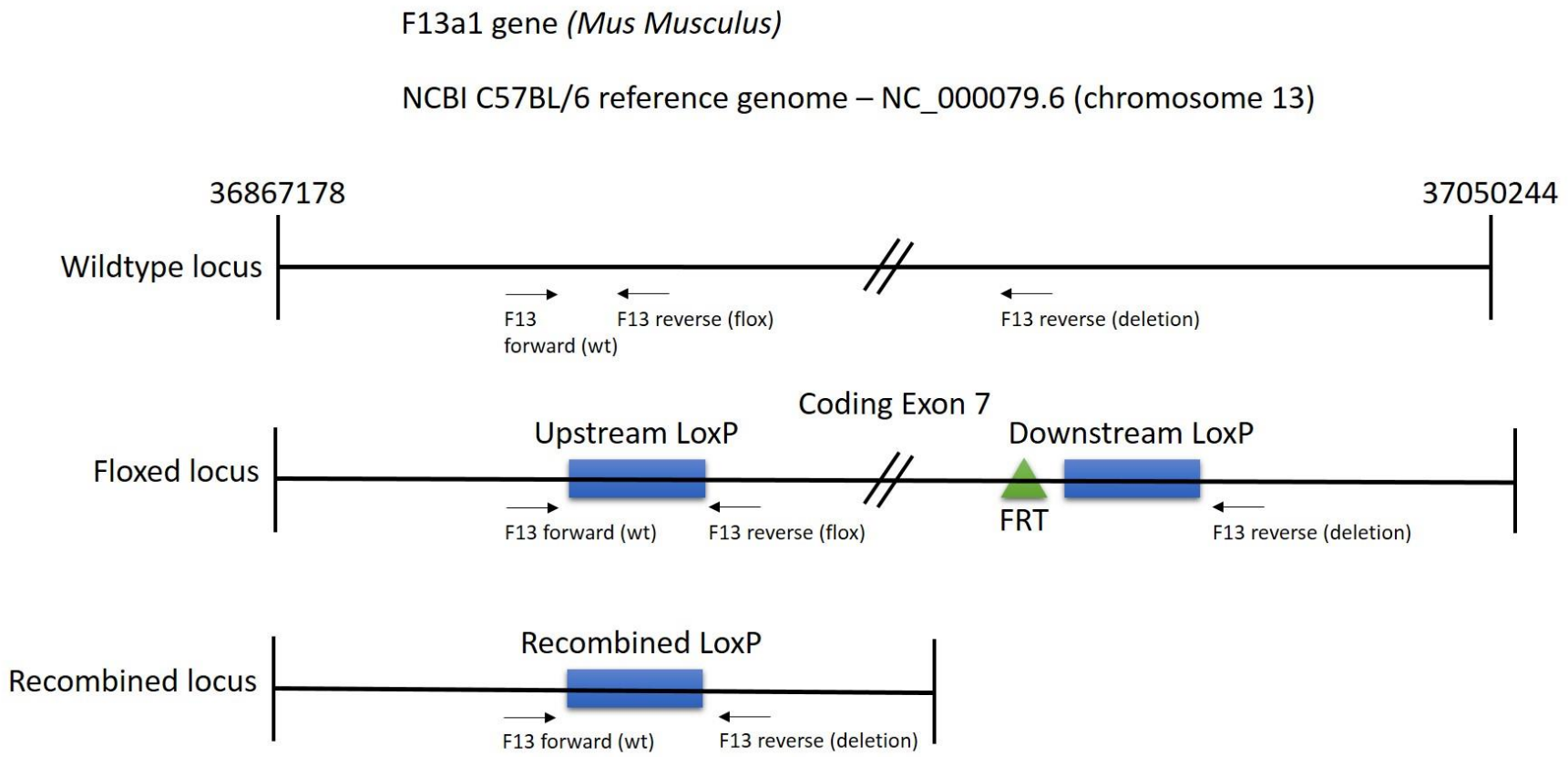

Figure 2-2 – Depiction of the wildtype and genetically modified FXIII-A locus

The FXIII-A gene was targeted by homologous recombination by GenOway. Flanking coding exon 7, a pair of LoxP sites were added along with a neomycin resistance cassette (which was enclosed between two FRT sites, and subsequently removed by recombination with Flp recombinase). Cre-mediated recombination removes coding exon 7 and the remaining recombined FRT site. Primer locations for genotyping are shown as labelled arrows.

2.4.2 Conditional FXIII-A Knockouts

To induce cell lineage specific deletion of FXIII-A, floxed mice were crossed with mice harbouring cre recombinase constructs fused to the promoter of one of four genes: Platelet Factor 4 (PF4) (Tiedt et al., 2007), Integrin Alpha M (CD11b) (Ferron and Vacher, 2005), Lysozyme 2 (LysM) (Faust et al., 2000) and Fms-related Tyrosine Kinase 3 (Flt3) (Benz et al., 2008). The PF4-cre transgene is present on an unidentified autosome(s) whereas the CD11b-cre and Flt3-cre transgenes reside on the Y chromosome and as such are only present in male mice. LysM-cre is a knock-in into the endogenous Lys2 gene.

PF4-cre utilises a 100Kb bacterial artifical chromosome to target expression of a codon-optimised cre recombinase to the megakaryocyte lineage (Tiedt et al., 2007). The construct comprises of PF4 (which has the first exon fused to the cre sequence) and 4 other chemokine genes. However, while PF4-cre has been used in a large number of studies, the endongeous PF4 gene has been reported to be expressed in other cell types (e.g. monocytes (Schaffner and Rhyn, 2005)). More recent evidence from (Pertuy et al., 2015) has demonstrated clear expression of the PF4-cre transgene outside of the megakaryocytic lineage in F4/80^{+} macrophage cells in the majority of mouse tissues (which are presumably tissue resident macrophages).

The PF4-cre^{+}.FXIII-A$^{flox/flox}$ mice were produced by crossing PF4-cre^{+}.FXIII-A$^{wt/wt}$ and FXIII-A$^{flox/flox}$ mice. This produces PF4-cre^{+}.FXIII-A$^{wt/flox}$ mice, which were then crossed against FXIII-A$^{flox/flox}$ mice to generate PF4-cre^{+}.FXIII-A$^{flox/flox}$ mice at a mendelian frequency of 1 in 2. Once generated, PF4-cre^{+}.FXIII-A$^{flox/flox}$ mice were crossed against

FXIII-A$^{flox/flox}$ mice to ensure a constant production of PF4-cre^{+}.FXIII-A$^{flox/flox}$ mice (Figure 2-3).

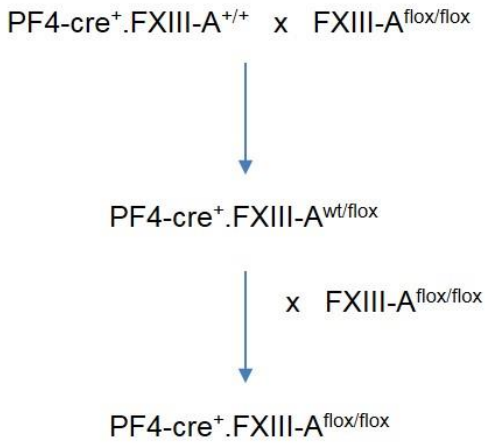

Figure 2-3 – Generation of 1 copy PF4-cre.FXIII-A floxed mice

Single copy PF4-cre.FXIII-A$^{flox/flox}$ mice were produced by crossing PF4-cre mice with the *de novo* FXIII-A$^{flox/flox}$ mouse as per the diagram.

In some studies a second PF4-cre allele was bred into these mice (Figure 2-4). These mice were bred through hemizygous crosses of PF4-cre^{+}.FXIII-A$^{flox/flox}$ and PF4-cre^{+}.FXIII-A$^{flox/flox}$. Real time PCR of genomic DNA was used to discrimate pups with one or two copies of the cre transgene (i.e. PF4-cre^{+} or PF4-cre^{++}).

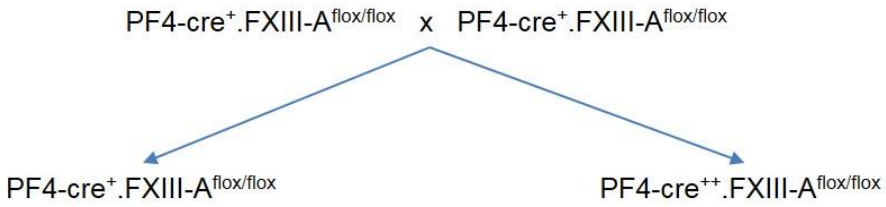

Figure 2-4 – Generation of 2 copy PF4-cre.FXIII-A floxed mice

Two copy PF4-cre.FXIII-A$^{flox/flox}$ mice were produced by crossing hemizygotic PF4-cre.FXIII-A$^{flox/flox}$ mice as per the schematic above.

LysM-cre^{+}.FXIII-A$^{flox/flox}$ mice were bred in a similar fashion to the single copy PF4-cre mice with LysM-cre^{+}.FXIII-A$^{flox/flox}$ crossed with FXIII-A$^{flox/flox}$ mice to

produce LysM-cre^{+}.FXIII-A$^{flox/flox}$ offspring. Pups were genotyped based on the presence or absence of the transgene using a 3 primer strategy with a common oligo hybridising just upstream of the insertion site.

CD11b-cre^{+}.FXIII-A$^{flox/flox}$ and Flt3-cre^{+}.FXIII-A$^{flox/flox}$ mice were bred using the same strategy as the single copy PF4-cre mice but as male mice only habour a single Y chromosome, only one cre allele can ever be present.

CD11b-cre^{+}.PF4-cre^{+}.FXIII-A$^{flox/flox}$ mice were bred by crossing CD11b-cre^{+}.FXIII-A$^{flox/flox}$ males with PF4-cre^{++}.FXIII-A$^{flox/flox}$ females which produce male mice that are hemizygous for both the CD11b-cre and PF4-cre alleles and homozygous for the floxed FXIII-A locus.

2.4.3 FXIII-A.TG2 (Double) Knockout

Double knockout, FXIII-A$^{-/-}$.TG2$^{-/-}$, (DKO) mice, were bred by crossing FXIII-A$^{-/-}$ males with TG2$^{-/-}$ females to produce FXIII-A$^{+/-}$.TG2$^{+/-}$ offspring. These offspring were backcrossed twice against TG2$^{-/-}$ mice to increase the

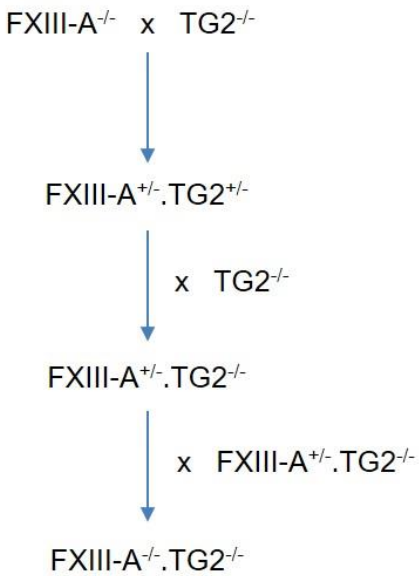

Figure 2-5 – Breeding of double knockout mice

Global FXIII-A and TG2 double deficient mice were produced by breeding mice deficient for the two genes through the scheme above.

C57BL/6 background of the mice resulting in FXIII-A$^{+/-}$.TG2$^{-/-}$ mice on a 97% C57BL/6 background. These mice were bred in sibling-sibling crosses to produce FXIII-A$^{-/-}$.TG2$^{-/-}$ offspring. Beyond this, mice were bred in trios consisting of a single FXIII-A$^{-/-}$.TG2$^{-/-}$ male and two FXIII-A$^{+/-}$.TG2$^{-/-}$ females and the DKO offspring used for study. This breeding strategy is summarised in Figure 2-5.

2.5 Routine Genotyping

Pups were ear notched at weaning (~3 weeks of age) and gDNA extracted by subjecting each individual sample to high temperature (95 ^{o}C) in 100 µL of an alkaline solution (final concentration of 25 mM NaOH and 0.2 mM EDTA) for 20 min followed by the addition of 100 µL of a pH neutralising solution containing Tris-HCl (final concentration of 20 mM, pH 5.5). These samples were frozen at -20 ^{o}C, if not immediately used for PCR.

PCR reactions were carried out in 25 µL total volumes containing 2 µL of the undiluted gDNA isolate along with 12.5 µL of MyTaq Red master mix (Bioline).

For all genotypes, common PCR reaction conditions were used;

1. 94 ºC for 2 min
2. 94 ºC for 15s
3. T_m (shown in 8.1) for 20s
4. 72 ºC for 45s
5. Repeat steps 2-4 another 29 times
6. 72 ºC for 5 min
7. Cool at 4 ºC

PCR primers, sequences and melting temperatures for each genotype are defined in 8.1.

Figure 2-6 shows the expected electrophoretic product sizes for each genotype.

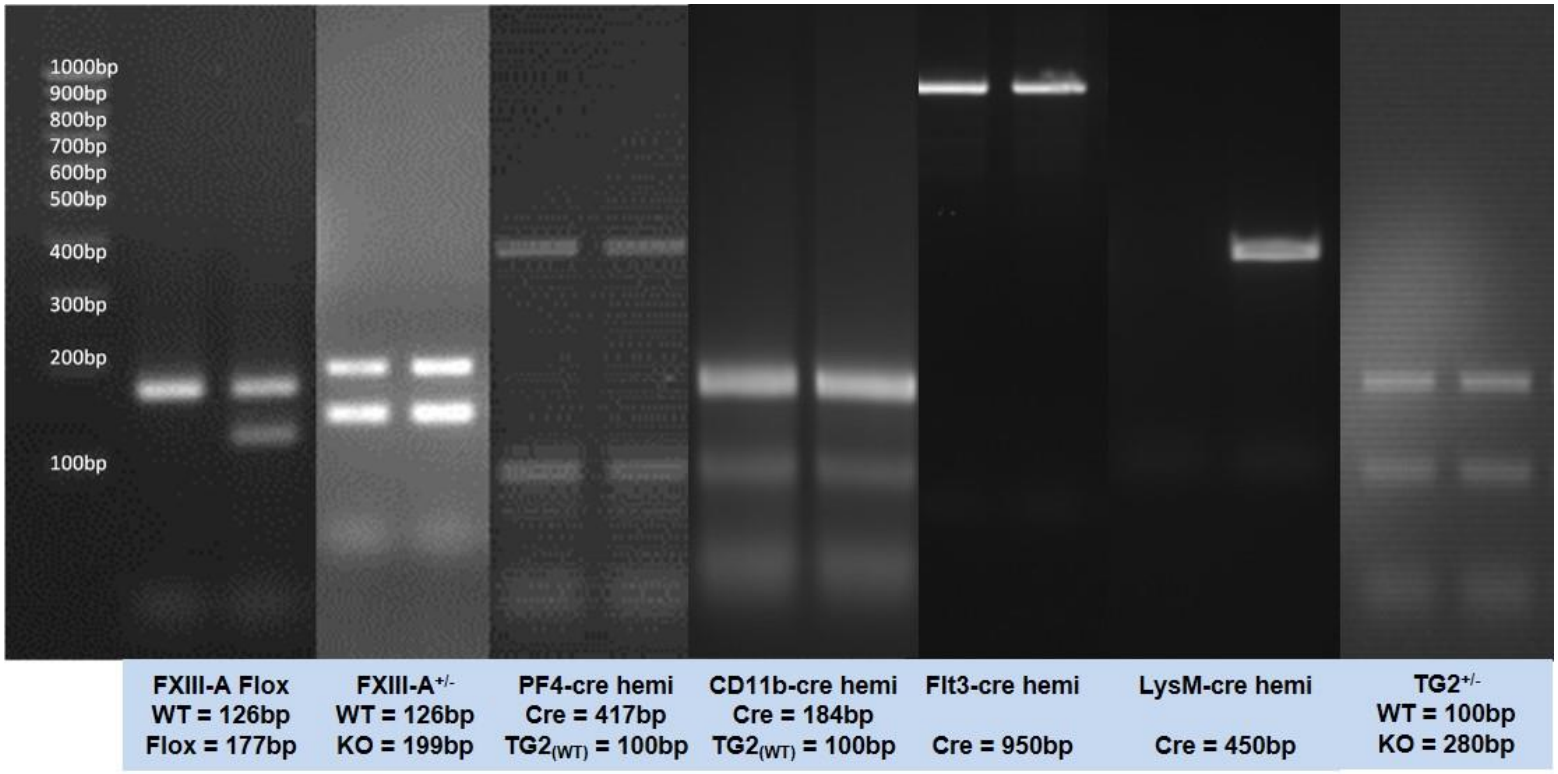

Figure 2-6 – Representative samples of PCR genotyping of mouse lines

Regions of gDNA were amplified by PCR to produce electrophoretic bands that show the presence of the floxed locus of FXIII-A (e.g. FXIII-A Flox), the wildtype or recombined alleles (e.g. FXIII-$A^{+/-}$ and $TG2^{+/-}$) or the presence or absence of the cre gene (e.g. -cre lines).

2.5.1 Agarose Gel Electrophoresis

To determine the genotype of the different mouse lines, PCR products (generated as outlined in 2.5 above) were separated using agarose gel electrophoresis, whereby smaller DNA molecules migrate through the gel faster than larger ones.

Gels were cast in 8 cm x 15 cm gel tanks with two 16 well combs embedded within. For all genotyping assays 2% (3 g/150 mL) agarose gels were used in a total volume of 150 mL of 1x TAE buffer (40 mM Tris-HCl, 20 mM acetic acid, 1 mM EDTA, pH 7.6). The agarose and TAE buffer were mixed in a 500 mL conical flask and brought to melting in an 800 W microwave. Once heated and the agarose totally dissolved, 1 µL of ethidium bromide solution (10 mg/mL, Sigma-Aldrich) was added to the gel mix. The tank was filled with 1x TAE buffer until the gel was submerged and 1 µL ethidium bromide solution added to the cathode end of the gel tank. Then, 5 µL (50 ng/µL) of 100bp GeneRuler Ladder (ThermoFisher Scientific) was added to the first lane and the total 25 µL PCR reaction added to subsequent wells. It was then connected to a PowerPac Basic power supply (Bio-Rad) and electrophoresis carried out at 125 V for 60 min.

After electrophoresis, gels were imaged on a G:Box (Syngene) using UV illumination and the genotyping gel images saved as JPG files. The genotypes of all mice were determined manually and corroborated by two independent parties and then recorded on the local mouse database if agreement was reached.

2.6 Mouse Blood Isolation

Eight week old mice were anaesthetised using inhaled Isoflurane gas and a laparotomy performed. The inferior *vena cava* was exposed and blood was taken using a 25G needle into 0.3 mL of CTAD (citrate, theophylline, adenosine and dipyridamole) anticoagulant. Syringes were weighed before and after blood sampling to determine the dilution factor of blood into CTAD.

2.7 Plasma FXIII-A Activity Assay

Whole blood isolated as described in 2.6 above was centrifuged at 200 xg for 10 min; the platelet-rich plasma was removed, centrifuged at 500 xg for 10 min and the platelet depleted supernatant removed for assay.

Plasma FXIII-A activity was measured by means of a microtiter plate assay using immobilised fibrinogen and 5-(biotinamido)pentylamine as substrates. This method was based on that described by (Song and Sheng, 1994). Nunc Immuno Maxisorp 96-well plates (Nunc A/S) were coated with 4 µg of fibrinogen (40 µg/mL in TBS, pH 8.3) (Calbiochem) per well overnight at 4 ^{o}C. The plate was emptied and washed 3 times with 300 µL of TBS (pH 8.3) followed by blocking of the plate by addition of 300 µL of 1% BSA and incubation at 37 ^{o}C for 90 min. The plate was washed 4 times with 300 µL of TBS and 1:100, 1:200, 1:400 CTAD-inhibited mouse plasma samples added in duplicate to wells. The crosslinking reaction was started by addition of 150 µL of the reaction mix (DTT (2.2 µM), biotinpentylamine (6.6 µM), $CaCl_2$ (220 µM) and thrombin (21.75U)).

The plate was incubated at 25 ^{o}C and the reaction stopped by addition of 200 µL of 200 mM EDTA at 7.5 min. The wells were washed 4 times with 300 µL TBS/Tween-20 (0.1%) followed by incubation with 100 µL of 10 µg/mL alkaline

phosphatase conjugated streptavidin at 37 ^{o}C for 1 h in 1% BSA, TBS and 0.1% Tween-20.

The wells were washed 4 times with 300 µL TBS/Tween-20 (0.1%) and colour was developed by addition of 100 µL of 1 mg/mL 4-nitrophenyl phosphate (Sigma-Aldrich) in 1 M diethanolamine and 0.5 mM $MgCl_2$ (pH 9.8) for 1 h at 30 ^{o}C. Absorbance readings, measured at 405 nm on a Labtek plate reader (ThermoScientific), were taken every 1 min for 1 h and rates derived from the linear portion of the reaction curve. Final activities were corrected for CTAD dilution of the whole blood in the initial sample.

2.8 Platelet Isolation and Characterisation

To determine the FXIII-A levels in mouse platelets, whole blood samples, described in 2.6 above, were centrifuged at 200 xg and the platelet rich plasma layer was retained. This platelet-rich plasma was re-centrifuged at 1000 xg to sediment the platelet cells and the plasma layer removed and stored for plasma FXIII-A assays. For FACS experiments the platelet activation inhibitors apyrase (0.02 U/mL, Sigma-Aldrich) and prostacyclin I_2 (0.5 uM, Cayman Chemical) were added prior to antibody labelling to prevent aggregation. For FXIII-A activity determination platelet pellets were washed twice with Tyrode's buffer (10 mM HEPES (pH 7.4), 134 mM NaCl, 12 mM $NaHCO_3$, 2.9 mM KCl, 0.34 mM Na_2HPO_4, 1 mM $MgCl_2$) to remove residual plasma proteins and the platelets stored at -80 ^{o}C until use.

2.8.1 Fluorescence Activated Cell Sorting of Mouse Platelets

To determine counts and morphology, the centrifuged and washed platelets were labelled with a monoclonal FITC-conjugated anti-CD42b antibody

(Emfret) in PBS supplemented with 1% BSA and FACS analysis was performed on a FACSAria II (Becton Dickinson).

2.8.2 FXIII-A Activity Assay

To normalise the FXIII-A activity measurement in the platelets of the various mouse lines, lactate dehydrogenase levels were determined (as described in 2.25.1.1 below) in the pelleted platelets. The LDH normalised platelet pellets were resuspended in a total volume of 100 µL which was added to 96-well Nunc Immuno Maxisorp 96-well plates (Nunc A/S) coated with 4 µg of fibrinogen (40 µg/mL in TBS, pH 8.3) (Calbiochem). The activity assay was then performed as per 2.7 above. The resulting activity was corrected for cell number and all genotypes normalised to the wildtype.

2.9 Mouse Organ Isolation

Following blood sampling as described in 2.6, mice were perfused via the left ventricle with 10 mL of saline to remove circulating blood. The animals were exsanguinated via the IVC and organs were harvested in the following order; liver, spleen, aorta and heart, into labelled 1.7 mL eppendorf tubes, snap-frozen in liquid nitrogen and then stored at -80 ^{o}C until use.

2.10 Genomic DNA Isolation

For assays relating to PF4-cre copy number determination (2.11) and genomic recombination (2.19), high purity gDNA ($A_{260/230}$ and $A_{260/280}$ >1.8) was required. gDNA was isolated from organs by incubating in 0.5-1 mL lysis buffer (2% SDS, 400 ng RNase A, 400 ng proteinase K) at 55 ^{o}C overnight. These samples were centrifuged at 14000 xg for 20 min to pellet insoluble material and the supernatant mixed 1:1 with 25:24:1 Phenol:Chloroform:Isoamyl Alcohol, shaken, and then left for 10 min at room temperature to equilibrate.

These samples were centrifuged at 14000 xg for 10 min and the upper layer containing DNA was removed to a new tube. This step was repeated twice in total. Residual phenol was removed from the sample by mixing 1:1 with bromochloropropane (BCP), the mixture was centrifuged and the upper layer removed to a new tube. This step was carried out twice in total. DNA was precipitated by addition of 0.1 volumes of 3 M sodium acetate (pH 5.2) and 2.2 volumes of 100% ethanol. These samples were left at -80 ^{o}C for 1 h followed by centrifugation at 14000 xg for 20 min at 4 ^{o}C. The pellet was washed 4 times with 70% ethanol and resuspended in 100-1000 µL of TE buffer depending on concentration (as determined by a NanoDrop 1000 Spectrophotometer).

2.11 PF4 Copy Number Determination

The location of the PF4-cre transgene within the genome is unknown but the initial report (Tiedt et al., 2007) describing the transgenic mouse suggests it may be present in more than one location depending on which transgenic founder was used.

To determine the copy number of the PF4-cre mice, 3 primers were designed to be compatible with real time PCR (optimal melting temperature of 60 ^{o}C and ~100 bp products). The forward primer hybridises with a common region in both the PF4-cre transgene and the endogenous PF4 gene and the two reverse primers each recognises a unique region in either the codon-optimised cre recombinase or the endogenous PF4 gene. The real time PCR reactions were set up in quadruplicate using 60 ng (all samples normalised to 15 ng/µL with ultrapure water) of gDNA (extracted using the method in 2.10), 10 µL of the Roche LightCycler 480 SYBR green I Master Mix and 500 nM of

each primer. The reactions were separated to generate a single product in each well and had a total volume of 20 µL.

The reaction conditions used were; 95 ^{o}C for 10 min, 45 cycles of 95 ^{o}C for 20 s, 64 ^{o}C for 20 s and 72 ^{o}C for 45 s, followed by a melting curve from 65 ^{o}C to 95 ^{o}C to ensure only a single product was made. The raw crossing points (Ct) were collected for each reaction and averaged per sample (if technical replicates were within 0.3 Ct). The average transgenic product Ct was subtracted from the endogenous product Ct giving a ΔCt which was converted into an amount of gene product by the Livak ($2^{-\Delta Ct}$) method. When plotted as a bar chart, the mice fell into groups identifiable as having 0, 1 or 2 copies of the PF4-cre gene.

2.12 Heart Fractionation

Heart fractionation was performed by Dr Sumia Bageghni and colleagues (University of Leeds) using the Neonatal Cardiac Fibroblast Isolation Kit (Miltenyi Biotech) after size exclusion of cardiomyocytes and RNA isolation samples from each purified fraction were kindly donated. The RNA samples were reverse transcribed as per 2.17 and real time PCR carried out as per 2.18 below.

2.13 Cell Isolation and Culture

2.13.1 Vascular Smooth Muscle Cell Culture

2.13.1.1 Poly-L-lysine Coating of Culture Plastic and Glassware

Five mg of poly-L-lysine hydrobromide with a molecular weight between 30-70 kDa (Sigma-Aldrich) was dissolved in 50 mL tissue culture grade sterile water. In a laminar flow hood, 150 µL or 300 µL of poly-L-lysine solution was added to 24- or 12-well plates. If cells grown in these wells were intended for

microscopy, then a single 6 mm glass coverslip was placed in each well and coated at the same time. The plates were incubated for 5 min at room temperature, the solution removed and the plates allowed to dry for 2 h at room temperature under laminar flow.

2.13.1.2 Vascular Smooth Muscle Cells

Aortas (descending aortic arch to iliac bifurcation) were harvested into 500 µL antimycotic solution (10 µL antimycotic in DMEM) (ThermoFisher Scientific) as described in 2.9 above. Following harvest, the adventitia was removed with straight forceps using a stripping motion originating in the centre of the tissue. Each individual aorta was placed in a 100 mm culture dish containing a small volume of culture medium (DMEM (ThermoFisher Scientific), 10% FCS, 1% antibiotic-antimycotic solution and 1% L-glutamine) and cut into several 2 mm pieces. The pieces were placed into a 1.7 mL eppendorf tube containing 100 µL of enzyme solution (7.5 mg collagenase type II (Merck Millipore) dissolved in 5.5 mL culture medium). The tubes were capped and taped awry to allow gas exchange and placed in a 37 ^{o}C/5% CO_2 incubator for 5 h to allow tissue digestion. Following digestion, dispersed cells were resuspended by gently flicking the tube. The cell suspension was moved to a 15 mL falcon tube, 3 mL of culture medium added to the suspension and the cells were pelleted by centrifugation (300 xg, 5 mins, 18 ^{o}C). The medium was removed by vacuum aspiration and the pellet washed in 5 mL of culture medium followed by centrifugation (300 xg, 5 mins, 18 ^{o}C). The pelleted cells were resuspended in 700 µL of culture medium, and the whole volume transferred to a single well of a poly-L-lysine coated 24-well plate where it was left undisturbed for 3 days in a 37 ^{o}C/5% CO_2 incubator. After 3 days, the media was refreshed and on day 5 the cells split (Ray et al., 2001; Bochaton-Piallat et al., 1992; Furmaniak-

Kazmierczak et al., 2007). For the immunocytochemistry, gene and protein expression experiments, the cells were split 1 in 4 into 2 wells of a coated 12-well plate (or into 4 wells of a 24-well plate with coverslips if required).

2.13.2 Macrophage Isolation and Culture

Fore and hind limbs were harvested (with epiphyses intact) from 8-week old wildtype mice into chilled in PBS on ice. The bones were cleaned of muscle and soft tissue and washed with PBS. The epiphyses were removed with strong surgical scissors and placed into a 0.7 mL eppendorf with the bottom 1 mm removed of the tube. The 0.7 mL tube was then placed inside a 1.7 mL eppendorf. The bones were centrifuged at 1200 xg to remove the bone marrow cells then the bones turned over and centrifuged again.

The isolated cells were plated in 100 mm tissue culture dishes (Nunc) using 10 mL media (RPMI-1640 supplemented with 10 ng/mL M-CSF) and cultured for 7 days until a point where other researchers have defined them as differentiated (Bellora et al., 2012). The cells were either harvested for RNA isolation or were trypsinised and seeded at a density of $5x10^6$ cells in 100 mm dishes (10 mL culture media) the night before being used for mRNA or clodronate assays.

2.14 RNA Isolation from Whole Organs

Messenger RNA isolated from mouse organs using a TissueLyser II (Qiagen) to homogenise the sample and TRIzol (ThermoFisher Scientific) to lyse the cells releasing the cellular contents (Chomczynski and Sacchi, 1987). TRIzol contains a mixture of guanidinium thiocyanate (a chaotrophic agent to aid in the denaturation of proteins) and phenol. The addition of BCP causes phase

separation in which the RNA moves to the aqueous layer, protein to the organic layer and DNA to the interphase.

The ribonucleic acid was precipitated from the aqueous layer using 100% ethanol and DNA removed using the “DNA-free” kit (ThermoFisher Scientific). This kit contains a highly active variant of deoxyribonuclease I which cleaves any residual single stranded or double stranded DNA molecules, the kit also removes any divalent metal ions (Ca^{2+}, Mg^{2+}, etc) which are required for ribonuclease activity.

2.15 RNA Isolation from the Liver

Livers were homogenised in 1 mL of Trizol (ThermoFisher Scientific). The RNA extraction protocol was the same as described in 2.14 above with the exception of taking 50 µL of the chloroform fraction for ethanol precipitation rather than the whole fraction (~600 µL) to avoid precipitating too large a quantity of RNA which would result in contaminated final samples.

2.16 RNA Isolation from Cells

2.16.1 Macrophages

Cultured macrophages (prepared as in 2.13.2 above) were washed twice with ice cold PBS and lysed in 1 mL of Trizol. The RNA was then isolated following the method in 2.14 above.

2.16.2 VSMCs

Total RNA was isolated from VSMCs (as in 2.13.1.2 above) cultured in 12-well plates. Due to the small cell numbers cultured (~3.5 $x10^5$ cells per well) the RNeasy Micro Kit (Qiagen) was preferred over the TRIzol based method (described in 2.13 above) as silica based extraction methods more readily

isolate small amounts of nuclei acids (Kim et al., 2012). The method described by the manufacturer was followed without alteration.

Quantitative qPCR was performed (as described in 2.18 below) on each sample in duplicate using 20 ng of cDNA per reaction for the following transcripts; Collagen I, Collagen III, Elastin, FXIII-A, TG2, MMP-2, MMP-9, MMP-12, αSMA, JNK1, c-Jun, Src, Sek1, ATF2, Lysyl Oxidase, β-actin, RPL32 (all primer sequences are described in 8.2).

2.17 Reverse Transcription

The resulting mRNA was reverse transcribed to cDNA using the High Capacity Reverse Transcription Kit (ThermoFisher Scientific). This uses a recombinant form of the Moloney mouse leukaemia virus reverse transcriptase to generate single stranded complementary DNA (cDNA) from single stranded RNA molecules. The cDNA produced was stored at -80 ^{o}C until required for real time PCR (qPCR).

2.18 Quantitative PCR

Real time quantitative polymerase chain reaction (qPCR) was used both for specialised genotyping (i.e. PF4-cre copy number) and for measurement of mRNA levels in tissue.

qPCR works on the principle that PCR is an exponential process, i.e. each cycle results in a doubling of the DNA product concentration (under optimal conditions). Therefore, a greater amount of input DNA produces more reaction product (and therefore more detected fluorescence). With Sybr Green detection, the point at which the fluorescence breaks through the background and begins exponential amplification, the Ct or crossing point, is reported.

The primers used in qPCR are designed to have an optimal annealing temperature of approximately 60^{o}C, this allowed multiple primer pairs to be run on the same reaction plate thereby improving throughput.

To detect whether or not the catalytic exon was present in the mature FXIII-A mRNA and determine the abundance of other gene transcripts, quantitative PCR was carried out with samples run in duplicate. The cycling conditions used were; 95 ^{o}C for 10 min, 45 cycles of 95 ^{o}C for 10 s, 60 ^{o}C for 1 min, followed by a melting curve to ensure a single product was amplified.

The first stage of processing the results from a qPCR assay involves normalising the determined Ct value for a target gene to the Ct of a housekeeper gene (i.e. a gene that does not vary its expression dependent on the experimental conditions). Typically, qPCR studies have relied upon the use of glyceraldehyde 3-phosphate dehydrogenase (GAPDH) as the housekeeper however, reports in the literature have suggested that this gene may show substantial variation within mouse tissues (Szabo et al., 2004; Barber et al., 2005). To combat this, other researchers have advocated for the use of multiple housekeeper genes, and the geometric mean of these genes used as the normaliser value (Thellin et al., 1999; Vandesompele et al., 2002).

Testing of mouse aortic tissue samples from our experimental genotypes by qPCR showed that the housekeeper genes β-actin (a cytoskeletal protein) and ribosomal protein L32 (RPL32) (a protein component of the 60S subunit of the ribosome) showed little variation between the genotype groups. For β-actin the average Ct was 26.69 +/- 0.31 and for RPL32 the average Ct was 24.61 +/- 0.07 (Figure 2-7). All qPCR assays of mRNA expression described in this

thesis used the geometric mean of β-actin and RPL32 to normalise all target genes.

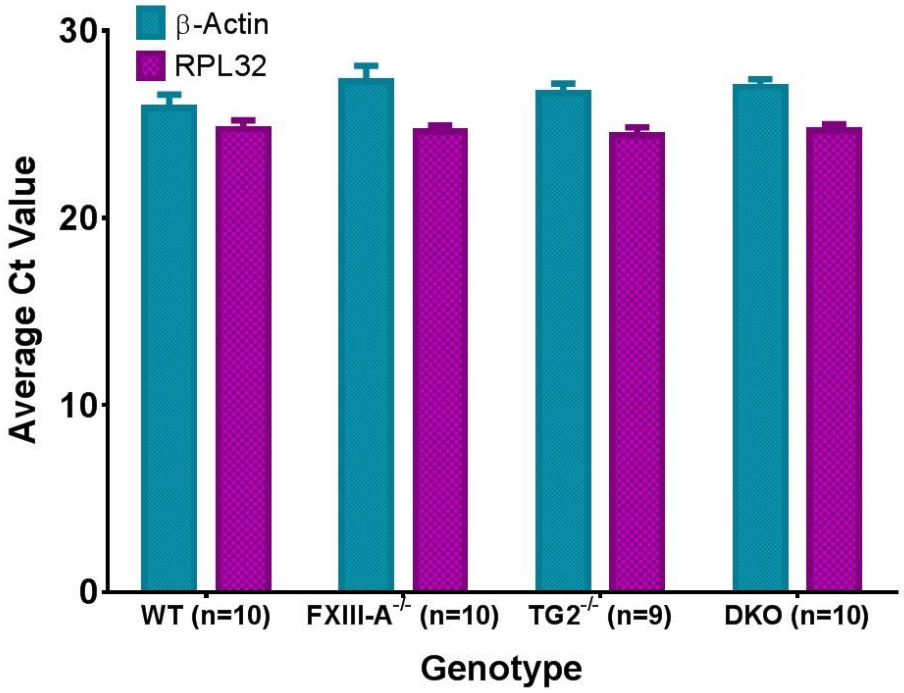

Figure 2-7 – Testing of qPCR housekeeper genes

The average Ct value (mean +/- SEM) of the housekeepers' β-actin and RPL32 across wildtype and global transglutaminase knockout groups.

The results (Ct values) generated were manipulated using the Livak method. This method calculates the exponential amount of DNA product produced from the Ct value by first subtracting the mean of the reference genes from the target gene Ct (giving the delta Ct, ΔCt), then transforming the normalised ΔCt by calculating $2^{-\Delta Ct}$ which converts the logarithmic ΔCt value into linear space. All results are shown as normalised to the geometric mean of the housekeeper genes β-actin and RPL32 and are depicted as the group mean +/- 95% confidence interval. To calculate the significance of the results, groups were compared to the wildtype by 2-way ANOVA and if significant by ANOVA then compared by Sidak's multiple comparisons method.

2.19 Quantification of Fractional Genomic Recombination

To enable measurement of the proportion of recombined floxed to unrecombined floxed FXIII-A alleles, an assay was established based on real time PCR. Utilising the FXIII-A multiplex genotyping primers in separate reactions, 300 ng of genomic DNA extracted organs (as described in 2.10) was mixed with 500 nM of each primer and 10 µL of the Roche LightCycler 480 SYBR Green I Master Mix in a total volume of 20 µL. The reaction conditions used were; 95 ^{o}C for 10 min, 45 cycles of 95 ^{o}C for 20 s, 63 ^{o}C for 20 s and 72 ^{o}C for 45 s, followed by a melting curve from 65 ^{o}C to 95 ^{o}C. The reactions were carried out in quadruplicate and normalised to an artificial 50% deletion reference which was run at the same time. This reference was made by mixing genomic DNA from a FXIII-A$^{flox/flox}$ mouse 1:1 with genomic DNA from a FXIII-A$^{-/-}$ mouse. Each sample Ct was subtracted from the respective 50% reference and the amount of product calculated using the Livak 2^{-Ct} method. The percentage of recombination in the sample was calculated by the following equation:

$$\%\ Recombination = \frac{Amount\ of\ recombined\ flox}{(Amount\ of\ recombined\ flox + Amount\ of\ unrecombined\ flox)}$$

2.20 Bicinchoninic Acid Assay

The bicinchoninic acid (BCA) assay was performed as per the manufacturer's recommended method (Sigma-Aldrich). The BCA assay relies on two reactions; the first is protein peptide bonds reducing Cu^{2+} ions in copper(II) sulphate to Cu^{+} and this is followed by chelation of these Cu^{+} ions by the bicinchoninic acid at a 1:2 molar ratio. The amount of Cu^{+} ions reduced is

proportional to the amount of protein present in solution and is detected by the bicinchoninic acid:Cu^{+} complex which absorbs light at 562 nm.

An appropriate volume of sample (up to a maximum of 25 µL) was added to a single well of a 96-well plate (Greiner) in duplicate. A standard curve was run on each plate made in duplicate, consisting of the following concentrations diluted from a 2 mg/mL stock of BSA (0, 25, 125, 250, 500, 750, 1000, 1500, 2000 µg/mL). To each well 200 µL of 50:1 mixed bicinchoninic acid:copper (II) sulphate solution was added and mixed for 30 s on a plate shaker. The plate was incubated at 37 ^{o}C for 30 min and the absorbance of each well read at 490 nm on an ELx808 (BioTek) plate reader. The values were then imported into Microsoft Excel and sorted by sample ID, duplicates were averaged and the blank subtracted for each average. A standard curve was plotted using the concentration in µg/mL as the x-axis and absorbance at 490 nm as the y-axis. The equation of the line ($y = mx + c$) was rearranged and used to calculate the concentration (x) of the unknown samples, $x = \frac{(y-c)}{m}$.

2.21 SDS-PAGE

The protein concentration was determined in each sample to be run by adding 25 µL of cleared lysate in duplicate to a microwell plate and a BCA assay carried out as per 2.20 above.

The required amount of protein per sample was chemically reduced and denatured by addition to a final concentration of 50 mM DTT and 1x SDS loading buffer (ThermoFisher Scientific) in a total volume of 20 µL. The samples were then heated to 70 ^{o}C for 10 min and 20 µL loaded per well into a 12-well 4-12% acrylamide gradient Novex bis-tris gels (ThermoFisher Scientific) along with 5 µL of Precision Plus Protein WesternC pre-stained

molecular weight marker (Bio-Rad). The gel was loaded into a Novex Mini Cell electrophoresis system (ThermoFisher Scientific) and the tank filled with 800 mL of 1x MOPS running buffer (ThermoFisher Scientific) and connected to a Powerpac Basic power supply (Bio-Rad) for 1 h at 160 V.

The electrophoresed gels were either further processed by western blotting or post-stained with Coomassie blue (45% methanol, 10% glacial acetic acid, 45% ultrapure water and 3 g/L Coomassie Brilliant Blue R250) for 1 h at room temperature with shaking. This was followed by 2 h of destaining (20% methanol, 10% glacial acetic acid, 70% ultrapure water) at room temperature with shaking. The gels were imaged post-stain on a G:Box imager (Syngene) using a white UV blocking screen.

2.22 MAPK Signalling in VSMCs

The VSMCs from individual mouse aortas were isolated and grown as described in 2.13.1.2 and on day 5 of culture split at a ratio of 1 in 4 into 2 wells of a 12-well plate. Standard culture conditions were maintained for a further 5 days until ~80% confluency. The media was removed and the cells washed twice with ice cold PBS before harvesting for gene expression or protein expression analysis.

2.22.1 Immunocytochemistry

The VSMCs seeded on 6 mm glass coverslips were first washed with sterile PBS, fixed by incubation in 3.7% paraformaldehyde for 10 min at room temperature and washed three times in PBS to remove the remaining PFA. Cell permeabilisation was carried out by immersing coverslips in PBS containing 0.2% Triton X-100 for 2 min at room temperature followed by two washes in PBS to remove the detergent. To reduce off-target staining

coverslips were incubated in 5% BSA for 30 min at room temperature. The primary antibody was diluted to its working concentration (as per 8.3 below) in 3% BSA and 125 µL of this solution added to each coverslip and incubated at room temperature (in the dark if fluorescent) for 2 h. Coverslips were washed 3 times in PBS for 10 min per wash; 5 µL of rhodamine labelled Phalloidin (ThermoFisher Scientific) in 200 µL of PBS was added to one of the washes if F-actin was to be visualised. To a frosted microscopy slide, a single drop of Vectashield soft-set mountant containing DAPI (Vectorlabs) was added and the coverslip, cell side down, placed on top. The slide was sealed with clear nail polish and left at room temperature for a minimum of 2 h to set before imaging.

The imaging of the slides was performed on a Zeiss LSM880 inverted confocal microscope using a 40x/1.4 oil Plan-Neofluar objective. Image analysis and processing was carried out using ImageJ v1.47 (NIH, USA).

2.22.2 SDS-PAGE of Cell Lysates

The cultured cells (from 2.13.1.2 above) were lysed in 150 µL of radio-immunoprecipitation assay (RIPA) buffer supplemented with a non-covalent protease and phosphatase inhibitor cocktail (Sigma-Aldrich) for 30 min at 4 ^{o}C on a shaking platform. The lysate was aspirated into separate 1.7 mL eppendorf tubes and centrifuged at 14000 xg for 30 min at 4 ^{o}C to pellet any insoluble material.

The protein concentration was determined in each sample by adding 25 µL of cleared lysate in duplicate to a microwell plate and a BCA assay carried out as per 2.20 above.

Fifteen micrograms of protein per sample was reduced and denatured by addition of 1x SDS reducing buffer and 1x (final concentration) SDS loading buffer (ThermoFisher Scientific) in a total volume of 60 µL. The samples were then heated to 70 ^{o}C for 10 min and 30 µL loaded per well into two single wells across two 12 well 4-12% Novex bis-tris gel (ThermoFisher Scientific) along with 5 µL of Precision Plus Protein WesternC pre-stained molecular weight marker (Bio-Rad). The two gels were loaded into a Novex Mini Cell electrophoresis system (ThermoFisher Scientific) and the tank filled with 800 mL of 1x MOPS running buffer (ThermoFisher Scientific) and connected to a Powerpac Basic power supply (Bio-Rad) for 1 h at 160 V.

2.22.3 Western Blotting of MAPK Pathway Antigens

After electrophoresis, the gel was transferred to a blotting cassette containing a 7 x 8.4 cm piece of methanol activated PVDF membrane placed between two pieces of blotting filter paper and two sponges which were soaked in Towbin transfer buffer (25 mM Tris base, 192 mM glycine, 20% v/v methanol, 0.1% SDS). A blotting tank containing the assembled cassettes was filled with 800 mL of transfer buffer and electrophoresis carried out at 100 V for 60 min.

The transfer was confirmed by presence of the prestained marker on the membrane. Each membrane was placed into a 50 mL falcon tube with the protein side facing into the tube and 5 mL of 5% BSA in TBS-T (19 mM Tris base (pH 7.4), 137 mM NaCl, 2.7 mM KCl, 0.1% Tween-20) added for 1 h with continuous rolling to block the membrane. The blocking solution was poured off and replaced with 3 mL of 5% BSA in TBS-T containing the primary antibody as per 8.3 and incubated overnight (16 h) at 4 ^{o}C with continuous rolling.

The membranes were washed 3 times with 5 mL TBS-T for 15 min per wash and the horseradish peroxidase conjugated secondary antibodies (as per 8.3 below) diluted in 5 mL of milk solution (1.25 g milk powder in 25 mL TBS-T) per membrane. The secondary incubation was carried out at room temperature for 1 h with constant rolling. The membrane was again washed three times in 5 mL of TBS-T for 15 min per wash.

The blots were visualised using the Clarity Western ECL blotting substrate (Bio-Rad) whereby 500 µL of the substrate was mixed with 500 µL of the enhancer solution and applied to the membrane which was placed between two acetate sheets. The membrane was incubated for 5 min before imaging on a G:Box (Syngene) at 428 nm.

After imaging, the membranes were stripped by incubation in 5 mL stripping buffer (200 mM glycine (pH 2.2), 0.1% SDS, 1% Tween-20) for 20 min with replacement of the buffer at 10 min, followed by two 10 min washes in PBS and two 5 min washes in TBS-T. The membranes were then blocked as before and probed for β-actin to use as a normaliser for densitometry.

Files were saved in the TIFF and proprietary SGD formats. Band densities were calculated by the inbuilt software using the ladder to define the size of the bands and the densities of the bands of interest were normalised to the β-actin density for each lane.

2.22.4 Calphostin C

For experiments using calphostin C, the drug was dissolved into 100% DMSO to make a 1000x stock and added to the cell media at 1x concentration (0.1% DMSO final concentration). Calphostin C mediated apoptosis was initiated by

illumination of the culture plates with an LED lamp. The control cells received the drug but no light treatment.

2.22.5 JNK Activity Assay

VSMCs cultured in 12-well plates using the same conditions described in 2.13.1.2 above were harvested by first washing the cells in ice cold PBS followed by 100 µL of cell lysis buffer containing 1% Triton X-100 (Cell Signalling Technology) on ice for 30 min. Lysates were centrifuged at 14000 xg for 10 min at 4 ^{o}C and the supernatant transferred to a new tube. 10 µL of cleared lysate was assayed for protein concentration using the BCA method described in 2.20 above. JNK activity was measured using the SAPK/JNK nonradioactive kinase activity assay kit (Cell Signalling Technology) following the manufacturer's recommended protocol.

Twenty micrograms of protein in 200 µL of lysis buffer was immunoprecipitated by incubation with 10 µL of immobilised phospho-SAPK/JNK (Thr183/Tyr185) rabbit mAb bead slurry overnight at 4 ^{o}C with gentle agitation. The cell lysate/slurry mix was centrifuged at 14000 xg for 30 s at 4 ^{o}C and the supernatant removed carefully without disturbing the pellet. The pellet was washed twice with 500 µL of cell lysis buffer and twice with 500 µL of kinase buffer with centrifugation between steps.

The kinase assay uses the precipitated phospho-JNK to catalyse the phosphorylation of a recombinant truncated form of c-Jun (residues 1-89) in an ATP-dependent reaction.

The pellet was resuspended in 50 µL of kinase buffer supplemented with 200 µM ATP and 1 µL of c-Jun fusion protein (Cell Signalling Technology). The reaction was allowed to proceed for 30 min at 30 ^{o}C and was terminated by

the addition of 4x SDS loading buffer containing DTT (final concentration: 1x loading buffer, 50 mM DTT).

Activity was measured by electrophoretic SDS-PAGE separation followed by blotting the reaction mixture on a PVDF membrane as described in 2.22.3 above and probing the membrane with a rabbit anti-phospho-c-Jun (Ser63) antibody. The image files were saved in the TIFF format and imported into ImageJ for densitometry analysis. The density of the resulting band was directly proportional to the activity of JNK in the sample.

2.22.6 In situ Transglutaminase Activity Determination

In order to assay cellular transglutaminase activity, cultured vascular smooth muscle cells were treated with 2 mM 5-(biotinamido)pentylamine (BPA) for 1 h before addition of the apoptosis-inducing agent calphostin C at 100 nM (0.1% DMSO) final concentration. Following treatment, the cells were harvested in RIPA buffer containing proteinase inhibitors for 2 h following calphostin C addition and a BCA assay performed as per 2.20 above to calculate the total protein concentration.

Once activated, TG2 will begin crosslinking substrates to each other as normal but also crosslinking the competitive reporter BPA to these substrates as well. It was hoped that these BPA crosslinked intracellular substrates could be affinity purified using streptavidin conjugated beads and identified using mass spectrometry techniques.

2.22.6.1 Kinetic Activity Assay

A continuously recording activity assay for transglutaminase activity was designed based upon the FXIII-A activity assay described in 2.7 above. One microgram of total protein, harvested in 2.22.6 above, was diluted in 50 µL of

coating buffer (TBS, pH 7.4) and applied to a 96-well Nunc Maxisorp plate in duplicate, overnight at 4 ^{o}C. Two hundred microlitres of blocking buffer (1% BSA in TBS) was added to each well and incubated for 2 h at 37 ^{o}C. The contents of each well were removed by shaking the plate upside down then washed with wash buffer (1% BSA, 0.1% Tween-20 in TBS) once. To detect the biotinylated proteins coated to the well, 100 µL of 10 µg/mL alkaline phosphatase conjugated streptavidin was added and incubated at 37 ^{o}C for 1 h. The plate was then washed 4 times with 300 µL of wash buffer. It was then dried by inversion on a paper towel and colour development initiated by the addition of 100 µL of 1 mg/mL 4-nitrophenyl phosphate and the reaction followed by reading absorbance at 405 nm every 1 min for 1 h on an ELx808 spectrophotometer (Biotek). The samples were blanked to the average of the wells coated with TBS (no protein) and the mean velocity over 1 h calculated by the software. Technical replicates were averaged and standard error of the mean calculated for each genotype.

2.22.6.2 Ligand Blot of Transglutaminase Crosslinked Proteins

Five micrograms of total protein were reduced, denatured and electrophoresis performed as per 2.22.2 above. The blots were incubated with horseradish peroxidase conjugated streptavidin (see 8.3 below for antibody dilutions) for 1 h at room temperature and imaged using the Clarity Western ECL blotting substrate (Bio-Rad) on a G:Box (Syngene). The blots showed proteins that were modified by transglutaminase activity and the total density of the resulting lanes provided qualitative evidence as to overall transglutaminase activity.

2.22.7 Protein Sequence Alignment

The protein sequences of DLK (MAP3K12) from 28 sequenced species, were aligned using Clustal-Omega (Söding, 2005) and consensus protein domains highlighted. Potential TG2 crosslinking sites (QxPΦ) were identified in each animal homolog using the ExPASy ScanProsite tool (Sigrist et al., 2002).

2.23 Identification of TG2 Substrates in Apoptosis

2.23.1 Enrichment of Biotinylated Proteins

Samples tested for *in situ* transglutaminase activity in 2.22.6 above were kept and later the biotinylated proteins (i.e. proteins to which TG2 had covalently attached biotinpentylamine) were enriched by streptavidin affinity using magnetic beads.

Fifty micrograms of cell lysate were diluted to 300 µL in binding buffer (50 mM Tris-HCl, 150 mM NaCl, pH 7.5) and added to 100 µL of washed magnetic streptavidin beads (GE Healthcare). The biotinylated proteins were left to bind to the beads for 30 min at room temperature with end-over-end mixing. The beads were pulled to the side of the tube using a magnet and the liquid removed. The beads were washed three times in total with 500 µL of washing buffer (50 mM Tris-HCl, 150 mM NaCl, 2 M urea, pH 7.5), removing the liquid each time. Dry samples were then frozen at -20 ^{o}C until trypsinisation and mass spectrometry analysis.

2.23.2 Protein Identification by LC-MS

The protein identification of the precipitated samples was performed by Dr James Ault in the Mass Spectrometry Facility, Faculty of Biological Sciences, University of Leeds.

2.24 Identification of TG2 Crosslinking Partners

2.24.1 Heart Protein Fractionation

Hearts were harvested from $TG2^{+/+}$ and $TG2^{-/-}$ mice as described in 2.9 above and shaken at 1000 rpm in 5 mL of wash buffer (PBS, 25 mM EDTA and 50 µL of 100x MS-SAFE proteinase and phosphatase inhibitors (Sigma-Aldrich) for 1 h (fraction 1; extracellular, non-covalent, non-electrostatically bound proteins). The hearts were not frozen to avoid cell rupture, and therefore contamination of extracellular fractions with intracellular proteins. Each of the hearts were sliced into 4 equal sized pieces using a scalpel and washed 3 times for 5 min each in PBS.

The heart segments were incubated for 2 h at room temperature with shaking in 5 mL salt buffer (500 mM NaCl, 10 mM Tris-base (pH 7.5), 25 mM EDTA, 50 µL 100x MS-SAFE inhibitors) and the supernatant was collected by centrifugation (14000 xg, 10 min, 4 ^{o}C) and stored at -80^{o}C (fraction 2; extracellular, non-covalent, electrostatically bound proteins). The tissue was washed 3 times in 5 mL salt buffer followed by 3 times in 5 mL distilled water.

The heart pellet was decellularised at room temperature with shaking in 5 mL of SDS buffer (0.5% w/v sodium dodecyl sulphate, 0.5% w/v sodium deoxycholate, 10 mM Tris-base (pH 7.5), 25 mM EDTA, 50 µL 100x MS-SAFE inhibitors) for 72 h and the buffer replaced at 36 h. The supernatant was collected by centrifugation (14000 xg, 10 min, 4 ^{o}C) and stored at -80^{o}C (fraction 3; intracellular protein). The remaining tissue (insoluble ECM) was washed 3 times with 5 mL of distilled water to remove any residual detergent.

Insoluble elastin was acid extracted by boiling (95 ^{o}C in a water bath) the ECM in 5 mL of 0.25 M oxalic acid for 2 h. Oxalic acid breaks desmosine-

isodesmosine isopeptide bonds with comparable kinetics and specificity to the enzyme pancreatic elastase (Partridge et al., 1955) generating the soluble product alpha-elastin. After boiling, the supernatant was collected by centrifugation (14000 xg, 10 min, 4 ^{o}C) and stored at -80^{o}C (fraction 4; elastin and elastin-bound proteins).

2.25 Biochemical Assays

Biochemical measurements were made in the uninjured aortas from the various mouse genotypes.

2.25.1 Vessel Biochemistry

Snap frozen aortas, harvested as described in 2.9 above, were first dehydrated under vacuum for 1 h and weighed to ascertain the dry weight of the tissue. Before the assays, the samples were lysed for 48 h at 4^{o}C in 750 µL of lysis buffer (50 mM sodium phosphate, 50 mM NaCl, 1% Triton X-100, 0.1% SDS, pH 7.4) followed by clarification by centrifugation (14000 xg for 10 min at 4 ^{o}C).

The resulting supernatant was used for measuring intracellular protein concentration (by BCA assay), lactate dehydrogenase activity (by commercial assay) and DNA concentration (using a fluorescent intercalating dye). The remaining tissue pellet was further processed and used to measure the elastin and collagen concentration. While the intracellular assays could be carried out on every sample, the elastin and collagen assays were incompatible with each other and therefore both measures could not be made on the same tissue. The values produced from the elastin and collagen assays were normalised to an intracellular measure to allow comparison between samples and groups.

2.25.1.1 Lactate Dehydrogenase Assay

Following lysis, the lactate dehydrogenase (LDH) activity was measured by a commercial colourimetric coupled assay (Promega CytoTox 96 LDH assay). Fifty microliters of sample and an aliquot of the supplied positive control enzyme were added to wells of a 96-well plate in triplicate. These samples were incubated for 30 min at room temperature with an equal volume of LDH substrate solution. LDH converts lactate into pyruvic acid which involves reduction of the cofactor NAD^+ to NADH. The production of NADH drives a diaphorase catalysed reaction whereby iodonitro-tetrazolium violet (a tetrazolium salt) was converted to the red formazan product. After 30 min this reaction was stopped by addition of 100 µL of stop solution (1 M acetic acid) and the resulting red colour was measured by visible absorbance at 490 nm on an ELx808 plate reader (BioTek). The resulting value was therefore proportional to the starting amount of LDH in the sample.

2.25.1.2 DNA Assay

After lysis, double stranded genomic DNA content was determined by binding of the fluorescent intercalating dye, Sybr Green I. Ten microlitres of sample was added to a 96-well plate in triplicate along with 200 µL of assay buffer (50 mM sodium phosphate, 2 M NaCl, pH 7.4) supplemented with a 1:20000 dilution of Sybr Green I gel stain (10000x concentrate, ThermoFisher Scientific). The samples were incubated for 2 h at room temperature in the dark. Fluorescence intensity was measured on a Varioskan fluorescence plate reader (ThermoFisher Scientific) with the following monochromator settings; 493 nm excitation, 530 nm emission, 12 nm bandwidth. The DNA concentrations were calculated by comparison with a gDNA standard curve (derived from mouse spleen) from 0 ng to 1000 ng.

2.25.1.3 Elastin Assay

Mice were perfused with PBS and aortas excised as in 2.9 above. In order to quantify the concentration of elastin present in the extracellular space, the aortas were boiled in 750 µL of 0.25 M oxalic acid for 3 h. The oxalic acid was replaced every 1 h and the supernatant (2.25 mL total) kept for analysis. The oxalic acid converts insoluble elastin fibres into soluble α-elastin by chemically cleaving the desmosine-isodesmosine crosslinks that hold the elastin polymer together. The amount of α-elastin present in each sample was quantified using the Fastin elastin assay kit (Biocolor) following the manufacturer's recommendations. Two hundred and fifty microlitres of oxalic acid treated aorta sample was run in duplicate alongside an 8 point (0, 15, 30, 45, 60, 75, 90 and 100 µg) α-elastin standard curve. All assays and replicates were carried out individually in 1.7 mL eppendorf tubes and the final coloured sample transferred to a 96-well plate and the absorbance of each well read at 490 nm using an ELx808 plate reader (BioTek). The concentration of α-elastin present in the sample was calculated by finding the equation of the straight line generated by the standard curve ($y = mx + c$).

This is rearranged to $x = \frac{(y-c)}{m}$ and the absorbance of the unknown sample (y) used to calculate the concentration (x).

2.25.1.4 Collagen Assay

The collagen content of harvested aortas was assayed following collagen fibre solubilisation by enzymatic treatment with 750 µL of 0.1 mg/mL Pepsin in 0.5 M acetic acid overnight at 4 ^{o}C. The enzymatic digestion of pepsin assists in cleaving the non-helical ends of the collagen molecules (known as telopeptides) which act as intermolecular crosslinks (Kiew and Don, 2013).

The concentration of solubilised collagen was measured using the Sircol collagen assay kit (Biocolor) according to the manufacturer's method. One hundred microlitres of pepsin solubilised aorta was assayed in duplicate along with an 8-point standard curve covering 0 to 50 µg of collagen. Each replicate was performed in separate 1.7 mL eppendorf tubes and the processed sample transferred to a 96-well plate before reading the absorbance of each well at 490 nm on an ELx808 plate reader (Biotek). The amount of collagen present was calculated using the equation of the straight line produced by the standard curve on each plate. This equation is rearranged to $x = \frac{(y-c)}{m}$ and the absorbance of the unknown sample (y) used to calculate the concentration (x).

2.26 Clodronate Liposome (Clodrosomes)

2.26.1 Preparation of Clodrosomes

Clodrosomes were prepared following the method detailed by (Rooijen and Hendrikx, 2010) whereby the small hydrophobic cytotoxic molecule clodronate is encapsulated in a phospholipid liposome made of phosphatidylcholine and cholesterol.

One millilitre stock solutions of 100 mg/mL phosphatidylcholine (Sigma-Aldrich), 10 mg/mL cholesterol (Sigma-Aldrich) using 100% ethanol as the solvent and 250 mg/mL clodronate in distilled water were prepared in separate 1.7 mL eppendorf tubes. Into each a new 1.7 mL eppendorf tube, 215 µL of phosphatidylcholine and 200 µL cholesterol were mixed and the ethanol removed by rotary evaporation under low vacuum at 40 ^{o}C (150 rpm). The sample was then dried until a thin phospholipid film was present at the bottom of the tube.

This film was dispersed in either 1 mL of the clodronate solution (to make active clodrosomes) or 1 mL of PBS (to make inactive control liposomes) with continuous gentle rotation at room temperature. Once resolubilised, the solution was held at room temperature for 2 h followed by sonication at 55 kHz for 3 min. The suspension was kept at 4 ^{o}C overnight to allow the liposomes to form. To limit the maximum size of the liposomes the solution was filtered through a 3 mm filter (Millipore) so as to avoid any risk of embolism once intravenously injected.

The filtrate was then ultracentrifuged at 24000 xg (average force, in a Beckman MLS-50 rotor) for 60 min at 10 ^{o}C to pellet the clodrosomes, the supernatant (unincorporated clodronate) was recovered and stored at 4 ^{o}C and then reused in future preparations.

The pelleted clodrosomes were then washed twice with 1 mL of PBS and re-pelleted, and if required, labelled with the fluorescent, lipophilic, label DiI following the manufacturer's method.

2.26.2 Testing of Clodrosomes

2.26.2.1 In vitro

Bone marrow derived macrophages were labelled with 1 µg/mL Hoechst 33258 (Sigma-Aldrich) to stain the nuclei and follow apoptosis (Hoechst increases in fluorescence as the nucleus condenses) and treated with 200 µL/10 mL of culture media of the DiI-labelled clodrosome preparation. The uptake and subsequent apoptosis of the cells was followed by imaging the brightfield, DAPI and Cy3 channels every 30 s for 1 h at 20x magnification with a water objective on a fluorescence microscope (Olympus).

2.26.2.2 In vivo

Eight-week old $Mpl^{-/-}$ mice were injected intravenously via the tail vein with 100 µL of the clodrosome preparation containing 3-5 mg/mL of encapsulated clodronate. The injections were repeated 3 times per week for 2 weeks, followed by a terminal blood sample and organ harvesting as per 2.6 and 2.9 above for plasma FXIII-A activity and FXIII-A mRNA determination.

2.27 Bone Marrow Transplantation

FXIII-$A^{+/-}$ mice were rederived behind a specific pathogen free (SPF) barrier at St James' University Hospital, Leeds. These FXIII-$A^{+/-}$ mice were crossed to produce both FXIII-$A^{+/+}$ and FXIII-$A^{-/-}$ mice for use.

Seven week old female FXIII-$A^{+/+}$ or FXIII-$A^{-/-}$ recipient mice were given access only to water containing enrofloxacin (50 µg/mL) (Bayer) for seven days prior to irradiation. Following this, the mice were subjected to total body lethal irradiation (8.45 Gy). This clears the fast replicating cells of the bone marrow, opening the niches for repopulation by the donor bone marrow cells.

Bone marrow from male donor mice was isolated by harvesting the femur bones under terminal anaesthesia. The bone marrow was extracted from the bones as per the method described in 2.26 above under sterile conditions. The cells were counted using a haemocytometer and $1x10^6$ cells/mL were injected via the tail vein into the irradiated recipients 24 h after ablation. The recipient mice were left to recover and to allow the engraftment to take place for 10 weeks.

Following this, blood and organs were harvested as per 2.6 and 2.9 above for plasma and platelet FXIII-A activity, FXIII-A mRNA level and FXIII-A genotype determination.

2.28 Rotational Thromboelastometry

Whole blood samples were taken from mice of the following genotypes; $FXIII^{+/+}$, $CD11b\text{-}cre^{+}.flox/flox$, $FXIII^{+/-}$, $PF4\text{-}cre^{+}.flox/flox$, $CD11b\text{-}cre^{+}.PF4\text{-}cre^{+}.flox/flox$, $FXIII^{-/-}$ and $Mpl^{-/-}$. Blood was drawn through the inferior *vena cava* as described in 2.6 above and clotting was inhibited by the addition of 10% v/v 0.1 M sodium citrate and the samples were kept on ice until use.

Rotational thromboelastometry (ROTEM) was performed on a ROTEM delta analyser (ROTEM.de). This technique gives a quantitative value to clot formation (and clot lysis if a thrombolytic agent is added). The system uses a cup and pin which is connected to an optical detector system. The rotational torque is transferred through the pin into the clot. As the fibrin clot forms, the impedance of rotation is detected using a laser and plotted as a value of amplitude in millimetres (mm). The greater the amplitude value, the more 'stiff' the clot (Luddington, 2005).

For all assays the INTEM protocol - which activates clotting through the intrinsic (contact activation) pathway - was utilised.

One hundred and five microlitres of well mixed whole blood was pipetted into a mini-cup. The sample was recalcified by addition of 7 µL of 0.2 M $CaCl_2$ and then clotting was initiated by addition of 7 µL of rabbit brain thromboplastin and mixed twice by gentle pipetting. The clot was formed at 37 ^{o}C and the reaction followed for 2 h.

2.29 Carotid Injury

Eight week old mice weighing 20-30 g were anaesthetised through inhalation of Isoflurane gas and anaethesia maintained through the use of a ventiliation mask. Mouse body temperature was regulated on a warmed operating table

set to 37 ^{o}C. With the mouse laying on its back facing away from the operator the neck was shaved and an incision, approximately 0.5 cm in length made to the right of the midline in the neck. Using a dissection microscope magnifying at 6x the thymus and salivary glands were separated using blunt dissection and the right common carotid artery exposed. The artery was isolated from the surrounding tissue using blunt curved forceps. 10% (0.617 M) iron (III) chloride heptahydrate (Sigma-Aldrich) was applied to the artery, below the birfucation, using a piece of Whatman grade 2 filter paper (1mm x 2mm) and left for 3 min. Utmost care was taken to avoid application of $FeCl_3$ to other structures. After 3 min, the filter paper was removed and the area thoroughly washed with 10 mL of saline. The wound was closed using 6/0 vicryl continuous sutures and animals allowed to recover in a warmed clean cage.

At selected timepoints following clot induction, mice were reanaesthetised as previously and prepared for a laparotomy. The mice were sacrificed by exsanguination through the inferior *vena cava* followed by opening of the chest cavity and perfusion of 5 mL of saline and 5 mL of 10% buffered formalin via cardiac puncture. The right common carotid artery was excised using vanus spring scissors from below the carotid bifurcation to its origin at the branch from the aortic arch and was then wax embedded for future sectioning (as per 8.5 below).

2.30 Statistical Analysis

All of the data described in this thesis is presented as mean +/- standard error of the mean, apart from real time PCR data which is shown as mean +/- 95% confidence intervals. Statistical significance was determined by several methods and accepted when the probability of the outcome occurring by chance was less than 5% (p=0.05).

First, data sets were imported into Graphpad Prism 7 (GraphPad Software, San Diego, CA, USA), technical replicates were averaged and normality was determined by the Shapiro-Wilks test. For two group comparisons the means were compared by a Student's unpaired t-test, for multiple group comparisons of one measure one-way ANOVA was used (with Dunnett's multiple comparison correction applied) and for multiple group comparisons of more than one measure two-way ANOVA (with Dunnett's correction) was used. For ANOVA testing, multiple comparisons were only tested if the F-test indicated significant variation in the dataset. For non-continuous data (i.e. knockout breeding numbers) the chi-squared test was applied and Fisher's exact test of proportions was used for the aneurysm development data.

Chapter 3 – Characterisation of transglutaminase knockout mice in the context of cardiac fibrosis and vascular injury

3.1 Introduction

Previous publications had highlighted a protective role for FXIII-A in the development of cardiac fibrosis in male mice (Souri et al., 2008). Further to this, evidence also suggested that transglutaminase 2 can compensate for (i.e. is upregulated) in states of FXIII-A deficiency (Bakker et al., 2006).

We sought to determine if this compensatory action does indeed exist and to also characterise the roles of the two transglutaminases in states of cardiovascular disease.

To do this, mice were bred which harboured either a single deletion of the FXIII-A or the TG2 gene or a double deletion of both the FXIII-A and TG2 genes. These mice were then allowed to age for the cardiac fibrosis study after which the heart was excised under terminal anaesthesia and stained for markers of fibrosis. For experiments relating to abdominal aorta aneurysm development, mice underwent laparotomy and peri-aortic application of 0.5 M $CaCl_2$ in order to induce the AAA. These mice were then left for 6 weeks or 6 months then the aorta was harvested and used for study.

This chapter also examines a potential role for maternal and embryonic FXIII-A, but not TG2, in pregnancy.

3.2 Aims

To determine the effect of FXIII-A and TG2 deficiency on the development of cardiac fibrosis and abdominal aortic aneurysm in mice by:

1. Breeding FXIII-A and TG2 single and double knockout mice.
2. Allowing these mice to age and harvesting the heart at 8 and 21 weeks to determine the extent of fibrosis by collagen deposition and haemosiderin staining.
3. Initiating aortic aneurysm by peri-aortic application of 0.5 M $CaCl_2$ followed by harvest of the aorta at 6 weeks and 6 months post-induction.

3.3 Hypothesis

FXIII-A and TG2 individually or co-operatively influence the outcome of cardiac fibrosis and abdominal aortic aneurysm in mice.

3.4 Results

3.4.1 Flox Sequencing

To identify the LoxP sites within the FXIII-A floxed mouse and to confirm that the gene was otherwise intact, sequencing of the locus was performed on products obtained from PCR of genomic DNA isolated from spleen.

The automated sequencing results were aligned using MultAlin (Corpet, 1988) to the deduced sequence for the floxed FXIII-A gene and showed perfect agreement with the expected sequence flanking coding exon 7 as judged by the sequence of the targeting construct (Figure 3-1). Confirmation of these sequences allowed us to define the floxed allele and from this information design 3 primer strategies to genotype future offspring.

The floxed mouse was further crossed with a CMV-cre mouse to produce a *de novo* global knockout as outlined in the methods.

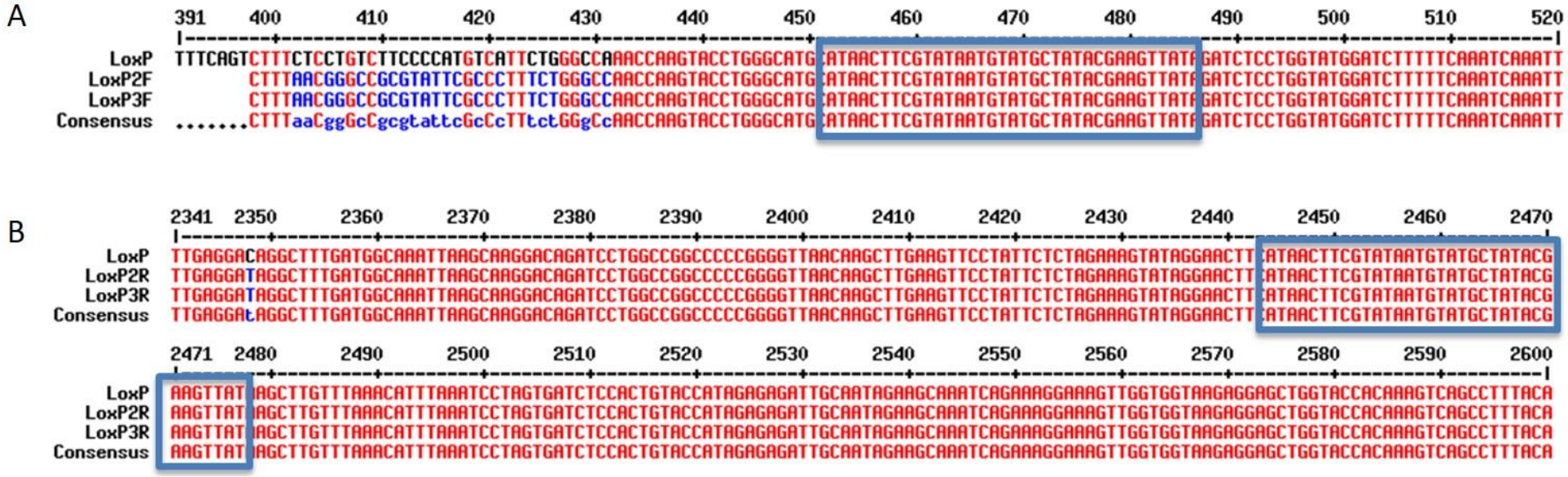

Figure 3-1 – Multiple sequence alignment of the FXIII-A floxed sequence with initial floxed breeders

The floxed FXIII-A locus was amplified by PCR from gDNA isolated from the initial FXIII-A$^{flox/flox}$ breeders, sequenced by automated Sanger sequencing and aligned to the deduced FXIII-A floxed sequence (LoxP) using MultAlin. **(A)** shows the upstream LoxP site and **(B)** shows the downstream site. The LoxP sites are highlighted by the blue boxes.

3.4.2 Mouse Breeding

Female global FXIII-A knockout C57BL/6 mice were fertile, however, it was previously reported that FXIII-A$^{-/-}$ mice are unable to survive pregnancy and die from uterine haemorrhage later on in pregnancy. This suggests that FXIII-A is critical for supporting the extensive vascular and structural remodelling that pregnancy requires. Despite this, a previous cohort of FXIII-A$^{-/-}$ mice derived from the “Dickneite” line which was obtained from Harland laboratories was able to complete pregnancy. To determine if this effect was seen in the newly derived knockout mouse, breeding was attempted in 4 FXIII-A$^{-/-}$ females derived from the new floxed mouse after discussion with CBS staff and the project licence holder. Unfortunately, this resulted in the deaths of all 4 of the females from extensive haemorrhage. To this end, FXIII-A heterozygous females were bred with FXIII-A$^{-/-}$ males in trios thus lowering the expected ratio of knockout progeny to 1 in 2.

The Mendelian frequency expected for generating FXIII-A$^{-/-}$ pups from this breeding strategy was signficantly less than expected (FXIII-A$^{-/-}$ observed 226, expected 296, p=<0.0001) which is closer to 1 in 3 than 1 in 2. Single deficiency of TG2 produced no difference in observed:expected pups (TG2$^{-/-}$ observed 80, expected 78, p=>0.99) and mice lacking both FXIII-A and TG2 showed the same reduced frequency of knockout pups produced as the FXIII-A$^{-/-}$ (DKO observed 265, expected 350, p=<0.0001). (Figure 3-3).

It is known that female C57BL/6 mice release on average 10.5 eggs per ovulation but only produce 6.2 (+/- 0.2) pups per litter (Nagasawa et al., 1973). Analysis of the litter sizes of each genotype showed a significant decrease in

litter sizes between the wildtype and FXIII-A$^{-/-}$ (6.8 vs 5.4, p=<0.01) and wildtype and DKO groups (6.8 vs 5.6, p=<0.01).

Transglutaminase deficient mice showed no gross or phenotypic abnormalities and grew at the same rate as the controls (Figure 3-2). Further to this, FXIII-A deficient mice showed no spontaneous deaths over the period of characterisation although as described in 3.5.1 some myocardial fibrosis was seen in these mice.

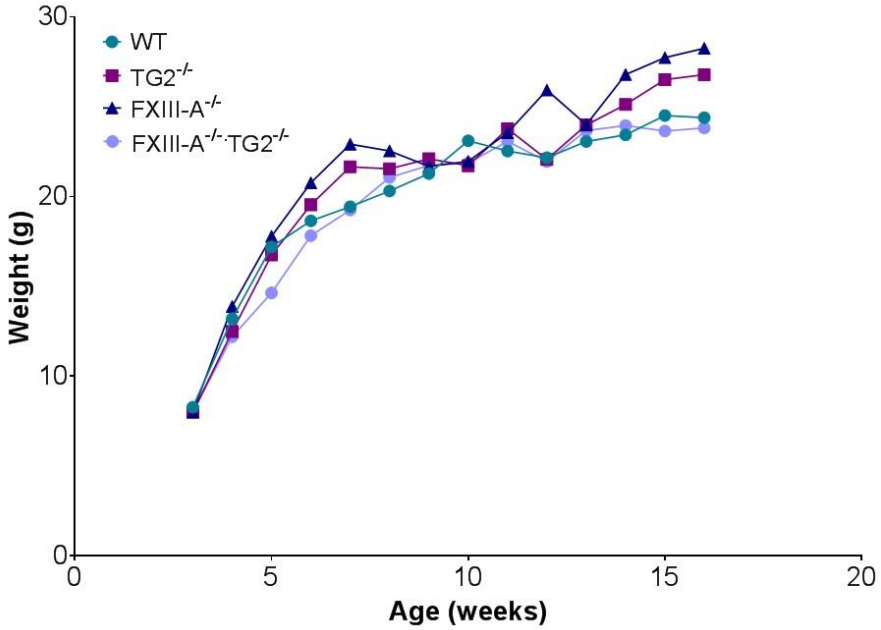

Figure 3-2 – Mouse growth curves

The global FXIII-A, TG2 and DKO mice were weighed weekly from weaning (week 3) through to week 16 (n=>4 per time point). No significant differences were seen between the weights of each genotype at any age. Data is expressed as weight in grams.

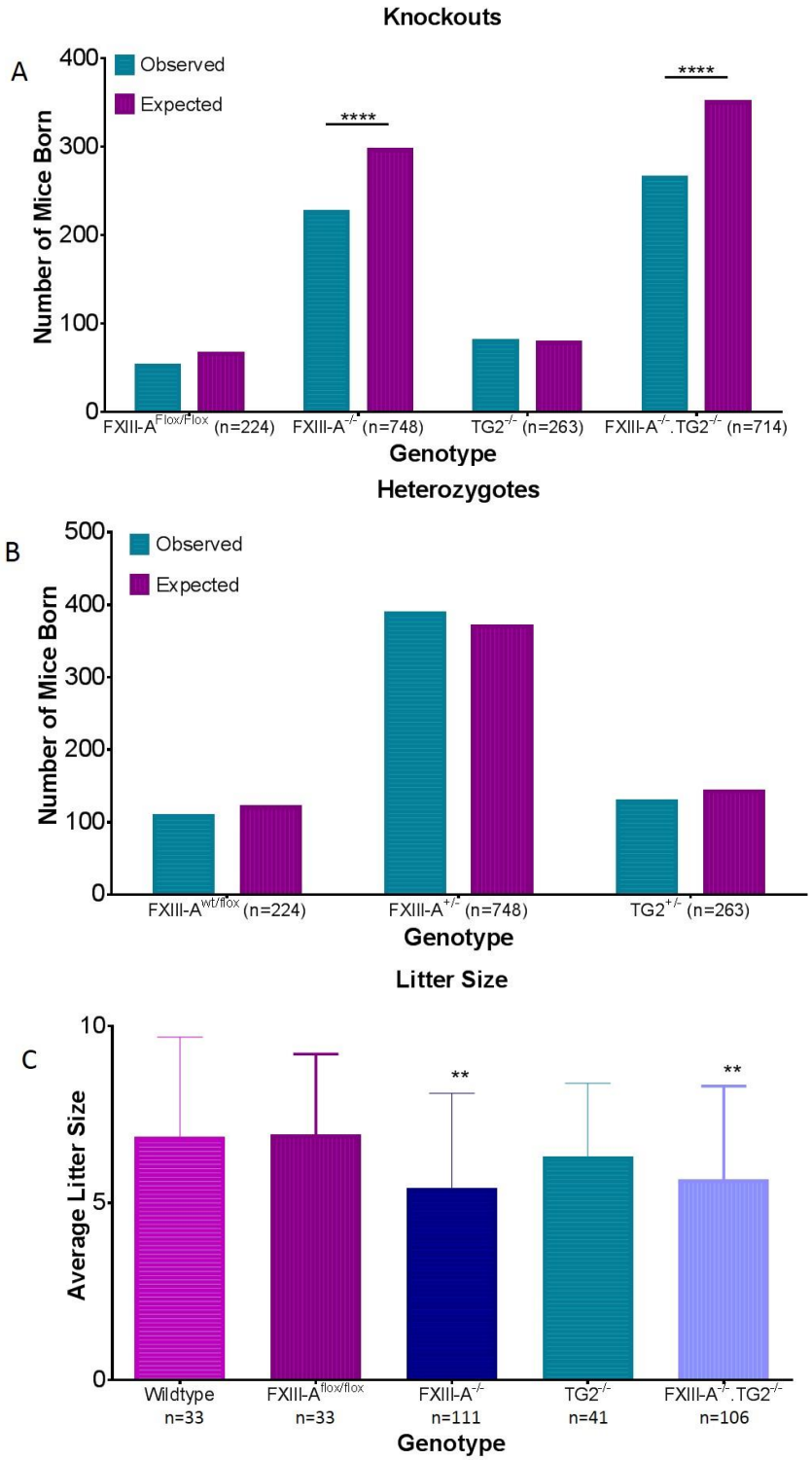

Figure 3-3 – Expected vs observed breeding and litter sizes

(A and B) Bar charts showing birth rates of mice. Significant differences were noted in the numbers of both FXIII-A$^{-/-}$ (p=0.00005) and DKO (p=0.000006) pups produced, however no differences were seen in FXIII-A$^{flox/flox}$ or TG2$^{-/-}$ pups. **(C)** Litter sizes were also significantly smaller in the FXIII-A$^{-/-}$ and DKO groups when compared to the wildtype (WT vs FXIII-A$^{-/-}$ p=<0.01) and (WT vs FXIII$^{-/-}$.TG2$^{-/-}$ p=<0.01). Data is expressed as mean +/- SEM, Chi-squared testing used for A and B and 1-way ANOVA for C to determine significance.

3.4.3 Biochemical Assays

3.4.3.1 Aortic Collagen and Elastin Content

Before any conclusions can be drawn about the effects of FXIII-A and TG2 on the vasculature following injury, the basal morphology must first be tested. To do this, measures of elastin and collagen content were seen as crucial, as were measures of cellularity which were determined by intracellular LDH and gDNA content normalised to detergent solubilised protein.

Previous reports in the literature have identified a role for FXIII-A and TG2 in the development of cardiac fibrosis (Sane et al., 2007; Souri et al., 2008) and it may be expected that if the lack of FXIII-A and/or TG2$^{-/-}$ also resulted in fibrotic changes within the vasculature that there would be a loss of cellularity and/or a relative increase in collagen deposition detected in the aortic tissue samples.

Figure 3-4A shows the results of the cellularity assays in which the LDH:protein ratio in the DKO mice was significantly reduced compared to the wildtype (mean +/- SEM) (WT 0.013 +/- 0.0009 OD/µg, DKO 0.009 +/- 0.0007 OD/µg, p=0.0124). Figure 3-4B depicts the results of the DNA:protein ratios and shows that both the FXIII A$^{-/-}$ and DKO groups have significantly reduced ratios (WT 0.003 +/- 0.0002 ng/µg, FXIII-A$^{-/-}$ 0.002 +/- 0.00017 ng/µg, DKO 0.002 +/- 0.0001, p=0.0002). These results indicate that mice lacking FXIII-A have a decreased cell mass within the aorta.

The concentrations of elastin and collagen were assayed; however, as the extraction methods used were incompatible with each other, each harvested aorta was assayed for *either* elastin or collagen, not both. This made calculating an elastin:collagen ratio difficult as it required a normalised value

for each sample (i.e. elastin:protein vs collagen:protein) to enable comparisons between genotype groups. A further issue was related to defining an error for the overall elastin:collagen ratio; methods do exist for calculating errors from non-matched data (e.g. bootstrapping) but these require sample sizes far larger than those presented here. Nevertheless, the results from these assays (Figure 3-5A&B) suggest that there are no differences in normalised aortic elastin content across the experimental genotypes but that there is a trend towards an increased normalised collagen content in the DKO group compared to the WT (WT 0.014 +/- 0.0017 µg/µg, DKO 0.017 +/- 0.0026 µg/µg) but this did not reach statistical significance. When taken together, the elastin:collagen ratios of all the experimental genotypes suggest that the DKO mice have a greater proportion of collagen in the aortic wall and that they may exhibit vascular fibrosis from an early age (Figure 3-6).

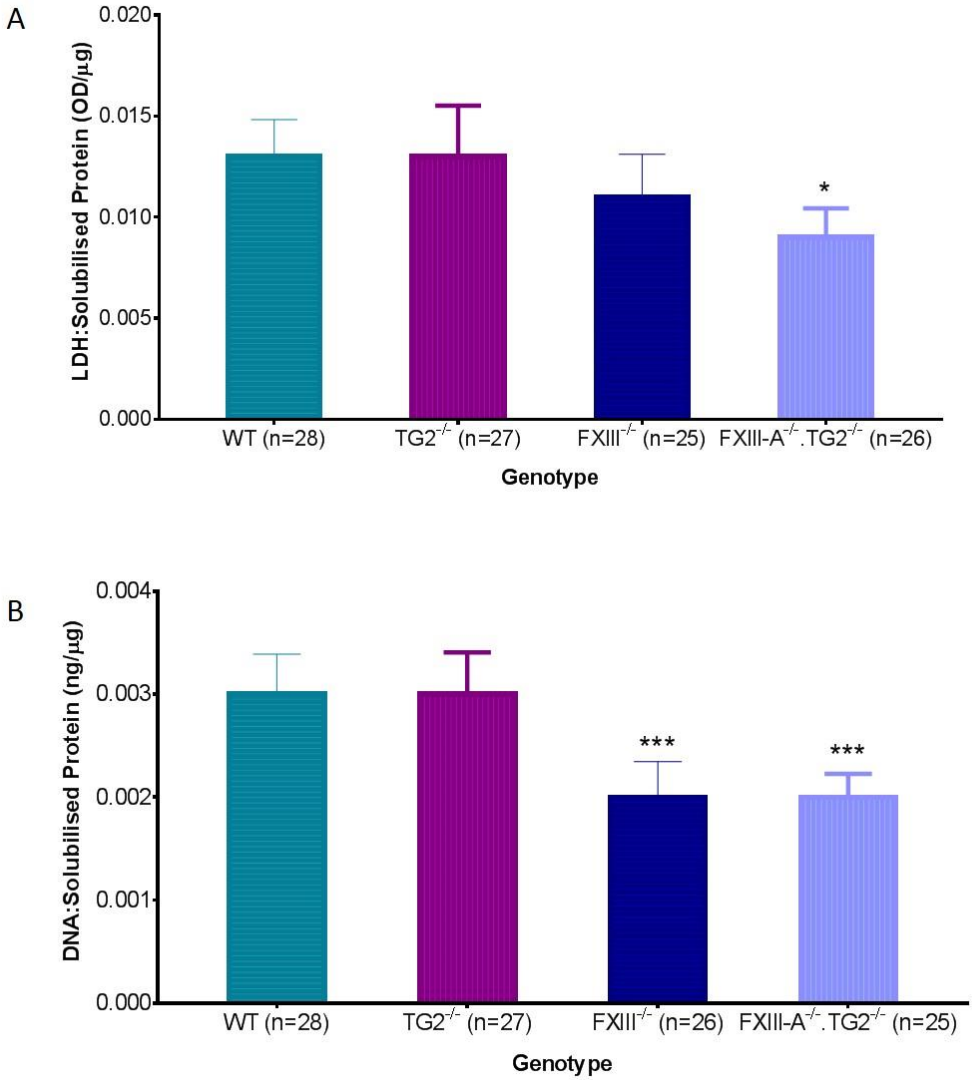

Figure 3-4 – Solubilised protein normalised LDH and DNA results

(A) Shows the aortic LDH:protein ratios (mean +/- SEM) of the experimental genotype groups. The DKO group shows a significantly decreased ratio (WT vs DKO p=0.0124). **(B)** is the aortic DNA:protein ratio and suggests that both the FXIII-$A^{-/-}$ and DKO groups have a significantly reduced ratio (WT vs FXIII-$A^{-/-}$ and WT vs DKO p=0.0002). 1-way ANOVA was used to determine significance.

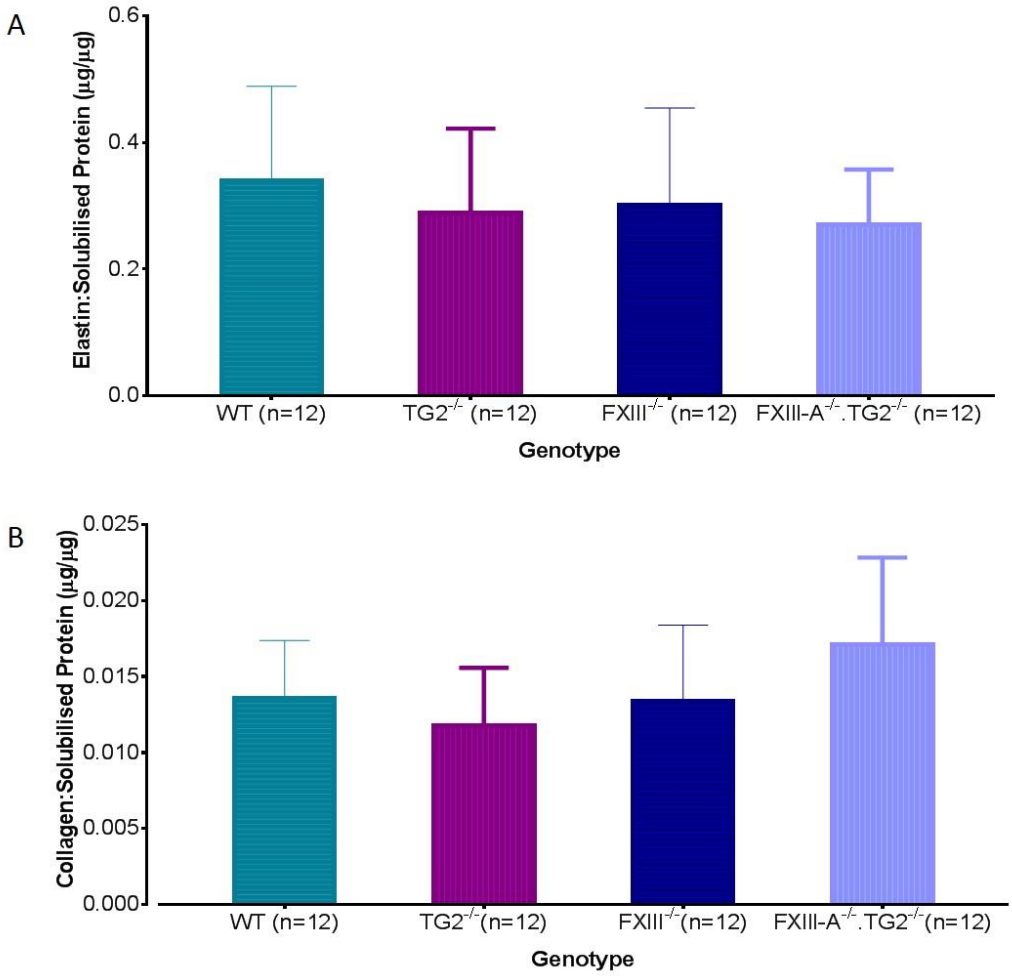

Figure 3-5 – Solubilised protein normalised aortic elastin and collagen measures

Soluble protein normalised elastin **(A)** and collagen **(B)** concentrations (mean +/- SEM) in mouse aorta. No significant difference (by 1-way ANOVA) in either elastin or collagen content was seen but there is a trend (p=0.34) towards an increased amount of collagen in the aortas of the DKO mice compared to the wildtypes.

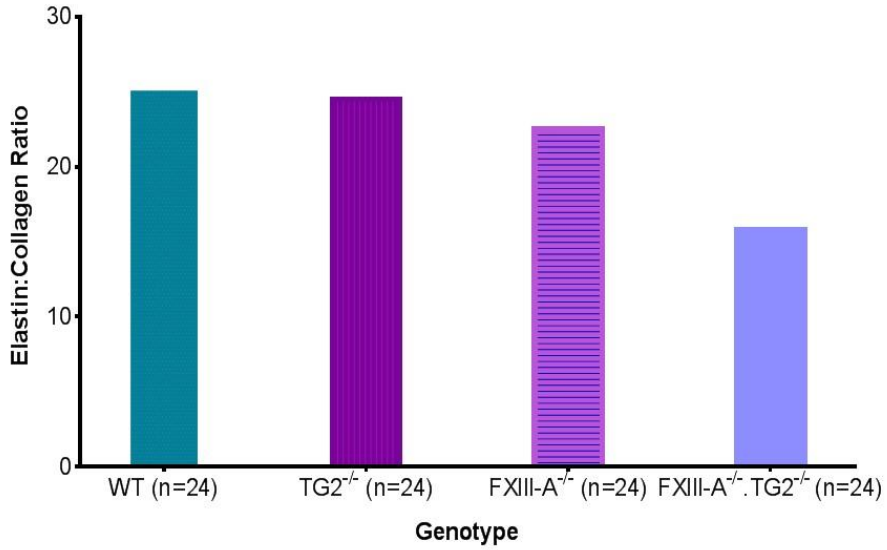

Figure 3-6 – Aortic elastin to collagen ratios

Aortic elastin:collagen ratios were calculated by dividing the collagen:protein by the elastin:protein values. This ratio illustrates the increase in collagen content in the vessel of the DKO mice and suggests that the vessels of these mice are potentially fibrotic. Data is shown as mean ratios without associated error as the methodology used did not allow sampling of both elastin and collagen content in the same mice and therefore represents non-matched data.

3.4.3.2 mRNA Measurements

3.4.3.2.1 Transglutaminase Family

As mammals code for 8 transglutaminase enzymes with closely related activities but distinct tissue expression patterns, it may be possible that if one of the family is defunct that upregulation of one or more of the others could compensate for the deficit. Real time PCR assays of transcripts of the transglutaminase family in both the aorta and heart showed that none of the transglutaminases were upregulated to compensate for the deficiency of FXIII-A (Figure 3-7 and Figure 3-8); in fact, in the aorta of the FXIII-A knockouts the TG2 mRNA was significantly decreased (2.1 vs 0.5, p=0.0001). Therefore, any phenotypes observed in these mice are not underestimated as a result of compensating transglutaminase action.

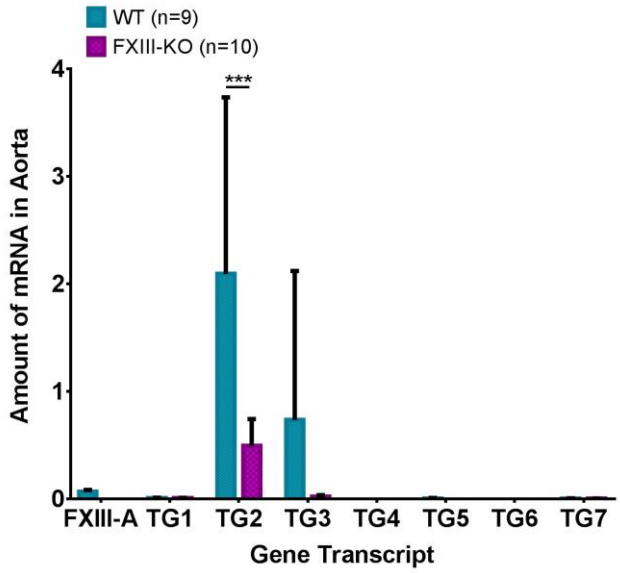

Figure 3-7 – Transglutaminase family mRNA in aorta

None of the other transglutaminases were upregulated in response to the loss of FXIII-A. The TG2 transcript shows a significant decrease in transcription in the FXIII-A knockout (WT vs TG2$^{-/-}$ p=0.0001). Data expressed as the mean +/- 95% confidence intervals and significance determined by 2-way ANOVA testing.

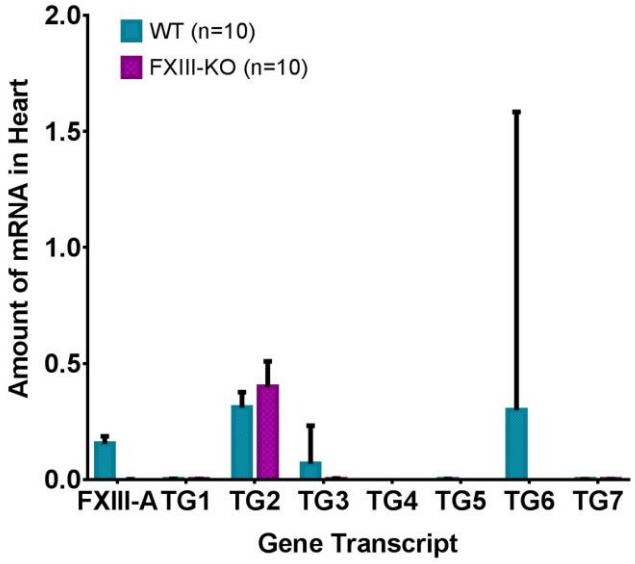

Figure 3-8 – Transglutaminase family mRNA in heart

The mRNA transcripts in the hearts of the FXIII-A$^{-/-}$ mice showed no compensatory changes in transglutaminase expression as a result of FXIII-A deficiency. Data shown as mean +/- 95% confidence intervals and 2-way ANOVA used for significance testing.

3.4.3.2.2 Basal Aortic Gene Expression

As part of determining the basal characteristics of the aorta, gene transcripts relating to ECM structural proteins, ECM degrading matrix metalloproteinases and a smooth muscle cell marker were assayed by real time PCR.

A significant decrease (>2-fold) in the alpha-smooth muscle actin transcript was seen in the $TG2^{-/-}$ mice when compared with the wildtype group (WT 68.6, $TG2^{-/-}$ 16.7, p=0.0005) but this was not replicated in the FXIII-$A^{-/-}$ or DKO groups (Figure 3-9). No difference was seen in any of the MMP genes for any of the genotype groups and of these genes, only MMP-2 was seen to be expressed in any large quantity (Ct <30) (Figure 3-10).

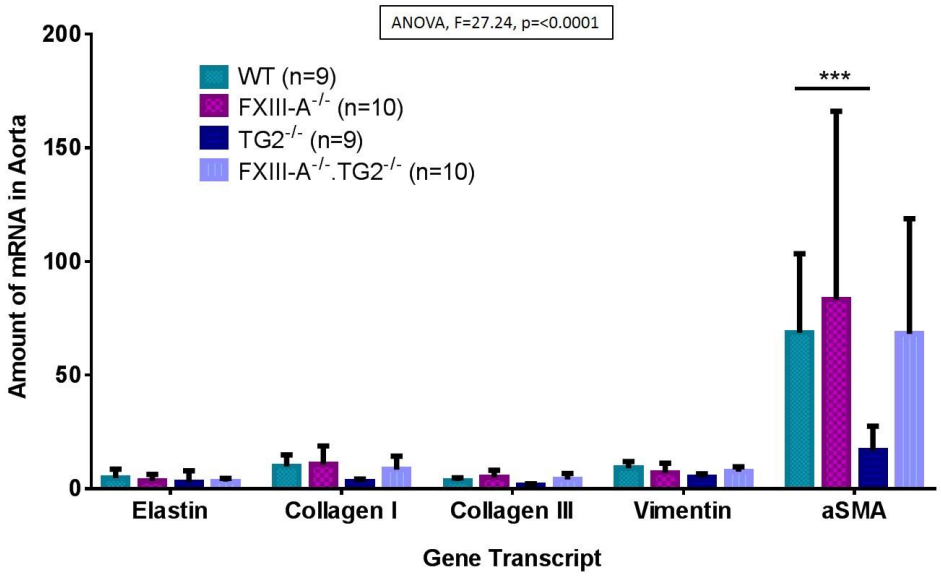

Figure 3-9 – Basal aortic structural protein expression

mRNA expression of four ECM proteins (elastin, collagen I, collagen III and vimentin) and a vascular smooth muscle cell marker was determined in basal mouse aorta. Significantly decreased mRNA amounts were found in the alpha-smooth muscle actin transcript in the $TG2^{-/-}$ group (WT vs $TG2^{-/-}$ p=0.0005). Data is shown as mean +/- 95% confidence interval and significance calculated by 2-way ANOVA.

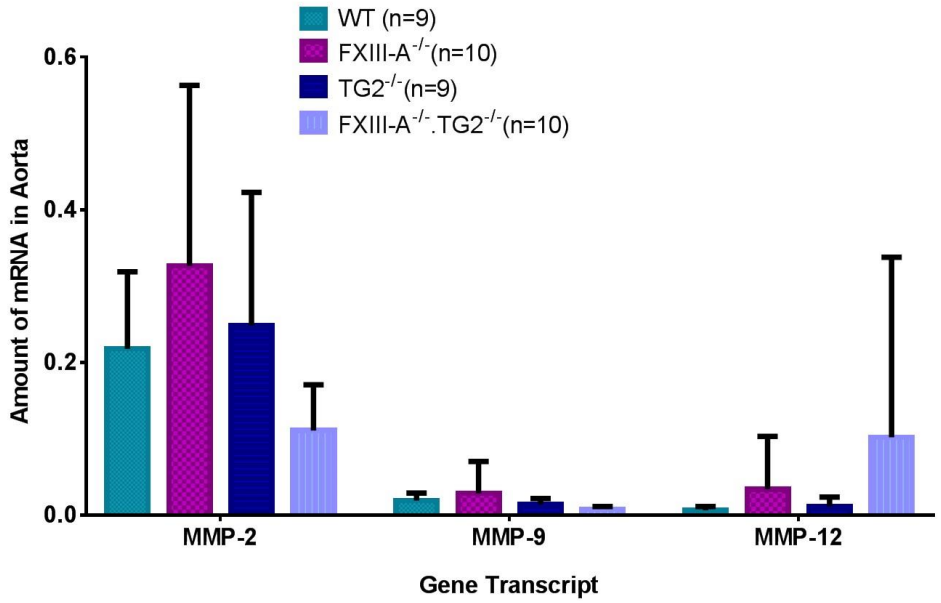

Figure 3-10 – Basal aortic expression of matrix metalloproteinases

mRNA expression of the three main matrix metalloproteinases (-2, -9 and -12) associated with a range of vascular pathologies was determined in basal mouse aortas. MMP-2 is the only gene that appears to be transcribed (Ct <30) the others are not (Ct >30). No significant difference was found in expression of any of the MMPs between the various genotype groups. Data is shown as mean +/- 95% confidence interval.

3.5 Parallel Work

Work was carried out in collaboration with other members of the group to further characterise the WT, FXIII-A$^{-/-}$, TG2$^{-/-}$ and DKO mice and the role that these genes play in the pathogenesis of vascular disorders.

3.5.1 Cardiac Fibrosis

Following the finding that the DKO mice develop spontaneous vascular fibrosis, work was carried out in collaboration with Dr Cora Beckers in our group to determine if this fibrosis was also present in the heart, a finding which has been previously seen in the literature in FXIII-A$^{-/-}$ mice (Souri et al., 2008).

To quantify the levels of cardiac fibrosis in the transglutaminase knockout mice produced above in 2.2, the amount of collagen and haemosiderin (haemoglobin degradation product) deposition was determined histochemically in sectioned tissue. This tissue was derived from mice aged 8 and 21 weeks of age which had been fed on a chow diet.

Collagen deposition was highlighted by Sirius Red staining and haemosiderin deposition by Prussian Blue staining. The proportion of stained area relative to the total tissue area was measured using ImageJ.

It was found that neither the wildtype nor the TG2$^{-/-}$ mice developed cardiac fibrosis at either time point. However, both the FXIII-A$^{-/-}$ (8 weeks 0.8 +/- 0.5% fibrotic area p=0.0001 and 21 weeks 2.4 +/- 2.3% p=<0.0001) and DKO (8 weeks 3.3 +/- 5.1% p=<0.0001 and 21 weeks 14.0 +/- 8.3% p=<0.0001) groups showed fibrotic changes, with the DKO mice showing significantly greater amounts of fibrosis than any of the other genotypes (Figure 3-11). Haemosiderin deposition in the cardiac tissue (a marker of red blood cell leakage into tissue) followed the same pattern as above whereby the DKO

mice showed significantly greater amounts of haemosiderin when compared to the wildtype at 21 weeks (WT 0.14 +/- 0.53%, DKO 0.76 +/- 0.35% p=<0.0001). This suggests that haemorrhage may be part of the pathological process which ultimately results in these (FXIII-$A^{-/-}$ and DKO) mice developing cardiac fibrosis.

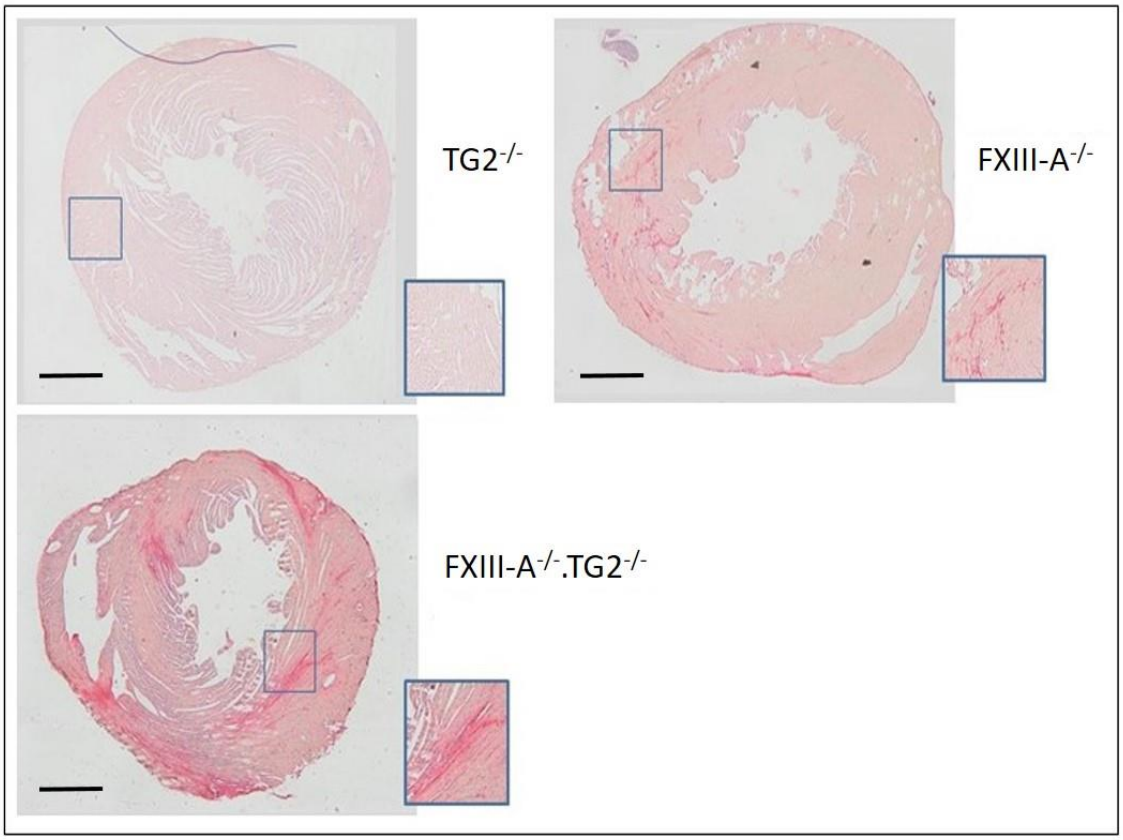

Figure 3-11 – Collagen deposition in the hearts of the knockout mice

Representative images of sections of heart tissue (4x magnification) from the single and double knockout mice (n=12). Sirius red staining was used to detect collagen deposition (dark pink). The FXIII-$A^{-/-}$ and FXIII-$A^{-/-}$.$TG2^{-/-}$ mice showed significantly greater collagen deposition compared to the control $TG2^{-/-}$ mice (p=<0.0001). Scale bar denotes 1

3.5.2 Abdominal Aortic Aneurysm

A mouse model of vascular injury was established in the group to try and determine the effect (if any) that FXIII-A and/or TG2 have in tissue repair. Abdominal aortic aneurysms were induced in 8 week old mice by peri-aortic calcium chloride application by Dr Kathryn Griffin (Figure 3-12).

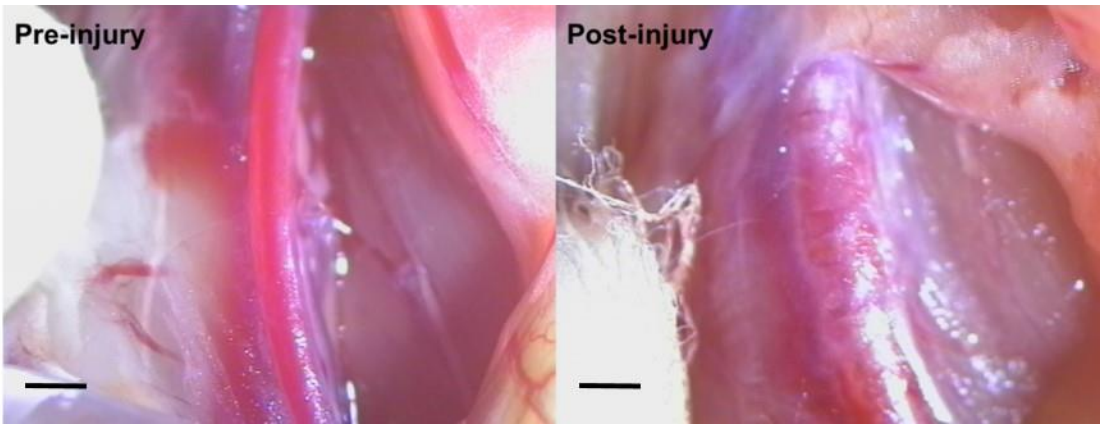

Figure 3-12 – $CaCl_2$ induced AAA development in a C57BL/6 mouse

A representative image from a C57BL/6 mouse before (left) and 6 months after (right) AAA induction with $CaCl_2$. Following injury, the artery dilates and becomes heavily calcified and inflamed. Scale bar denotes 1 mm.

A significant mortality was observed in both the FXIII-$A^{-/-}$ (41% mortality rate, 23/56 died) and DKO (62% mortality rate, 47/77 died) (FXIII-$A^{-/-}$ vs DKO p=0.01 by T-test) groups compared to the wildtype and TG2 groups which showed a far lower mortality rate (9%, 6/70 died and 7%, 6/88 died respectively) (WT vs FXIII-$A^{-/-}$ p=<0.0001) meaning that this phenomenon was not a result of the aneurysm induction procedure. The majority of the FXIII-$A^{-/-}$ and DKO mice which had died prematurely exhibited cardiac pathology or other distal morphology upon post-mortem examination. Blackened, thrombus filled atria (Figure 3-13) were found suggesting that in these animals, non-stable thrombi were produced which embolised to the heart causing sudden cardiac death.

Figure 3-13 – Post-mortem pathology of FXIII-A$^{-/-}$ and DKO mice

Representative post-mortem image of a DKO heart isolated from a mouse that had undergone a sham procedure and was found dead on post-op day 2. Blood was found in the thoracic cavity and the atrium of the heart contained a large clot.

If TG2 and FXIII-A play a big role in repair, then it would be expected that a large effect would be seen following arterial insult. Images of the aorta were taken before AAA induction and before AAA excision. I measured the aortic diameters at both time points as a blinded observer and calculated a percentage change. No significant difference was seen in aortic diameter following AAA induction with $CaCl_2$ between any of the single knockout or double knockout mice at 6 weeks post injury (Figure 3-15). However, if the animals were left for 6 months following injury (Figure 3-14) a significant increase in aortic diameter was seen in the TG2$^{-/-}$ when compared to the WT mice (WT 64% increase, TG2$^{-/-}$ 90% increase p=0.031). This finding suggests that the aneurysm had continued to develop in the TG2$^{-/-}$ mice and that TG2 is perhaps involved in repair in the later stages of the aneurysm model.

However, due to the mortality of the FXIII-A$^{-/-}$ and DKO mice, data at 6 months after injury was not available in these groups.

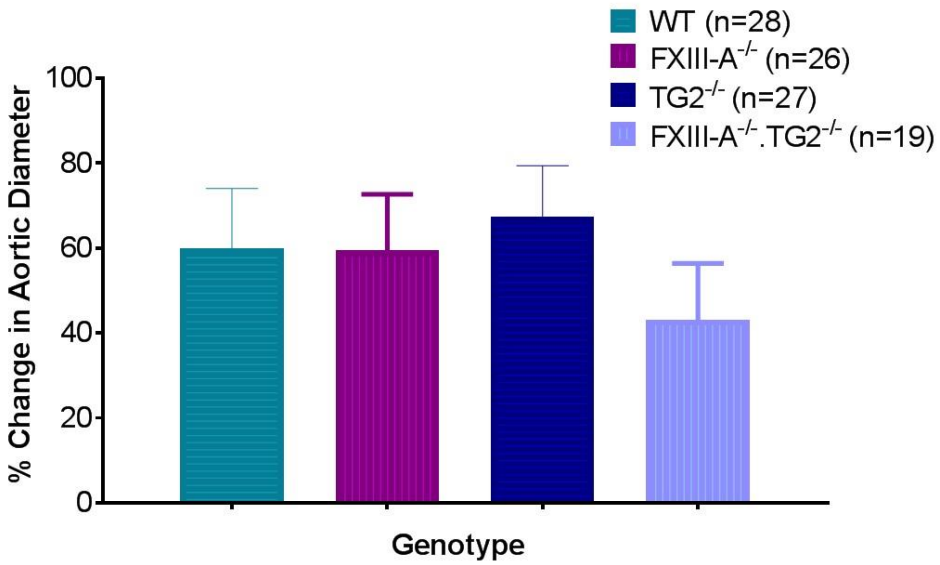

Figure 3-15 – Short term $CaCl_2$ induced AAA – change in vessel diameter

Graph shows the 6-week post-injury percentage change in aortic diameter compared to the pre-injury diameter. No significant difference (p=0.097) was seen between any of the genotype groups. Data is shown as mean +/- SEM and significance determined by 1-way ANOVA.

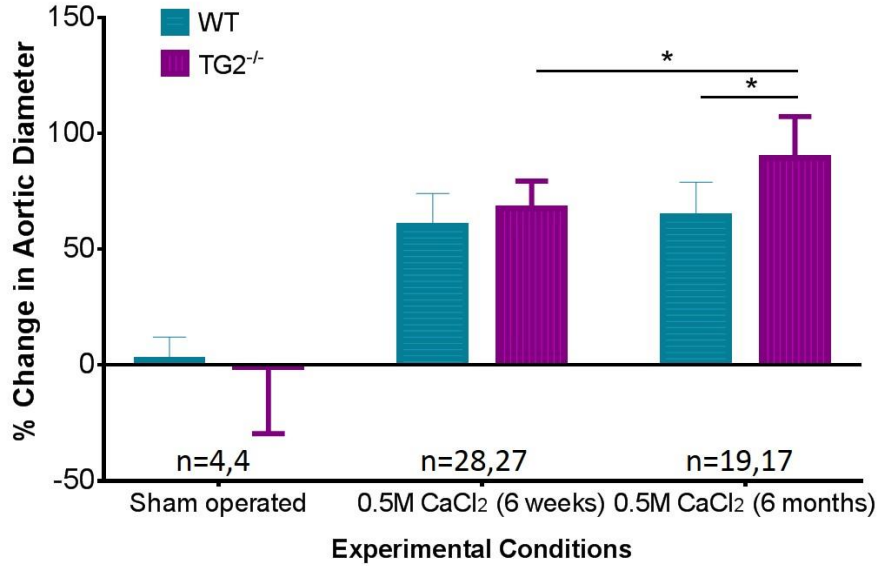

Figure 3-14 – Long term $CaCl_2$ induced AAA – change in vessel diameter

Graph shows the summary data of the sham operated, 6-week post injury and 6-month post-injury changes in aortic diameter in the wildtype and $TG2^{-/-}$ groups. Significant increases were seen in the $TG2^{-/-}$ group between 6 weeks and 6 months (p=0.025) and the WT and $TG2^{-/-}$ groups at 6 months (p=0.03). Data is presented as mean +/- SEM and 2-way ANOVA used to determine significance.

3.6 Discussion

3.6.1 Maternal FXIII-A is required for survival through pregnancy whilst embryonic FXIII-A supports foetal development

The data presented in this chapter suggests that FXIII-A is required to maintain pregnancy, as with a previous study (Koseki-Kuno et al., 2003) spontaneous haemorrhage was observed late in pregnancy in all of the FXIII-A global knockout female mice who were allowed to breed. Congenital FXIII-A deficiency also causes spontaneous miscarriage in human females (Seitz et al., 1996). These findings signify that FXIII-A plays an important (if not crucial) role in pregnancy and is perhaps required for the extensive vascular remodelling. Whether the FXIII-A involved in this process is derived from the plasma or a tissue resident cell (such as a uterine macrophage), or is a mixture of both, is unknown, however, FXIII-A supplementation therapy is known to allow FXIII-A deficient humans to complete pregnancy.

Further, FXIII-A knockout embryos stand a greater chance of death *in utero* than either FXIII-$A^{+/-}$ or FXIII-$A^{+/+}$ littermates as the number of FXIII-$A^{-/-}$ (and DKO) pups was found to be significantly lower than expectation. Previously reported evidence on this subject has suggested that in FXIII-$A^{-/-}$ embryos there is a failure of blastocyst implantation that could represent a loss of an integrin crosslinking event which is normally catalysed by FXIII-A (Illera et al., 2000).

It may be that both of these explanations are true, and that as the FXIII-$A^{-/-}$ embryos begin to implant into the uterine wall something goes awry resulting in the death of the embryo which blocks the implantation site for other embryos and produces the smaller litter sizes seen.

3.6.2 Deficiency of both TG2 and FXIII-A may cause fibrosis of both the vessel and the heart

The biochemical data presented in this chapter suggest that while the single and double knockout mice show no obvious gross phenotypic abnormalities, the DKO, and perhaps the FXIII-$A^{-/-}$, mice show signs of both cardiac and vascular fibrosis and reduced vascular cellularity. While this fibrosis does not appear to pose an issue to these mice normally, vascular injury (e.g. $CaCl_2$ application to the aorta) in the FXIII-$A^{-/-}$ mice resulted in a significant mortality rate, this mortality was further increased in the DKO mice. While this may be explained by unstable clot formation in these mice, the fact that added deficiency of TG2 produced a far worse outcome argues for a second role beyond clotting, perhaps in microvascular structure and/or repair.

The mechanism behind this spontaneous fibrosis development is unclear however, it may be a result of increased vascular leakage or permeability as both FXIII-A and TG2 have been implicated in maintaining the endothelial barrier (Noll et al., 1999; Lee et al., 2016). Further evidence for this hypothesis is provided from children undergoing open-heart surgery. It was shown by (Schroth et al., 2006) that children who showed increased pleural effusion had lower plasma FXIII-A levels than controls and when these children were given supplemental FXIII-A they showed rapidly decreased effusion for the first 24 hours after surgery.

Previous literature (Bakker et al., 2006) has shown that while there may be some compensatory action between FXIII-A and TG2, in $TG2^{-/-}$ mice there is no upregulation of FXIII-A. In this thesis, it is shown that the opposite is also true whereby in FXIII-$A^{-/-}$ mice, TG2 is not upregulated and is actually downregulated by 75%. While this finding suggests that any effects of FXIII-A

are not masked by overexpression of TG2 (or any other transglutaminase) it may be that the phenotype of the FXIII-A$^{-/-}$ mouse is exacerbated by the decrease in TG2 transcription. However, the evidence for this is provided only at the transcriptional level. While it usually holds true that an increase (or a decrease) in the amount of a specific protein associated with an increase (or decrease) in the amount of mRNA, the correlation between the two has recently been determined to only be ~40% (Vogel and Marcotte, 2012). It would therefore be important to confirm the findings of decreased enzyme levels by comparing the mRNA levels with measures of FXIII-A and TG2 protein amount by western blotting for example.

3.7 Conclusion

This chapter focusses on the characterisation of mice with either single or double deficiency of FXIII-A and TG2. We have shown that FXIII-A is crucial for maternal survival through pregnancy and is also important for embryonic survival. Further to this, there appears to be no compensatory mechanisms for upregulating the transglutaminase family genes following deletion of either FXIII-A or TG2.

Finally, loss of FXIII-A on its own produces cardiac fibrosis which is worsened by additional deficiency of FXIII-A and TG2 and insult in these mice causes significant mortality.

These findings suggest that transglutaminases may play differing roles that are site and/or context specific. With FXIII-A and TG2 aiding vessel stability in microvessels (i.e. cardiac fibrosis) and in large vessels expression of FXIII-A is perhaps destined for secretion into the circulation to maintain the plasma pool rather than being involved in repair processes.

3.8 Summary of Key Findings

- FXIII-A$^{-/-}$ and DKO pups are born at a lower rate and in smaller litter sizes than expected.

- No gene upregulation or compensation of the other transglutaminases is seen in response to knockout of FXIII-A and/or TG2.

- The FXIII-A$^{-/-}$ and DKO mice show development of spontaneous cardiac fibrosis at 8 weeks of age.

- The DKO mice showed characteristic biochemical changes of vascular fibrosis (e.g. reduced cellularity and increased collagen deposition) by 8 weeks of age (Table 3-1).

Genotype	LDH:Protein	DNA:Protein	Elastin	Collagen	Elastin:Collagen
Wildtype	---	---	---	---	---
FXIII-A$^{-/-}$	↓	↓↓↓	---	---	---
TG2$^{-/-}$	---	---	---	---	---
DKO	↓↓↓	↓↓↓	---	↑↑↑	↓↓↓

Table 3-1 - Overview of aortic biochemical data

Findings from the biochemical assays showing decreased cellularity and increased collagen deposition in the DKO mice.

- The FXIII-A$^{-/-}$ mice suffer a high mortality (41%) following injury, this mortality is further significantly increased in the DKO mice (62%) and suggests that this phenomenon is more than just a clotting defect.

Chapter 4 – Identification of the cell type that maintains the pool of plasma FXIII-A

4.1 Introduction

The conclusion from our group that the platelet is not the cellular source of plasma FXIII-A was based on blood samples from $Mpl^{-/-}$ mice imported from Professor Benjamin Kile (Walter and Eliza Hall Institute, Australia) and from in-house breeding and characterisation of the $Bcl\text{-}x^{plt20/plt20}$ mice. Both lines were previously reported by our group (Cordell et al., 2010) to have normal levels of plasma FXIII-A. To further confirm the findings in the $Mpl^{-/-}$ mice and to determine that platelet size and FXIII-A content were unchanged a new line of Mpl mice was established and characterised.

In addition, cre-lox technology was used to allow production of mouse lines where the FXIII-A gene was inactivated in specific cell types.

As macrophage-like cells in the heart had previously been seen to be expressing FXIII-A (Souri et al., 2008), as had blood monocytes (Henriksson et al., 1985; Töröcsik et al., 2005; Muszbek et al., 1985), macrophage specific cre constructs were used to resolve their role in maintaining the plasma pool. However, as monocyte/macrophages are known to be highly heterogeneous it was seen as necessary to use two independent and supposedly granulocyte/macrophage-specific promoters, CD11b and LysM.

Finally, Flt3-cre was chosen to differentiate between primitive and definitive cells and determine if one (or both) were the source of plasma FXIII-A. Flt3 is required for differentiation of adult long term HSCs into short term HSCs. The use of Flt3-cre excludes all of the haematopoietic cell-types derived from the

bone marrow from contributing to the plasma pool (by recombining the FXIII-A gene in the HSC) whilst leaving any primitive cells alone (i.e. yolk sac-derived tissue resident macrophages in the heart, aorta and brain, amongst others).

To complement the findings of the Flt3-cre mouse, bone marrow transplants were performed to determine if plasma FXIII-A could be restored by stem cell transplantation.

4.2 Aims

To find the cell responsible for maintaining and secreting plasma FXIII-A by:

1. Breeding mice with tissue specific recombination of the FXIII-A gene using cre-lox technology.
2. Determine the plasma and platelet FXIII-A levels in these mice and correlating them with tissue FXIII-A mRNA levels.
3. Establish a method to allow quantification of the extent of genomic recombination in the cre-lox crosses.
4. Perform bone marrow transplantation to determine the effect of resident macrophage turnover on the plasma FXIII-A activity.

4.3 Hypothesis

A cell type that is not the platelet maintains the circulating pool of plasma FXIII-A.

4.4 Results

4.4.1 Plasma FXIII-A Assay

Platelet depleted plasma was purified from whole mouse blood by serial centrifugation. Plasma FXIII-A activity was determined from these samples with allowance for the dilution with anticoagulant (as described in 2.7 above) in the wildtype, FXIII-A floxed, all cre-flox crosses, FXIII-A heterozygotes, FXIII-A global knockouts and Mpl knockout mice and the results are shown in Figure 4-3 below.

The FXIII-A heterozygous mouse had a residual activity of 61% which suggests that the cell that maintains the plasma pool has no way of sensing the plasma concentration and therefore has no mechanism whereby the gene can be upregulated, which validates the cre-lox approach.

Flow cytometry analysis of stained platelets from the thrombocytopenic ($Mpl^{-/-}$) mice showed them to have a platelet count of ~6% compared to a wildtype, and to have normal levels of FXIII-A (95% of wildtype). The Mpl mice also showed normal platelet sizes and showed no compensatory mechanism for storing more FXIII-A in the residual platelets meaning that the platelet cannot be the cellular source of plasma FXIII-A.

The mice in which FXIII-A deletion had been targeted to macrophages (CD11b-cre and LysM-cre) showed a residual plasma activity of 61% and 20% respectively. Despite exclusion of the platelet as the cellular source of plasma FXIII-A, the supposed megakaryocyte specific cre, PF4-cre, depleted the plasma pool of FXIII-A to a level of 18%.

Individually, CD11b-cre and PF4-cre reduced the plasma pool to 61% and 18% respectively. If taken as separate lineage-specific genes then in theory,

together they would deplete more than 100% of the plasma pool. In practice addition of both cre constructs into one mouse leaves a residual FXIII-A activity of 9% (however this is not significant over the single copy PF4-cre mouse, p=0.17). This suggests that at least 12% of the plasma pool originates from a cell line (most likely a tissue resident macrophage) expressing both platelet factor 4 and integrin alpha M (CD11b) with the remaining 9% coming from a separate PF4/CD11b-independent source.

Two copy PF4-cre mice were bred to determine whether the residual 18% activity of the single copy PF4-cre mice was a result of suboptimal expression of the PF4-cre gene. As described in 2.11 above, the PF4-cre insertion site is unknown and therefore a real time PCR approach was employed to genotype 2-copy PF4-cre mice.

Figure 4-1 is an example of the results obtained and shows that mouse genotyping could be categorised into clearly distinct groups with a 2 copy mouse showing twice the fluorescence following qPCR than a 1 copy mouse. The copy number determination is supported by running known copy number controls alongside *de novo* samples and also by knowing the parental genotypes. Genotypes were confirmed by breeding mice suggested as 2-copy with each other followed by genotyping the offspring, which should all be 2-copy. The genotype confirmed mice were then used for study. To aid copy number determination, breeding pairs were set up with known zygosity.

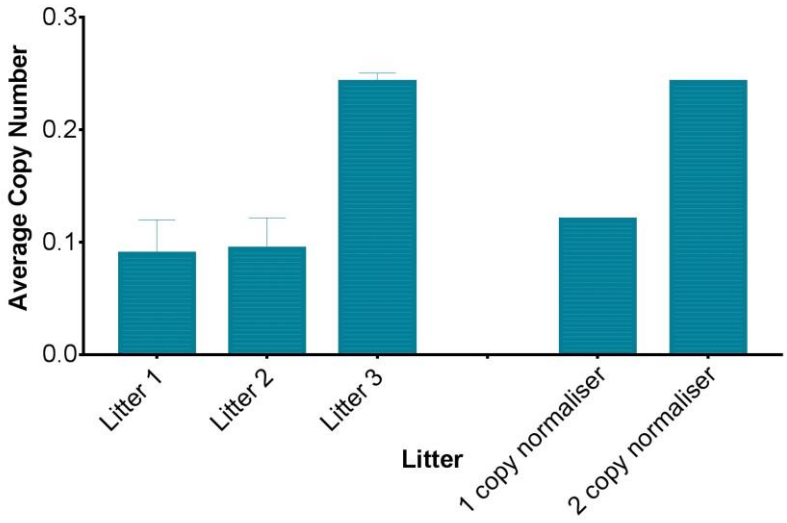

Figure 4-1 – PF4 copy number determination

Results from the PF4 copy number assays. Parents with known genotypes were crossed to produce pups with either 1 copy of PF4-cre (litter 1, n=6, and 2, n=6) or 2 copies of PF4-cre (litter 3, n=8). The numbers shown are the average copy number +/- SEM for all of the pups in each litter and known copy number controls are included as visual normalisers.

Addition of a second PF4-cre allele has a minor, but non-significant (p=0.77), effect on further depleting the plasma pool suggesting that a single cre allele produces a sufficiently high cre recombinase enzyme concentration to ensure complete recombination of the floxed locus in those cells within which PF4-cre is expressed.

Flt3-cre depleted the plasma pool to a residual 34% in one case and left it totally intact in 10 other cases. It is known that Flt3-cre has variable penetrance in mice (Boyer et al., 2011) and this appears to be the case here. The one mouse that recombined ‘efficiently’ showed genomic recombination in the bone marrow by PCR (Figure 4-2) whereas the others did not. The above plasma FXIII-A activity results are summarised in Figure 4-3.

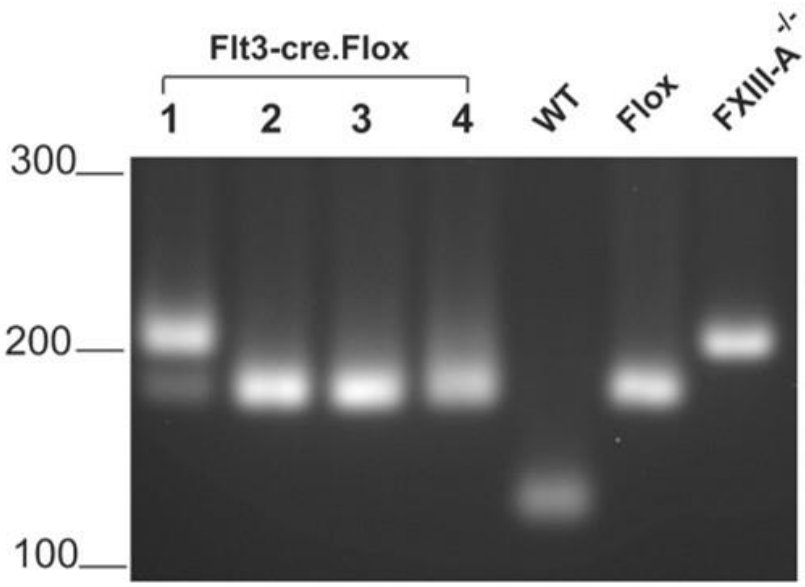

Figure 4-2 – Flt3-cre bone marrow recombination

Isolated whole bone marrow was genotyped for the FXIII-A locus by standard PCR and showed that one mouse **(1)** recombined and this mouse showed efficient depletion of the plasma pool of FXIII-A. Whereas, the other Flt3-cre mice showed no evidence of genomic recombination **(2-4)**. The last three lanes are known genotype samples used for visual comparison. Molecular weight guidelines are shown as base pairs (bp).

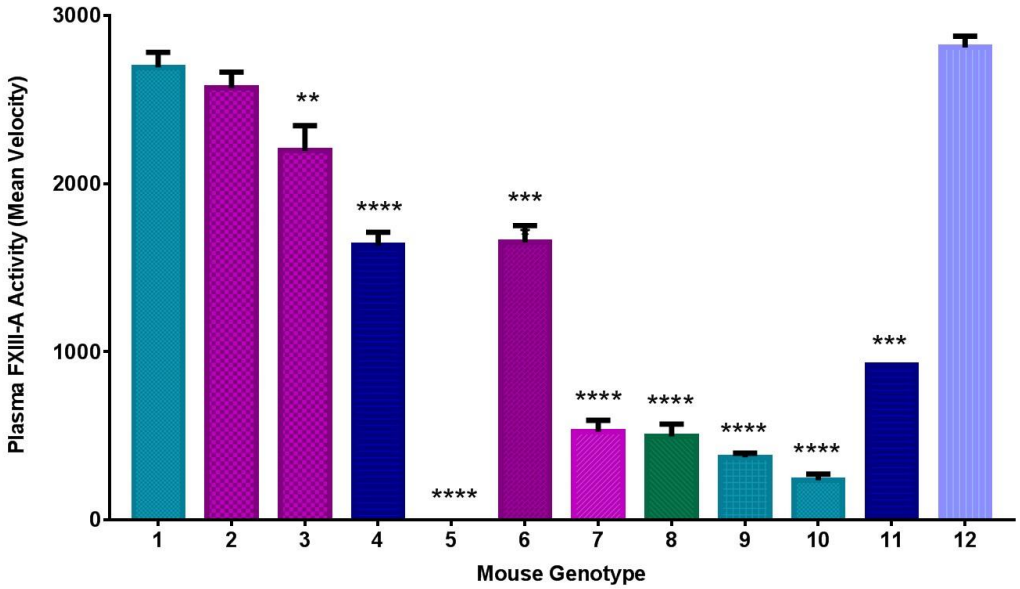

1 Wildtype (n=30)
2 c-Mpl$^{-/-}$ (n=18)
3 FXIII-A$^{flox/flox}$ (n=18)
4 FXIII-A$^{+/-}$ (n=10)
5 FXIII-A$^{-/-}$ (n=12)
6 CD11b-cre^{+}.FXIII-A$^{flox/flox}$ (n=25)
7 LysM-cre$^{+/+}$.FXIII-A$^{flox/flox}$ (n=13)
8 Pf4-cre^{+}.FXIII-A$^{flox/flox}$ (n=32)
9 PF4-cre^{++}.FXIII-A$^{flox/flox}$ (n=6)
10 CD11b-cre^{+}.PF4-cre^{+}.FXIII-A$^{flox/flox}$ (n=11)
11 Flt3-cre^{+}.FXIII-A$^{flox/flox}$ high efficiency (n=1)
12 Flt3-cre^{+}.FXIII-A$^{flox/flox}$ low efficiency (n=10)

Figure 4-3 - Plasma FXIII-A activity assay

Plasma FXIII-A activity levels were assayed in wildtype, Mpl$^{-/-}$ mice as well as the cre-lox crosses. Significant reductions in FXIII-A activity were seen in the FXIII-A$^{flox/flox}$ (p=0.001), FXIII$^{+/-}$, FXIII-A$^{-/-}$, CD11b-cre, LysM-cre, PF4-cre^{+}, PF4-cre^{++} and CD11b-cre.PF4-cre (p=<0.0001) and also the Flt3-cre high efficiency group (p=0.001). No significant difference was seen in either the Mpl$^{-/-}$ (p=0.99) or Flt3-cre low efficiency (p=0.99). All results were compared to the wildtype group and are shown as mean +/- SEM, significance was determined by 1-way ANOVA.

As described earlier, human deficiency of FXIII-A is defined as <10% of the “normal” activity of the enzyme in the plasma. People with plasma activities of >10% FXIII-A usually show none of the phenotypes associated with deficiency (e.g. spontaneous brain haemorrhage) and do not require supplementation therapy.

To try and explain the lack of clotting deficiency seen in the cre-lox mice, human plasma FXIII-A was assayed. The basal FXIII-A activity of the wildtype mouse was compared with that of four human platelet depleted plasma samples. Human plasma samples were diluted 1 in 5, 1 in 10 and 1 in 20 and mouse plasma samples diluted 1 in 10, 1 in 20 and 1 in 40 to bring assay readings into the sensitivity range of the assay. The assay results showed that human plasma FXIII-A activity was 392.3 +/- 67.3 ΔOD_{405} min^{-1} (n=4) and mouse C57BL/6 plasma FXIII-A was 2691.7 +/- 89.5 ΔOD_{405} min^{-1} (n=30) suggesting that mice have approximately a 7-fold greater excess of plasma FXIII-A activity when compared to humans. Data shown is the mean activity +/- SEM (Figure 4-4).

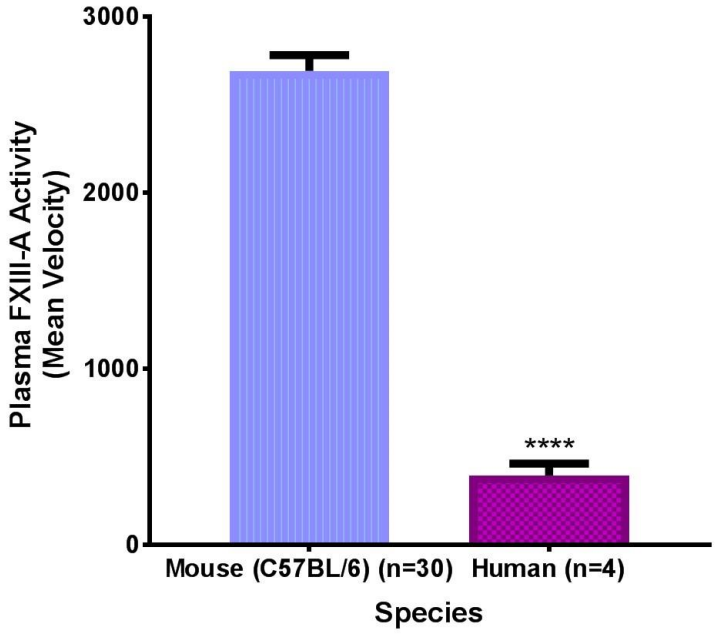

Figure 4-4 – Comparison of human and mouse plasma FXIII-A activity

The results showed that mice have approximately 7 times more plasma FXIII-A per volume of plasma than humans (p=<0.0001). Data is shown as mean +/- SEM, an unpaired t-test was used to determine significance.

Total mRNA was isolated from the livers of wildtype and global FXIII-A deficient mice. Real time PCR (Figure 4-5) showed no transcriptional changes in the acceptor B subunit of FXIII (fibrinogen chain genes shown for comparison). The results also confirmed that the liver does not produce any FXIII-A even though it contains a store of active HSCs left over from foetal haematopoiesis (Crosbie et al., 1999; Taniguchi et al., 1996) and has been suggested as a possible tissue source of FXIII-A by earlier studies.

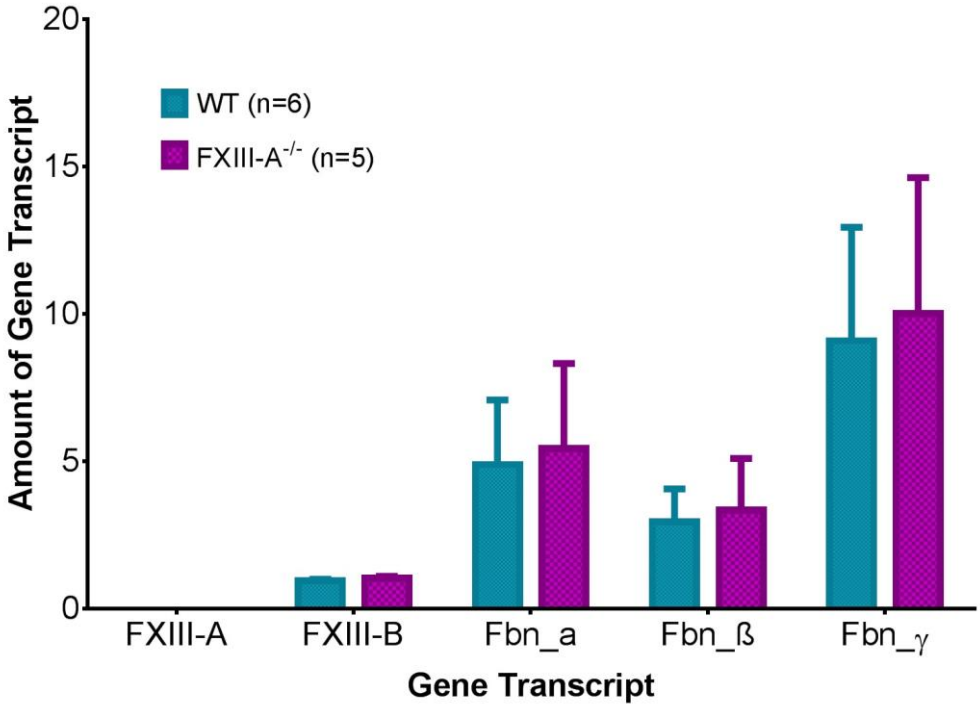

Figure 4-5 – mRNA analysis of liver expressed clotting factors

Liver mRNA isolated from wildtype and FXIII-A global knockout mice was assayed for gene transcripts relating to clotting factors. No significant differences were seen in any of the transcripts tested and of note no FXIII-A is made in the mouse liver, contrary to previous reports suggesting the liver maybe the tissue source of the plasma enzyme. Data is expressed as mean +/- 95% confidence intervals.

4.4.2 Platelet FXIII-A Assay

Platelets were purified from mouse whole blood by centrifugation, lysed and the FXIII-A activity of these lysates was determined by kinetic assay.

Figure 4-6 shows platelet FXIII-A activity per cell presented as mean +/- SEM. Of note, the Mpl knockout mice have a “normal” amount of FXIII-A per cell i.e. thrombocytopaenia does not in itself induce compensatory mechanisms to increase FXIII-A production. The single copy PF4-cre platelets are entirely depleted of their FXIII-A, showing that complete cre recombination has occurred in the megakaryocyte lineage and reinforcing the conclusion that the plasma pool cannot be maintained by the platelet.

The unexpected recombination behaviour of the Flt3-cre mouse is also shown in this assay as evidenced by the normal FXIII-A activity in the platelets of these mice. In the single Flt3-cre mouse that did appear to recombine, i.e. recombination of FXIII-A in the bone marrow was evident by PCR, there was a marked depletion of platelet FXIII-A activity to 13% of the wildtype.

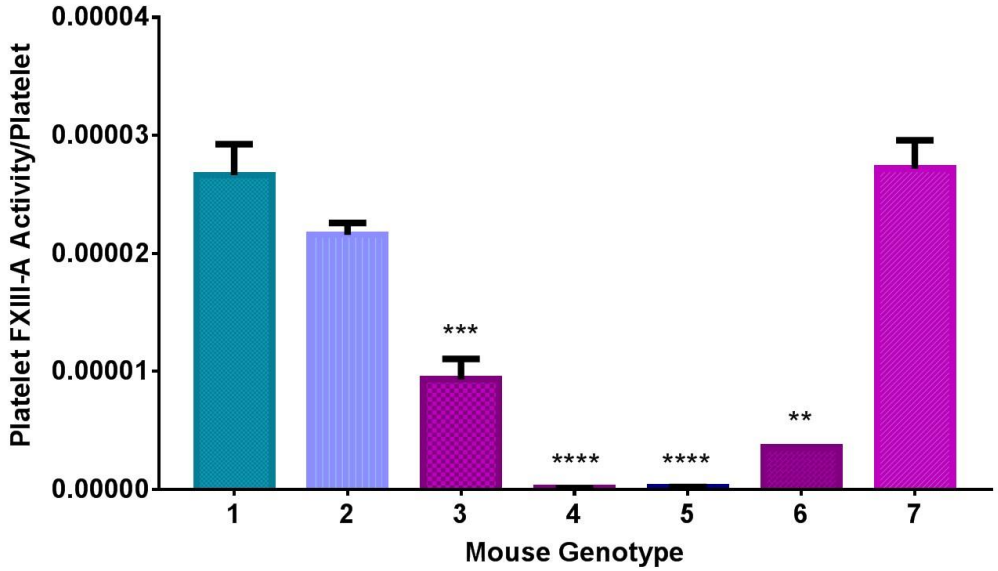

1 Wildtype (n=10)
2 c-Mpl$^{-/-}$ (n=7)
3 FXIII-A$^{+/-}$ (n=3)
4 FXIII-A$^{-/-}$ (n=3)
5 PF4-cre^{++}.FXIII-A$^{flox/flox}$ (n=5)
6 Flt3-cre^{+}.FXIII-A$^{flox/flox}$ high efficiency (n=1)
7 Flt3-cre^{+}.FXIII-A$^{flox/flox}$ low efficiency (n=10)

Figure 4-6 – Platelet FXIII-A activity

Platelet FXIII-A activity was determined by kinetic assay and normalised to the platelet count as determined by FACS analysis. Significant decreases in FXIII-A activity/platelet when compared to the wildtype group were seen in the FXIII-A$^{+/-}$ (p=0.0009), FXIII-A and PF4-cre^{++} (0.0001) and Flt3-cre high efficiency (p=0.006) groups but not in the Mpl$^{-/-}$ (p=0.37) or Flt3-cre low efficiency groups (p=0.9997). Data is expressed as mean +/- SEM and significance determined using 1-way ANOVA.

4.4.3 Quantification of Genomic Recombination

To be able to quantify the extent of genomic recombination in tissue samples from the cre-flox crosses it was necessary to design a novel PCR based method. This is outlined in 2.19 above and essentially compares the proportion of floxed FXIII-A allele to the knockout FXIII-A allele in a given sample.

To test the efficacy of the method, samples of 60 ng/µL gDNA from spleens of FXIII-$A^{flox/flox}$ and FXIII-$A^{-/-}$ mice were mixed in differing ratios to generate samples that would reflect experimental conditions (0-100% recombination in 5% increments). Figure 4-7 verifies the utility of the method, which accurately estimated the extent of deletion at all ranges and has proven to be reliable and reproducible. The proportion of knockout loci to the floxed and knockout (FXIII-$A^{flox/flox}$ x CMV-cre) loci was calculated to show the amount of recombination in that tissue.

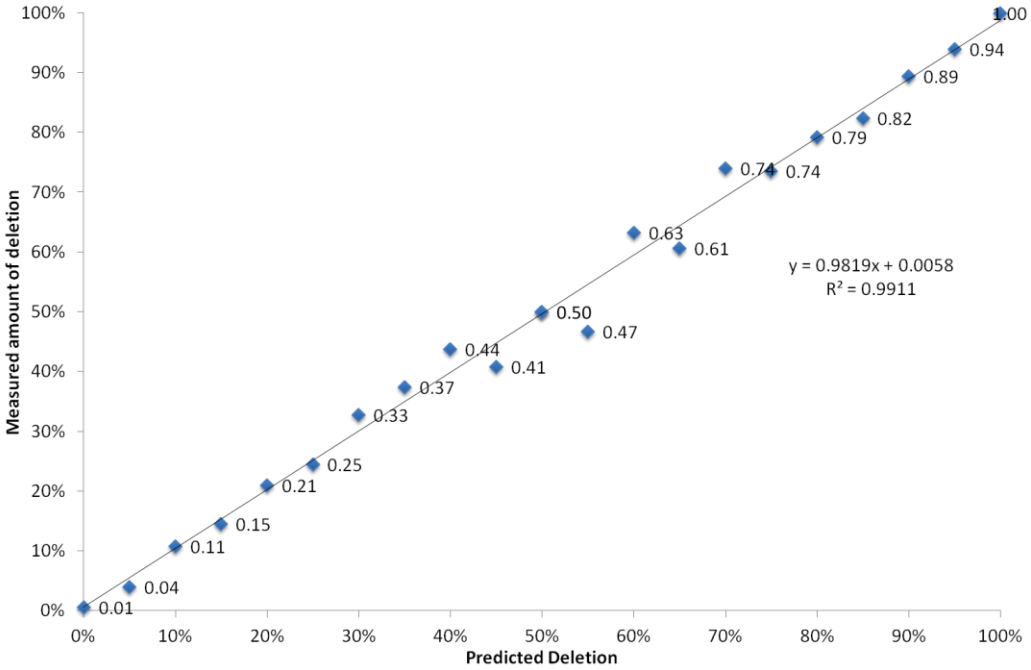

Figure 4-7 – Calibration graph of defined mixtures of FXIII-A genomic DNA

Genomic DNA isolated from spleens of FXIII-A$^{flox/flox}$ and FXIII-A$^{-/-}$ mice were mixed in defined ratios from 0-100% in 5% intervals. Each sample was assayed using qPCR and the calculated amount of recombination compared to the expected amount. Linear regression showed a near perfect correlation (R^2 = 0.9911) between the two groups of values.

Figure 4-8 shows the calculated proportion of genomic recombination (assayed as described in 2.19) in both the PF4-cre$^+$.FXIII-A$^{flox/flox}$ and CD11b-cre$^+$.FXIII-A$^{flox/flox}$ mice. The data supports the notion that PF4-cre is specific and not promiscuous in its tissue specific recombination activity. The PF4-cre mice show low levels of cre recombination in all of the organs tested, 3-4% in the heart and aorta, 2% in the liver and spleen and 0.5% in the brain.

However, it does suggest that cell type(s) beyond the megakaryocyte express the endogenous PF4 gene and are therefore able to switch on the PF4-cre gene as haematopoiesis is not known to occur in the heart, aorta and brain and the tissues were perfused to remove circulating contaminating platelets. This finding of off-target recombination replicates that of (Pertuy et al., 2015)

who found that mice expressing PF4-cre show gene recombination in resident macrophage cells in all tissues.

The CD11b-cre mice show larger amounts of genomic recombination and the results obtained appear to be in close agreement with the original report by (Ferron and Vacher, 2005) and also with the known proportion of macrophage cells living within those tissues.

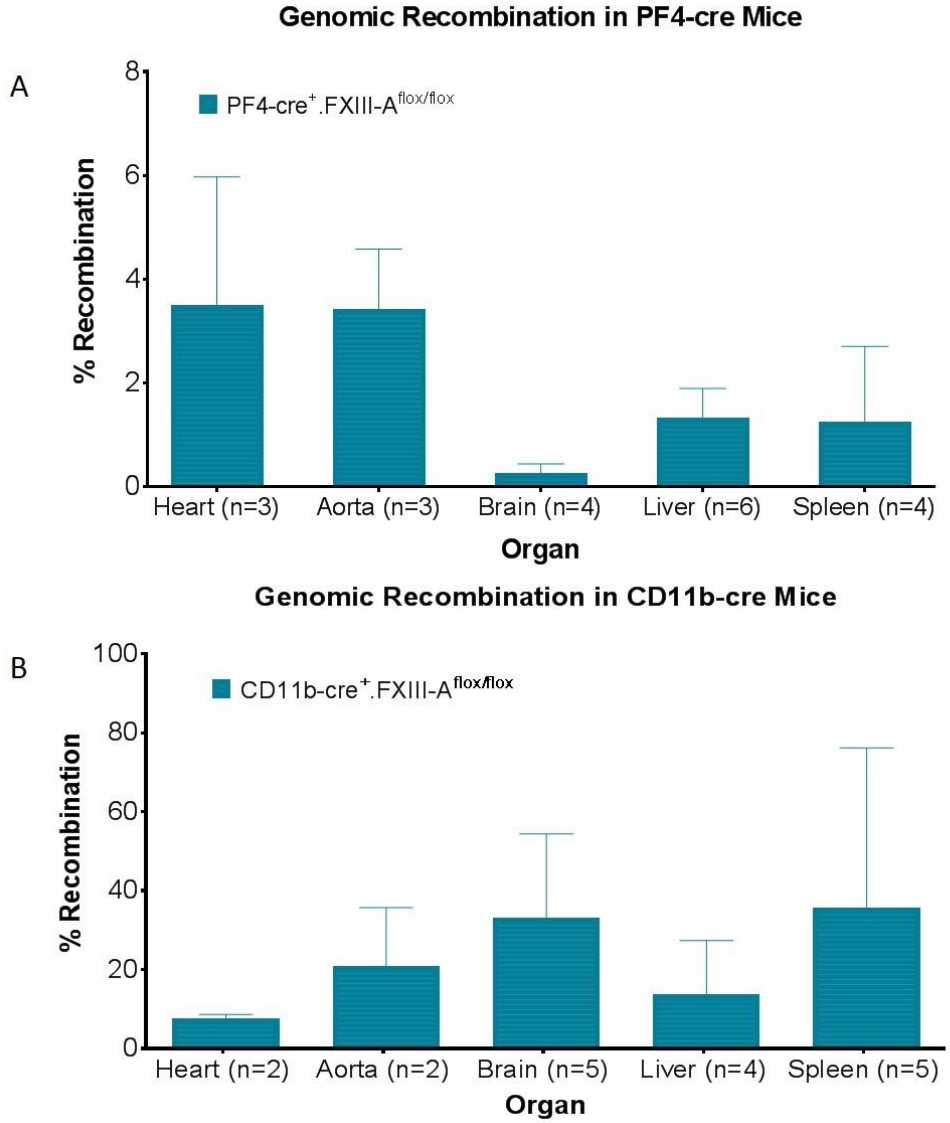

Figure 4-8 – Genomic recombination in the conditional cre-lox crosses

Proportional recombination of the FXIII-A locus was determined in the heart, aorta, brain, liver and spleen of PF4-cre and CD11b-cre FXIII-A$^{flox/flox}$ crosses. **(A)** PF4-cre appears to show limited and targeted recombination of <4% in the tissues tested whilst **(B)** CD11b-cre shows far higher amounts of recombination (10-40%), which may reflect the numbers of tissue resident macrophages within those tissues. Data is expressed as mean +/- SEM.

4.4.4 Messenger RNA Measurements

Expression of the FXIII-A gene in whole mouse organs and fractionated cells was determined by qPCR.

4.4.4.1 Gene Expression in Whole Organs

Figure 4-9 shows the transcription of the FXIII-A gene in the heart, aorta, brain, liver, spleen and bone marrow. It was determined that all of these organs apart from the liver and spleen produce FXIII-A with the heart and aorta being the major sites of FXIII-A expression.

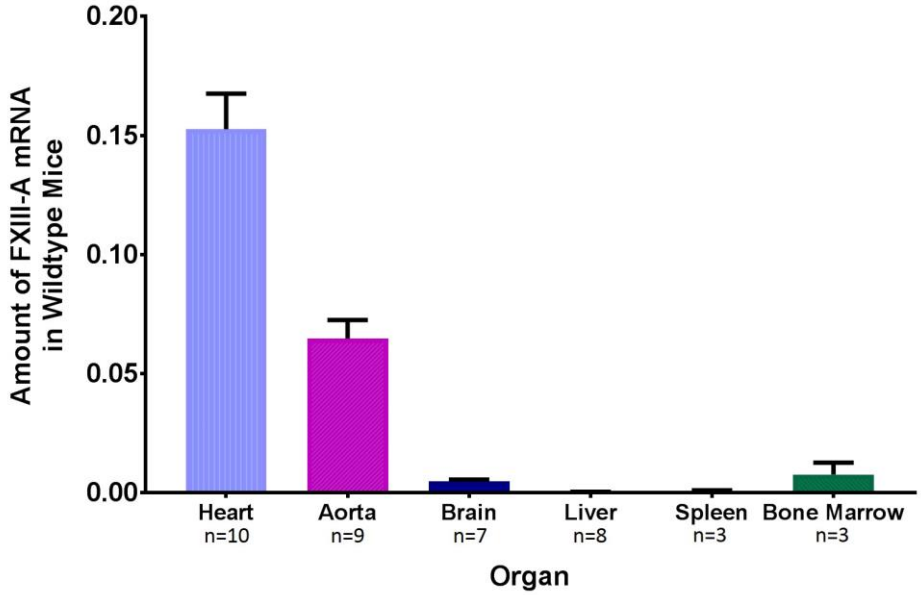

Figure 4-9 – FXIII-A gene expression in the organs of wildtype mice

Gene transcription of FXIII-A was determined by qPCR in a number of organs in wildtype mice. The heart, aorta, brain and bone marrow all express FXIII-A whereas the liver and spleen do not. Data is shown as mean +/- 95% confidence intervals.

No significant difference in FXIII-A transcription was found in either the aortas (74% of WT) or hearts (102% of WT) of the FXIII-$A^{flox/flox}$ mice compared to the wildtype mice which agrees with the essentially normal plasma and platelet levels of FXIII-A in the floxed mice and shows that the targeting construct is not interfering with transcription of the gene.

FXIII-A protein expression has previously been observed in the walls of both the heart and the vasculature (Figure 4-10). It had been expected that these cells would be identified as tissue resident macrophages and that this pool of cells expressing FXIII-A would be depleted in the CD11b-cre mice. However, FXIII-A mRNA levels in the aorta and heart of CD11b-cre^{+}.FXIII-A$^{flox/flox}$ were 54% and 103% of wildtype, respectively. LysM-cre^{+}.FXIII-A$^{flox/flox}$ mice had a remaining FXIII-A mRNA signal of 37% in the aorta and 20% in the heart.

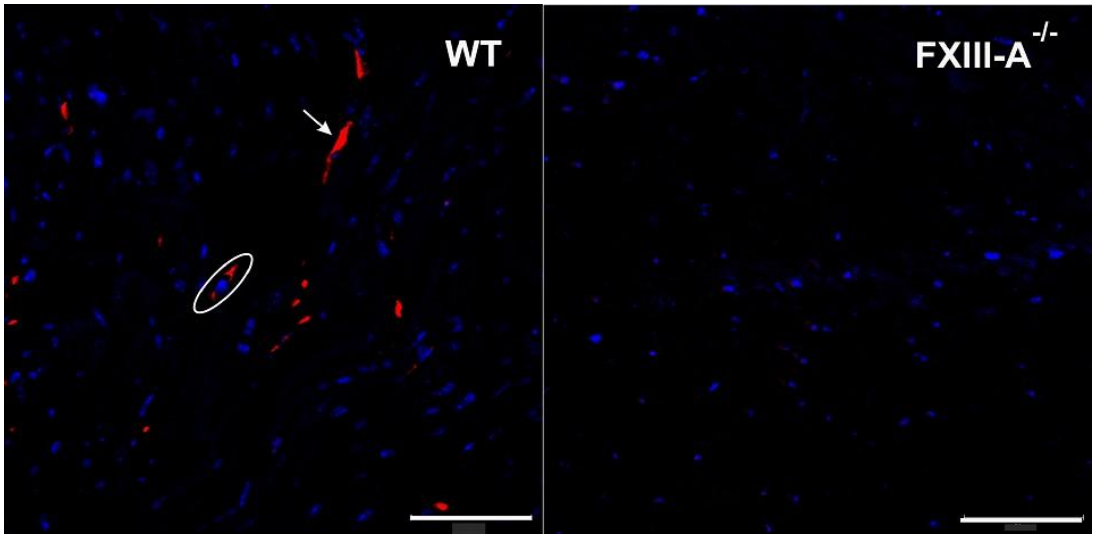

Figure 4-10 – Immunofluorescent detection of FXIII-A in mouse heart

Work in collaboration with Dr Paul Cordell in the group has shown FXIII-A in sections of mouse heart using an anti-sheep FXIII-A antibody (SAF13A-AP). The WT hearts show FXIII-A signal (red) in select cells whereas the FXIII-A$^{-/-}$ sections show no staining. In the WT heart, a proportion of labelled cells are nucleated (DAPI, blue, circled cell), whereas others adopt a spindle-shaped morphology that is distinctive of cardiac macrophages (arrow). Scale bar denotes 10 μm.

The FXIII-A mRNA signal in the PF4-cre^{+}.FXIII-A$^{flox/flox}$ mice was decreased to a residual 12% and 1% (aorta and heart respectively) when compared to the wildtype group.

The residual signal in the aortas of the CD11b-cre.PF4-cre.FXIII-A$^{flox/flox}$ mice is 9% and essentially 0% in the heart. This data suggests that the majority of cells expressing FXIII-A also express PF4; a smaller population of cells co-express FXIII-A, PF4 and CD11b and a tiny proportion of the FXIII-A expressing cells express CD11b.

The above data is summarised in Figure 4-11 and Figure 4-12.

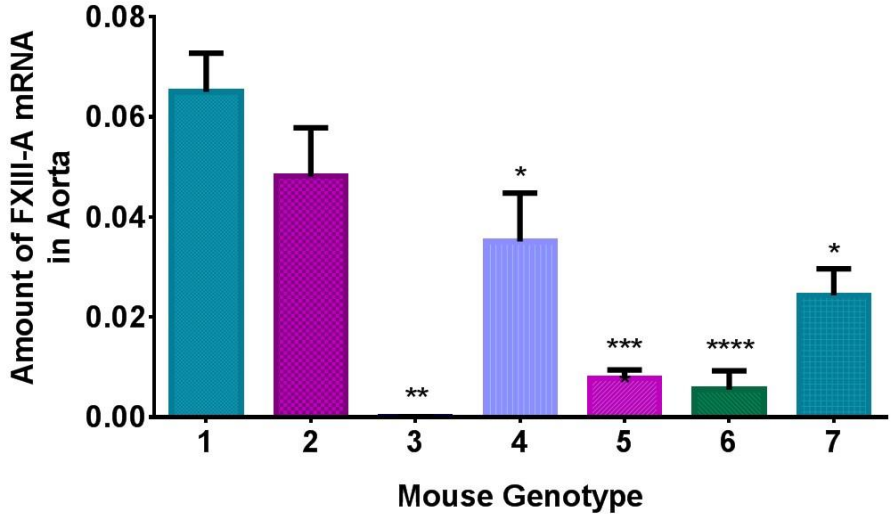

1 Wildtype (n=9)
2 FXIII-A$^{Flox/Flox}$ (n=10)
3 FXIII-A$^{-/-}$ (n=10)
4 CD11b-cre^{+}.FXIII-A$^{Flox/Flox}$ (n=10)
5 PF4-cre^{+}.FXIII-A$^{Flox/Flox}$ (n=10)
6 CD11b-cre^{+}.PF4-cre^{+}.FXIII-A$^{Flox/Flox}$ (n=6)
7 LysM-cre^{+}.FXIII-A$^{Flox/Flox}$ (n=3)

Figure 4-11 – Aortic FXIII-A mRNA in FXIII-A conditional and global knockout mice

Figure shows FXIII-A mRNA expression in aorta. The results show significantly decreased gene expression in the FXIII-A (p=0.002), CD11b-cre (p=0.02), PF4-cre (p=0.0001), CD11b-cre.PF4-cre (p=0.0001) and LysM-cre (p=0.02) groups but no significant decrease was seen in the FXIII-A$^{flox/flox}$ (p=0.34) group. Data is shown as mean +/- 95% confidence intervals and significance was determined by 1–way ANOVA.

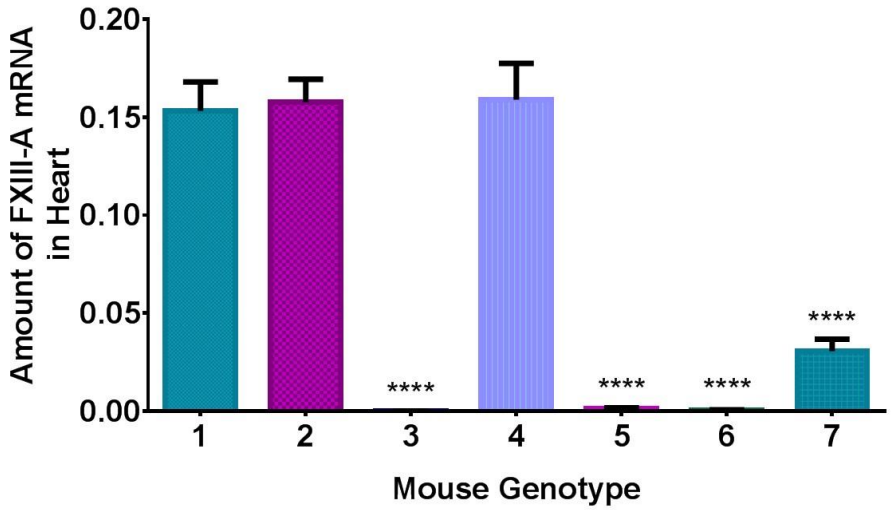

1 Wildtype (n=9)
2 FXIII-A$^{Flox/Flox}$ (n=10)
3 FXIII-A$^{-/-}$ (n=10)
4 CD11b-cre^{+}.FXIII-A$^{Flox/Flox}$ (n=10)
5 PF4-cre^{+}.FXIII-A$^{Flox/Flox}$ (n=10)
6 CD11b-cre^{+}.PF4-cre^{+}.FXIII-A$^{Flox/Flox}$ (n=6)
7 LysM-cre^{+}.FXIII-A$^{Flox/Flox}$ (n=3)

Figure 4-12 – Cardiac FXIII-A mRNA in global and conditional FXIII-A knockout mice

The FXIII-A mRNA signal was seen to be significantly decreased in the FXIII-A$^{-/-}$ (p=0.0001), PF4-cre (p=0.0001), CD11b-cre.PF4-cre (p=0.0001) and LysM-cre (p=0.0001) groups but not significantly decreased in the FXIII-A$^{flox/flox}$ (p=0.9996) or CD11b-cre (p=0.9982) groups. Data is expressed as mean +/- 95% confidence intervals and significance was determined by 1–way ANOVA.

To determine whether loss of the Mpl receptor affected the FXIII-A mRNA signal (i.e. which might be the case if platelets are trapped in the tissue or that the cells are produced through an Mpl dependent pathway) qPCR was performed on aorta and heart samples isolated from these mice. Mpl deficiency had no significant effect on FXIII-A mRNA signal in either the aorta or heart, however, there does appear to be a near doubling of FXIII-A mRNA in the aorta (235% of WT). The Mpl data is shown in Figure 4-14 and Figure 4-13.

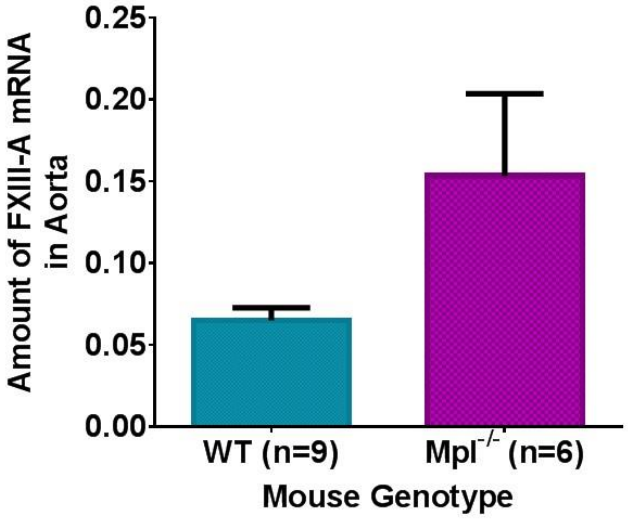

Figure 4-14 – Aortic FXIII-A mRNA in Mpl knockout mice

The Mpl knockout mouse appeared to cause an increase in FXIII-A gene expression in the aorta however this was not found to be significant (p=0.053). Data is shown as mean +/- 95% confidence intervals and significance was determined by an unpaired t-test.

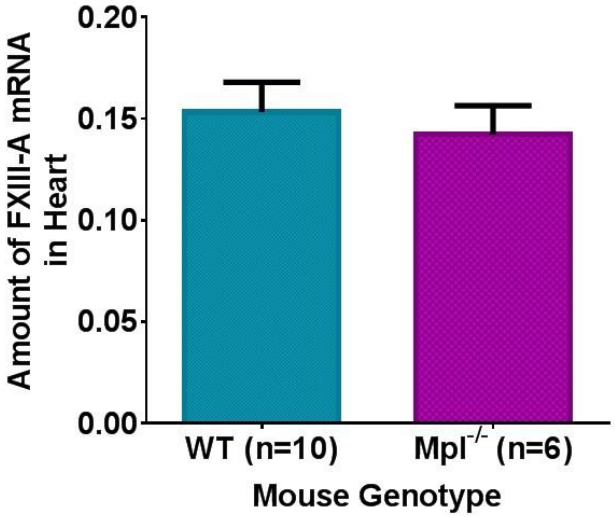

Figure 4-13 – Heart FXIII-A mRNA in Mpl knockout mice

In the heart of the Mpl knockout mouse the amount of FXIII-A gene expression remained unchanged (p=0.62). Results are shown as mean +/- 95% confidence intervals and significance was determined by an unpaired t-test.

The results above might be consistent with a macrophage origin of FXIII-A. Therefore, to determine if macrophages were able to be recombined by PF4-cre and to assess the level of endogenous expression of PF4 and CD11b, macrophages were cultured and mRNA isolated (as described in

2.13.2 above). Figure 4-15 shows that macrophages are able to express PF4 which is in agreement with the view that PF4 (and therefore PF4-cre) is expressed outside the megakaryocyte lineage.

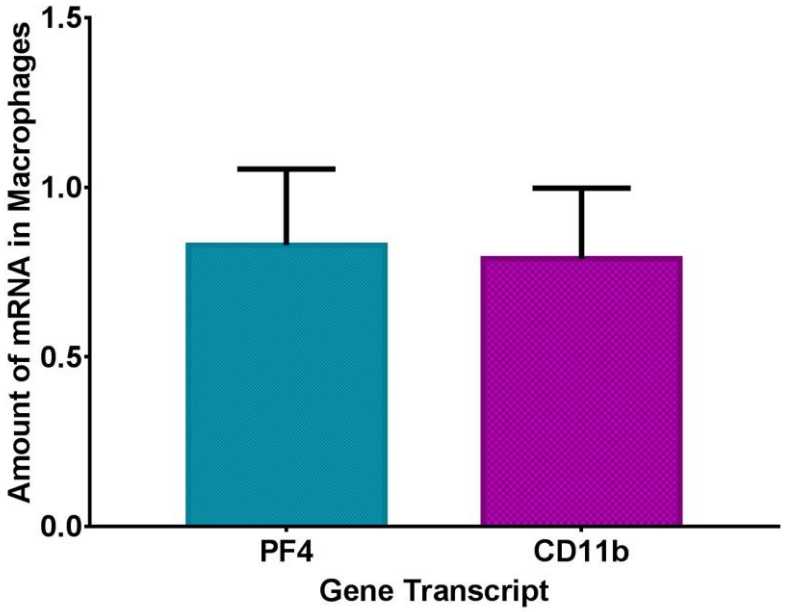

Figure 4-15 – mRNA expression in cultured macrophages

mRNA analysis of cultured wildtype bone marrow-derived macrophages which are known to express CD11b also express the supposedly platelet/megakaryocyte specific gene, PF4. Both genes are expressed at the same level. Data is shown as mean +/- 95% confidence intervals (n=7 per group).

In parallel studies to confirm the phenotype of this cell population, the cultured macrophage cells were shown to be strongly phagocytic towards zymosan coated beads and my work has shown that they are extensively killed by clodrosomes (6.2.2 below).

4.4.4.2 Gene Expression in Fractionated Hearts

We were aware that other groups within our Institute were fractionating heart cells and attempted to use this methodology to determine if the cells which produce the FXIII-A in heart were amenable to isolation.

Heart cells isolated from 3-4 week old mice (obtained after removal of cardiomyocytes by a size exclusion filter) were fractionated with the mouse Neonatal Cardiac Fibroblast Isolation Kit (Miltenyi) and total mRNA was isolated by Dr Sumia Bageghni and colleagues.

The hearts were fractionated into 4 pools, by cell number they were; 50% cardiomyocytes, which were discarded, 32% non-fibroblast (assumed to be endothelial cells), 16% fibroblast pool A (shown to be Thy-1 negative) and 2% fibroblast pool B (shown to be Thy-1 positive cells). The overall enrichment of the gene transcripts was shown by comparison with RNA samples isolated from whole hearts.

Figure 4-16 depicts the results from each assayed fraction as $2^{-\Delta Ct}$ (normalised to β-actin and RPL32) +/- 95% confidence intervals, all the results are normalised to the FXIII-A bar in fraction fibroblast pool B. Fibroblast pool B shows the greatest enrichment of FXIII-A over the whole heart along with both the endogenous genes PF4 and CD11b. This fraction was calculated to be 2% of the entire cell number of a heart and corresponds closely with the 3% of heart cells that recombined their genomic DNA in the PF4-cre^{+}.FXIII-A$^{flox/flox}$ mice when assayed in 4.4.3 above. This suggests that these cells are most likely the rare FXIII-A positive cells of interest seen in the previous immunohistochemistry images (Figure 4-10).

While bone marrow-derived macrophages and THP-1 cells were not seen to be secretory *in vitro*, the spindle-like morphology of the *in vivo* cells may represent a cytoskeletal change within these cells when *in situ* which is associated with changes that allow secretion of FXIII-A.

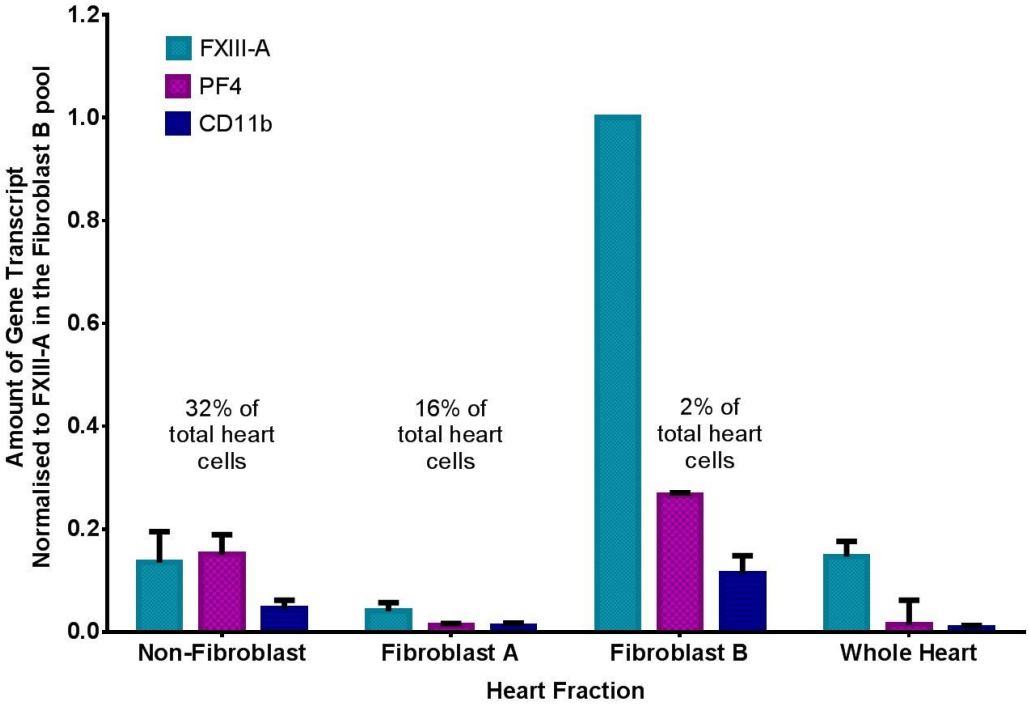

Figure 4-16 – Gene expression in fractionated hearts

mRNA was extracted and analysed from hearts fractionated using the Miltenyi neonatal cardiac fibroblast isolation kit (n=4). The kit produces 3 fractions of cells. FXIII-A, PF4 and CD11b transcript levels were determined in each fraction and compared to levels in a whole heart. Fibroblast fraction B showed the greatest enrichment of FXIII-A, PF4 and CD11b but only made up approximately 2% of the entire cell number. This number is in line with the percentage of recombination in the hearts of the PF4-cre mice and may point to the cell population being sought.

4.4.5 Bone Marrow Transplantation

To further elucidate the contribution of the bone marrow to the plasma pool, bone marrow transplant experiments were performed. Bone marrow, isolated from wildtype mice, was transplanted into lethally irradiated wildtype and FXIII-$A^{-/-}$ mice and subsequently, plasma FXIII-A activity, platelet FXIII-A activity and organ FXIII-A mRNA levels were determined.

The plasma FXIII-A activity (Figure 4-17) was shown to be maintained but not increased in the WT into WT group (100%) and plasma FXIII-A was reconstituted to 74.6% in the WT into KO group. The platelet FXIII-A activity (Figure 4-18) showed near 50% reconstitution in the WT into WT group and 78% in the WT into KO group. Taken together, this data suggests that the majority of plasma FXIII-A, in mice, is maintained by a bone marrow-derived cell which can be displaced by irradiation and restored by cell transplantation.

Both the hearts and brains of the FXIII-$A^{-/-}$ mice were repopulated with FXIII-$A^{+/+}$ expressing cells whereas the aorta showed incomplete reconstitution (25%). However, the real time PCR assay that determined the repopulation within the aorta showed very high Ct values for both the FXIII-A and housekeeper transcripts so this value may underestimate the actual repopulation that took place.

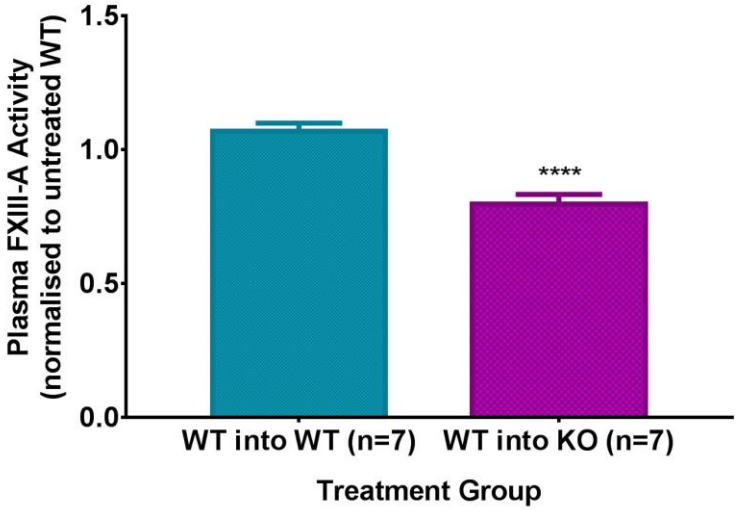

Figure 4-17 – Reconstitution of plasma FXIII-A activity in the bone marrow transplant recipient mice

Plasma FXIII-A was assayed in both wildtype and FXIII-A$^{-/-}$ mice that had been lethally irradiated and injected with bone marrow isolated from wildtype mice. The plasma FXIII-A activity was restored to 74.6% in the wildtype bone marrow into FXIII-A$^{-/-}$ group which is significantly lower than the WT into WT group (p=<0.0001). Data is shown as mean +/- SEM and significance determined using an unpaired t-test.

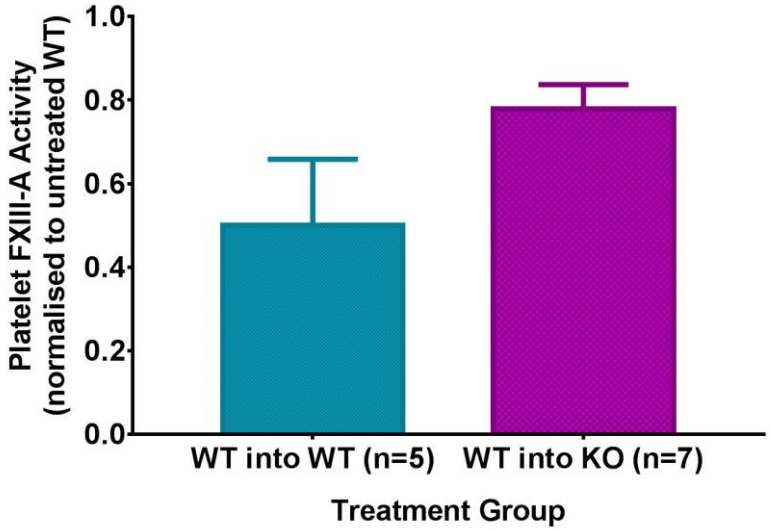

Figure 4-18 – Reconstitution of platelet FXIII-A activity in the bone marrow transplant recipient mice

Platelet FXIII-A was measured in bone marrow recipients (WT and FXIII-A$^{-/-}$) that had received WT bone marrow. The platelet FXIII-A activity was returned to 50% in the WT into WT group and 78% in the KO into KO group. Data is expressed as mean +/- SEM and significance determined using an unpaired t-test.

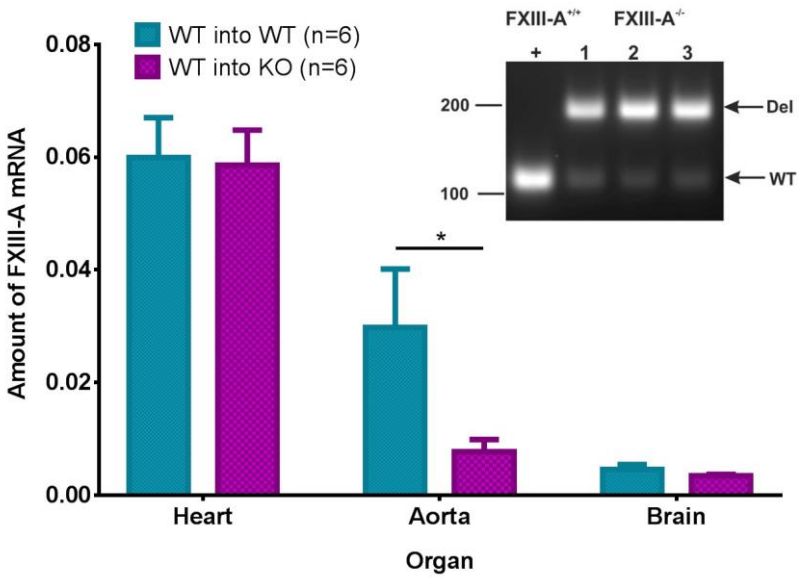

Figure 4-19 – Reconstitution of FXIII-A mRNA in bone marrow transplant assays

Organs were harvested from wildtype and FXIII-A$^{-/-}$ mice that had been lethally irradiated and injected with bone marrow harvested from healthy wildtype mice. In the FXIII-A$^{-/-}$ mice, the heart and brain showed near perfect reconstitution of FXIII-A mRNA (heart 97.7%, p=0.99 and brain 73.6%, p=0.99) whilst the aorta showed incomplete reconstitution (25.8%, p=0.03). Data shown as a percentage of the control group (wildtype bone marrow transplanted into lethally irradiated wildtype mice). Inset is PCR genotyping of liver tissue from WT and FXIII-A$^{-/-}$ bone marrow recipients of WT bone marrow showing that the mice were originally FXIII-A$^{-/-}$ but now contain WT FXIII-A after transplantation suggesting haematopoietic cells in the liver had converted to the donor genotype. Molecular weight scale is shown as base pairs (bp).

4.4.6 Plasma FXIII-A and Clot Structure

An unresolved question in the literature regards whether FXIII-A is a potential anti-thrombotic target. Mouse lines were generated in this thesis that expressed different levels of FXIII-A and this allowed us to examine the effect of lowering plasma FXIII-A concentration on clot strength. This involved *in vitro* testing of mouse whole blood samples by rotational thromboelastometry which provides a real time output of clot strength as the clot forms. A caveat of this study however (as shown in Figure 4-4) is that mice have a greater activity of plasma FXIII-A than humans (approximately 7-fold higher).

The thrombocytopenic Mpl mice showed the same rate of increase of clot firmness compared to the wildtype but overall have a lower maximal firmness which is presumably a result of having less platelet material incorporated into the clot. The FXIII-$A^{-/-}$ mice also showed a greatly perturbed clotting phenotype both in terms of clot firmness and formation time, which is in line with human reports of FXIII-A deficiency (Figure 4-20A).

Finally, neither clot firmness nor formation time is affected in the conditional knockout mice compared to the wildtype (Figure 4-20B&C) suggesting that a residual FXIII-A activity of 9% may be enough to form a ‘normal’ clot. This is unlike the human condition whereby a person with <10% FXIII-A has significantly impaired clotting parameters and this may be due to mice having a greater activity of plasma FXIII-A than humans.

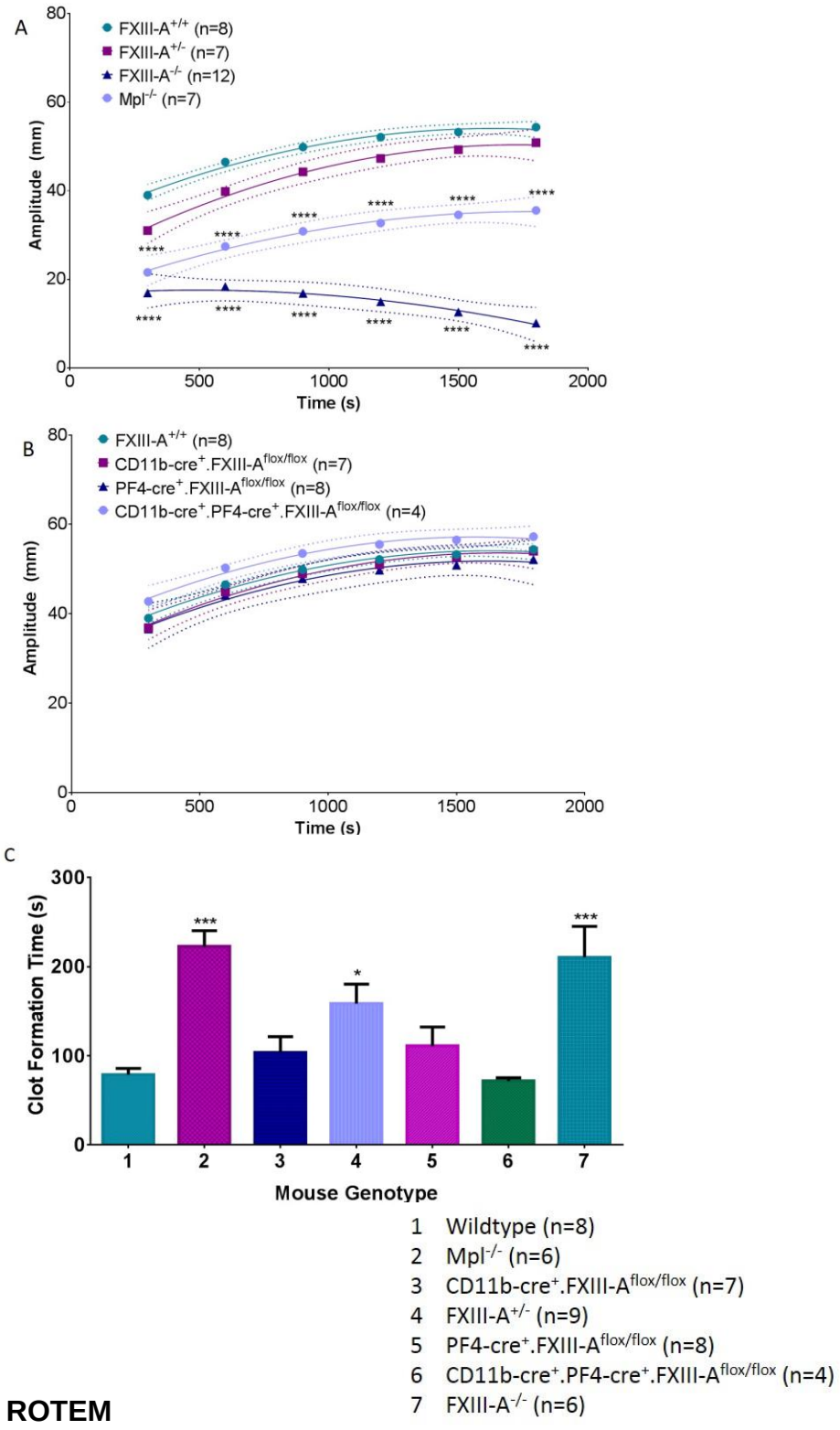

Figure 4-20 – ROTEM

Whole blood ROTEM was performed to determine clotting parameters. **(A)** shows the amplitude (clot stiffness) at 6 time points. Significant decreases in clot stiffness were seen in the FXIII-$A^{-/-}$ and $Mpl^{-/-}$ groups at all time points (p=<0.0001). **(B)** None of the conditional FXIII-A knockouts showed any statistical difference in clot formation. Data is shown as mean +/- 95% confidence intervals. **(C)** shows the clot formation time for each genotype and significant increases were seen in the $Mpl^{-/-}$ (p=<0.001), FXIII-$A^{+/-}$ (p=<0.05) and FXIII-$A^{-/-}$ (p=<0.001) mice compared to the wildtype. Data is expressed as mean +/- SEM and significance determined by 2-way ANOVA for A and B and 1-way ANOVA for C.

4.5 Discussion

4.5.1 Platelets do not maintain the plasma pool

The plasma FXIII-A activity assay data shows that the PF4-cre mice, (supposedly a megakaryocyte specific cre construct) depleted almost all of the plasma FXIII-A. The thrombocytopenic $Mpl^{-/-}$ mice on the other hand (which have ~6% of the normal platelet number) were found to have normal levels of plasma FXIII-A. This is consistent with previous reports from our group of plasma FXIII-A in two different lines of thrombocytopenic mice (Cordell et al., 2010). FACS analysis of platelets derived from $Mpl^{-/-}$ mice show no changes in cell size or volume compared to the wildtype and when equal numbers of platelets are assayed from both groups identical FXIII-A activities are seen. This suggests that there are no compensatory mechanisms involved (e.g. larger platelets containing more FXIII-A or normal sized platelets containing a higher concentration of FXIII-A) and therefore refutes the notion that platelets are the cellular source of FXIII-A.

Analysis of genomic recombination in the PF4-cre mice shows that the targeting construct is specific and not simply recombining in every cell. However the mRNA data demonstrates that cultured bone marrow-derived macrophages can express the endogenous PF4 gene under normal conditions further confirming that this construct is able to be expressed outside of the megakaryocyte lineage.

Previous reports, which had suggested an extrahaematological source of plasma FXIII-A had hypothesised that the liver could be the source of plasma FXIII-A (Poon et al., 1989; Pihusch et al., 2002). The results of our mRNA assays show that the liver, spleen, brain and bone marrow (which contain

FXIII-A positive macrophages) contain negligible amounts of FXIII-A mRNA and therefore would be unlikely sources of plasma FXIII-A production. In contrast, the heart and aorta do contain high quantities of FXIII-A mRNA. Immunohistochemistry data has previously shown that the heart contains spindle-like cells which stain positively for FXIII-A antigen, which are believed to be tissue resident macrophages (Souri et al., 2008) and account for approximately 3-5% of the total cell number.

4.5.2 Fingerprinting of cre-lox mice suggests the aorta is the site that maintains the plasma pool of FXIII-A

Figure 4-21 is an overview of the results produced from real time PCR assays of heart and aorta mRNA samples from the cre-lox crosses and $Mpl^{-/-}$ mice and shows FXIII-A gene transcript level and plasma FXIII-A activity assay results for each of the genotypes.

The data presented in this thesis suggests that tissue resident macrophages express PF4, which has been shown previously by (Schaffner and Rhyn, 2005), with a minority also expressing CD11b. These cells can be readily isolated from heart tissue using cardiomyocyte depletion and what is presumed to be positive selection with an anti-Thy1.2 antibody. This may also be possible to achieve in aortic samples; however, this has not yet been attempted.

From this overview of the data, it appears that the aorta is the prime candidate for the tissue source of plasma FXIII-A, the heart seems less likely or perhaps plays a lesser role in maintaining the plasma pool. The reasons for discounting the heart are; 1) PF4-cre almost entirely depletes the FXIII-A mRNA signal in the heart but does not completely deplete the plasma protein whereas the aorta is not completely exhausted, this is the same story with the

CD11b-cre.PF4-cre mice; 2) The CD11b-cre^{+}.FXIII-A$^{flox/flox}$ mouse shows a parallel decrease in both aortic mRNA and plasma FXIII-A activity but the cardiac mRNA does not fall to the same level; 3) in the LysM-cre mice aorta mRNA and plasma activity levels match but the heart again shows a decrease greater than that seen in plasma activity; 4) the bone marrow transplant assays show complete restitution of FXIII-A mRNA in the heart but both the plasma FXIII-A activity (74.6%) and aorta also show incomplete reconstitution of FXIII-A mRNA; 5) the non-recombined floxed mouse shows a reduction in plasma FXIII-A activity but no commensurate drop in heart mRNA signal whereas the aorta does show a reduction, which may suggest a different transcriptional mechanism for FXIII-A destined for the plasma (i.e. the aortic cells) and that destined for repair (i.e. the cardiac cells).

When taken together these results build a picture of the aorta playing the primary role in maintaining the levels of plasma FXIII-A. It may also be true that this isn't just taking place in the aorta but in the entire vasculature due to the large concentration of FXIII-A in the plasma and its apparent short half-life. However, due to the difficulties in isolating mRNA from the aortas of mice due to the small size of the vessel, it was not possible to look at other sites, an example being the carotid arteries where unsuccessful attempts were made in trying to extract mRNA.

In the future, extraction of RNA from smaller vessels or from other species (e.g. rat or rabbit) will be attempted using the methodology described in 2.16.2 above using silica columns. It would also be pertinent to test the lungs for expression of FXIII-A as this was suggested previously as an extrahaematological source of plasma FXIII-A.

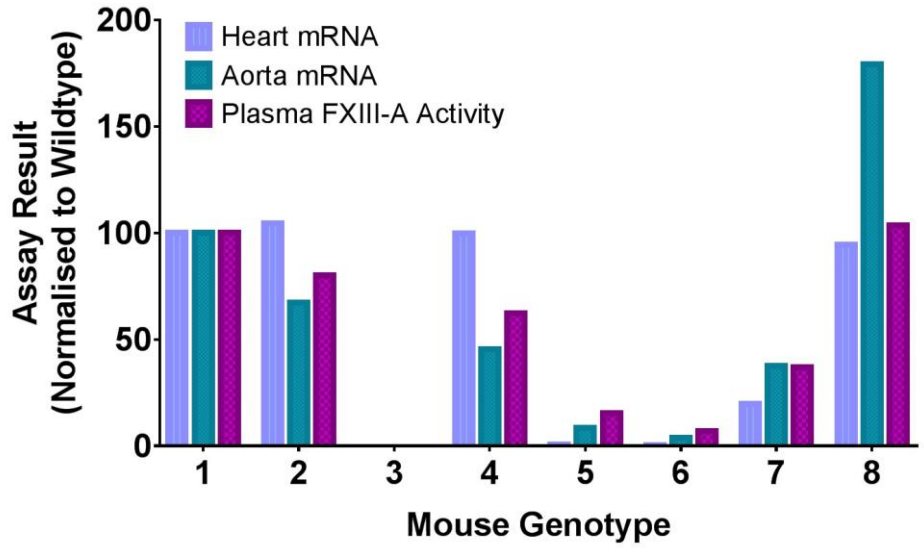

1 Wildtype
2 FXIII-A$^{Flox/Flox}$
3 FXIII-A$^{-/-}$
4 CD11b-cre^{+}.FXIII-A$^{Flox/Flox}$
5 PF4-cre^{+}.FXIII-A$^{Flox/Flox}$
6 CD11b-cre^{+}.PF4-cre^{+}.FXIII-A$^{Flox/Flox}$
7 LysM-cre^{+}.FXIII-A$^{Flox/Flox}$
8 Mpl$^{-/-}$

Figure 4-21 – Fingerprinting of FXIII-A mRNA and plasma activity following cre-lox deletion

An overview of the data from the plasma FXIII-A activity assays and FXIII-A gene transcription in the heart and aorta. When comparing the two tissues to the plasma activity, the data points to the aorta being the tissue source of FXIII-A as the aortic mRNA appears to mirror the plasma activity more closely than the heart mRNA does.

4.5.3 Tissue resident macrophages are the probable cellular source of FXIII-A

Figure 4-22 summarises the above work into a working hypothesis of how the plasma and platelet cellular sources of FXIII-A arise. The results suggest that the cellular source of plasma FXIII-A is maintained by a population of resident tissue cells, which appear to be macrophages, in the aorta and possibly the heart.

Tissue resident macrophages in the aorta and heart, as well as those in the brain, skin, lungs and liver, arise initially from the foetal yolk sac. These cells originate from primitive (Flt3-independent) haematopoiesis and migrate to the early dorsal aorta (aorto-gonadal mesonephros) (Medvinsky et al., 2011; Perdiguero et al., 2014) which perhaps makes the finding that the aorta may serve as the tissue source less surprising than it first appears. These cells are able to undergo local proliferation within the tissue in order to maintain their numbers and can also be replaced by circulating monocytes from the bone marrow which appear to differentiate into tissue resident macrophages when *in situ* (Epelman et al., 2014; Molawi et al., 2014). These bone marrow-derived cells arise through definitive haematopoiesis which differentiate from a stem cell derived from the HSC (Flt3-dependent) but not from a cell-type that is a precursor to the megakaryocyte (Mpl independent).

As the animal ages, these cells can be displaced by invading adult bone marrow-derived macrophages naturally as a result of cell turnover (Molawi et al., 2014), or as a result of injury (Epelman et al., 2014). Fms-like tyrosine kinase 3 (Flt3) is required for the differentiation of long-term haematopoietic stem cells (LT-HSCs) into short-term haematopoietic stem cells (ST-HSCs). These ST-HSCs are the cells which are able to differentiate into the many lineages of cells that the bone marrow produces (namely, megakaryocytes and monocytes) through the common myeloid precursor.

These resident tissue cells, both yolk sac- and bone marrow-derived, appear to express the genes PF4 in the aorta and heart and potentially Thy1.2 in the heart. This is reinforced by calculating the recombination efficiency of the PF4-cre mouse in the heart and aorta, which reports that approximately 3-4%

of cells in the aorta and heart have undergone cre-lox recombination. Fractionation of 3-4 week old mouse hearts using a positive selection strategy involving what is believed to be an anti-Thy1.2 antibody produced a cell fraction that accounts for approximately 2% of the entire cell number of the heart and these cells show the greatest enrichment of FXIII-A, PF4 and CD11b transcripts over a whole heart.

There are differing reports of what happens after birth to the yolk-sac derived macrophages. There are three hypotheses with good evidence supporting each of them; 1) the yolk-sac cells persist and divide but are not replaced by adult cells (Hashimoto et al., 2013; Schulz et al., 2012; Yona et al., 2013; Guilliams et al., 2013; Epelman et al., 2014); 2) the yolk-sac cells are replaced entirely at birth or following injury by bone marrow-derived cells (van Amerongen et al., 2007; Nahrendorf et al., 2007); 3) the yolk-sac cells persist and divide, but are slowly displaced by, and co-exist alongside, bone marrow-derived macrophages (Ensan et al., 2016; Perdiguero and Geissmann, 2016; Molawi et al., 2014).

The results presented here suggest that hypothesis 3 is the most likely as the Flt3-cre FXIII-A assays which show that the plasma activity is depleted to 34% of the wildtype which would mean that by around 8 weeks of age a C57BL/6 mouse has displaced approximately 65% of its (yolk sac derived, Flt3-independent) FXIII-A secreting cells with bone marrow-derived (Flt3-dependent) cells.

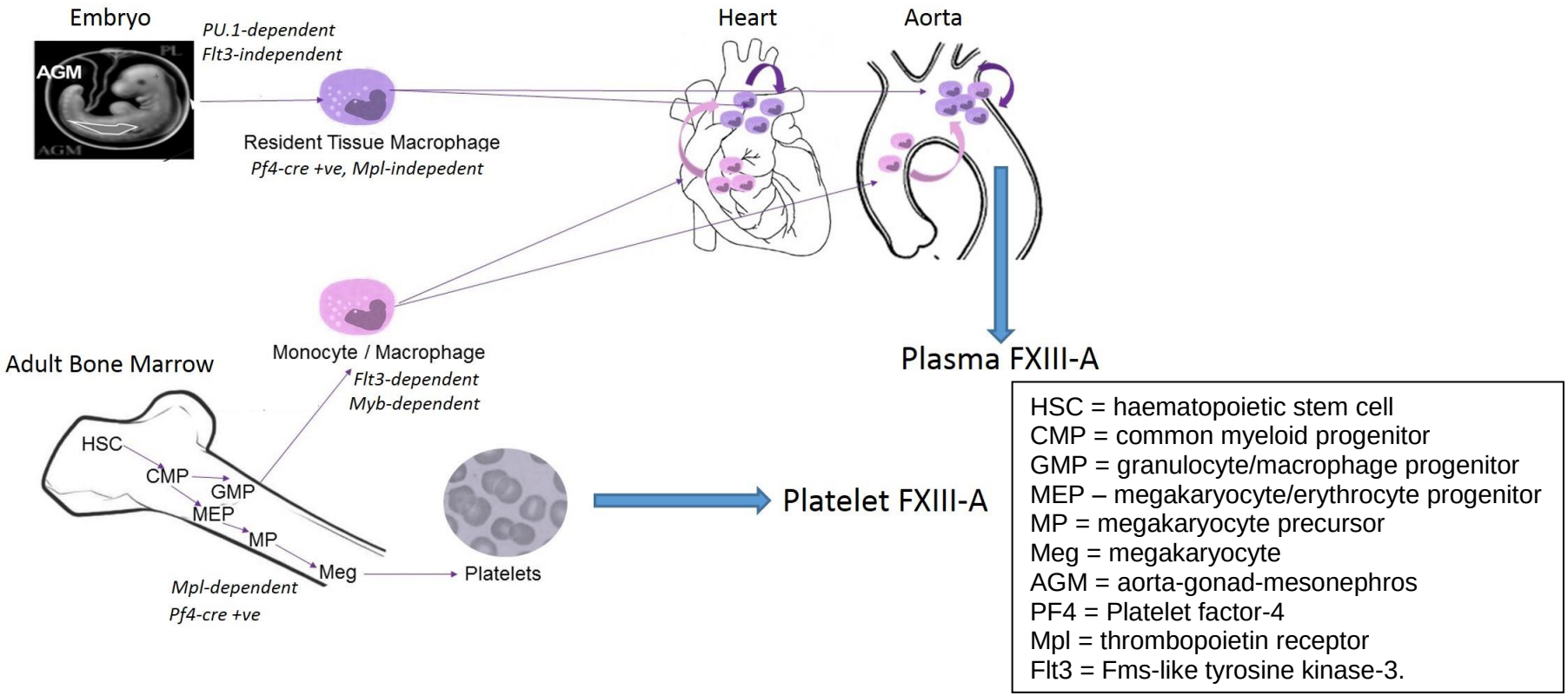

Figure 4-22 – Proposed mechanism by which FXIII-A positive resident tissue macrophages arise in the heart and aorta

Diagram summarising the origins of tissue resident macrophages in the heart and aorta and how they contribute to the plasma pool of FXIII-A. These cells originate from the embryo and are generated from flt3-independent primitive haematopoiesis which takes place in the yolk sac. These cells then migrate into the early aorta and heart and persist throughout embryogenesis. It is known that these cells can undergo self-renewal and maintain their numbers by mitosis but also can be displaced by bone marrow-derived macrophages produced by flt3-dependent adult haematopoiesis.

4.5.4 Differing expression of Flt3-cre between pups

Flt3-cre, peculiarly, has been reported to have variable penetrance in mice. (Boyer et al., 2011) described two groups of mice derived from Flt3-cre mediated recombination of the dual-colour reporter mT/mG mouse. They coined the terms “high-efficiency” and “low-efficiency” floxers. The high-efficiency mice showed recombination and therefore expression of the GFP reporter in all haematopoietic lineages whereas the low-efficiency mice showed switching on of the reporter in lymphoid cells only. This thesis reports similar findings whereby FXIII-A was not recombined in the platelets of the majority of the Flt3-cre offspring and recombination was only detected in one of eleven pups. To date, no one has established why this variable recombination occurs and in the future a new line of Flt3-cre mice, which are known to produce high-efficiency pups, would have to be imported.

A potential reason for this difference in cre expression in these mice may be due to epigenetic silencing of the transgene. While it has been generally assumed that all epigenetic modifications are erased from the germline, it has been shown that certain epigenetic modifications of gene loci can be inherited in mice an example of this being the agouti locus. (Morgan et al., 1999; Roemer et al., 1997).

4.5.5 Mice have limitations for modelling human FXIII-A deficiency

FXIII-A deficient mice were generated by cre-lox recombination using tissue specific cre constructs. This allowed depletion of circulating FXIII-A from 100% (FXIII-$A^{+/+}$) down to 61% (CD11b-cre and FXIII-$A^{+/-}$), 18% (PF4-cre), 9% (PF4-cre.CD11b-cre) and 0% (FXIII-$A^{-/-}$).

An *in vitro* assessment of clot formation was performed using ROTEM in all mouse lines and while differences were found in the global FXIII-A knockout and $Mpl^{-/-}$ groups, which was expected, no differences were found in any of the conditional knockout mice. The reduction in firmness in the Mpl knockout group is probably a result of the lack of platelet mass in the clot and as platelets have a wide range of functions in clotting (e.g. retraction and as a source of clotting factors) it is unsurprising that these mice have perturbed clotting function.

The strong sequence homology between mouse and human FXIII-A suggest that there will be no difference in the specific activities of enzymes between the two species. This would imply that mice have approximately 7 times more enzyme molecules of FXIII-A than humans per volume of blood. If the effects of clinical human deficiency begin to be apparent at 10% of “normal” FXIII-A (i.e. an activity of ~40 in the assay) then an equivalent “human deficient” mouse model would require a residual enzyme activity of approximately 1.5% or lower in order to mimic this.

$$(39.2 \div 2691.7) \times 100 = 1.45\%$$

This means that the PF4-cre^{+}.CD11b-cre^{+}.FXIII-$A^{flox/flox}$ mouse, which has 9% residual FXIII-A when compared to a wildtype mouse, is actually equivalent to a human with approximately 70% plasma FXIII-A assuming that other blood parameters are unchanged. Such an individual would be asymptomatic, and this would therefore explain the results of the ROTEM assays. The excess of plasma FXIII-A in mice could be explained by a need to clot quickly due to their small blood volume but this would have to be balanced by rapid clot lysis as most blood clots would presumably be occlusive. This may be a result of

mice having blood cells which are of a comparable size to humans (mice RBCs are 6 μm in diameter, human RBCs are 7.9 μm in diameter) (Milo et al., 2010) but smaller vessels.

It may be that using mice to model human FXIII-A deficiency is impractical as a mouse with a residual activity of 1.5% (i.e. a mouse with <10% “human” FXIII-A activity) is beyond the limits of cre-lox recombination even with the use of a tamoxifen-inducible cre recombinase (e.g. ROSA26).

A future line of enquiry which could prove interesting would be to investigate whether the plasma activity of FXIII-A is inversely proportional to the blood volume of the animal by looking at other small (e.g. hamsters), and large rodents (e.g. rats) as well as larger mammals such as pigs and sheep.

4.6 Conclusion

The aim of this project was to define the role that platelets play in maintaining the circulating source of plasma FXIII-A. The results presented here not only provide substantial evidence to refute the idea that platelets maintain the plasma pool but also suggests that yolk sac-derived and later bone marrow-derived tissue resident macrophages, most likely present in the aorta (and perhaps the entire vasculature), are the cellular source which maintains the plasma pool of FXIII-A.

4.7 Summary of Key Findings

- Normal plasma FXIII-A activity and lack of compensation in platelet size or platelet FXIII-A content in the $Mpl^{-/-}$ mouse discounts the platelet as the cellular source of plasma FXIII-A (Table 4-1).

Genotype	Plasma Activity	Platelet Activity/Cell	Cardiac mRNA	Aortic mRNA
Wildtype	95%	75%	102%	74%
$Mpl^{-/-}$	95%	81%	93%	236%
CD11b-cre^{+}.FXIII-$A^{flox/flox}$	61%	63%	103%	54%
LysM-cre^{+}.FXIII-$A^{flox/flox}$	20%	71%	20%	37%
PF4-cre^{+}.FXIII-$A^{flox/flox}$	18%	0%	1%	12%
CD11b-cre^{+}.PF4-cre^{+}.FXIII-$A^{flox/flox}$	9%	0%	0%	9%
Flt3-cre^{+}.FXIII-$A^{flox/flox}$	34%	13%	n.d.	n.d.
FXIII-$A^{-/-}$	0%	0%	0%	0%

Table 4-1 - Summary of the cre-lox fingerprinting data

Table showing residual plasma and platelet FXIII-A activity and expression of FXIII-A mRNA in the heart and aorta of the cre-lox crossed mice. All data is shown as the average value normalised to the wildtype.

- Cultured bone marrow-derived macrophages were seen to express PF4 and therefore depletion in the PF4-cre may suggest a macrophage origin for plasma FXIII-A.

- Fingerprinting of the cre-lox crosses shows that plasma FXIII-A closely matches the aortic FXIII-A mRNA profile.

- BMT of FXIII-$A^{+/+}$ bone marrow cells into FXIII-$A^{-/-}$ mice restores plasma and platelet FXIII-A but also organ FXIII-A mRNA.

- Mice have 7 fold more plasma FXIII-A than humans hence modelling FXIII-A deficiency in mice may be impractical.

Chapter 5 – Examining the effect of TG2 deficiency on apoptosis

5.1 Introduction

So far, no large vessel repair deficit has been seen in the experimental aneurysm studies of the $TG2^{-/-}$ mice. Is this because TG2 does not have a repair role or is it due to it having an equally important role in cell apoptosis?

Previous reports have suggested that a transglutaminase is able to increase the activation of MAPK through interaction with the first kinase in the cascade, DLK. This interaction has been suggested to be a crosslinking reaction whereby DLK oligomerises and is stabilised by a transglutaminase which results in increased apoptotic potential of the cell (Robitaille et al., 2004; Robitaille et al., 2008; Hébert et al., 2000).

Activation of apoptosis typically involves a rapid influx of calcium and hence, to mimic this, calphostin C was used to induce apoptosis in our cellular models. Calphostin C is a potent, light dependent, inhibitor of protein kinase C which results in rapid mobilisation of intracellular calcium stores resulting in activation of the typical caspase-dependent apoptosis cascade.

Vascular smooth muscle cells were chosen as the model system for this study due to their particular relevance in aortic aneurysm disease. Vascular smooth muscle cell apoptosis is a key component of aneurysm pathology (McCarthy, 2000; Rowe et al., 2000). Since VSMCs also represent the bulk cell population of the artery wall their isolation and culture is relatively straightforward and well described in the literature (Bochaton-Piallat et al., 1992; Ray et al., 2001).

5.2 Aims

To define the effects of TG2 deficiency on JNK activation and gene expression by:

1. Culturing vascular smooth muscle cells derived from the aortas of wildtype and $TG2^{-/-}$ mice.
2. Determine the phospho-JNK antigen levels and total JNK activity in these cells as a readout of MAPK activation.
3. Measure the transglutaminase activity levels under apoptotic conditions.
4. Examine the protein sequence of DLK to try and identify any potential TG2 crosslinking sites.

5.3 Hypothesis

Transglutaminase 2 is involved in the activation of c-Jun N-terminal kinase (JNK) therefore TG2-null vascular smooth muscle cells will show defects in JNK activation and apoptosis.

5.4 Results

5.4.1 Vascular Smooth Muscle Cell Culture and Phenotype

Mouse aortic vascular smooth muscle cells were isolated from whole aortas (aortic arch to iliac bifurcation). The culture conditions were optimised to provide maximum cell numbers for study. To determine this, cells were split at 1 in 4, 1 in 8 and 1 in 16 and it was found that splitting at a density lower than 1 in 4 did not establish viable cultures. Therefore, the culture conditions used were a total culture time of 10 days and a single passage at a 1 in 4 ratio.

The cultured cells grew as monolayers, as examined by phase contrast microscopy, and took on the characteristic 'hill-and-valley' morphology as expected of smooth muscle cells (Endlich et al., 2000) following fixation and confocal microscopy. They also showed features of both the synthetic (rhomboidal) and contractile (elongated) phenotypes both of which stain positively for alpha-smooth muscle actin (Figure 5-1).

Real time PCR of total mRNA data from these cells confirms that they are indeed vascular smooth muscle cells (αSMA positive) and not endothelial cells (CD31 negative). This is in agreement with the <1% contamination of endothelial cells reported in the original published method (Ray et al., 2001). This data also confirms that VSMCs express the pro-apoptotic MAP kinase pathway (DLK and JNK) and also TG2 (but as expected, not FXIII-A). However, in the $TG2^{-/-}$ cells, the transcripts relating to the MAPK pathway appear to be transcribed at lower levels than in the wildtype cells and therefore these cells may have lower amounts of those proteins (Figure 5-2).

Whilst synthetic VSMCs are known to express MMP-2 and -9 it has also been shown that VSMCs are able to express the macrophage metalloelastase,

MMP-12 (Wu et al., 2003; Harris et al., 2010). This was confirmed in this work. Macrophage metalloelastase, as its name suggests, was first characterised in invading inflammatory macrophages and contributes to the excessive degradation of the elastic ECM seen in numerous inflammatory disorders (e.g. aortic aneurysm and emphysema). Its constitutive expression in VSMCs further implicates these cells as important drivers of the destructive process within the vessel.

VSMCs in culture also express the ECM synthesis machinery (e.g. lysyl oxidase, collagens and elastin) suggesting a wider role for VSMCs in remodelling the vasculature, and not just in modulating vessel tone and ECM turnover.

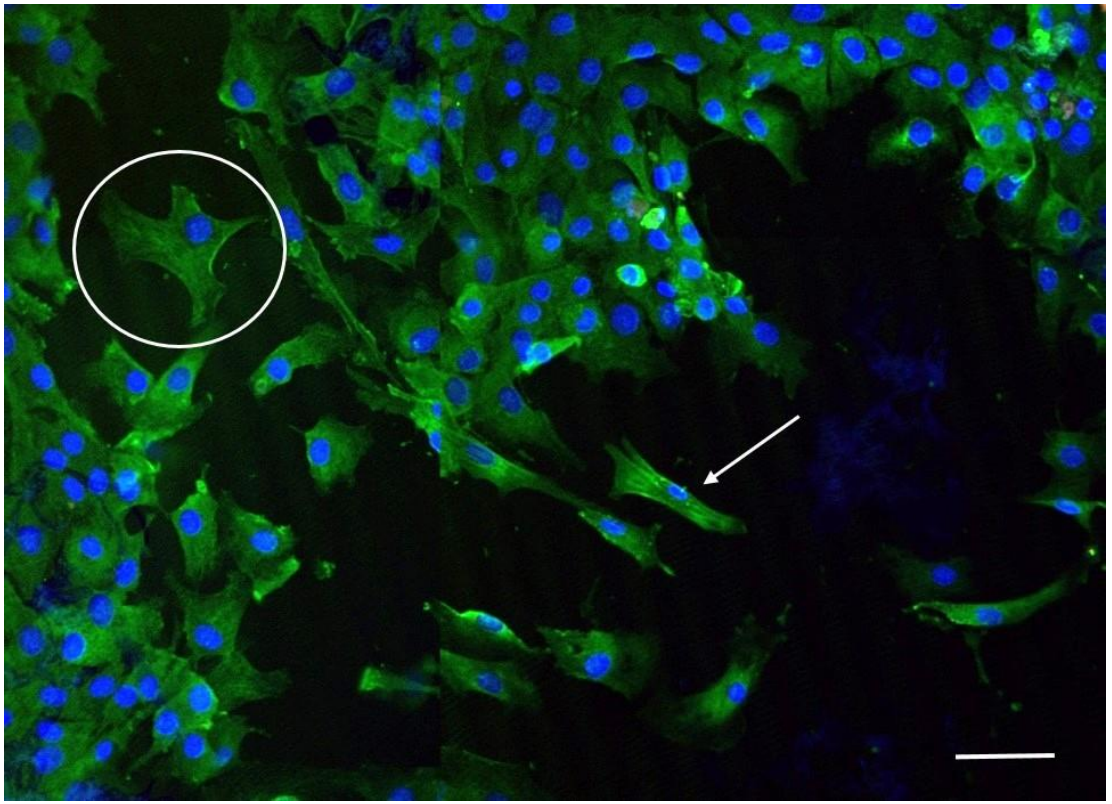

Figure 5-1 – Confocal micrograph of VSMCs

200x magnification of VSMCs cultured without calphostin C on coverslips, fixed with paraformaldehyde, permeabilised with Triton X-100 and stained with DAPI (nucleus, blue) and an Alexa Fluor 488 conjugated α-smooth muscle actin antibody (clone 1A4, green). Image analysis of the cultured cells showed that they grew in monolayers and that all cells were nucleated and reacted with the 1A4 antibody suggesting that the cells were VSMCs and not endothelial cells or other contaminating cells. A mixed population of VSMCs were seen, containing both rhomboidal synthetic cells (circled) and elongated contractile cells (arrow). Scale bar denotes 5 μm.

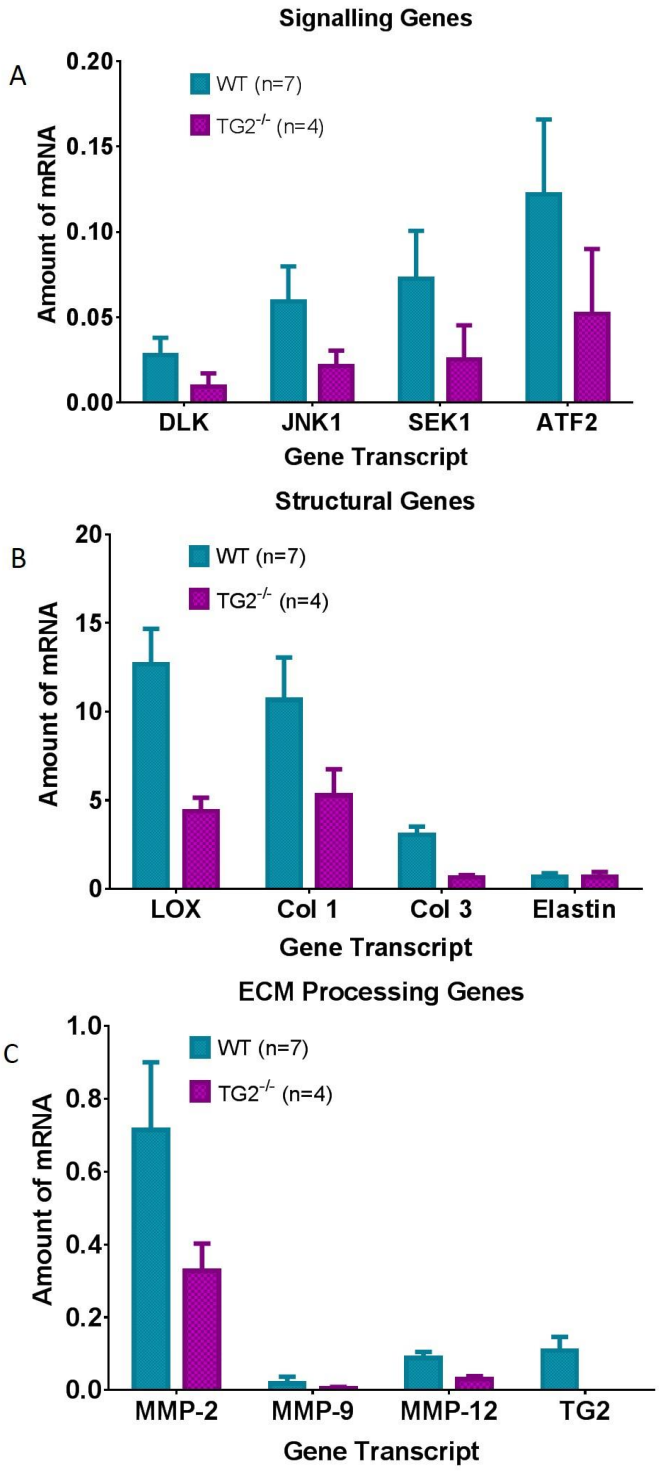

Figure 5-2 – Real time PCR of VSMCs

Bar graphs showing real time PCR data from WT and TG2$^{-/-}$ VSMCs. Data is shown as mean +/- 95% confidence intervals.

5.4.2 JNK Antigen and Activity

The ability of a cell to undergo programmed cell death (apoptosis) depends upon sustained activation of one or more of a number of receptors, all of which funnel through JNK, which is the final kinase in the MAPK pathway. A commercial activity assay was used to determine the activity of phospho-JNK (the active form) immunoprecipitated from cell lysates.

In 80% confluent TG2$^{-/-}$ cells it was found that total JNK activity was significantly decreased to 30% of the wildtype group (p=0.01). Phospho-JNK immunoblot levels in the same cells were decreased to 38% for p54 JNK (p=0.001) and 42% for p46 JNK (Figure 5-3).

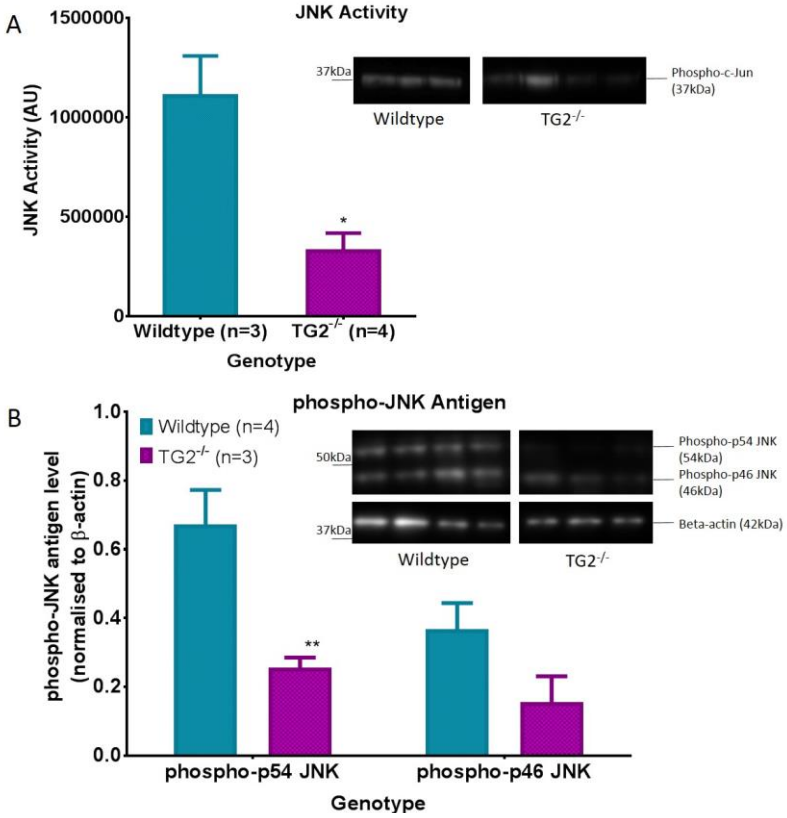

Figure 5-3 – JNK Activity and Antigen

Cell lysates from WT and TG2$^{-/-}$ VSMCs cultured without calphostin C were assayed for **(A)** JNK activity and **(B)** phospho-JNK antigen. TG2$^{-/-}$ were shown to have significantly less basal JNK activity (p=0.01) and phospho-p54 JNK (p=0.001) and a trend towards less phospho-p46 JNK (p=0.18) when compared to WT. Data is presented as mean +/- SEM (with western blot images inset) and significance determined by unpaired t-test for A and 1-way ANOVA for B.

5.4.3 Transglutaminase Activity

It has been postulated on the basis of inhibitor studies, but not formally shown, that TG2 is involved in potentiating apoptosis. Therefore, VSMCs from wildtype and $TG2^{-/-}$ mice were labeled with 2 mM biotinpentylamine, a transglutaminase substrate, and challenged with 100 nM calphostin C for 2 h to induce apoptosis.

Transglutaminase activity was determined by detection of biotinylated proteins from cultured VSMCs which were immobilised on a 96-well plate. Cell lysates were also ligand blotted using horseradish peroxidase labelled streptavidin to visualise biotinpentylamine labelled proteins.

Figure 5-4 shows the results of this activity assay and ligand blot. The activity assay is presented as the mean reaction velocity normalised to the non-apoptotic control. This value is the fold induction of total cell transglutaminase activity under apoptotic conditions. There is a significant difference in transglutaminase activity between the wildtype and $TG2^{-/-}$ groups (13-fold induction vs 3-fold, $p=0.004$) which supports the idea that this process is a TG mediated pathway and that the principal transglutaminase involved is TG2, rather than TG1 or TG4, both of which have been shown to be expressed by VSMCs (Johnson et al., 2012). It is also possible that this process is universal to all cells as TG2 is ubiquitously expressed.

The ligand blot (inset) shows transglutaminase crosslinking substrates in apoptosis (+/- calphostin C treatment). Interestingly, the number of bands appears to be limited, when compared to an SDS-PAGE gel of total intracellular protein, suggesting that TG2 is not indiscriminately crosslinking acceptor proteins together, and rather that there is selection in the glutamine

residue of substrate proteins. This signifies that the action is targeted and therefore is not just protecting against spillage of intracellular proteins into the extracellular space as has previously been suggested (Piredda et al., 1997).

Future work will aim to identify these labelled proteins which should be amenable to enrichment by magnetic streptavidin beads prior to identification by LC-MS.

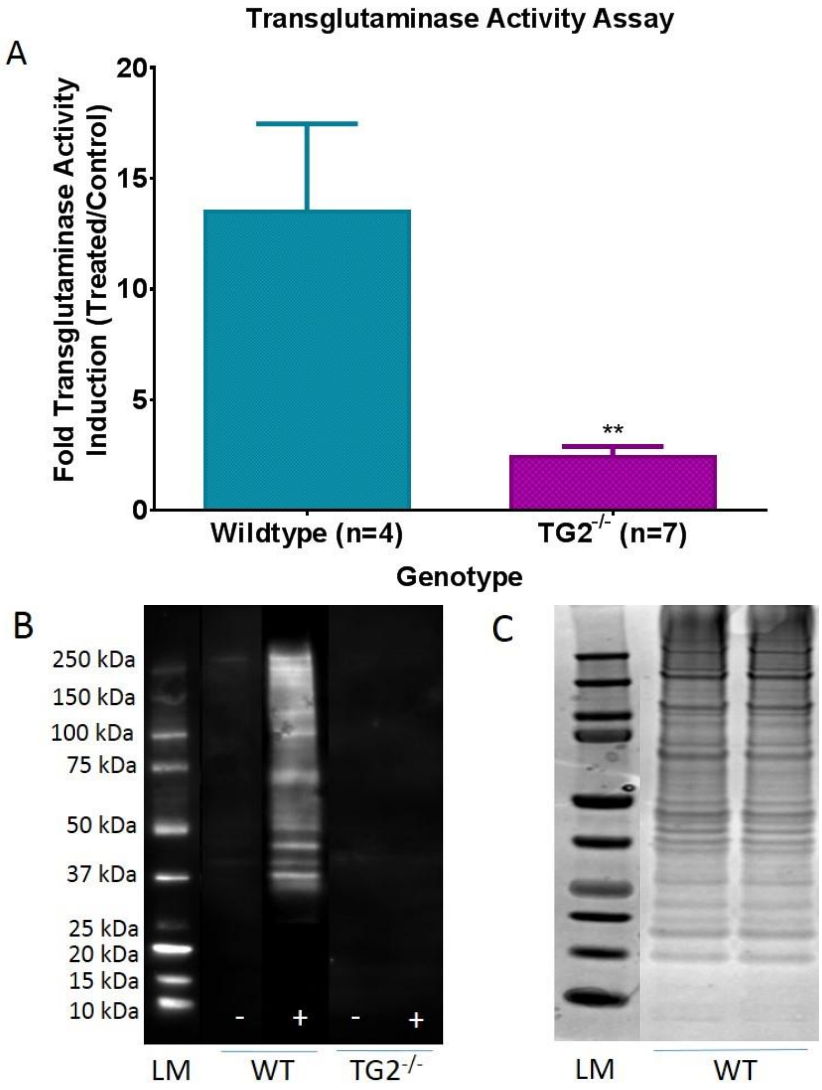

Figure 5-4 – TG2 activity and western blot of crosslinked proteins

Apoptosis was induced, by addition of calphostin C, in cultured VSMCs which had the transglutaminase substrate, biotinpentylamine, supplemented in the cell media. After 2 h of apoptotic stimuli, cells were lysed and **(A)** assayed for transglutaminase activity, **(B)** ligand blotted with streptavidin conjugated alkaline phosphatase to show crosslinked proteins and **(C)** SDS-PAGE gel of total intracellular proteins. Data in A is expressed as mean +/- SEM and an unpaired t-test used to determine significance.

5.4.4 Transglutaminase Activity in Apoptosis

Figure 5-5 shows the proportion of dead cells based upon an assay of protein mass after 2 h of calphostin C treatment.

TG2 knockout cells appear to resist apoptosis, as after 2 h of calphostin C treatment only 5% of cells had undergone apoptosis whereas 21% (p=0.03) of the wildtype cells had died.

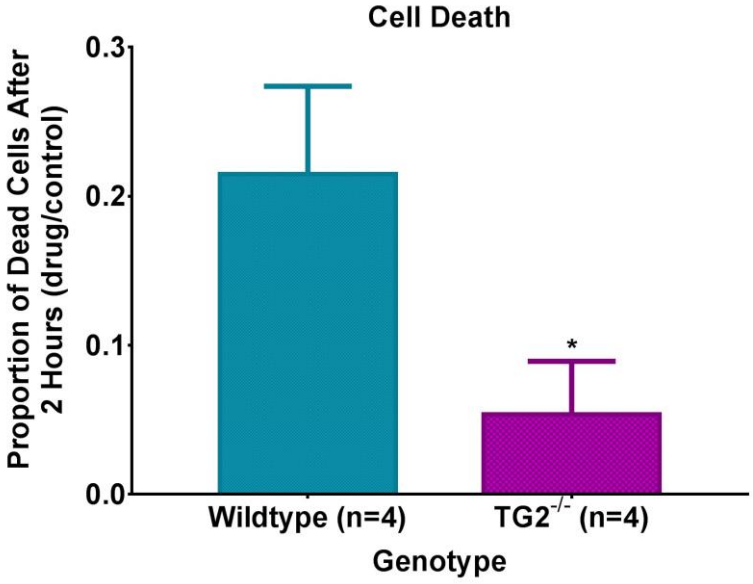

Figure 5-5 – VSMC death following apoptosis

The numbers of dead cells following calphostin C treatment was estimated by protein concentration of the harvest cell lysates (BCA assay) which were normalised to control cells (not treated with calphostin C). The data shows that significantly more WT cells had died than $TG2^{-/-}$ cells after 2 h (p=0.03). Data is shown as mean +/- SEM and significance determined by unpaired t-test.

5.4.5 DLK Protein Sequence Alignment

As it is known that TG2 preferentially crosslinks glutamines residing in Q-x-P-Φ motifs, protein alignment of the DLK amino acid sequence was performed. Figure 5-6 shows the findings of the alignment which revealed a conserved consensus TG2 crosslinking motif (QAPC) in all 28 animal species on Uniprot which contain a DLK homolog.

UniprotKB ID	Species	Q-X-P-ϕ motif	Residues
Q12852	Human	QAPC	182-185
Q60700	Mouse	QAPC	215-218
Q63796	Rat	QAPC	215-218
I3L8B0	Pig	QAPC	215-218
G1M1P0	Giant Panda	QAPC	215-218
H2Q625	Chimpanzee	QAPC	182-185
G1PF07	Brown Bat	QAPC	215-218
G1SPG5	Rabbit	QAPC	215-218
F1N791	Bovine	QAPC	215-218
I3N0G2	Ground Squirrel	QAPC	215-218
F7HKF1	Rhesus Macaque	QAPC	215-218
W5Q4M9	Sheep	QAPC	215-218
F7CZR4	Horse	QAPC	215-218
G1K8Z9	American Chameleon	QAPC	224-227
G3SQU1	African Elephant	QAPC	215-218
G3S5Z3	Gorilla	QAPC	215-218
Q6NYW1	Zebrafish	QAPC	206-209
E2RLX4	Dog	QAPC	215-218
M3WHK7	Cat	QAPC	215-218
H0WJ90	Bushbaby	QAPC	215-218
G3VYX8	Tasmanian Devil	QAPC	215-218
H0UV51	Guinea Pig	QAPC	215-218
M3Y3K1	Ferret	QAPC	215-218
H3DBH7	Pufferfish	QAPC	230-233
H2NHH3	Orangutan	QAPC	182-185
W5L5F1	Cave Fish	QAPC	208-211
H3A267	Coelacanth	QAPC	216-219
F6WAZ2	Platypus	QAPC	216-219

Figure 5-6 - Sequence alignment of DLK

Alignment of the DLK protein sequence of the 28 animal species available on the Uniprot database reveals a conserved TG2 recognition motif proximal to the kinase domain (QAPC).

Sequence annotation of the mouse homolog of DLK reveals that this potential crosslinking site resides within the protein kinase domain between the ATP binding and active sites. This crosslink could serve to either simply tether DLK molecules together or to promote cooperativity between the monomers and therefore greatly increase activity. Figure 5-7 shows the sequence alignment of mouse DLK and highlights the protein kinase domain (residues 137-405, yellow), the ATP binding site (K185, red), the active site (D269, pink) and the proposed TG2 crosslinking site (QAPC, 215-218, green).

```
        10         20         30         40         50
MACLHETRTP SPSFGGFVST LSEASMRKLD PDTSDCTPEK DLTPTQCVLR
        60         70         80         90        100
DVVPLGGQGG GGPSPSPGGE PPPEPFANSV LQLHEQDTGG PGGATGSPES
       110        120        130        140        150
RASRVRADEV RLQCQSGSGF LEGLFGCLRP VWTMIGKAYS TEHKQQQEDL
       160        170        180        190        200
WEVPFEEILD LQWVGSGAQG AVFLGRFHGE EVAVKKVRDL KETDIKHLRK
       210        220        230        240        250
LKHPNIITFK GVCTQAPCYC ILMEFCAQGQ LYEVLRAGRP VTPSLLVDWS
       260        270        280        290        300
MGIAGGMNYL HLHKIIHRDL KSPNMLITYD DVVKISDFGT SKELSDKSTK
       310        320        330        340        350
MSFAGTVAWM APEVIRNEPV SEKVDIWSFG VVLWELLTGE IPYKDVDSSA
       360        370        380        390        400
IIWGVGSNSL HLPVPSSCPD GFKILLRQCW NSKPRNRPSF RQILLHLDIA
       410        420        430        440        450
SADVLSTPQE TYFKSQAEWR EEVKLHFEKI KSEGTCLHRL EEELVMRRRE
       460        470        480        490        500
ELRHALDIRE HYERKLERAN NLYMELNALM LQLELKEREL LRREQALERR
       510        520        530        540        550
CPGLLKSHPS RGLLHGNTME KLIKKRNVPQ KLSPHSKRPD ILKTESLLPK
       560        570        580        590        600
LDAALSGVGL PGCPKGPPSP GRSRRGKTRH RKASAKGSCG DLPGLRAALP
       610        620        630        640        650
PHEPGGLGSP GGLGVGPSAW DACPPALRGL HHDLLLRKMS SSSPDLLSAA
       660        670        680        690        700
LGARGRGATG GARDPGSPPP PQGDTPPSEG SAPGSTSPDS PGGAKGEPPP
       710        720        730        740        750
PVGPGEGVGL LGTGREGTAG RGGNRAGSQH LTPAALLYRA AVTRSQKRGI
       760        770        780        790        800
SSEEEEGEVD SEVELPPSQR WPQGPNMRQS LSTFSSENPS DVEEGTASEP
       810        820        830        840        850
SPSGTPEVGS TNTDERPDER SDDMCSQGSE IPLDLPTSEV VPEREASSLP
       860        870        880
MQHQDGQGPN PEDSDCDSTE LDNSNSIDAL RPPASLPP
```

Figure 5-7 – Protein sequence annotation of mouse DLK

Consensus protein sequence of mouse DLK (MAP3K12) with the protein kinase domain highlighted in yellow (137-405), ATP acceptor (K185) in red, active site (D269) in pink and the potential TG2 crosslinking motif (QAPC, 215-218) highlighted in green.

5.5 Discussion

5.5.1 Transglutaminase 2 interacts with the apoptotic MAPK cascade

It has previously been proposed that a transglutaminase is involved in the activation and/or potentiation of apoptosis and studies utilising non-specific inhibitors (which among other actions would inhibit transglutaminase activity) have shown a commensurate reduction in the formation of DLK oligomers (and therefore MAPK activation) and caspase cleavage following initiation of apoptosis with calphostin C (Robitaille et al., 2008).

The results presented here corroborate those put forward by (Robitaille et al., 2008) and identify that TG2 is the main transglutaminase that potentiates apoptosis through the MAPK cascade. Aortic VSMCs derived from global TG2 knockout mice show defects in JNK activity as a result of lower levels of phosphorylation at the activating TPY motif in JNK. Further to this, protein alignment of DLK homologs revealed a conserved TG2 crosslinking site within DLK which is located in the protein kinase domain. This oligomerisation and subsequent crosslinking may serve to promote cooperativity between the active sites of the DLK molecules thereby resulting in the increased activity seen when oligomerised in previous reports (Robitaille et al., 2004).

However, the decrease in JNK phosphorylation, activity and amount of cell apoptosis seen in the $TG2^{-/-}$ VSMCs could be due to the decrease in the concentrations of the target molecules (i.e. DLK and JNK) as seen in the qPCR measurements and not necessarily due to a lack of TG2 catalysed crosslinking of DLK oligomers. In order to clarify this total JNK (and DLK)

antigen levels, for which antibodies are available, would need to be determined in the same samples.

The previous studies into TG2's involvement with the MAPK pathway have used caspase cleavage assays to determine the amount of apoptosis (Robitaille et al., 2004; Robitaille et al., 2008). This thesis used intracellular protein concentration as a surrogate for measuring intact cells. This method is not a measure of apoptosis and other methods would need to be employed in order to determine this. Examples of such assays would be the use of quenched-fluorescent caspase substrates (e.g. DEVD peptides) which tether a DNA binding dye to the cytosol until activation of caspase 3 and/or 7 which cleave the peptide and release the dye resulting in a measureable fluorescence signal, quantitation of the amount of DNA laddering and nuclear condensation as a result of nuclease activation and Annexin V staining of the outer cell membrane as a result of phosphatidylserine being externalised as part of the apoptotic cascade.

A potential therapeutic avenue could be explored by developing inhibitors of DLK oligomerisation. If this oligomerisation and covalent stabilisation occurs purely in apoptotic states when TG2's transamidation activity is activated, then this pathway would be a more preferable target for slowing cellular apoptosis than global JNK inhibition as it would not disturb JNK-dependent proliferation.

Figure 5-8 depicts this pathway as a flow chart, with the dotted horizontal line representing TG2 transamidation activity and vertical lines labelled with ATP signifying kinase activity.

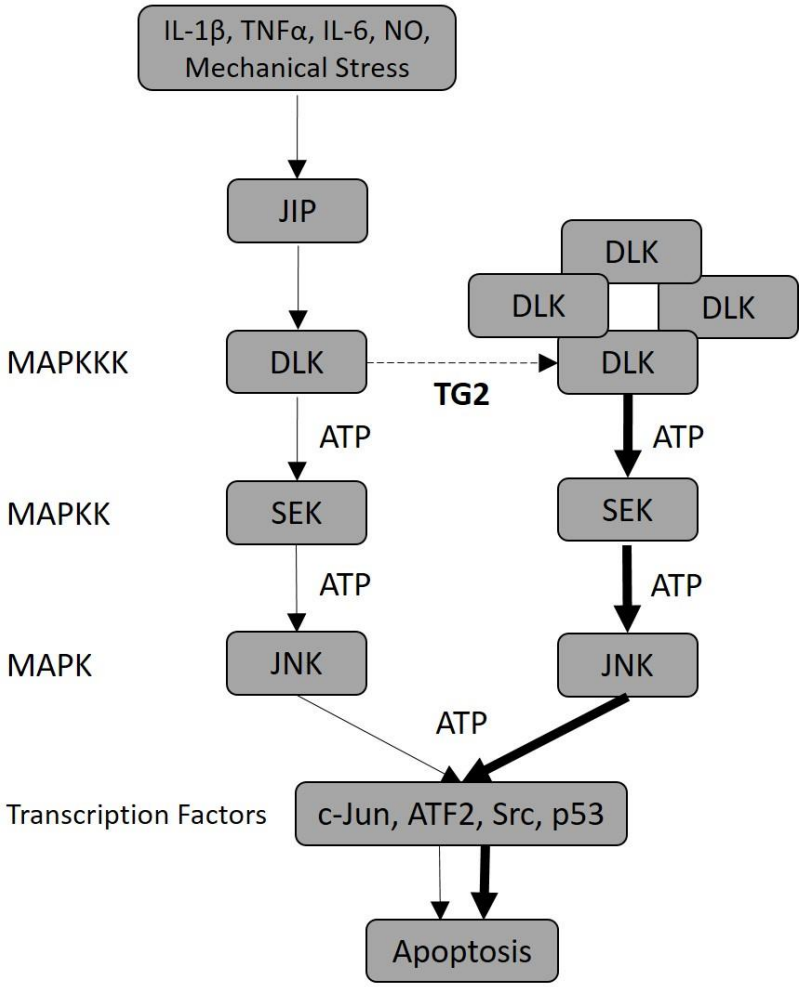

Figure 5-8 – Proposed mechanism of apoptotic MAPK activation

The data from this study and others suggests that TG2 is able to potentiate apoptosis through the MAPK pathway. Previous work suggested a transglutaminase was able to covalently oligomerise the MAPKKK, DLK, resulting in greater activation of the downstream cascade and therefore a greater activation of apoptotic signalling. Solid vertical arrow represents kinase activity and the dotted horizontal arrow shows transamidation activity.

5.6 Conclusion

This study aimed to build on the previously reported findings that a transglutaminase is involved in potentiating apoptosis through the MAPK pathway (Robitaille et al., 2004).

From the results presented above, it can be concluded that TG2 is the principal transglutaminase involved in potentiating apoptosis and that TG2 deficient cells show less ability to be able to undergo apoptosis.

This observation may be a result of either lower target concentrations of signalling molecules or a lack of TG2-catalysed stabilisation of DLK oligomers (Robitaille et al., 2004).

5.7 Summary of Key Findings

- Previous reports suggested that a transglutaminase (potentially TG2) crosslinks an upstream MAPK pathway kinase (DLK) resulting in an increased activation of the pathway and an increased potential for the cell to undergo apoptosis.

- $TG2^{-/-}$ VSMCs show reduced JNK activity and phospho-JNK levels.

- TG2 is the main transglutaminase involved in calphostin C-induced apoptosis and $TG2^{-/-}$ cells show resistance to apoptosis.

- Bioinformatics analysis of DLK reveals a conserved potential TG2 crosslinking site proximal to the kinase domain.

Chapter 6 – Preliminary Data and Suggestions for Future Work

6.1 Introduction

This thesis has provided evidence for a role for arterial FXIII-A in maintaining the plasma pool and also a role for TG2 in potentiating cellular apoptosis. However, some questions still remain unanswered.

This chapter describes work that has been carried out during the PhD study which require further attention and discusses some potential avenues for future work.

6.2 Results

6.2.1 Identification of TG2 Substrates

The literature suggests several important roles for TG2 but very little evidence in the way of identified *in vivo* substrates. The two roles of interest probed in this thesis relate to the promotion of apoptosis and the crosslinking of proteins in the extracellular space. Within the extracellular space there are two potential functions for TG2; the first is in the basal structure of the ECM and some potential *in vitro* substrates have been identified for this (shown earlier in 1.1.3), and the second is in repair whereby TG2 potentially becomes activated following tissue damage.

6.2.1.1 Substrates in Apoptosis

Proteins extracted from VSMCs (in 5.4.3 above), in which apoptosis had been induced with calphostin C, were labelled with biotinpentylamine, which was crosslinked into cellular proteins. These proteins were selectively enriched using streptavidin magnetic beads, trypsinised and peptide spectra identified by LC-MS. This methodology was seen as a viable strategy to allow efficient identification of TG2-crosslinked proteins due to the limited number of crosslinked bands detected by ligand blotting and a recent report (Schiapparelli et al., 2014) that suggested that direct trypsinisation of the biotin-streptavidin complexes produced more identifiable peptides in biotinylated HEK 293T cells than with traditional elution.

While the presence of biotinpentylamine was determined in the cell lysates the mass spectrometer detected no peptide peaks that were not derived from streptavidin. This is more than likely due to the amount of streptavidin magnetic beads used, which in retrospect will have been in too great an

excess for the amount of biotinylated proteins in the sample. Therefore, when the beads were trypsinised the resulting cellular peptides were swamped by the over abundant streptavidin peptides, thus masking the signal.

6.2.1.2 Substrates in the Extracellular Matrix

While the work presented earlier in this thesis identified a role for TG2 in the intracellular space (namely, in apoptosis), it is also known that TG2 is present in the ECM and in certain circumstances may become active in the extracellular space. Hearts were chosen to try and identify substrates because of their large relative size and amount of protein available compared to smaller tissues and also due to the link with a possible repair role for TG2 in myocardial fibrosis (3.5.1 above). To try and identify some novel extracellular TG2 substrates heart proteins were fractionated;

1. PBS soluble – extracellular, non-electrostatically bound, non-covalently bound proteins.
2. 0.5 M NaCl soluble – extracellular, electrostatically bound, non-covalently bound proteins.
3. Detergent soluble – intracellular and membrane proteins.
4. 0.25 M oxalic acid soluble – extracellular, elastin-bound proteins.

This scheme was based upon approaches described by others (de Castro Brás et al., 2013; Kim et al., 2014) and the expectation that TG2 crosslinks proteins that are already associated with the ECM (most likely by forming an initial electrostatic interaction). Therefore, the fractions containing the crosslinked proteins of interest would be the salt and acid soluble fractions with the salt fraction showing a greater abundance of protein in the $TG2^{-/-}$ mouse.

To characterise the fractions, several assays were performed; protein concentration was determined, SDS-PAGE to see any gross changes in abundant proteins, agarose gel electrophoresis to confirm the extracellular fractions were free of gDNA, and finally, protein identification by LC-MS.

Figure 6-1A shows the results of the BCA assay which provides evidence that the $TG2^{-/-}$ hearts have more protein electrostatically attached to the ECM (salt fraction, $TG2^{-/-}$ had 272.5 +/- 29.6 µg/mL vs 149.2 +/- 5.8 µg/mL for the WT) but less elastin crosslinked protein (oxalic acid fraction, $TG2^{-/-}$ 208.3 +/- 10.2 µg/mL, WT 266.7 +/- 8.0 µg/mL) compared to the wildtype.

The SDS-PAGE analysis of the salt fractions of the two groups (Figure 6-1B), showed that a ~250 kDa protein was differentially expressed in the $TG2^{-/-}$

hearts (brighter band, which does not appear in the wildtype). This may well be a protein that is usually crosslinked to the ECM by TG2 but in the knockouts has remained electrostatically associated to the ECM. Alternatively, the protein highlighted by SDS-PAGE could have been induced to compensate for the lack of TG2.

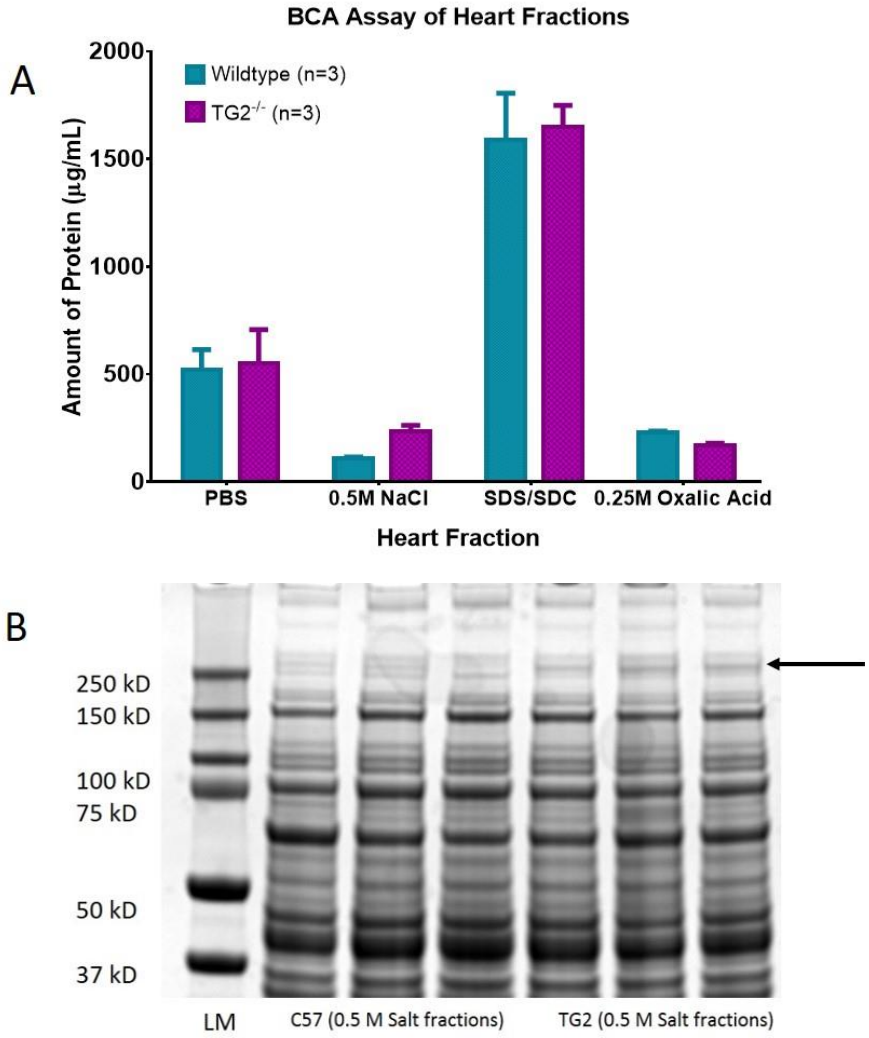

Figure 6-1 – Characterisation of heart protein fractions

Mouse hearts were fractionated using different conditions to sequentially extract groups of proteins potentially crosslinked by TG2. Four fractions of proteins were produced, PBS soluble, 0.5 M NaCl soluble, detergent soluble and 0.25 M oxalic acid soluble. **(A)** Protein concentrations were determined using the BCA assay. **(B)** SDS-PAGE analysis of the salt soluble fractions.

Because the BCA assay consistently showed an increased protein concentration in the salt fraction and there was evidence of a difference in protein composition, this fraction was further analysed.

Fifty micrograms of total protein was precipitated with 100% acetone and washed once with 100% acetone. These samples were then sent for protein identification by LC-MS. Table 8-4 details the results of the mass spectrometry which identified 50 proteins in the fractions. However, the proteins identified did not appear to be ECM derived proteins, with the most abundant being serum albumin. Amongst the remaining proteins many were identified as intracellular with numerous enzymes of the glycolytic pathway being found, thus suggesting that cell lysis had occurred and contaminated the samples. These proteins are so abundant that they mask the signal from any less abundant proteins and therefore no novel TG2 substrates were identified.

To try and establish if cellular damage had occurred during sample preparation, agarose gel electrophoresis (Figure 6-2) was performed on both the salt (NCP) and detergent (ICP) fractions to detect the presence of genomic DNA. As expected, large amounts of high molecular weight nucleic acid were found in the ICP fraction as cell and nuclear membranes are detergent soluble. Small amounts of nucleic acid were seen in the salt fractions along with light smears of ethidium bromide stained material (presumably fragmented gDNA) which suggests that a number of cells had indeed lysed and released intracellular material into the extracellular space, thus removing any expectation of detecting any of the extracellular, potentially crosslinkable, proteins.

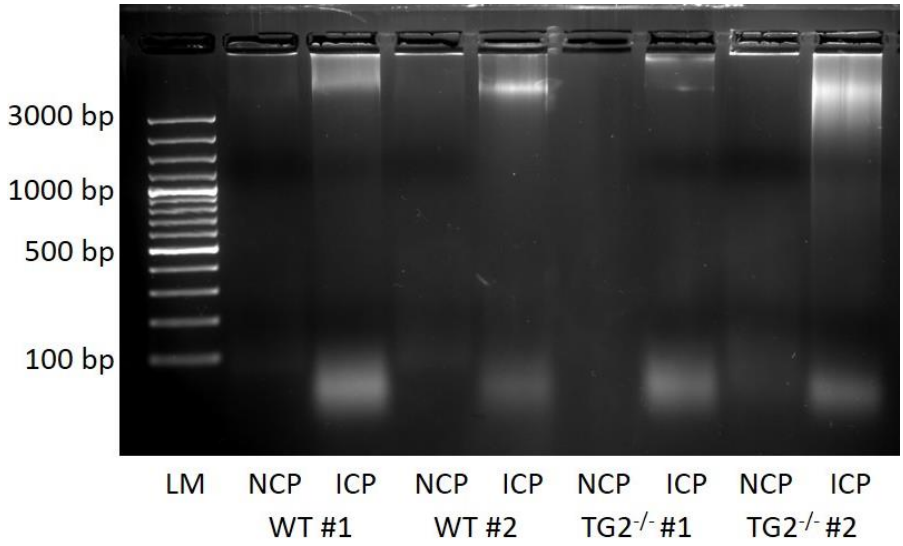

Figure 6-2 – Localisation of gDNA in heart fractions

Image of ethidium bromide stained 2% agarose gel electrophoresis of wildtype (WT) and $TG2^{-/-}$ salt and detergent soluble heart protein fractions. LM = DNA ladder, NCP = non-covalently bound protein fraction, ICP = intracellular protein fraction.

6.2.2 Clodronate

To determine if resident macrophages maintain the plasma pool of FXIII-A we attempted to selectively kill these cells by delivering the cytotoxic drug clodronate encapsulated within liposomes to mice and cultured bone marrow-derived macrophages. Only phagocytic cells exposed to these liposomes will engulf them, and be affected by the drug and die.

6.2.2.1 In vitro

Figure 6-3A shows cultured macrophages efficiently ingesting the DiI-labelled clodrosomes (red) and cells (blue). Once ingested, cells rapidly underwent apoptosis as expected. These cells showed the characteristic morphological changes associated with apoptosis, cell shrinkage, membrane blebbing and chromatin condensation followed by DNA fragmentation. As the DNA fragments, more sites for Hoechst dye binding are revealed resulting in a direct increase in fluorescence, this is shown in Figure 6-3B (green spots). Cells 1, 2 and 3 (labelled) show a time-dependent increase in fluorescence whereas cell 4 does not change its fluorescence throughout imaging.

Figure 6-3C&D show the characterisation of the clodrosome preparations and hence confirms that 3-5 mg of clodronate is encapsulated per mL of liposomes which is in line with expectation from the published method.

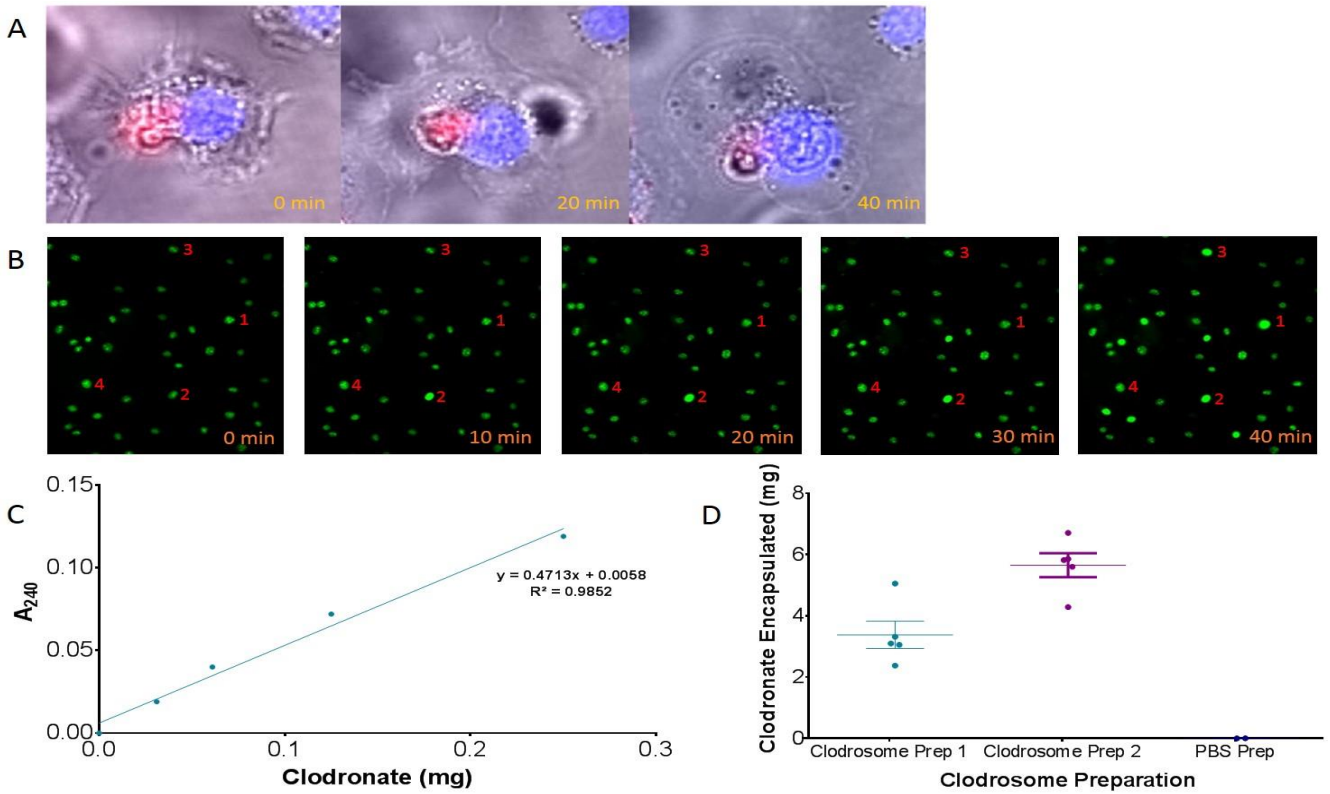

Figure 6-3 – *In vitro* testing of clodrosomes

Clodrosomes, clodronate-encapsulated liposomes, were given to phagocytic bone marrow-derived macrophages (BMDM) to test their cytotoxic potential. **(A)** shows a BMDM (nuclei, blue) phagocytosing a clodrosome (red) and then undergoing apoptosis and shows the characteristic cell shrinkage, membrane blebbing and intracellular vesicle formation. **(B)** is a fluorescence image showing Hoechst 33258 stained nuclei (green), as the chromatin condenses (in apoptosis) more sites for dye binding become accessible and fluorescence intensity increases. Cells 1, 2 and 3 show increases in fluorescence whilst 4 does not. **(C)** shows the clodronate encapsulation efficiency of the liposomes and demonstrates that the clodrosomes contain 3-5 mg/mL of clodronate.

6.2.2.2 In vivo

Literature in this area suggested that resident tissue macrophages living in the liver, spleen and bone marrow (Rooijen and Sanders, 1994) are all susceptible to clodronate treatment and there is evidence that cardiac macrophages are accessible too (Epelman et al., 2014; Fujiu et al., 2014) even though they do not contain fenestrated capillaries. However, as the liposomes cannot cross the blood-brain barrier (unless mannosylated), the brain microglial cells are not affected and can therefore serve as a negative control of cell death. The liver is known to be well targeted by the clodrosomes as a result of it containing fenestrated capillaries and can act as a positive control of cell death. We chose $Mpl^{-/-}$ mice for this experiment as any fall in plasma FXIII-A would be easier to see as the platelet contribution to the FXIII-A background is significantly reduced (as described in 4.4.2 above).

Either PBS-liposomes or Clodrosomes were injected via the tail vein 3 times per week for 2 weeks into $Mpl^{-/-}$ mice. Terminal blood samples were taken from these mice and age matched C57BL/6 controls for plasma FXIII-A activity determination and tissue was taken for mRNA determination.

Macrophage cell death in the *in vivo* assays was determined by assaying gene transcripts of cell differentiation markers, namely, the macrophage markers; CD163, heme oxygenase-1, F4/80 and CD68; the dendritic cell marker, CD11c; and CCR2 which is the receptor that allows the uptake of mononuclear cells into the tissue space. Alongside these markers the FXIII-A gene transcript was assayed to see if a proportional drop was seen. A wide range of supposedly pan-macrophage markers were chosen as a result of the large heterogeneity seen within a population of cells known as ‘macrophages’.

A dendritic marker was included as these cells are known to be tissue resident and also phagocytic and CCR2 was chosen as a reuptake marker to see if clodronate treatment induced macrophage flux into the tissue from the blood.

Figure 6-4 shows the real time PCR results of the above transcripts in heart (a), aorta (b), brain (c), liver (d), spleen (e), and bone marrow (f).

Of note, the highest transcribed macrophage marker was CD68, a surface glycoprotein which binds oxidised low density lipoprotein and is supposed to be a common marker representing all monocytes and macrophages (Heidt et al., 2014; Deonarine et al., 2007; Côté et al., 2013) and is therefore best placed to show a reduction if these cells are cleared by the clodrosomes.

The results show that the brain is unaffected by the clodrosomes, as expected, because the liposomes were not made with mannosylated reagents. The liver, which is expected to be sensitive to clodrosomes, showed a distinct drop in CD68 and HO-1, however not to zero. The heart appeared to be susceptible to clodrosomes and showed a drop in CD68 and was the only organ to show a demonstrable drop in FXIII-A. The spleen was also supposed to be sensitive to clodrosomes but it is arguable as to whether there is a drop in CD68 level. Whereas, the aorta and bone marrow appeared insensitive to clodrosome treatment. Of these, the bone marrow result appeared unpredicted as the clodrosomes are meant to be taken up through fenestrated vessels, which the bone marrow contains (as this is how cells are released from the bone marrow into the circulation, e.g. platelets).

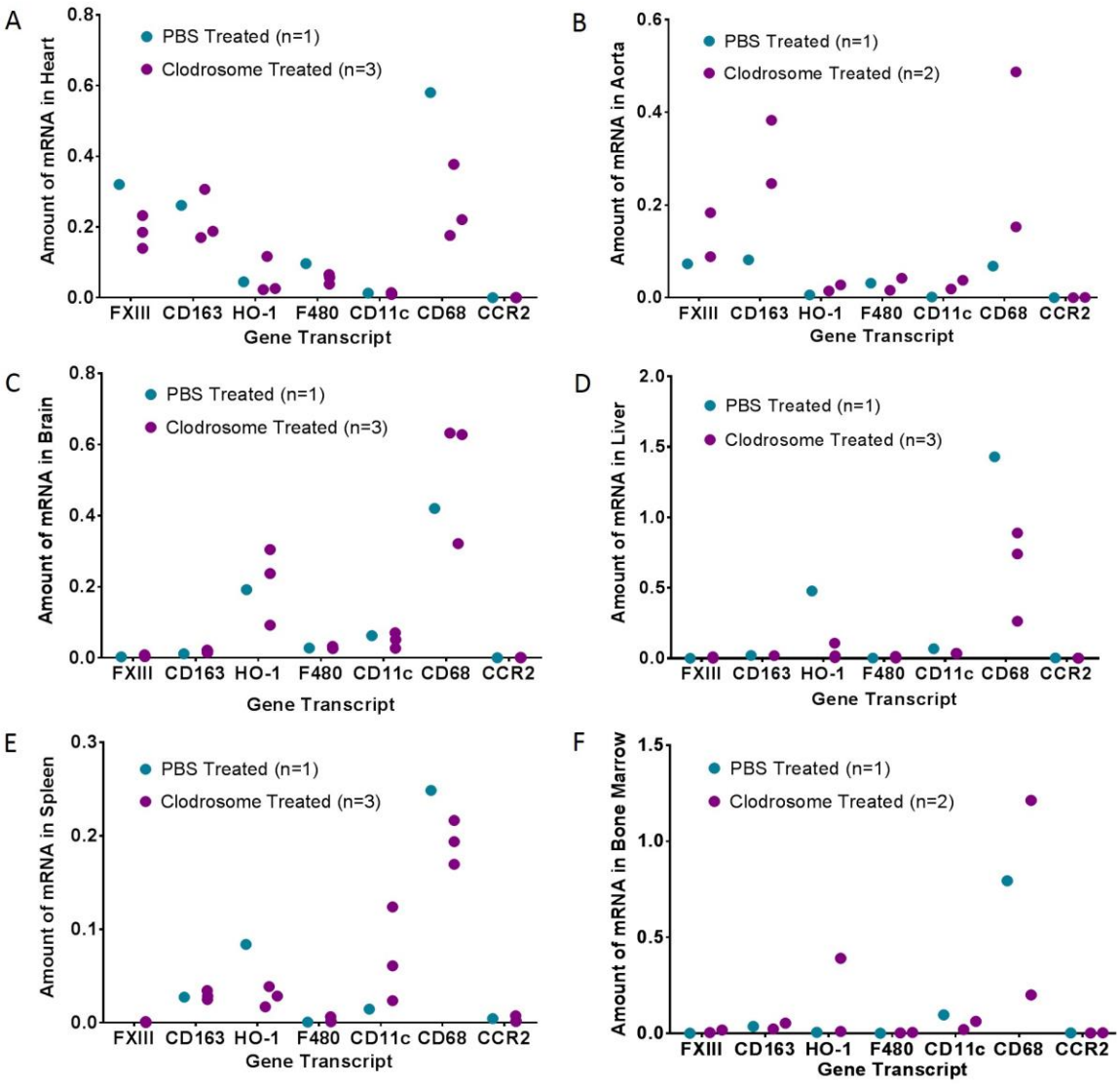

Figure 6-4 – mRNA data from clodrosome-treated mice

FXIII-A and cell marker mRNA expression in **(A)** heart, **(B)** aorta, **(C)** brain, **(D)** liver, **(E)** spleen and **(F)** bone marrow.

Blood samples from the clodrosome and control treated mice were taken and Figure 6-5 shows the results of the plasma FXIII-A activity assay. No reduction was seen in the clodrosome treated group when compared to either the PBS-liposome treated or wildtype control groups.

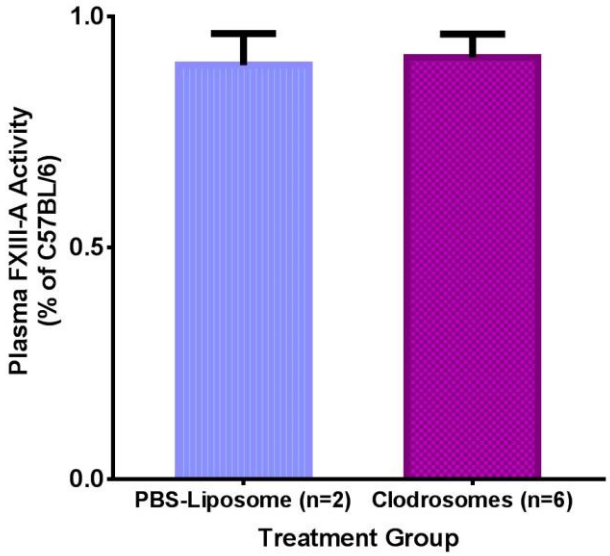

Figure 6-5 – FXIII-A plasma activity assay in clodrosome-treated mice

Mpl$^{-/-}$ mice were given intravenous injections of cytotoxic clodrosomes to deplete blood and, hopefully, tissue resident macrophages. Following treatment, plasma FXIII-A assay was determined and compared to the control liposome treated mice. No difference in plasma FXIII-A activity was seen between the two groups. Data is shown as mean +/- SEM.

The *in vivo* use of the clodrosomes was to try and determine whether or not there was an easy option for depletion of tissue resident macrophages and whether or not they contribute to the circulating levels of FXIII-A. However, the results presented here suggest that while the clodrosomes did kill macrophages *in vitro*, sporadic depletion was seen *in vivo*, and therefore future use of the clodrosomes will have to be carefully considered and if pursued would require further optimisation.

Ideally, to assay the *in vivo* effectiveness of the clodrosomes, circulating monocyte numbers should have been assayed as these cells readily ingest the liposomes and would have provided an index of cell depletion.

6.2.3 Carotid Injury

It remains unclear whether or not the lack of a clotting defect seen in the conditional knockout mice in the ROTEM assays fully represent the *in vivo* situation. It might still be expected that the FXIII-$A^{-/-}$ mouse would show an effect in clot formation in this model.

Several preliminary carotid injury procedures were carried out in wildtype mice to establish the technique. The procedure itself is summarised visually in Figure 6-6.

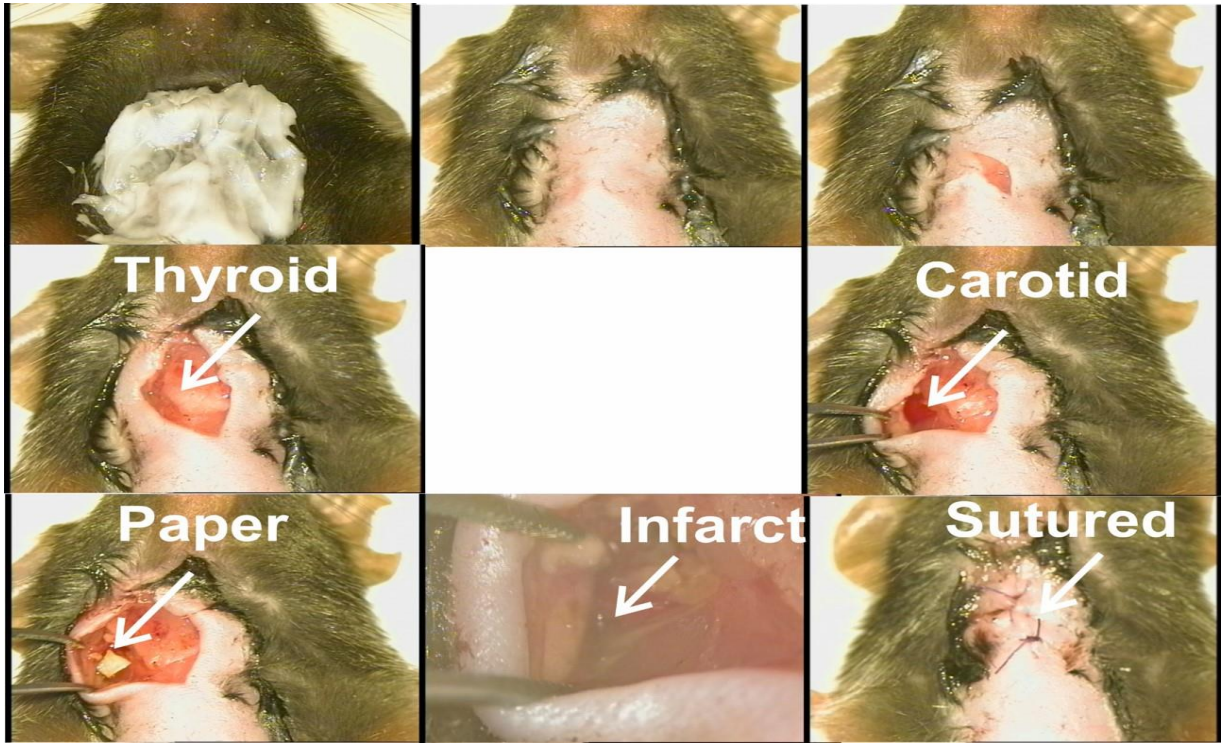

Figure 6-6 – *In vivo* carotid injury model

Eight week old C57BL/6 mice were anaesthetised using inhaled Isoflurane and maintained using a face mask. Once asleep, the mouse was placed on its back and the hair removed from the neck using an electric razor and dilapidating cream. The right carotid artery was exposed by making an incision to the right of the trachea and blunt dissecting away the soft tissue. 10% $FeCl_3$ on a 1 x 2 mm^2 piece of filter paper was placed on the artery for 3 min to induce thrombosis. The filter paper was then removed and the site washed with sterile PBS. The incision was then sutured using 6/0 vicryl and the mouse allowed to recover in a heated hospital cage.

The findings of (Evans et al., 2009) suggested that a clot in the common carotid artery of a wildtype C57BL/6 mouse has an area of 39 µm +/- 6 µm. Based upon this data, this study would require large group sizes to have the power to see differences in this parameter between the genotypes (n=6 per time point to have the power to see a 50% drop in clot area). In order to try and reduce the numbers of mice required for this study other methodologies, besides serial sectioning of the carotid artery, were explored including contrast-enhanced ultrasonography utilising fibrin-targeted microbubbles as well as standard ultrasonography (Figure 6-7).

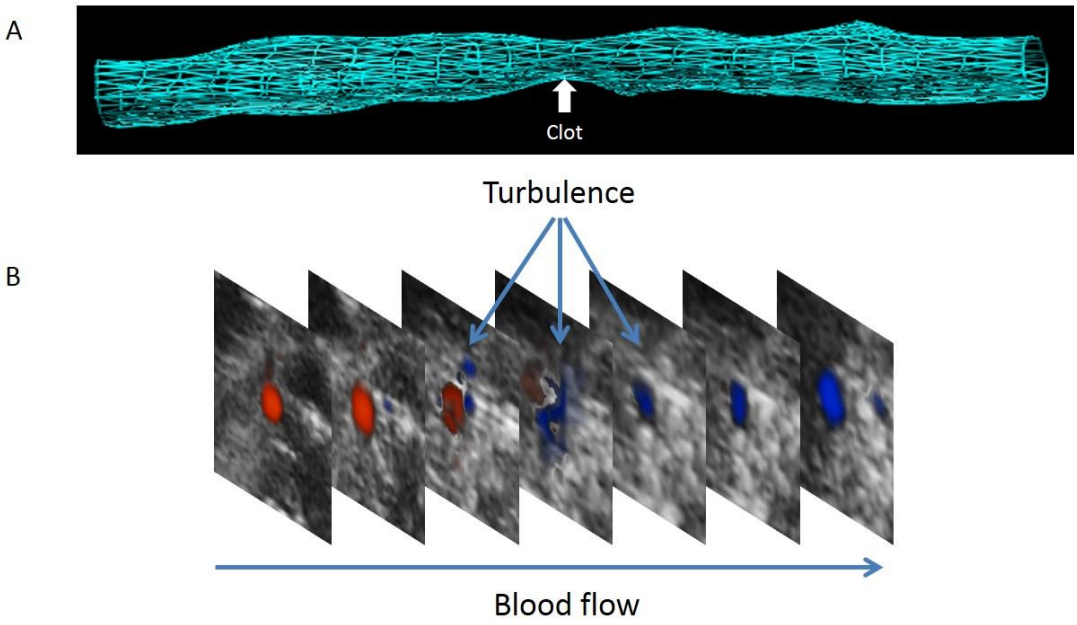

Figure 6-7 – Ultrasound imaging of a carotid thrombus

(A) shows an ultrasound 3D reconstruction of the right carotid artery of a FXIII-$A^{+/+}$ mouse following $FeCl_3$-induced thrombosis. **(B)** is individual 1 mm short-axis non-contrast enhanced ultrasound sections through the vessel with colour Doppler overlaid (red = flow towards probe, blue = flow away from probe).

6.3 Discussion

6.3.1 Composition of the extracellular matrix in the TG2$^{-/-}$ mice

While the presence of TG2 in the intracellular and extracellular spaces is unquestioned, the enzyme itself appears dormant under most conditions. Little is known about the substrates of TG2 and while this appears to be an obvious question, to date there are no reports that identify them *in vivo*. Therefore, as part of this thesis, work was undertaken to try and develop a method to be able to identify some potential targets.

While it was expected that the ECM-derived salt fraction in the TG2$^{-/-}$ mice would contain a greater concentration of protein, and the oxalic acid fraction less, when compared to the wildtype, it is unclear as to what this represents. The simplest explanation would be that the proteins usually crosslinked to the matrix in the wildtype are not crosslinked in the TG2$^{-/-}$ mice and therefore appear in the salt fraction. However, the mass spectrometry data does not reflect this notion. Instead, what this may suggest is that either the tissue is softer and therefore easier for sample preparation to cause cell lysis (as evidenced by protein identification of intracellular proteins) or it could represent an increase in vascular permeability in the TG2 knockouts (seen as an increase in albumin in the ECM).

These possibilities could be tested by techniques already established in the literature. Tissue strength can be determined through mechanical testing such as resistance to stretching and crushing (Miller, 2005) and calorimetry (Sun and Leung, 2008), whereas vascular permeability can be assayed by intravenous injection of Evan's blue dye into mice and subsequent measurement of the dye in excised tissues (Radu and Chernoff, 2013).

6.3.2 Clodronate did not deplete the cells that maintain the plasma pool

On review of the literature it became apparent that groups were attempting and reporting success in using clodronate-encapsulated liposomes to deplete both circulating monocytes as well as more importantly already established tissue resident macrophages. It was known that liver, spleen and bone marrow could be readily targeted by these clodrosomes (Rooijen and Sanders, 1994; Rooijen and Hendrikx, 2010) but more surprisingly that also cardiac (Epelman et al., 2014) and aortic cells (Psaltis et al., 2014) could be depleted.

Clodrosomes are made available to the tissue as they are able to travel out of the capillary through fenestrations in the wall of the vessel (Sercombe et al., 2015). The liver, spleen and bone marrow should all be targeted by clodrosomes as they all contain these discontinuous, fenestrated, capillaries. How the aorta and heart were targeted was more curious as they do not contain fenestrated capillaries and therefore the clodrosomes should have no access to the cells residing within the tissue. The brain is protected from clodrosome depletion as they cannot be transported across the blood-brain barrier unless mannosylated (Rooijen and Sanders, 1994).

The results presented in this thesis suggest that the clodrosomes, as expected, contained 3-5 mg/mL clodronate and that only the liver and heart are susceptible to clodrosome treatment through intravenous administration. However, the aorta, spleen and bone marrow show no depletion which contradicts the previous literature on the subject and suggests that the clodrosomes produced do work *in vitro* but were not evenly distributed *in vivo*. However, if the clodrosomes had spared cardiac macrophages and plasma FXIII-A but depleted bone marrow resident macrophages and monocytes then

this would have been good evidence for a role of resident macrophages in maintaining the plasma pool of FXIII-A.

A further question is raised as to how plasma proteins are degraded and removed from the circulation. This degradation may in part be mediated by blood monocyte/macrophages which if depleted by the clodrosomes may result in the circulating levels of FXIII-A not falling at the expected rate based on the known half-life of FXIII-A. This would make interpretation of the residual plasma FXIII-A activity levels following clodrosome treatment difficult as the levels of FXIII-A may remain “normal” for an extended period of time.

6.4 Future Work and Direction

While the work presented in this thesis lends evidence to arterial cells being involved in the maintenance of the plasma FXIII-A pool and intracellular TG2 playing a key role in apoptosis, there are still many unanswered questions. The ideas for future work are described below and concern the elucidation of the cellular source of plasma FXIII-A and the secretory mechanism as well as identifying novel substrates of TG2 both in the intracellular and extracellular spaces.

6.4.1 Macrophage Adoptive Transfer

In view of the failure of the clodronate assays but the success of bone marrow transplantation; two experiments would be worth carrying out.

The first is the reverse experiment to the one described earlier whereby FXIII-$A^{-/-}$ bone marrow would be transplanted into lethally irradiated FXIII-$A^{+/+}$ recipients to determine the cell displacement efficiency within the bone marrow as well as the organs of interest.

The second is to attempt adoptive transfer of wildtype cultured or isolated macrophages into FXIII-$A^{-/-}$ mice to see if the FXIII-A secreting niches can be repopulated without bone marrow ablation by irradiation and if they are able to reconstitute the plasma levels of FXIII-A. This would provide useful evidence as to the mechanism by which tissue macrophage niches are turned over as well as testing a possible treatment option for human patients deficient in FXIII-A. Adoptive transfer of macrophages has been established by other groups who have shown that macrophage adoptive transfer; prevents type 1 diabetes in NOD mice (Parsa et al., 2012), ameliorates renal fibrosis (Nishida

et al., 2005) and alleviates bronchial hyperresponsiveness (Careau and Bissonnette, 2004).

6.4.2 Purification of FXIII-A Secreting Cells

This thesis reports on a method to potentially purify these cells from 3-4 week old mouse heart tissue using (what is thought to be) an anti-Thy1.2 antibody, and if the same cells that colonise the early aorta are the same as the cells that are present in the heart then this methodology may be applicable to isolating those as well.

Beyond this, the evidence points toward the cells of interest in the aorta and heart expressing PF4. (Pertuy et al., 2015) described that F4/80^{+} macrophage-like cells in the lung, kidney, brain, heart, liver and stomach are able to be recombined by PF4-cre using an mT/mG mouse. The mT/mG mouse is a dual colour reporter whereby a stop codon placed downstream of the first colour reporter (Tomato) are flanked by LoxP sites. Upon cre recombination the Tomato and stop codon are cut out therefore allowing the GFP gene to be expressed. Therefore, when crossed with the PF4-cre mouse, this system would produce pups in which all of the cells express Tomato (red) fluorescing cells except for the PF4 expressing cells which would express GFP (green). Using the methodology described by Pertuy *et al*, these green fluorescing cells could be identified in the aorta (which the original study did not examine) and fluorescent cells isolated from organs using FACS and either cultured or assayed directly for FXIII-A expression and evidence of FXIII-A secretion.

6.4.3 Clodronate

The data presented in 6.2.2 above shows that *in vitro* cultured macrophages are phagocytic however no characterisation of these cells was carried out. It would be pertinent to characterise these cells in terms of FXIII-A mRNA and expression of PF4 and Thy1.2 and to verify that the FXIII-A mRNA disappears with clodronate treatment. It would also be important to determine if the heart cells from fibroblast B fraction isolated in 4.4.4.2 above are able to be cultured. If they are then two questions would need to be answered. The first, does treatment with clodrosomes cause apoptosis in this cell population which would suggest that they are capable of phagocytosis and therefore provide evidence that they are macrophages. The second question would be does clodrosome treatment result in a reduction of the FXIII-A mRNA signal implying that the population may represent a cell type capable of secreting FXIII-A.

Due to the findings of the *in vivo* assays whereby the clodrosomes did not produce the same findings as presented in the literature there are no immediate plans for attempting more *in vivo* clodronate assays.

A more effective way to determine the role that bone marrow-derived monocytes and macrophages have in maintaining the plasma pool of FXIII-A may be to characterise a mouse line that is monocytopenic. The $Csf1^{op/op}$ mouse carries a homozygous mutation in the colony stimulating factor-1 gene and therefore shows defects in producing monocytes through definitive haematopoiesis. As a result, this mouse produces 10% of the number of total leukocytes compared to a wildtype (Yoshida et al., 1990). It would be

predicted that these mice would show the same plasma FXIII-A levels as the Flt3-cre mice but with intact platelet FXIII-A.

6.4.4 Quantitation of Apoptosis in an Injury Model

Whilst the data presented in this thesis show that *in vitro* TG2 plays a role in cell death there is no substantive *in vivo* evidence as yet. A model of AAA has been established within the group as described in 3.5 above and it would be interesting to determine if there is a difference in apoptosis between the wildtype and $TG2^{-/-}$ groups by looking at DNA fragmentation levels using TUNEL staining in sectioned aneurysmal tissue. To balance this, staining would also be carried out using an anti-Ki67 antibody to determine any difference in cellular proliferation within the aneurysmal tissue.

A simple method for validating the idea that TG2 can slow apoptosis *in vivo* would be to utilise the mouse paracetamol overdose model. Cell death following paracetamol overdose is known to occur through a JNK dependent pathway (Win et al., 2011) and is relatively straightforward to carry out. Paracetamol is metabolised to the toxic product NAPQI in the liver and further reduced to a non-toxic product requiring glutathione. As the cellular stores of glutathione are depleted NAPQI builds up within the cell and beings binding mitochondrial proteins and inhibiting function leading to cell death. This methodology requires male C57BL/6 wildtype and $TG2^{-/-}$ mice (10-12 weeks old) which have been fasted for 12 hours (to normalise liver glutathione levels between mice). Following fasting, 300 mg/kg paracetamol (15 mg/mL in saline) is injected intraperitoneally and access to food is given. Mice are then sacrificed at 4 hours and 12 hours after injury and serum levels of alanine transferase are determined to show liver injury, liver lysates used to show

activation of the MAPK pathway, transglutaminase activity and caspase activation and sectioned tissue used for Annexin V staining (Mossanen and Tacke, 2015).

6.4.5 Cell Apoptosis

It has been suggested in this thesis that TG2 promotes the pro-apoptotic pathway and a potential crosslinking site within DLK, which is proximal to the kinase domain, has been identified in this work but has not been previously reported. Work will be undertaken to confirm that this site is crosslinked by TG2, both by *in vivo* cell labelling with biotinpentylamine and mass spectrometry identification of crosslinked DLK and also by recombinant protein methods.

As previously stated, TG2 is a ubiquitously expressed enzyme and therefore its role in apoptosis could be global. Further work is planned to determine if this pro-apoptotic function is present in other vascular cells e.g. fibroblasts, macrophages and endothelial cells.

A number of cell types, e.g. monocytes, macrophages and megakaryocytes, express FXIII-A. While FXIII-A is known to be secreted, albeit by an unknown mechanism, and is present in µg/mL quantities in the plasma it has also been shown to be retained intracellularly by some cell types (Adány and Bárdos, 2003; Cordell et al., 2010; Muszbek et al., 2011). FXIII-A, like TG2, is activated by increased Ca^{2+} ion concentration and carries out the same catalytic transglutamination reaction.

The vascular smooth muscle cells described here in this thesis were shown by real time PCR to not express FXIII-A however it would be interesting to see

if in cultured monocytes, which do express FXIII-A, there is a redundant role for FXIII-A in crosslinking DLK in apoptosis in the $TG2^{-/-}$ mice.

6.4.6 Substrates of TG2 in the ECM and within Apoptotic Cells

TG2 plays a role in cell apoptosis and it was shown in 5.4.4 above that proteins could be labelled with a small biotinylated molecule by TG2 which could potentially be enriched using streptavidin magnetic beads. Mass spectrometry will then be used to identify proteins crosslinked by TG2 in apoptosis.

In the ECM, isolation of crosslinkable proteins proved more challenging due to the highly crosslinked and insoluble nature of the matrix. In the future, decellularised hearts will be subjected to cyanogen bromide digestion to produce peptides of crosslinked proteins which should be suitable for mass spectrometry. Contamination with elastin should be avoided as it contains no methionine residues (which cyanogen bromide cleaves after) however collagen derived peptides may prove to be an issue. If this endeavour proves successful then TG2's role in repair could be studied by performing proteomic analysis on fibrotic hearts for example.

Chapter 7 – General Discussion and Conclusion

For quite some time the general consensus in the literature has been that the plasma pool of FXIII-A is maintained by the platelet. The work presented in this thesis describes the generation of a novel FXIII-A floxed mouse and not only discounts the platelet as the cellular source (as suggested by previous reports) but puts forward substantial evidence that circulating FXIII-A is secreted from a cell identical to, or closely resembling, the aortic tissue resident macrophage. Several experiments presented here suggest that these cells express the cell marker, PF4 and also perhaps Thy1.2. There is an emerging theory in the literature that tissue resident macrophages are seeded into the developing organs during embryogenesis, the earliest of which originate from the yolk sac. These cells then remain within the organs until long after birth and the majority of the reports suggest that while these cells are able to maintain their own cell numbers, they are slowly displaced by bone marrow-derived macrophages throughout life.

The evidence from the bone marrow transplantation studies presented in this thesis suggests that these resident cells can be displaced by irradiation and the results from the Flt3-cre mice show that these cells undergo simple turnover as the mouse ages. While FXIII-A deficiency in humans is rare, those that suffer with it require regular injections of recombinant protein to mitigate their symptoms. For these patients, transfer of cells expressing wildtype FXIII-A could serve as a long term therapy. What remains to be seen is whether or not tissue resident cells can be displaced by adoptive transfer (i.e. cell transfer without radiation) as this would allow restoration of the plasma

pool without the side-effects of bone marrow ablation therapy. However, further work is needed to confirm these findings. Once the cellular source is defined and a method designed to isolate the cells, substantial effort will need to be expended to elucidate the unknown mechanism of secretion from the cell.

While there does appear to be a convincing role for FXIII-A in microvascular repair (e.g. fibrosis) the results reported in this thesis and those from our group seem to discount the notion that TG2 and FXIII-A play a cooperative role in bone formation or macrovascular protection. However, there does appear to be a role for maternal FXIII-A in pregnancy which may well prove to be a macrovascular function, e.g. remodelling of the placental artery.

Despite the finding that TG2 is involved in apoptosis *in vitro*, which has been suggested previously, little in the way of *in vivo* evidence for this role has been shown. The work presented here reaffirms and builds on those findings and while it is known that apoptosis is required for a number of crucial developmental processes such as finger and toe formation, brain growth and septum formation in the heart (Haanen and Vermes, 1996; Watanabe et al., 2001), the $TG2^{-/-}$ mouse used in this thesis showed no gross phenotypic differences compared to the wildtype. This leads to the possible concern that a decreased apoptotic potential is incompatible with an otherwise phenotypically normal mouse. However, both of these could be rationalised if developmental apoptosis is controlled through a separate pathway to the TG2-JNK “stress” pathway. There are several previous reports detailing apoptosis during embryogenesis (Nelson, 1996; Uckan et al., 1997; Brill et al., 1999)

which suggest that this process is driven by Fas signalling which does not require JNK or any of the other MAPK components.

While global JNK inhibitors are in development for clinical use with the hope of efficacy in treating numerous conditions, it may be that this is ill-advised due to the findings in the compound knockout mouse that JNK is involved in proliferative signalling. It may well instead be prudent to target an upstream kinase in the MAPK pathway, of which DLK is identified as pro-apoptotic, and either inhibit its kinase activity directly or the potential oligomerisation sites, thus inhibiting apoptotic MAPK signalling without disturbing potential proliferative pathways.

Finally, while FXIII-A and TG2 appear to have distinct roles in biology, they do appear to have some cooperative function in protection against the development of both cardiac and vascular fibrosis, a deficit which is only seen in the double knockout mice and not in the single knockouts. Beyond this, it was shown in a model of aortic aneurysm that the double knockout mice were less susceptible to aneurysm formation at 6-weeks post injury which may be a result of the underlying fibrosis protecting the vessel from dilatation.

In summary, this thesis presents some common and distinct functions of the transglutaminases FXIII-A and TG2, for example in pregnancy and the development of cardiac and vascular fibrosis. Beyond this, significant exploration of the cellular source of plasma FXIII-A was undertaken and as a result plasma FXIII-A is suggested to originate from the aorta. Finally, the role of TG2 in potentiating apoptosis was investigated and TG2 was found to be the main transglutaminase involved in calphostin C-induced apoptosis in VSMCs. Also, a potential novel crosslinking site was identified in DLK, an

upstream MAPK component previously reported to be crosslinked by a transglutaminase, and this site could potentially be exploited as an avenue for therapy to better treat those conditions currently targeted by JNK inhibitors.

Chapter 8 – Appendices

8.1 Routine PCR Genotyping Conditions

Genotype	Primer Name	Sequence (5'-3')	T_M (^oC)
FXIII-A	F13-intron8FL	TCTGGGCCAAACCAAGTACCTGG	63
	F13-intron8R2	CAAGACCAGACTGTGCAAAGGG	
	F13-intron9R2	GGGGACTTGCTCCCATGTAAA	
PF4-cre	PF4common	CATTGGAGATGTGGATCCTGCT	55
	PF4endog_rev	CATGTCAAGAGGGTGCCACTGGA	
	PF4transgene	ATGTCCATCAGGTTCTTCCTGAC	
CD11b-cre	CD11b_F	CGACCAGGTTCGTTCACTCA	55
	CD11b_R	CAGCGTTTTCGTTCTGCCAA	
	ApoE_F	CTCTGTGGGCCGTGCTGTTGGTCACATTGC	
	ApoE_R	CTCGAGCTGATCTGTCACCTCCGCTCTCC	
TG2	TG2_P1_Long	GGAGCACACAGGCCTTATGAGCTGAAG	64
	TG2_P2_Long	GCACAGATAGGGATACAAGAACATTGAAG	
	TG2_P3_Long	GTCCTCGGATGACAAGGTGACAGAGCA	
c-Mpl	Cmpl_common	CAGGAACCTGAGGGGCTGGC	58
	Cmpl_WT	GTTTGGAAGGGCCAAGAGGA	
	Cmpl_bGal	AAGCGCCATTCGCCATTCAG	
LysM-cre	LysM_common	GGGCTGCCAGAATTTCTC	64
	LysM_WT	ACTCCATAGTAGCCAGCCATTCC	
	LysM_mutant	GGTTATTCAACTTGCACCATGCC	
Flt3-cre	Flt3fw2	ACGGAGTCCAGGCAACTTCCC	68
	Flt3ex1rev1	GCTGCGCCAACGCCCGCAT	
	Flt3crerev	GAAGCATGTTTAGCTGGCCC	

Table 8-1 – Routine PCR genotyping primers and melting temperatures

8.2 Quantitative PCR Primer Sequences

Gene	Forward Primer	Reverse Primer
Elastin	AAAGCCTGGGAAAGTTCCTG	TACACCTGGAAGACCAACAC
Collagen I	ATGGATTCCCGTTCGAGTACG	TCAGCTGGATAGCGACATCG
Collagen III	CACCCTTCTTCATCCCACTCTTA	ACCAAGGTGGCTGCATCC
Vimentin	CGGAAAGTGGAATCCTTGCA	CACATCGATCTGGACATGCTGT
aSMA	ACTGGGACGACATGGAAAAG	GTTCAGTGGTGCCTCTGTCA
MMP2	CTGATAACCTGGATGCCGTCGT	TGCTTCCAAACTTCACGCTCTT
MMP9	GTCTCGGGAAGGCTCTGCTGTT	CTCTGGGGATCCACCTTCTGAG
FXIII-A	TGCTGGTGTCTTTAACACATTTTTAA	TGGGCCGAGAATGAATTGGT
TG1	TTCGCTACCCGTACCGTCA	CTTCATCCAGCAGTCGTT
TG2	ATTGGCAGTGTGGACATTC	TCGTGGGCGGAGTTGTA
TG3	AAGAAGCTGACCATGAGTGCTTT	TGCGCCCTTCGATTCATAG
TG4	CCCATCTATTTGACCATAACTTTGAA	GCGAGAAACACCCTTGATT
TG5	AGGCAGGATTCTGGAGAATATG	GGGCCACAGCCACAGCAGTAGAG
TG6	TCCGAGTCAATGTGAGCG	GTCTTCTGTCAGGTCTCCTTTGTA
TG7	ATGTGCACGGTAATGAGATGCT	TGTGTGCAGAATGGAAATTGG
CD163	ATGGGTGGACACAGAATGGTT	CAGGAGCGTTAGTGACAGCAG
tPA	CAACAGCGGCCTGGTACAA	CCCCATTGAAGCATCTTGGTT
uPA	GAAACCCTACAATGCCCACAGA	GACAAACTGCCTTAGGCCAATC
Perilipin	CTGTGTGCAATGCCTATGAGA	CTGGAGGGTATTGAAGAGCCG
PAI-1	ACGGTGATGCGATATAATGTAAACG	CATTCCTGAGAAACACAGCATTG
Fibrillin 1	CCTGTGCTATGATGGGTTCA	AGGTCCCACTAAGGCAGATG
Fibrillin 2	CCACTCCTATTGCTGCCCAG	TTGGGGCGGGAACAGAATC
MT-MMP	CCCAAGGCAGCAACTTCA	CAATGGCAGCTGAGAGTGAC
HO-1	AACAAGCAGAACCCAGTCTATG	TGAGCAGGAAGGCGGTCTTA
MMP12	GCTAGAAGCAACTGGGCAAC	ACCGCTTCATCCATCTTGAC
TIMP1	GTGGGAAATGCCGCAGAT	GGGCATATCCACAGAGGCTTT
TIMP2	CCAGAAGAAGAGCCTGAACCA	GTCCATCCAGAGGCACTCATC
TGFB	CACCGGAGAGCCCTGGATA	TGTACAGCTGCCGCACACA
B-Actin	CGTGAAAAGATGACCCAGATCA	TCGTACGACCAGAGGCATACAG
RPL32	AAAATTAAGCGAAACTGGCGG	TGTTGCTCCCATAACCGATG
DLK	GGTGTGGGAAGCAACAGTCT	GCAGCAAGATCTGTCGGAAT
JNK1	ATGCAAATCTTTGCCAAGTG	AGGCTTTAAGTCCCGATGAA
cJun	AGCAGGGACCCATGGAAGTT	AAAGATGACCTTTGCTTGTGCAT
Src	AGCAACAAGAGCAAGCCCAAGGAC	GTGACGGTGTCCGAGGAGTTGAAG
SEK1	TCGGACCTCCAGCTTCTG	TAAACCCTGCTGTCGATTTG
ATF2	ACTGCCATGGCCTTTTACAG	CCTCTCCTCAACCAGTCCAG
LOX	GTGACATTCGCTACACAGGACATC	CCAAACACCAGGTACGGCTTTATC
CD31	CTGGTGCTCTATGCAAGCCT	AGTTGCTGCCCATTCATCAC

Table 8-2 – Quantitative PCR primer names and sequences

8.3 Antibody Dilutions

Antibody	Host	Type	Source	Product Code	Dilution
Phospho-JNK	Rabbit	Monoclonal	CST	4668	1:1000 (WB)
DLK (MAP3k12)	Rabbit	Polyclonal	Thermofisher	PA5-32173	1:1000 (WB)
Streptavidin-HRP	n/a	n/a	R&D Systems	4800-30-06	1:1000 (WB)
β-actin	Rabbit	Monoclonal	CST	8457	1:1000 (WB)
Anti-rabbit HRP	Goat	Polyclonal	CST	7074	1:2000 (WB)
α-smooth muscle actin (Alexa Fluor 488)	Mouse	Monoclonal	Abcam	Ab184675	1:150 (ICC)

Table 8-3 – Western blot and immunocytochemistry antibody dilutions

8.4 Mass Spectrometry Peptide Identification

Table 8-4 – LC-MS protein identification from a heart salt fraction

ID	Description	-10lgP	Coverage (%)	# Peptide	# Unique	PTM	Avg. Mass
1	Albumin 1 OS=Mus musculus GN=Alb PE=2 SV=1	248.41	49	27	27	Y	68693
2	Myosin-binding protein C, cardiac-type OS=Mus musculus GN=Mybpc3 PE=1 SV=1	239.29	26	25	25	Y	141308
3	Fructose-bisphosphate aldolase OS=Mus musculus GN=Aldoa PE=2 SV=1	198.76	36	12	12	Y	39356
4	Aspartate aminotransferase, cytoplasmic OS=Mus musculus GN=Got1 PE=1 SV=3	189.16	49	18	18	Y	46248
5	Eno3 protein OS=Mus musculus GN=Eno3 PE=2 SV=1	187.2	37	15	13	Y	46998
6	Myoglobin OS=Mus musculus GN=Mb PE=2 SV=1	181.78	55	15	15	Y	17070
7	Creatine kinase M-type OS=Mus musculus GN=Ckm PE=2 SV=1	174.56	33	14	14	Y	43045
8	Glyceraldehyde-3-phosphate dehydrogenase OS=Mus musculus GN=Gapdh PE=1 SV=2	155.14	28	8	8	Y	35810
9	Triosephosphate isomerase OS=Mus musculus GN=Tpi1 PE=1 SV=4	154.54	34	10	10	Y	32192
10	L-lactate dehydrogenase B chain OS=Mus musculus GN=Ldhb PE=1 SV=2	154.27	30	11	9	Y	36572
11	Malate dehydrogenase, cytoplasmic OS=Mus musculus GN=Mdh1 PE=1 SV=3	145.02	26	8	8	Y	36511
12	Actin, aortic smooth muscle OS=Mus musculus GN=Acta2 PE=1 SV=1	144.51	21	7	7	N	42009
13	Glycogen phosphorylase, muscle form OS=Mus musculus GN=Pygm PE=1 SV=3	134.35	15	11	6	Y	97286
14	Pyruvate kinase PKM OS=Mus musculus GN=Pkm PE=1 SV=4	133.97	20	8	8	Y	57845
15	Phosphoglycerate kinase 1 OS=Mus musculus GN=Pgk1 PE=1 SV=4	132.26	21	7	7	Y	44550
16	Alpha-enolase OS=Mus musculus GN=EG433182 PE=2 SV=1	130.85	14	5	3	Y	47141
17	Tropomyosin alpha-1 chain OS=Mus musculus GN=Tpm1 PE=1 SV=1	127.87	30	9	9	Y	32699
18	Phosphoglycerate mutase 2 OS=Mus musculus GN=Pgam2 PE=1 SV=3	122.28	30	9	9	Y	28827
19	Phosphatidylethanolamine-binding protein 1 OS=Mus musculus GN=Pebp1 PE=1 SV=3	121.67	33	4	4	N	20830
20	L-lactate dehydrogenase (Fragment) OS=Mus musculus GN=Ldha PE=2 SV=1	120.89	24	8	6	Y	34503

21	Elongation factor 1-alpha 2 OS=Mus musculus GN=Eef1a2 PE=1 SV=1	116.23	13	6	6	N	50454
22	Adenylate kinase isoenzyme 1 OS=Mus musculus GN=Ak1 PE=1 SV=1	116.03	30	4	4	Y	21540
23	Fatty acid binding protein 3, muscle and heart OS=Mus musculus GN=Fabp3 PE=2 SV=1	110.29	35	6	6	Y	14819
24	Putative uncharacterized protein (Fragment) OS=Mus musculus GN=Akr1b3 PE=2 SV=1	106.13	18	6	6	Y	35052
25	Histone H1.4 OS=Mus musculus GN=Hist1h1e PE=1 SV=2	103.1	17	5	5	N	21977
26	Myomesin-1 OS=Mus musculus GN=Myom1 PE=1 SV=1	101.42	4	6	6	N	175480
27	Peroxiredoxin-1 (Fragment) OS=Mus musculus GN=Prdx1 PE=1 SV=6	101	28	5	5	N	18870
28	Glucose-6-phosphate isomerase OS=Mus musculus GN=Gpi1 PE=2 SV=1	98.92	14	4	4	N	38283
29	Heat shock protein 84b OS=Mus musculus GN=Hsp90ab1 PE=2 SV=1	89.45	9	5	5	N	83281
30	Nucleoside diphosphate kinase OS=Mus musculus GN=Nme2 PE=2 SV=1	86.3	32	5	5	Y	17363
31	Myosin light chain 3 OS=Mus musculus GN=Myl3 PE=1 SV=1	86.23	19	2	2	Y	14227
32	Glutathione S-transferase Mu 1 OS=Mus musculus GN=Gstm1 PE=1 SV=2	83.04	15	4	2	N	25970
33	Myomesin 2 OS=Mus musculus GN=Myom2 PE=1 SV=1	80.4	4	5	5	Y	164737
34	ATP-dependent 6-phosphofructokinase, muscle type OS=Mus musculus GN=Pfkm PE=1 SV=3	77.39	5	3	3	N	85269
35	Troponin C, slow skeletal and cardiac muscles OS=Mus musculus GN=Tnnc1 PE=1 SV=1	77.36	17	2	2	N	18421
36	Putative uncharacterized protein (Fragment) OS=Mus musculus GN=Hspa8 PE=2 SV=1	75.73	5	2	2	N	50464
37	Selenium-binding protein 2 OS=Mus musculus GN=Selenbp2 PE=1 SV=2	74.95	7	3	3	N	52610
38	Superoxide dismutase [Cu-Zn] OS=Mus musculus GN=Sod1 PE=1 SV=2	74.15	15	3	3	Y	15943
39	Protein Hbb-bs (Fragment) OS=Mus musculus GN=Hbb-bs PE=1 SV=1	73.89	22	2	2	N	11084
40	Troponin I, cardiac 3 OS=Mus musculus GN=Tnni3 PE=2 SV=1	67.5	12	2	2	N	24259
41	Peroxiredoxin-6 OS=Mus musculus GN=Prdx6 PE=1 SV=1	63.29	13	3	3	Y	22494
42	Protein deglycase DJ-1 OS=Mus musculus GN=Park7 PE=1 SV=1	60.16	16	3	3	Y	20021
43	PDZ and LIM domain protein 5 OS=Mus musculus GN=Pdlim5 PE=1 SV=1	56.24	12	2	2	N	23793

44	Troponin T, cardiac muscle OS=Mus musculus GN=Tnnt2 PE=1 SV=1	53.44	7	2	2	N	35001
45	Putative uncharacterized protein (Fragment) OS=Mus musculus GN=Prdx5 PE=2 SV=1	53.12	10	2	2	N	20713
46	Cofilin-2 OS=Mus musculus GN=Cfl2 PE=2 SV=1	52.49	11	2	2	N	18710
47	Annexin OS=Mus musculus GN=Anxa6 PE=2 SV=1	51.13	4	3	3	N	75273
48	Putative uncharacterized protein OS=Mus musculus GN=H1f0 PE=2 SV=1	47.97	9	2	2	N	19253
49	Serotransferrin OS=Mus musculus GN=Tf PE=1 SV=1	45.98	2	2	2	N	76724
50	Peroxiredoxin-2 OS=Mus musculus GN=Prdx2 PE=1 SV=3	44.86	8	2	2	N	21779

8.5 Tissue Processing Settings

70% ethanol	30 min
70% ethanol	30 min
70% ethanol	30 min
90% ethanol	1 h
100% ethanol	2 h
100% ethanol	2 h 30 min
100% ethanol	3 h
Histoclear	30 min
Histoclear	1 h 30 min
Histoclear	1 h 30 min
Paraffin	1 h 30 min
Paraffin	2 h

8.6 Home Office Module 1-4 Certificate

Animals (Scientific Procedures) Act, 1986
Universities' Training Group

No: 33889

This is to certify that **Kingsley Simpson**
of **University of Leeds**

has successfully completed a programme of training approved by the Universities' Accreditation Scheme

Modules	Species
1-4	Rat Mouse

Signed: ..... for Universities' Training Group
(L. Taylor - Secretary)

Date: 20 March 2013

8.7 Home Office Personal Licence

Home Office

No. PIL 70/25614

ANIMALS (SCIENTIFIC PROCEDURES) ACT 1986

PERSONAL LICENCE

to

carry out regulated procedures on living animals.

In pursuance of the powers vested in him by the above Act, the Secretary of State hereby licenses

Mr K R Simpson
LIGHT Laboratories
University of Leeds
Leeds
LS2 9JT

to apply regulated procedures of the category or categories specified in column a of paragraph 8 of the attached Schedule to the kinds of animals in column b of the same paragraph at places specified in authorised project licences subject to the restrictions and provisions contained in the Act, and subject also to the limitations and conditions contained in this licence and to such other conditions as the Secretary of State may from time to time prescribe.

This licence shall be in force until revoked by the Secretary of State and shall be periodically reviewed by him.

Home Office
2 Marsham Street
London SW1P 4DF

For the Secretary of State

17 September 2013

NB. This licence does not authorise the licensee to perform any of the procedures specified in it unless they are carried out in the course of a project for which there is a project licence in force under the Act.

8.8 Mouse Ear Notch Identification

All mice were ear notched at point of weaning by University of Leeds CBS staff. The following notch identification system was used with all mice within the facility.

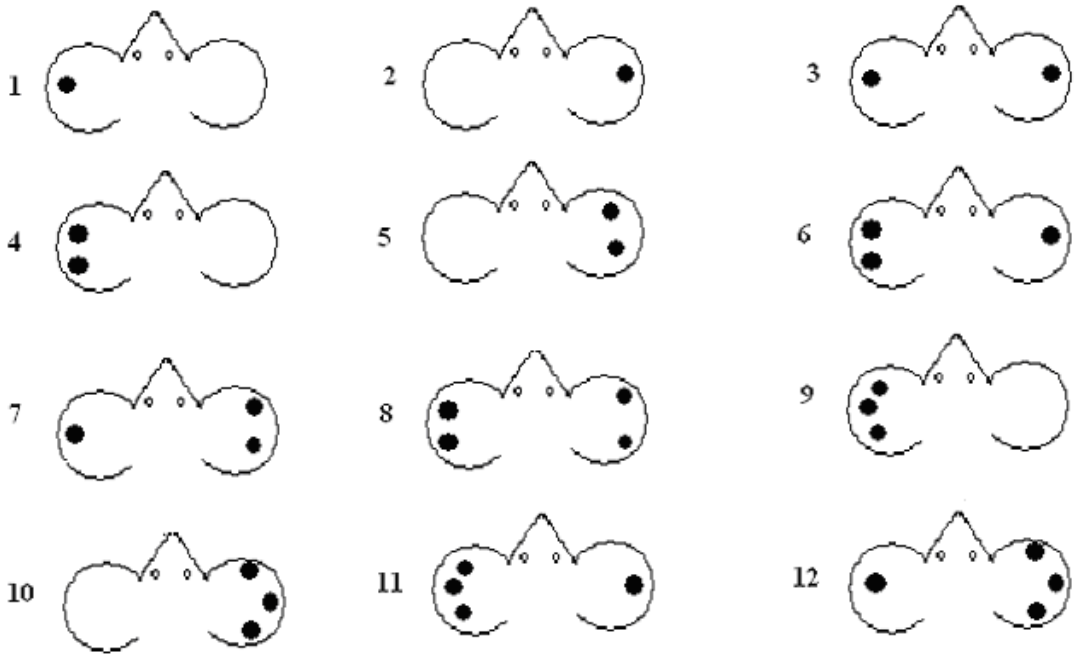

Figure 8-1 – CBS mouse ear notch identification chart

● = site of ear notching

References

Adány, R. and Bárdos, H. 2003. Factor XIII subunit A as an intracellular transglutaminase. *Cellular And Molecular Life Sciences : CMLS*. [Online]. **60**(6),pp.1049–60.

Adány, R., Bárdos, H., Antal, M., Módis, L., Sárváry, A., et al. 2001. Factor XIII of blood coagulation as a nuclear crosslinking enzyme. *Thrombosis And Haemostasis*. [Online]. **85**(5),pp.845–51.

Aeschlimann, D. and Paulsson, M. 1994. Transglutaminases: protein cross-linking enzymes in tissues and body fluids. *Thrombosis And Haemostasis*. [Online]. **71**(4),pp.402–15.

Aeschlimann, D., Wetterwald, A., Fleisch, H. and Paulsson, M. 1993. Expression of tissue transglutaminase in skeletal tissues correlates with events of terminal differentiation of chondrocytes. *The Journal Of Cell Biology*. [Online]. **120**(6),pp.1461–70.

Ailawadi, G., Eliason, J.L. and Upchurch, G.R. 2003. Current concepts in the pathogenesis of abdominal aortic aneurysm. *Journal Of Vascular Surgery*. [Online]. **38**(3),pp.584–8.

van den Akker, J., van Weert, A., Afink, G., Bakker, E.N.T.P., van der Pol, E., et al. 2012. Transglutaminase 2 is secreted from smooth muscle cells by transamidation-dependent microparticle formation. *Amino Acids*. [Online]. **42**(2-3),pp.961–73.

Alberts B, Johnson A, L.J. 2002. Molecular Biology of the Cell. 4th edition. *In*: New York, NY: Garland Science.

Alexander, W.S., Roberts, A.W., Nicola, N.A., Li, R. and Metcalf, D. 1996. Deficiencies in progenitor cells of multiple hematopoietic lineages and defective megakaryocytopoiesis in mice lacking the thrombopoietic receptor c-Mpl. *Blood*. [Online]. **87**(6),pp.2162–70.

van Amerongen, M.J., Harmsen, M.C., van Rooijen, N., Petersen, A.H. and van Luyn, M.J. a 2007. Macrophage depletion impairs wound healing and increases left ventricular remodeling after myocardial injury in mice. *The American Journal Of Pathology*. [Online]. **170**(3),pp.818–29.

Bakker, E.N.T.P., Pistea, A., Spaan, J.A.E., Rolf, T., de Vries, C.J., et al. 2006. Flow-dependent remodeling of small arteries in mice deficient for tissue-type transglutaminase: possible compensation by macrophage-derived factor XIII. *Circulation Research*. [Online]. **99**(1),pp.86–92.

Barber, R.D., Harmer, D.W., Coleman, R.A. and Clark, B.J. 2005. GAPDH as a housekeeping gene: analysis of GAPDH mRNA expression in a panel of 72 human tissues. *Physiological Genomics*. [Online]. **21**(3),pp.389–95.

Bauer, V. and Sotníková, R. 2010. Nitric oxide--the endothelium-derived relaxing factor and its role in endothelial functions. *General Physiology And Biophysics*. [Online]. **29**(4),pp.319–40.

Bauriedel, G., Hutter, R., Welsch, U., Bach, R., Sievert, H., et al. 1999. Role of smooth muscle cell death in advanced coronary primary lesions:

implications for plaque instability. *Cardiovascular Research*. [Online]. **41**(2),pp.480–8.

Bellora, F., Castriconi, R., Doni, A., Cantoni, C., Moretta, L., et al. 2012. M-CSF induces the expression of a membrane-bound form of IL-18 in a subset of human monocytes differentiating in vitro toward macrophages. *European Journal Of Immunology*. [Online]. **42**(6),pp.1618–26.

Bennett, B.L., Sasaki, D.T., Murray, B.W., O'Leary, E.C., Sakata, S.T., et al. 2001. SP600125, an anthrapyrazolone inhibitor of Jun N-terminal kinase. *Proceedings Of The National Academy Of Sciences Of The United States Of America*. [Online]. **98**(24),pp.13681–6.

Bennett, M.R. and Boyle, J.J. 1998. Apoptosis of vascular smooth muscle cells in atherosclerosis. *Atherosclerosis*. [Online]. **138**(1),pp.3–9.

Benz, C., Martins, V.C., Radtke, F. and Bleul, C.C. 2008. The stream of precursors that colonizes the thymus proceeds selectively through the early T lineage precursor stage of T cell development. *The Journal Of Experimental Medicine*. [Online]. **205**(5),pp.1187–99.

Bernassola, F., Federici, M., Corazzari, M., Terrinoni, A., Hribal, M.L., et al. 2002. Role of transglutaminase 2 in glucose tolerance: knockout mice studies and a putative mutation in a MODY patient. *FASEB Journal : Official Publication Of The Federation Of American Societies For Experimental Biology*. [Online]. **16**(11),pp.1371–8.

Biernacka, A. and Frangogiannis, N.G. 2011. Aging and Cardiac Fibrosis. *Aging And Disease*. [Online]. **2**(2),pp.158–173.

Board, P.G., Losowsky, M.S. and Miloszewski, K.J. 1993. Factor XIII: inherited and acquired deficiency. *Blood Reviews*. [Online]. **7**(4),pp.229–42.

Bochaton-Piallat, M.L., Gabbiani, F., Ropraz, P. and Gabbiani, G. 1992. Cultured aortic smooth muscle cells from newborn and adult rats show distinct cytoskeletal features. *Differentiation; Research In Biological Diversity*. [Online]. **49**(3),pp.175–85.

Bockamp, E., Maringer, M., Spangenberg, C., Fees, S., Fraser, S., et al. 2002. Of mice and models: improved animal models for biomedical research. *Physiological Genomics*. [Online]. **11**(3),pp.115–32.

Boyer, S.W., Schroeder, A. V, Smith-Berdan, S. and Forsberg, E.C. 2011. All hematopoietic cells develop from hematopoietic stem cells through Flk2/Flt3-positive progenitor cells. *Cell Stem Cell*. [Online]. **9**(1),pp.64–73.

Brill, A., Torchinsky, A., Carp, H. and Toder, V. 1999. The role of apoptosis in normal and abnormal embryonic development. *Journal Of Assisted Reproduction And Genetics*. [Online]. **16**(10),pp.512–9.

Cafueri, G., Parodi, F., Pistorio, A., Bertolotto, M., Ventura, F., et al. 2012. Endothelial and smooth muscle cells from abdominal aortic aneurysm have increased oxidative stress and telomere attrition. *PloS One*. [Online]. **7**(4),p.e35312.

Calaminus, S.D.J., Guitart, A., Sinclair, A., Schachtner, H., Watson, S.P., et al. 2012. Lineage tracing of Pf4-Cre marks hematopoietic stem cells and their progeny. *PloS One*. [Online]. **7**(12),p.e51361.

Careau, E. and Bissonnette, E.Y. 2004. Adoptive transfer of alveolar macrophages abrogates bronchial hyperresponsiveness. *American Journal Of Respiratory Cell And Molecular Biology*. [Online]. **31**(1),pp.22–7.

de Castro Brás, L.E., Ramirez, T.A., DeLeon-Pennell, K.Y., Chiao, Y.A., Ma, Y., et al. 2013. Texas 3-step decellularization protocol: looking at the cardiac extracellular matrix. *Journal Of Proteomics*. [Online]. **86**,pp.43–52.

Caux, C., Vanbervliet, B., Massacrier, C., Dezutter-Dambuyant, C., de Saint-Vis, B., et al. 1996. CD34+ hematopoietic progenitors from human cord blood differentiate along two independent dendritic cell pathways in response to GM-CSF+TNF alpha. *The Journal Of Experimental Medicine*. [Online]. **184**(2),pp.695–706.

Chomczynski, P. and Sacchi, N. 1987. Single-step method of RNA isolation by acid guanidinium thiocyanate-phenol-chloroform extraction. *Analytical Biochemistry*. [Online]. **159**,pp.156–159.

Coffey, E.T. 2014. Nuclear and cytosolic JNK signalling in neurons. *Nature Reviews. Neuroscience*. [Online]. **15**(5),pp.285–99.

Cordell, P.A., Kile, B.T., Standeven, K.F., Josefsson, E.C., Pease, R.J., et al. 2010. Association of coagulation factor XIII-A with Golgi proteins within monocyte-macrophages: implications for subcellular trafficking and secretion. *Blood*. [Online]. **115**(13),pp.2674–81.

Cordell, P.A., Newell, L.M., Standeven, K.F., Adamson, P.J., Simpson, K.R., et al. 2015. Normal Bone Deposition Occurs in Mice Deficient in Factor XIII-A and Transglutaminase 2. *Matrix Biology : Journal Of The International Society For Matrix Biology*. [Online]. **43**,pp.85–96.

Corpet, F. 1988. Multiple sequence alignment with hierarchical clustering. *Nucleic Acids Research*. [Online]. **16**(22),pp.10881–10890.

Côté, C.H., Bouchard, P., van Rooijen, N., Marsolais, D. and Duchesne, E. 2013. Monocyte depletion increases local proliferation of macrophage subsets after skeletal muscle injury. *BMC Musculoskeletal Disorders*. [Online]. **14**,p.359.

Crosbie, O.M., Reynolds, M., McEntee, G., Traynor, O., Hegarty, J.E., et al. 1999. In vitro evidence for the presence of hematopoietic stem cells in the adult human liver. *Hepatology (Baltimore, Md.)*. [Online]. **29**(4),pp.1193–8.

Cui, J., Zhang, M., Zhang, Y.-Q. and Xu, Z.-H. 2007. JNK pathway: diseases and therapeutic potential. *Acta Pharmacologica Sinica*. [Online]. **28**(5),pp.601–8.

Daugherty, A., Manning, M.W. and Cassis, L.A. 2000. Angiotensin II promotes atherosclerotic lesions and aneurysms in apolipoprotein E-deficient mice. *The Journal Of Clinical Investigation*. [Online]. **105**(11),pp.1605–12.

Davies, M.J., Richardson, P.D., Woolf, N., Katz, D.R. and Mann, J. 1993. Risk of thrombosis in human atherosclerotic plaques: role of extracellular lipid, macrophage, and smooth muscle cell content. *British Heart Journal*. [Online]. **69**(5),pp.377–81.

Deimann, W. and Fahimi, H.D. 1978. Peroxidase cytochemistry and ultrastructure of resident macrophages in fetal rat liver. A developmental study. *Developmental Biology*. [Online]. **66**(1),pp.43–56.

Deonarine, K., Panelli, M.C., Stashower, M.E., Jin, P., Smith, K., et al. 2007. Gene expression profiling of cutaneous wound healing. *Journal Of Translational Medicine*. [Online]. **5**,p.11.

Eckert, R.L., Kaartinen, M.T., Nurminskaya, M., Belkin, A.M., Colak, G., et al. 2014. Transglutaminase regulation of cell function. *Physiological Reviews*. [Online]. **94**(2),pp.383–417.

Endlich, N., Endlich, K., Taesch, N. and Helwig, J.J. 2000. Culture of vascular smooth muscle cells from small arteries of the rat kidney. *Kidney International*. [Online]. **57**(6),pp.2468–75.

Ensan, S., Li, A., Besla, R., Degousee, N., Cosme, J., et al. 2016. Self-renewing resident arterial macrophages arise from embryonic CX3CR1(+) precursors and circulating monocytes immediately after birth. *Nature Immunology*. [Online]. **17**(2),pp.159–68.

Epelman, S., Lavine, K.J., Beaudin, A.E., Sojka, D.K., Carrero, J.A., et al. 2014. Embryonic and adult-derived resident cardiac macrophages are maintained through distinct mechanisms at steady state and during inflammation. *Immunity*. [Online]. **40**(1),pp.91–104.

Evans, D.J.W., Jackman, L.E., Chamberlain, J., Crosdale, D.J., Judge, H.M., et al. 2009. Platelet P2Y(12) receptor influences the vessel wall response to arterial injury and thrombosis. *Circulation*. [Online]. **119**(1),pp.116–22.

Faust, N., Varas, F., Kelly, L.M., Heck, S. and Graf, T. 2000. Insertion of enhanced green fluorescent protein into the lysozyme gene creates mice with green fluorescent granulocytes and macrophages. *Blood*. [Online]. **96**(2),pp.719–26.

Feng, J.F., Readon, M., Yadav, S.P. and Im, M.J. 1999. Calreticulin down-regulates both GTP binding and transglutaminase activities of transglutaminase II. *Biochemistry*. **38**(33),pp.10743–10749.

Ferron, M. and Vacher, J. 2005. Targeted expression of Cre recombinase in macrophages and osteoclasts in transgenic mice. *Genesis (New York, N.Y. : 2000)*. [Online]. **41**(3),pp.138–45.

Fesus, L., Madi, A., Balajthy, Z., Nemes, Z. and Szondy, Z. 1996. Transglutaminase induction by various cell death and apoptosis pathways. *Experientia*. [Online]. **52**(10-11),pp.942–9.

Fesus, L., Thomazy, V. and Falus, A. 1987. Induction and activation of tissue transglutaminase during programmed cell death. *FEBS Letters*. [Online]. **224**(1),pp.104–8.

Fleming, Y., Armstrong, C.G., Morrice, N., Paterson, A., Goedert, M., et al. 2000. Synergistic activation of stress-activated protein kinase 1/c-Jun N-terminal kinase (SAPK1/JNK) isoforms by mitogen-activated protein kinase kinase 4 (MKK4) and MKK7. *The Biochemical Journal*. [Online]. **352 Pt 1**,pp.145–54.

Folk, J.E. and Finlayson, J.S. 1977. The epsilon-(gamma-glutamyl)lysine crosslink and the catalytic role of transglutaminases. *Advances In Protein*

Chemistry. [Online]. **31**,pp.1–133.

Fujiu, K., Wang, J. and Nagai, R. 2014. Cardioprotective function of cardiac macrophages. *Cardiovascular Research*. [Online]. **102**(2),pp.232–9.

Furmaniak-Kazmierczak, E., Crawley, S.W., Carter, R.L., Maurice, D.H. and Côté, G.P. 2007. Formation of extracellular matrix-digesting invadopodia by primary aortic smooth muscle cells. *Circulation Research*. [Online]. **100**(9),pp.1328–36.

Garcia, M.D. and Larina, I. V. 2014. Vascular development and hemodynamic force in the mouse yolk sac. *Frontiers In Physiology*. [Online]. **5**(August),p.308.

Geng, Y.J. and Libby, P. 1995. Evidence for apoptosis in advanced human atheroma. Colocalization with interleukin-1 beta-converting enzyme. *The American Journal Of Pathology*. [Online]. **147**(2),pp.251–66.

Gertz, S., Kurgan, A. and Eisenberg, D. 1988. Aneurysm of the rabbit common carotid artery induced by periarterial application of calcium chloride in vivo. *Journal Of Clinical Investigation*. [Online]. **81**(March),pp.649–656.

Ginhoux, F. and Jung, S. 2014. Monocytes and macrophages: developmental pathways and tissue homeostasis. *Nature Reviews. Immunology*. [Online]. **14**(6),pp.392–404.

Greenberg, C.S., Birckbichler, P.J. and Rice, R.H. 1991. Transglutaminases: multifunctional cross-linking enzymes that stabilize tissues. *FASEB Journal : Official Publication Of The Federation Of American Societies For Experimental Biology*. [Online]. **5**(15),pp.3071–7.

Guilliams, M., De Kleer, I., Henri, S., Post, S., Vanhoutte, L., et al. 2013. Alveolar macrophages develop from fetal monocytes that differentiate into long-lived cells in the first week of life via GM-CSF. *The Journal Of Experimental Medicine*. [Online]. **210**(10),pp.1977–92.

Gupta, S., Campbell, D., Dérijard, B. and Davis, R.J. 1995. Transcription factor ATF2 regulation by the JNK signal transduction pathway. *Science (New York, N.Y.)*. [Online]. **267**(5196),pp.389–93.

Haanen, C. and Vermes, I. 1996. Apoptosis: programmed cell death in fetal development. *European Journal Of Obstetrics, Gynecology, And Reproductive Biology*. [Online]. **64**(1),pp.129–33.

Hada, M., Kaminski, M., Bockenstedt, P. and McDonagh, J. 1986. Covalent crosslinking of von Willebrand factor to fibrin. *Blood*. [Online]. **68**(1),pp.95–101.

Hao, H., Gabbiani, G. and Bochaton-Piallat, M.-L. 2003. Arterial smooth muscle cell heterogeneity: implications for atherosclerosis and restenosis development. *Arteriosclerosis, Thrombosis, And Vascular Biology*. [Online]. **23**(9),pp.1510–20.

Harris, L.K., Smith, S.D., Keogh, R.J., Jones, R.L., Baker, P.N., et al. 2010. Trophoblast- and vascular smooth muscle cell-derived MMP-12 mediates elastolysis during uterine spiral artery remodeling. *The American Journal Of Pathology*. [Online]. **177**(4),pp.2103–15.

Hashimoto, D., Chow, A., Noizat, C., Teo, P., Beasley, M.B., et al. 2013.

Tissue-resident macrophages self-maintain locally throughout adult life with minimal contribution from circulating monocytes. *Immunity*. [Online]. **38**(4),pp.792–804.

Hébert, S.S., Daviau, a, Grondin, G., Latreille, M., Aubin, R. a, et al. 2000. The mixed lineage kinase DLK is oligomerized by tissue transglutaminase during apoptosis. *The Journal Of Biological Chemistry*. [Online]. **275**(42),pp.32482–90.

Heidt, T., Courties, G., Dutta, P., Sager, H.B., Sebas, M., et al. 2014. Differential contribution of monocytes to heart macrophages in steady-state and after myocardial infarction. *Circulation Research*. [Online]. **115**(2),pp.284–95.

Henriksson, P., Becker, S., Lynch, G. and MacDonagh, J. 1985. Identification of intracellular factor XIII in human monocytes and macrophages. *Journal Of Clinical Investigation*. **76**(2),pp.528–534.

Hsieh, L. and Nugent, D. 2008. Factor XIII deficiency. *Haemophilia : The Official Journal Of The World Federation Of Hemophilia*. [Online]. **14**(6),pp.1190–200.

Ichinose, A., Bottenus, R.E. and Davie, E.W. 1990. Structure of transglutaminases. *The Journal Of Biological Chemistry*. [Online]. **265**(23),pp.13411–4.

Illera, M.J., Cullinan, E., Gui, Y., Yuan, L., Beyler, S. a, et al. 2000. Blockade of the alpha(v)beta(3) integrin adversely affects implantation in the mouse. *Biology Of Reproduction*. [Online]. **62**(5),pp.1285–90.

Inbal, A., Muszbek, L. and Lubetsky, A. 2004. Platelets but not monocytes contribute to the plasma levels of factor XIII subunit A in patients undergoing autologous peripheral blood stem cell transplantation. *Blood Coagulation & …*. [Online],pp.249–253.

Jin, X., Stamnaes, J., Klöck, C., DiRaimondo, T.R., Sollid, L.M., et al. 2011. Activation of extracellular transglutaminase 2 by thioredoxin. *The Journal Of Biological Chemistry*. [Online]. **286**(43),pp.37866–73.

Johnson, K.B., Petersen-Jones, H., Thompson, J.M., Hitomi, K., Itoh, M., et al. 2012. Vena cava and aortic smooth muscle cells express transglutaminases 1 and 4 in addition to transglutaminase 2. *American Journal Of Physiology. Heart And Circulatory Physiology*. [Online]. **302**(7),pp.H1355–66.

Kaetsu, H., Hashiguchi, T., Foster, D. and Ichinose, a 1996. Expression and release of the a and b subunits for human coagulation factor XIII in baby hamster kidney (BHK) cells. *Journal Of Biochemistry*. [Online]. **119**(5),pp.961–9.

Kiew, P.L. and Don, M.M. 2013. *Modified Lowry's Method for Acid and Pepsin Soluble Collagen Measurement from Clarias Species Muscles*.

Kim, E.K. and Choi, E.-J. 2010. Pathological roles of MAPK signaling pathways in human diseases. *Biochimica Et Biophysica Acta*. [Online]. **1802**(4),pp.396–405.

Kim, M.-S., Pinto, S.M., Getnet, D., Nirujogi, R.S., Manda, S.S., et al. 2014. A draft map of the human proteome. *Nature*. [Online]. **509**(7502),pp.575–

81.

Kim, S.Y., Jeitner, T.M. and Steinert, P.M. 2002. Transglutaminases in disease. *Neurochemistry International*. [Online]. **40**(1),pp.85–103.

Kim, Y.-K., Yeo, J., Kim, B., Ha, M. and Kim, V.N. 2012. Short structured RNAs with low GC content are selectively lost during extraction from a small number of cells. *Molecular Cell*. [Online]. **46**(6),pp.893–5.

Klöck, C., DiRaimondo, T.R. and Khosla, C. 2012. Role of transglutaminase 2 in celiac disease pathogenesis. *Seminars In Immunopathology*. **34**(4),pp.513–522.

Kluwe, J., Pradere, J., Gwak, G., Mencin, A., De Minicis, S., et al. 2010. Modulation of hepatic fibrosis by c-Jun-N-terminal kinase inhibition. *Gastroenterology*. [Online]. **138**(1),pp.347–59.

Komáromi, I., Bagoly, Z. and Muszbek, L. 2011. Factor XIII: novel structural and functional aspects. *Journal Of Thrombosis And Haemostasis : JTH*. [Online]. **9**(1),pp.9–20.

Kondo, M., Wagers, A.J., Manz, M.G., Prohaska, S.S., Scherer, D.C., et al. 2003. Biology of hematopoietic stem cells and progenitors: implications for clinical application. *Annual Review Of Immunology*. [Online]. **21**(1),pp.759–806.

Korsgren, C., Lawler, J., Lambert, S., Speicher, D. and Cohen, C.M. 1990. Complete amino acid sequence and homologies of human erythrocyte membrane protein band 4.2. *Proceedings Of The National Academy Of Sciences Of The United States Of America*. [Online]. **87**(2),pp.613–7.

Koseki-Kuno, S., Yamakawa, M., Dickneite, G. and Ichinose, A. 2003. Factor XIII A subunit-deficient mice developed severe uterine bleeding events and subsequent spontaneous miscarriages. *Blood*. [Online]. **102**(13),pp.4410–4412.

Kuan, C.Y., Yang, D.D., Samanta Roy, D.R., Davis, R.J., Rakic, P., et al. 1999. The Jnk1 and Jnk2 protein kinases are required for regional specific apoptosis during early brain development. *Neuron*. **22**(4),pp.667–676.

Lacolley, P., Regnault, V., Nicoletti, A., Li, Z. and Michel, J.B. 2012. The vascular smooth muscle cell in arterial pathology: A cell that can take on multiple roles. *Cardiovascular Research*. **95**(2),pp.194–204.

Lakatta, E.G. 2003. Arterial and cardiac aging: major shareholders in cardiovascular disease enterprises: Part III: cellular and molecular clues to heart and arterial aging. *Circulation*. [Online]. **107**(3),pp.490–7.

De Laurenzi, V. and Melino, G. 2001. Gene disruption of tissue transglutaminase. *Molecular And Cellular Biology*. [Online]. **21**(1),pp.148–55.

Lee, Y.-J., Jung, S.-H., Kim, S.-H., Kim, M.-S., Lee, S., et al. 2016. Essential Role of Transglutaminase 2 in Vascular Endothelial Growth Factor-Induced Vascular Leakage in the Retina of Diabetic Mice. *Diabetes*. [Online]. **65**(8),pp.2414–28.

Lieu, Y.K. and Reddy, E.P. 2009. Conditional c-myb knockout in adult hematopoietic stem cells leads to loss of self-renewal due to impaired

proliferation and accelerated differentiation. *Proceedings Of The National Academy Of Sciences Of The United States Of America*. [Online]. **106**(51),pp.21689–94.

Lorand, L. 2000. Sol Sherry Lecture in Thrombosis : research on clot stabilization provides clues for improving thrombolytic therapies. *Arteriosclerosis, Thrombosis, And Vascular Biology*. [Online]. **20**(1),pp.2–9.

Lorand, L. and Conrad, S.M. 1984. Transglutaminases. *Molecular And Cellular Biochemistry*. [Online]. **58**(1-2),pp.9–35.

Lorand, L. and Graham, R.M. 2003. Transglutaminases: crosslinking enzymes with pleiotropic functions. *Nature Reviews. Molecular Cell Biology*. [Online]. **4**(2),pp.140–56.

Luddington, R.J. 2005. Thrombelastography/thromboelastometry. *Clinical And Laboratory Haematology*. [Online]. **27**(2),pp.81–90.

Majesky, M.W., Dong, X.R., Hoglund, V., Mahoney, W.M. and Daum, G. 2011. The adventitia: a dynamic interface containing resident progenitor cells. *Arteriosclerosis, Thrombosis, And Vascular Biology*. [Online]. **31**(7),pp.1530–9.

Mason, K.D., Carpinelli, M.R., Fletcher, J.I., Collinge, J.E., Hilton, A.A., et al. 2007. Programmed Anuclear Cell Death Delimits Platelet Life Span. *Cell*. **128**(6),pp.1173–1186.

Mastroberardino, P.G., Iannicola, C., Nardacci, R., Bernassola, F., De Laurenzi, V., et al. 2002. 'Tissue' transglutaminase ablation reduces neuronal death and prolongs survival in a mouse model of Huntington's disease. *Cell Death And Differentiation*. [Online]. **9**(9),pp.873–80.

McCarthy, N. 2000. The regulation of vascular smooth muscle cell apoptosis B. J. Hunt, L. Poston, M. Schachter, & A. W. Halliday, eds. *Cardiovascular Research*. [Online]. **45**(3),pp.747–755.

Medvinsky, A., Rybtsov, S. and Taoudi, S. 2011. Embryonic origin of the adult hematopoietic system: advances and questions. *Development (Cambridge, England)*. [Online]. **138**(6),pp.1017–31.

Meier, I.D., Bernreuther, C., Tilling, T., Neidhardt, J., Wong, Y.W., et al. 2010. Short DNA sequences inserted for gene targeting can accidentally interfere with off-target gene expression. *FASEB Journal : Official Publication Of The Federation Of American Societies For Experimental Biology*. [Online]. **24**(6),pp.1714–24.

Milakovic, T., Tucholski, J., McCoy, E. and Johnson, G.V.W. 2004. Intracellular localization and activity state of tissue transglutaminase differentially impacts cell death. *The Journal Of Biological Chemistry*. [Online]. **279**(10),pp.8715–22.

Miller, K. 2005. Method of testing very soft biological tissues in compression. *Journal Of Biomechanics*. [Online]. **38**(1),pp.153–8.

Milo, R., Jorgensen, P., Moran, U., Weber, G. and Springer, M. 2010. BioNumbers--the database of key numbers in molecular and cell biology. *Nucleic Acids Research*. [Online]. **38**(Database issue),pp.D750–3.

Mishra, S. and Murphy, L.J. 2006. The p53 oncoprotein is a substrate for tissue transglutaminase kinase activity. *Biochemical And Biophysical Research Communications*. **339**(2),pp.726–730.

Molawi, K., Wolf, Y., Kandalla, P.K., Favret, J., Hagemeyer, N., et al. 2014. Progressive replacement of embryo-derived cardiac macrophages with age. *Journal Of Experimental Medicine*. [Online]. **211**(11),pp.2151–2158.

Morgan, H.D., Sutherland, H.G., Martin, D.I. and Whitelaw, E. 1999. Epigenetic inheritance at the agouti locus in the mouse. *Nature Genetics*. **23**(3),pp.314–318.

Mossanen, J.C. and Tacke, F. 2015. Acetaminophen-induced acute liver injury in mice. *Laboratory Animals*. [Online]. **49**(1 Suppl),pp.30–6.

Muszbek, L., Adány, R., Szegedi, G., Polgár, J. and Kávai, M. 1985. Factor XIII of blood coagulation in human monocytes. *Thrombosis Research*. [Online]. **37**(3),pp.401–10.

Muszbek, L., Bereczky, Z., Bagoly, Z., Komáromi, I. and Katona, É. 2011. Factor XIII: a coagulation factor with multiple plasmatic and cellular functions. *Physiological Reviews*. [Online]. **91**(3),pp.931–72.

Muszbek, L., Yee, V.C. and Hevessy, Z. 1999. Blood coagulation factor XIII: Structure and function. *Thrombosis Research*. **94**(5),pp.271–305.

Muzumdar, M.D., Tasic, B., Miyamichi, K., Li, L. and Luo, L. 2007. A global double-fluorescent Cre reporter mouse. *Genesis (New York, N.Y. : 2000)*. [Online]. **45**(9),pp.593–605.

Nagasawa, H., Miyamoto, M. and Fujimoto, M. 1973. [Reproductivity in inbred strains of mice and project for their efficient production (author's transl)]. *Jikken Dobutsu. Experimental Animals*. [Online]. **22**(2),pp.119–26.

Nahrendorf, M., Hu, K., Frantz, S., Jaffer, F. a, Tung, C.-H., et al. 2006. Factor XIII deficiency causes cardiac rupture, impairs wound healing, and aggravates cardiac remodeling in mice with myocardial infarction. *Circulation*. [Online]. **113**(9),pp.1196–202.

Nahrendorf, M., Swirski, F.K., Aikawa, E., Stangenberg, L., Wurdinger, T., et al. 2007. The healing myocardium sequentially mobilizes two monocyte subsets with divergent and complementary functions. *The Journal Of Experimental Medicine*. [Online]. **204**(12),pp.3037–47.

Naito, M., Takahashi, K. and Nishikawa, S. 1990. Development, differentiation, and maturation of macrophages in the fetal mouse liver. *Journal Of Leukocyte Biology*. [Online]. **48**(1),pp.27–37.

Nakamura, K., Bossy-Wetzel, E., Burns, K., Fadel, M.P., Lozyk, M., et al. 2000. Changes in endoplasmic reticulum luminal environment affect cell sensitivity to apoptosis. *The Journal Of Cell Biology*. [Online]. **150**(4),pp.731–40.

Nanda, N., Iismaa, S.E., Owens, W.A., Husain, A., Mackay, F., et al. 2001. Targeted inactivation of Gh/tissue transglutaminase II. *The Journal Of Biological Chemistry*. [Online]. **276**(23),pp.20673–8.

Nara, K., Ito, S., Ito, T., Suzuki, Y., Ghoneim, M.A., et al. 1994. Elastase inhibitor elafin is a new type of proteinase inhibitor which has a

transglutaminase-mediated anchoring sequence termed ‘cementoin’. *Journal Of Biochemistry*. [Online]. **115**(3),pp.441–8.

Nelson, D.M. 1996. Apoptotic changes occur in syncytiotrophoblast of human placental villi where fibrin type fibrinoid is deposited at discontinuities in the villous trophoblast. *Placenta*. [Online]. **17**(7),pp.387–91.

Nestle, F.O., Zheng, X.G., Thompson, C.B., Turka, L.A. and Nickoloff, B.J. 1993. Characterization of dermal dendritic cells obtained from normal human skin reveals phenotypic and functionally distinctive subsets. *Journal Of Immunology (Baltimore, Md.: 1950)*. [Online]. **151**(11),pp.6535–45.

Ng, A.P., Kauppi, M., Metcalf, D., Hyland, C.D., Josefsson, E.C., et al. 2014. Mpl expression on megakaryocytes and platelets is dispensable for thrombopoiesis but essential to prevent myeloproliferation. *Proceedings Of The National Academy Of Sciences Of The United States Of America*. [Online]. **111**(16),pp.5884–9.

Nielsen, V.G., Gurley, W.Q. and Burch, T.M. 2004. The impact of factor XIII on coagulation kinetics and clot strength determined by thrombelastography. *Anesthesia And Analgesia*. [Online]. **99**(1),pp.120–3.

Nielsen, V.G., Kirklin, J.K., Hoogendoorn, H., Ellis, T.C. and Holman, W.L. 2007. Thrombelastographic method to quantify the contribution of factor XIII to coagulation kinetics. *Blood Coagulation & Fibrinolysis : An International Journal In Haemostasis And Thrombosis*. [Online]. **18**(2),pp.145–50.

Niemann, A., Takatsuki, A. and Elsässer, H.P. 2000. The lysosomotropic agent monodansylcadaverine also acts as a solvent polarity probe. *The Journal Of Histochemistry & Cytochemistry*. **48**(2),pp.251–258.

Nikolajsen, C.L., Dyrlund, T.F., Poulsen, E.T., Enghild, J.J. and Scavenius, C. 2014. Coagulation Factor XIIIa Substrates in Human Plasma: Identification and Incorporation Into the Clot. *The Journal Of Biological Chemistry*. [Online]. **289**(10),pp.6526–34.

Nishida, M., Okumura, Y., Fujimoto, S.-I., Shiraishi, I., Itoi, T., et al. 2005. Adoptive transfer of macrophages ameliorates renal fibrosis in mice. *Biochemical And Biophysical Research Communications*. [Online]. **332**(1),pp.11–6.

Noll, T., Wozniak, G., McCarson, K., Hajimohammad, A., Metzner, H.J., et al. 1999. Effect of factor XIII on endothelial barrier function. *The Journal Of Experimental Medicine*. [Online]. **189**(9),pp.1373–82.

Nurminskaya, M. and Kaartinen, M.T. 2006. Transglutaminases in mineralized tissues. *Frontiers In Bioscience : A Journal And Virtual Library*. [Online]. **11**,pp.1591–606.

Nurminskaya, M., Magee, C., Nurminsky, D. and Linsenmayer, T.F. 1998. Plasma transglutaminase in hypertrophic chondrocytes: expression and cell-specific intracellular activation produce cell death and externalization. *The Journal Of Cell Biology*. [Online]. **142**(4),pp.1135–44.

O’Blenes, S.B., Zaidi, S.H., Cheah, A.Y., McIntyre, B., Kaneda, Y., et al. 2000.

Gene transfer of the serine elastase inhibitor elafin protects against vein graft degeneration. *Circulation*. [Online]. **102**(19 Suppl 3),pp.III289–95.

Orkin, S.H. and Zon, L.I. 2008. Hematopoiesis: an evolving paradigm for stem cell biology. *Cell*. [Online]. **132**(4),pp.631–44.

Owens, G.K., Kumar, M.S. and Wamhoff, B.R. 2004. Molecular regulation of vascular smooth muscle cell differentiation in development and disease. *Physiological Reviews*. [Online]. **84**(3),pp.767–801.

Park, D., Choi, S.S. and Ha, K.-S. 2010. Transglutaminase 2: a multi-functional protein in multiple subcellular compartments. *Amino Acids*. [Online]. **39**(3),pp.619–31.

Parsa, R., Andresen, P., Gillett, A., Mia, S., Zhang, X.-M., et al. 2012. Adoptive transfer of immunomodulatory M2 macrophages prevents type 1 diabetes in NOD mice. *Diabetes*. [Online]. **61**(11),pp.2881–92.

Partridge, S.M., David, H.F. and Adair, G.S. 1955. The chemistry of connective tissues. 2. Soluble proteins derived from partial hydrolysis of elastin. *The Biochemical Journal*. [Online]. **61**(1),pp.11–21.

Pawlinski, R., Fernandes, A., Kehrle, B., Pedersen, B., Parry, G., et al. 2002. Tissue factor deficiency causes cardiac fibrosis and left ventricular dysfunction. *Proceedings Of The National Academy Of Sciences Of The United States Of America*. [Online]. **99**(24),pp.15333–8.

Perdiguero, E.G. and Geissmann, F. 2016. The development and maintenance of resident macrophages. *Nature Immunology*. [Online]. **17**(1),pp.2–8.

Perdiguero, E.G., Klapproth, K., Schulz, C., Busch, K., Azzoni, E., et al. 2014. Tissue-resident macrophages originate from yolk-sac-derived erythro-myeloid progenitors. *Nature*. [Online].

Pertuy, F., Aguilar, A., Strassel, C., Eckly, A., Freund, J.-N., et al. 2015. Broader expression of the mouse platelet factor 4-cre transgene beyond the megakaryocyte lineage. *Journal Of Thrombosis And Haemostasis : JTH*. [Online]. **13**(1),pp.115–25.

Pihusch, R., Salat, C., Göhring, P., Hentrich, M., Wegner, H., et al. 2002. Factor XIII activity levels in patients with allogeneic haematopoietic stem cell transplantation and acute graft-versus-host disease of the gut. *British Journal Of Haematology*. [Online]. **117**(2),pp.469–76.

Pinkas, D.M., Strop, P., Brunger, A.T. and Khosla, C. 2007. Transglutaminase 2 undergoes a large conformational change upon activation. *PLoS Biology*. [Online]. **5**(12),p.e327.

Piredda, L., Amendola, A., Colizzi, V., Davies, P.J., Farrace, M.G., et al. 1997. Lack of 'tissue' transglutaminase protein cross-linking leads to leakage of macromolecules from dying cells: relationship to development of autoimmunity in MRLIpr/Ipr mice. *Cell Death And Differentiation*. [Online]. **4**(6),pp.463–72.

Ponce, R. a, Visich, J.E., Heffernan, J.K., Lewis, K.B., Pederson, S., et al. 2005. Preclinical safety and pharmacokinetics of recombinant human factor XIII. *Toxicologic Pathology*. [Online]. **33**(4),pp.495–506.

Poon, M.C., Russell, J.A., Low, S., Sinclair, G.D., Jones, A.R., et al. 1989. Hemopoietic origin of factor XIII A subunits in platelets, monocytes, and plasma. Evidence from bone marrow transplantation studies. *The Journal Of Clinical Investigation*. [Online]. **84**(3),pp.787–92.

Psaltis, P.J., Puranik, A.S., Spoon, D.B., Chue, C.D., Hoffman, S.J., et al. 2014. Characterization of a resident population of adventitial macrophage progenitor cells in postnatal vasculature. *Circulation Research*. [Online]. **115**(3),pp.364–75.

Pyo, R., Lee, J.K., Shipley, J.M., Curci, J.A., Mao, D., et al. 2000. Targeted gene disruption of matrix metalloproteinase-9 (gelatinase B) suppresses development of experimental abdominal aortic aneurysms. *The Journal Of Clinical Investigation*. [Online]. **105**(11),pp.1641–9.

Radu, M. and Chernoff, J. 2013. An in vivo assay to test blood vessel permeability. *Journal Of Visualized Experiments : JoVE*. [Online]. (73),p.e50062.

Rahaman, S.O., Lennon, D.J., Febbraio, M., Podrez, E.A., Hazen, S.L., et al. 2006. A CD36-dependent signaling cascade is necessary for macrophage foam cell formation. *Cell Metabolism*. [Online]. **4**(3),pp.211–21.

Ramirez-Alcantara, V., LoGuidice, A. and Boelsterli, U.A. 2009. Protection from diclofenac-induced small intestinal injury by the JNK inhibitor SP600125 in a mouse model of NSAID-associated enteropathy. *American Journal Of Physiology. Gastrointestinal And Liver Physiology*. [Online]. **297**(5),pp.G990–8.

Ramsay, R.G. and Gonda, T.J. 2008. MYB function in normal and cancer cells. *Nature Reviews. Cancer*. [Online]. **8**(7),pp.523–34.

Ray, J.L., Leach, R., Herbert, J.M. and Benson, M. 2001. Isolation of vascular smooth muscle cells from a single murine aorta. *Methods In Cell Science : An Official Journal Of The Society For In Vitro Biology*. [Online]. **23**(4),pp.185–8.

Rensen, S.S.M., Doevendans, P.A.F.M. and van Eys, G.J.J.M. 2007. Regulation and characteristics of vascular smooth muscle cell phenotypic diversity. *Netherlands Heart Journal : Monthly Journal Of The Netherlands Society Of Cardiology And The Netherlands Heart Foundation*. [Online]. **15**(3),pp.100–8.

Richardson, V.R., Cordell, P., Standeven, K.F. and Carter, A.M. 2013. Substrates of Factor XIII-A: roles in thrombosis and wound healing. *Clinical Science (London, England : 1979)*. [Online]. **124**(3),pp.123–37.

Robinson, B.R., Houng, a. K. and Reed, G.L. 2000. Catalytic Life of Activated Factor XIII in Thrombi : Implications for Fibrinolytic Resistance and Thrombus Aging. *Circulation*. [Online]. **102**(10),pp.1151–1157.

Robitaille, K., Daviau, a, Lachance, G., Couture, J.-P. and Blouin, R. 2008. Calphostin C-induced apoptosis is mediated by a tissue transglutaminase-dependent mechanism involving the DLK/JNK signaling pathway. *Cell Death And Differentiation*. [Online]. **15**(9),pp.1522–31.

Robitaille, K., Daviau, a, Tucholski, J., Johnson, G.V.W., Rancourt, C., et al. 2004. Tissue transglutaminase triggers oligomerization and activation of dual leucine zipper-bearing kinase in calphostin C-treated cells to facilitate apoptosis. *Cell Death And Differentiation*. [Online]. **11**(5),pp.542–9.

Roemer, I., Reik, W., Dean, W. and Klose, J. 1997. Epigenetic inheritance in the mouse. *Current Biology : CB*. **7**(i),pp.277–280.

Rooijen, N. Van and Hendrikx, E. 2010. *Liposomes* [Online] (V. Weissig, ed.). Totowa, NJ: Humana Press.

Rooijen, N. Van and Sanders, A. 1994. Liposome mediated depletion of macrophages: mechanism of action, preparation of liposomes and applications. *Journal Of Immunological Methods*. [Online]. **174**(1-2),pp.83–93.

Rowe, V.L., Stevens, S.L., Reddick, T.T., Freeman, M.B., Donnell, R., et al. 2000. Vascular smooth muscle cell apoptosis in aneurysmal, occlusive, and normal human aortas. *Journal Of Vascular Surgery*. [Online]. **31**(3),pp.567–76.

Samokhvalov, I.M. 2014. Deconvoluting the ontogeny of hematopoietic stem cells. *Cellular And Molecular Life Sciences : CMLS*. [Online]. **71**(6),pp.957–78.

Sane, D.C., Kontos, J.L. and Greenberg, C.S. 2007. Roles of transglutaminases in cardiac and vascular diseases. *Frontiers In Bioscience : A Journal And Virtual Library*. [Online]. **12**(12),pp.2530–45.

Sárváry, A., Szucs, S., Balogh, I., Becsky, A., Bárdos, H., et al. 2004. Possible role of factor XIII subunit A in Fcgamma and complement receptor-mediated phagocytosis. *Cellular Immunology*. [Online]. **228**(2),pp.81–90.

Sauer, B. and Henderson, N. 1988. Site-specific DNA recombination in mammalian cells by the Cre recombinase of bacteriophage P1. *Proceedings Of The National Academy Of Sciences Of The United States Of America*. [Online]. **85**(14),pp.5166–70.

Schaffner, A. and Rhyn, P. 2005. Regulated expression of platelet factor 4 in human monocytes—role of PARs as a quantitatively important monocyte activation pathway. *Journal Of Leukocyte …*. [Online],pp.202–209.

Schiapparelli, L.M., McClatchy, D.B., Liu, H.H., Sharma, P., Yates, J.R., et al. 2014. Direct detection of biotinylated proteins by mass spectrometry. *Journal Of Proteome Research*. **13**(9),pp.3966–3978.

Schroth, M., Meissner, U., Cesnjevar, R., Weyand, M., Singer, H., et al. 2006. Plasmatic [corrected] factor XIII reduces severe pleural effusion in children after open-heart surgery. *Pediatric Cardiology*. [Online]. **27**(1),pp.56–60.

Schulz, C., Gomez Perdiguero, E., Chorro, L., Szabo-Rogers, H., Cagnard, N., et al. 2012. A lineage of myeloid cells independent of Myb and hematopoietic stem cells. *Science (New York, N.Y.)*. [Online]. **336**(6077),pp.86–90.

Schütze, S., Machleidt, T., Adam, D., Schwandner, R., Wiegmann, K., et al. 1999. Inhibition of receptor internalization by monodansylcadaverine

selectively blocks p55 tumor necrosis factor receptor death domain signaling. *The Journal Of Biological Chemistry*. [Online]. **274**(15),pp.10203–12.

Schwartz, M.L., Pizzo, S. V., Hill, R.L. and McKee, P.A. 1973. Human Factor XIII from plasma and platelets. Molecular weights, subunit structures, proteolytic activation, and cross-linking of fibrinogen and fibrin. *The Journal Of Biological Chemistry*. [Online]. **248**(4),pp.1395–407.

Seitz, R., Duckert, F., Lopaciuk, S., Muszbek, L., Rodeghiero, F., et al. 1996. ETRO Working Party on Factor XIII questionnaire on congenital factor XIII deficiency in Europe: status and perspectives. Study Group. *Seminars In Thrombosis And Hemostasis*. [Online]. **22**(5),pp.415–8.

Sercombe, L., Veerati, T., Moheimani, F., Wu, S.Y., Sood, A.K., et al. 2015. Advances and Challenges of Liposome Assisted Drug Delivery. *Frontiers In Pharmacology*. [Online]. **6**(DEC),p.286.

Sigrist, C.J.A., Cerutti, L., Hulo, N., Gattiker, A., Falquet, L., et al. 2002. PROSITE: a documented database using patterns and profiles as motif descriptors. *Briefings In Bioinformatics*. [Online]. **3**(3),pp.265–74.

Söding, J. 2005. Protein homology detection by HMM-HMM comparison. *Bioinformatics (Oxford, England)*. [Online]. **21**(7),pp.951–60.

Song, Y. and Sheng, D. 1994. A microtiter assay for factor XIII using fibrinogen and biotinylcadaverine as substrates. *Analytical …*. [Online].

Soriano, P. 1999. Generalized lacZ expression with the ROSA26 Cre reporter strain. *Nature Genetics*. [Online]. **21**(1),pp.70–1.

Souri, M., Koseki-Kuno, S., Takeda, N., Yamakawa, M., Takeishi, Y., et al. 2008. Male-specific cardiac pathologies in mice lacking either the A or B subunit of factor XIII. *Thrombosis And Haemostasis*. [Online]. **99**(2),pp.401–8.

Stamnaes, J., Pinkas, D.M., Fleckenstein, B., Khosla, C. and Sollid, L.M. 2010. Redox regulation of transglutaminase 2 activity. *Journal Of Biological Chemistry*. **285**(33),pp.25402–25409.

Stephens, P., Grenard, P., Aeschlimann, P., Langley, M., Blain, E., et al. 2004. Crosslinking and G-protein functions of transglutaminase 2 contribute differentially to fibroblast wound healing responses. *Journal Of Cell Science*. [Online]. **117**(Pt 15),pp.3389–403.

Stieler, M., Weber, J., Hils, M., Kolb, P., Heine, A., et al. 2013. Structure of active coagulation factor XIII triggered by calcium binding: basis for the design of next-generation anticoagulants. *Angewandte Chemie (International Ed. In English)*. [Online]. **52**(45),pp.11930–4.

Sugimura, Y., Hosono, M., Wada, F., Yoshimura, T., Maki, M., et al. 2006. Screening for the preferred substrate sequence of transglutaminase using a phage-displayed peptide library: identification of peptide substrates for TGASE 2 and Factor XIIIA. *The Journal Of Biological Chemistry*. [Online]. **281**(26),pp.17699–706.

Sun, W.Q. and Leung, P. 2008. Calorimetric study of extracellular tissue matrix degradation and instability after gamma irradiation. *Acta Biomaterialia*. [Online]. **4**(4),pp.817–26.

Szabo, A., Perou, C.M., Karaca, M., Perreard, L., Palais, R., et al. 2004. Statistical modeling for selecting housekeeper genes. *Genome Biology*. [Online]. **5**(8),p.R59.

Szondy, Z., Sarang, Z., Molnar, P., Nemeth, T., Piacentini, M., et al. 2003. Transglutaminase 2-/- mice reveal a phagocytosis-associated crosstalk between macrophages and apoptotic cells. *Proceedings Of The National Academy Of Sciences Of The United States Of America*. [Online]. **100**(13),pp.7812–7.

Takahashi, K., Takahashi, H., Naito, M., Sato, T. and Kojima, M. 1983. Ultrastructural and functional development of macrophages in the dermal tissue of rat fetuses. *Cell And Tissue Research*. [Online]. **232**(3),pp.539–52.

Takahashi, K., Yamamura, F. and Naito, M. 1989. Differentiation, maturation, and proliferation of macrophages in the mouse yolk sac: a light-microscopic, enzyme-cytochemical, immunohistochemical, and ultrastructural study. *Journal Of Leukocyte Biology*. [Online]. **45**(2),pp.87–96.

Taniguchi, H., Toyoshima, T., Fukao, K. and Nakauchi, H. 1996. Presence of hematopoietic stem cells in the adult liver. *Nature Medicine*. [Online]. **2**(2),pp.198–203.

Tarantino, U., Oliva, F., Taurisano, G., Orlandi, A., Pietroni, V., et al. 2009. FXIIIA and TGF-beta over-expression produces normal musculo-skeletal phenotype in TG2-/- mice. *Amino Acids*. [Online]. **36**(4),pp.679–84.

Thellin, O., Zorzi, W., Lakaye, B., De Borman, B., Coumans, B., et al. 1999. Housekeeping genes as internal standards: use and limits. *Journal Of Biotechnology*. [Online]. **75**(2-3),pp.291–5.

Tiedt, R., Schomber, T., Hao-Shen, H. and Skoda, R.C. 2007. Pf4-Cre transgenic mice allow the generation of lineage-restricted gene knockouts for studying megakaryocyte and platelet function in vivo. *Blood*. [Online]. **109**(4),pp.1503–6.

Töröcsik, D., Bárdos, H., Nagy, L. and Adány, R. 2005. Identification of factor XIII-A as a marker of alternative macrophage activation. *Cellular And Molecular Life Sciences : CMLS*. [Online]. **62**(18),pp.2132–9.

Tournier, C., Hess, P., Yang, D.D., Xu, J., Turner, T.K., et al. 2000. Requirement of JNK for stress-induced activation of the cytochrome c-mediated death pathway. *Science (New York, N.Y.)*. [Online]. **288**(5467),pp.870–4.

Tucholski, J. and Johnson, G.V.W. 2002. Tissue transglutaminase differentially modulates apoptosis in a stimuli-dependent manner. *Journal Of Neurochemistry*. [Online]. **81**(4),pp.780–91.

Uckan, D., Steele, A., Cherry, Wang, B.Y., Chamizo, W., et al. 1997. Trophoblasts express Fas ligand: a proposed mechanism for immune privilege in placenta and maternal invasion. *Molecular Human Reproduction*. [Online]. **3**(8),pp.655–62.

Vandesompele, J., De Preter, K., Pattyn, F., Poppe, B., Van Roy, N., et al. 2002. Accurate normalization of real-time quantitative RT-PCR data by

geometric averaging of multiple internal control genes. *Genome Biology*. [Online]. **3**(7),p.RESEARCH0034.

Verma, G. and Datta, M. 2010. IL-1beta induces ER stress in a JNK dependent manner that determines cell death in human pancreatic epithelial MIA PaCa-2 cells. *Apoptosis : An International Journal On Programmed Cell Death*. [Online]. **15**(7),pp.864–76.

Vogel, C. and Marcotte, E.M. 2012. Insights into the regulation of protein abundance from proteomic and transcriptomic analyses. *Nature Reviews. Genetics*. [Online]. **13**(4),pp.227–32.

Watanabe, M., Jafri, A. and Fisher, S. a 2001. Apoptosis is required for the proper formation of the ventriculo-arterial connections. *Developmental Biology*. [Online]. **240**(1),pp.274–88.

Weston, C.R. and Davis, R.J. 2007. The JNK signal transduction pathway. *Current Opinion In Cell Biology*. [Online]. **19**(2),pp.142–9.

Win, S., Than, T.A., Han, D., Petrovic, L.M. and Kaplowitz, N. 2011. c-Jun N-terminal kinase (JNK)-dependent acute liver injury from acetaminophen or tumor necrosis factor (TNF) requires mitochondrial sab protein expression in mice. *Journal Of Biological Chemistry*. **286**(40),pp.35071–35078.

Wölpl, A., Lattke, H., Board, P.G., Arnold, R., Schmeiser, T., et al. 1987. Coagulation factor XIII A and B subunits in bone marrow and liver transplantation. *Transplantation*. [Online]. **43**(1),pp.151–3.

Wu, L., Tanimoto, A., Murata, Y., Sasaguri, T., Fan, J., et al. 2003. Matrix metalloproteinase-12 gene expression in human vascular smooth muscle cells. *Genes To Cells : Devoted To Molecular & Cellular Mechanisms*. [Online]. **8**(3),pp.225–234.

Wynn, T.A. 2008. Cellular and molecular mechanisms of fibrosis. *The Journal Of Pathology*. [Online]. **214**(2),pp.199–210.

Xu, H., Noria, F., Sandoval-Cooper, M.J., Menchen, H., Donahue, D.L., et al. 2009. Severe deficiency of coagulation Factor VII results in spontaneous cardiac fibrosis in mice. *The Journal Of Pathology*. [Online]. **217**(3),pp.362–71.

Xu, Z., Castellino, F.J. and Ploplis, V.A. 2010. Plasminogen activator inhibitor-1 (PAI-1) is cardioprotective in mice by maintaining microvascular integrity and cardiac architecture. *Blood*. [Online]. **115**(10),pp.2038–47.

Yang, J., Zhang, L., Yu, C., Yang, X.-F. and Wang, H. 2014. Monocyte and macrophage differentiation: circulation inflammatory monocyte as biomarker for inflammatory diseases. *Biomarker Research*. [Online]. **2**(1),p.1.

Yona, S., Kim, K.-W., Wolf, Y., Mildner, A., Varol, D., et al. 2013. Fate mapping reveals origins and dynamics of monocytes and tissue macrophages under homeostasis. *Immunity*. [Online]. **38**(1),pp.79–91.

Yorifuji, H., Anderson, K., Lynch, G.W., Van de Water, L. and McDonagh, J. 1988. B protein of factor XIII: differentiation between free B and complexed B. *Blood*. [Online]. **72**(5),pp.1645–50.

Yoshida, H., Hayashi, S.-I., Kunisada, T., Ogawa, M., Nishikawa, S.-I., et al. 1990. The murine mutation osteopetrosis is in the coding region of the macrophage colony stimulating factor gene. *Nature*. [Online]. **345**(6274),pp.442–4.

Yoshimura, K., Aoki, H., Ikeda, Y., Furutani, A., Hamano, K., et al. 2006. Regression of abdominal aortic aneurysm by inhibition of c-Jun N-terminal kinase in mice. *Annals Of The New York Academy Of Sciences*. [Online]. **1085**,pp.74–81.

Zhang, J., Lesort, M., Guttmann, R.P. and Johnson, G. V 1998. Modulation of the in situ activity of tissue transglutaminase by calcium and GTP. *The Journal Of Biological Chemistry*. [Online]. **273**(4),pp.2288–95.